A dissertation entitled

Experimental and numerical investigations of design parameters for a shell and tube latent heat storage unit

Submitted in partial fulfilment of the requirements for
the award of the degree of

DOCTOR OF PHILOSOPHY
in
MECHANICAL ENGINEERING

By

LOKESH KALAPALA

(Roll No: 717122)

Supervisor

Dr. D. JAYA KRISHNA

(Associate Professor)

Department of Mechanical Engineering

National Institute of Technology,

Warangal (TS), India.

January 2021

Thesis approval for Ph.D

This thesis entitled "**Experimental and numerical investigations of design parameters for a shell and tube latent heat storage unit**" is approved for the degree of Doctor of Philosophy.

Examiners

_____

_____

_____

Supervisor

(Dr. D. Jaya Krishna)
Associate Professor
Department of Mechanical Engineering
National Institute of Technology Warangal

Chairman

(Prof. A. Kumar)
Head
Department of Mechanical Engineering
National Institute of Technology Warangal

DEPARTMENT OF MECHANICAL ENGINEERING

NATIONAL INSTITUTE OF TECHNOLOGY,

WARANGAL (TS), INDIA - 506004

CERTIFICATE

This is to certify that the dissertation work entitled "**Experimental and numerical investigations of design parameters for a shell and tube latent heat storage unit**" which is being submitted by **Mr. Lokesh Kalapala (Roll No:717122)**, is a bonafide work submitted to the Department of Mechanical Engineering, National Institute of Technology Warangal in partial fulfilment of the requirement for the award of the degree of **Doctor of Philosophy in Mechanical Engineering**.

To the best of our knowledge, the work incorporated in this thesis has not been submitted elsewhere for the award of any degree.

Dr. D. Jaya Krishna

(Supervisor)
Associate Professor
Department of Mechanical Engineering
National Institute of Technology Warangal

Prof. A. Kumar

Head
Department of Mechanical Engineering
National Institute of Technology Warangal

DECLARATION

This is to certify that the work presented in the thesis entitled "**Experimental and numerical investigations of design parameters for a shell and tube latent heat storage unit**" is a bonafide work done by me under the supervision of **Dr. D. Jaya Krishna**, and was not submitted elsewhere for the award of any degree.

I declare that this written submission represents my ideas in my own words, and where other ideas or words have been included, I have adequately cited and referenced the original sources. I also declare that I have adhered to all principles of academic honesty and integrity and have not misrepresented or fabricated or falsified any idea/data/fact/source in my submission. I understand that any violation of the above will be a cause for disciplinary action by the Institute and can also evoke penal action from the sources which have thus not been properly cited or from whom proper permission has not been taken when needed.

Date: (**Lokesh Kalapala**)

(Roll No: 717122)

ACKNOWLEDGEMENT

My Ph. D tenure at NIT Warangal is largely responsible for the level of research expertise that I have been able to gain in the past few years and the person primarily responsible for this is my supervisor **Dr. D. Jaya Krishna**. I would like to thank him for his outstanding support, encouragement, and guidance. I am also thankful to him for giving me an initiation into research and technical writing.

I am grateful to the institute administration, especially Head of the Mechanical Engineering Department **Prof. A. Kumar** for providing necessary facilities and for creating a wonderful research environment in the department. I would also like to thank other faculty members, non-teaching staff who extended their support during the entire period of my doctoral program.

I express my deepest gratitude towards doctoral scrutiny committee (DSC) members, **Dr. V. R. K. Raju** (Associate professor, MED), **Dr. G. Naga Srinivasulu** (Associate professor, MED) and **Dr. P. V. Suresh** (Associate professor, CHED) who continuously monitored my research work, and their valuable suggestions helped a lot in the improvement of my thesis.

I would like to thank my seniors at the lab, **Dr. G. Uma Maheswararao, Dr. T. N. Suri**, and **Mr. T. Markandeyulu** for laying the groundwork in creating highly academic environment in the lab and for the productive technical discussions we had to enhance the quality of the work. I am also thankful to my juniors **Mr. Sandip Khobragade**, and **A. Gopi Krishna** for carrying forward the legacy. All these people made our lab such a wonderful place to work. I would also like to thank my fellow scholars, **Mr. P. Rajkumar, Mr. M. Sateesh Kumar, Mr. P. Mahesh**, and **Mr. M. Nitin Kumar** for their continuous encouragement and the fun without which life would have been wearisome.

I greatly thank SERB - Fast Track Scheme for Young Scientists, Department of Science and Technology (DST), Government of India to provide the financial support for this research work thorough the project No. SB/FTP/ETA-0130/2014.

Finally, I would like to thank my wife **Rohini Srilakshmi** for her ceaseless sacrifice and for the moral support. She is the person who motivated me to pursue Ph. D, without her support it would have not been possible for me to complete my Ph. D in three years of time and I always feel lucky to have such a wonderful wife. I would also like to thank our baby **Samanvitha** who

brought charm in our lives and made our lives beautiful. I am also grateful to my parents and in-laws for their support and unconditional love towards me.

Lokesh Kalapala

Abstract

The utilization of solar heat for various industrial processes and residential applications help us to overcome the current predicament of increased pollution and depletion of conventional energy sources. Due to the innate intermittency of solar radiation thermal energy storage is necessary. In this regard, latent heat storage is proven to be a promising option to store thermal energy because of its diverse desirable advantages such as high energy storage density, isothermal heat recovery, etc. Out of various configurations available for latent heat energy storage units (LHSU), shell and tube configuration is the most prominent in which phase change material (PCM) is placed in the annular space of shell and tube and heat transfer fluid (HTF) is passed through the tube. Thermal performance of LHSU depends on charging and discharging rates in other words total melting and solidification times of PCM. Various operating and design parameters of LHSU influence the melting and solidification behavior of PCM and thus affect the thermal performance of LHSU. One drawback of PCMs is their low thermal conductivity because of which energy storage/release rates are hindered. To augment the heat transfer rate various techniques are available out of which employing annular fins is simple yet efficient. Design parameters of fins also affect the thermal performance of LHSU and thus needs to be optimized.

The present research work is aimed at analyzing the influence of various parameters on the melting and solidification behavior of PCM. Adding fins is considered for heat transfer enhancement and optimization of fin parameters is carried out to make LHSU energy and exergetically efficient. Finally, shell geometry is modified as a conical shell for the effective utilization of natural convection. Additionally, the effect of fin parameters is also analyzed in the conical shell. To achieve these objectives, an experimental setup was designed and fabricated. Also, the numerical simulations based on the enthalpy porosity approach are carried out to have a thorough understanding of PCM phase changing behavior.

Initially, the effect of various parameters on the melting characteristics of PCM impregnated in a shell and tube LHSU is analyzed numerically. It is observed that the melt front proceeded in a conical manner and the melting is assisted by natural convection but towards the end, melting has become conduction dominant. Out of all the parameters, Stefan number and Rayleigh number (a non-dimensional form of HTF inlet temperature and shell diameter) are the most influencing parameters. 60.78% reduction in melting time is noted by increasing the

inlet temperature by 40° C i.e. by increasing Stefan number from 0.2 to 0.6. Similarly, 36.37% reduction in total non-dimensional melting time is observed by increasing the Rayleigh number from 2.04×10^5 to 2.32×10^6. The developed correlation for total melting time as a function of all the influential parameters accurately estimated the total melting time with a maximum error of 5%.

Experimental investigations are carried out to realize the effect of LHSU orientation on its thermal performance. Initially, experiments were performed on unfinned LHSU, then a comparative analysis is made among the role of solid fins and perforated fins on heat transfer enhancement. When fins are not attached to the tube, horizontal configuration took 37.17% lesser time to melt half of the PCM, whereas for complete melting vertical configuration required the least time. Exergy efficiency is also noted to be higher for vertical orientation. Vertical configuration exhibited a higher melting rate even when fins are employed. However, providing perforations is observed to be beneficial in vertical configuration during the initial stages of melting. Among solid fins and perforated fins, a higher energy storage rate is obtained with solid fins. The effectiveness of the solid fins is 5% more than the effectiveness of perforated fins during the melting process. The solidification process is unaffected by the orientation of LHSU with and without fins.

Solid fins in the vertical configuration are noted to offer better thermal performance of LHSU but optimization of fin parameters is necessary as the excessive number of fins and fin diameter may deteriorate the heat transfer rate. Fin diameter and number of fins are taken as fin parameters and optimization is carried out to minimize melting time and entropy generated. An increase in the number of fins reduced entropy generation but melting time got increased after a certain number of fins. An increase in diameter increased the melting rate but showed a negative impact on entropy generation. By carrying out multi-objective optimization based on ratio analysis (MOORA), optimized fin parameters are: number of fins = 15, fin diameter = 80 mm. the corresponding non dimensional parameters are: non-dimensional fin spacing = 0.373, non-dimensional fin diameter = 0.8.

Passive heat transfer enhancement technique (modification of shell geometry to conical shape) resulted in better utilization of natural convection as it packed more amount of PCM at the top. Initially, a comparison is made between the cylindrical shell and conical shell without fins. By adopting a conical shell design, 34.46% reduction in melting time is obtained but solidification time increased by 63.17%. When the effect of fin parameters is analyzed it is observed that the

effect of fin diameter depended on the fin number. At higher number of fins (15 or more), an increase in fin diameter caused a reduction in melting rate because the higher diameter of fins led to poor thermal mixing. For both melting and solidification processes it is recommended to employ a higher number of fins with lesser fin diameter.

The developed correlation for total melting time and the presented optimized values of fin parameters are expected to be very handy in the design of a latent heat storage system. Employing perforations and conical shell design also showed promising results for the melting process but further studies are necessary especially in terms of optimizing the configuration of perforations and geometry of the shell.

Keywords: Phase change material, Latent heat storage, Melting and solidification, Exergy, Orientation, MOORA, conical shell, Annular fins, Perforated fins.

CONTENTS

LIST OF FIGURES

LIST OF TABLES

NOMENCLATURE

C	Mushy zone constant (kg/m^3 s)
c	Melt fraction
c_p	Specific heat (J/kg K)
D	Diameter (m)
D_f	Fin diameter (mm)
E	Energy (J)
Ex	Exergy (J)
e	Eccentricity (mm)
Gr	Grashof number
g	Gravitational acceleration (m/s^2)
h	Enthalpy (J/kg), heat transfer coefficient (W/m^2 K)
h_f	Heat transfer coefficient (W/m^2 K)
$\overrightarrow{J_q}$	Heat flux (W/m^2)
k	Thermal conductivity (W/m-K)
L	Latent heat (J/kg)
m	Mass of the PCM (kg)
$\dot{m}$	Mass flow rate (kg/s)
N	Number of fins
$\overline{Nu}$	Average Nusselt number
Pr	Prandtl number
p	Pressure (N/m^2)
p_f	Fin pitch (mm)
$\dot{q}$	Heat transfer rate (J/s)
R	Radius (m)
R_T	Thermal resistance (K/W)
Ra	Rayleigh number
Re	Reynolds number
r	Radius (m)
r, z	Dimensional space coordinates (m)
S	Source term in governing equations

S_p	Entropy generation (W/K)
T	Temperature (K)
T_o	Ambient temperature (K)
t	Time (s)
t_f	Thickness of the fin (mm)
St	Stefan number
U	Overall heat transfer coefficient (W/m^2 K)
u, v	Velocities in r and z directions (m/s)
V	Volume (m^3)
W	Characteristic dimension of LHSU (m)
w	Weighting factor
w_i	Weighing factor of the ith attribute
X	Decision matrix
x	Dimensional space coordinate (m)
x_{ij}	Performance value of ith alternative corresponding to jth attribute
x_{ij}^*	Normalized performance value of ith alternative corresponding to jth attribute
y_i	Assessment value of ith alternative

Greek

Θ	Non-dimensional temperature
η	Non-dimensional space coordinate, energy efficiency
τ	Non-dimensional time, strain tensor
ρ	Density (kg/m^3)
α	Thermal diffusivity (m^2/s)
δ	Thickness of melt layer (m)
δX	uncertainty in measuring X
$\delta(t)$	Position of interface with respect to time
λ	Dimensionless number in solution to Neumann's problem, Ratio of shell diameter to tube diameter, ratio of fin diameter to shell diameter
β	Thermal expansion coefficient (1/K)
ϵ	Porosity
ε	Effectiveness
ρ	Density (kg/m^3)

α	Thermal diffusivity (m^2/s)
β	Thermal expansion coefficient (1/K)
δ	Thickness of tube (m)
ϵ	Porosity
μ	Dynamic viscosity (N s/m^2)
ν	Kinematic viscosity (m^2/s)
φ	Ratio of thermal diffusivities of tube material and PCM
ψ	Exergy efficiency
σ	Ratio of tube thickness to shell diameter

Subscripts

app	apparent
cm	complete melting
dis	discharged
En	energy
eff	effective
i	inner surface, i^{th} control volume
in	inlet
ini	initial
l	liquid
m	melting
max	maximum
o	outer surface
ref	reference
ret	retrieved
s	solidus
st	stored
t	total
w	wall

Symbols

Δ	Difference, stress tensor
$\overline{\Delta T_m}$	Melting temperature span

$\vec{\nabla}.$	Divergence operator

Abbreviations

DSC	Differential scanning calorimeter
Fo	Fourier number $(\alpha t/(R_{shell} - R_{o_{tube}})^2)$
HTF	Heat transfer fluid
LHSU	Latent heat storage unit
LPM	Liters per minute
MF	Melt fraction
MOORA	Multi-objective optimization based on ratio analysis
NTU	Number of transfer units
PCM	Phase change material
PID	Proportional integral derivative
SS	Stainless steel
TES	Thermal energy storage

Chapter 1

Introduction

Industrialization coupled with technological advancement benefitted mankind by showcasing so many advantages like higher productivity, efficient ways of accomplishing any task, improved communication, comfortable traveling, upgraded medical facilities, etc. Many technological innovations in day to day life contributed towards higher living standards and one cannot imagine human life without these technologies in today's world. However, rapid industrial growth and enormous technological improvement continue to escalate energy demand. As per the International Energy Agency (IEA) report, energy consumption throughout the world has been increasing by 2.5% every year which is equivalent to 600 TWh [1]. To meet the increased energy demand, excessive exploitation of fossil fuels is taking place owing to the fact that the world largely depends on fossil fuels for energy production. The imprudent utilization of fossil fuels has become a menace to the environment and the pollution levels are increasing at a frightening rate [2]. To combat these challenges of alarming pollution levels and decrement in fossil fuel reserves, cleaner energy production from renewable sources of energy is the best viable solution.

Various renewable energy sources include solar, wind, biomass, and geothermal energy sources. Undoubtedly all the sources are beneficial, but solar energy emerges as the most valuable of all because of its diverse desirable advantages. Besides being location-specific, wind and geothermal power sources are developed as large-scale utilities and are generally set up by the government. On the other hand, solar installation can be set up almost anywhere and can be adopted directly by every individual. Solar power is much more versatile because of which a huge variety of solar-powered consumer products are available in the market. Electricity production from solar radiation on a larger scale requires a lot of space and incurs a high initial cost. But for residential applications like water heating, space heating, and cooking, etc., solar radiation can be easily tapped using very well-established technologies such as solar flat plate collectors and evacuated tube collectors. The heat produced with the help of these technologies can also be used for various industrial processes such as cleaning, drying, boiling, etc. With the cost of installation is dropping year after year harnessing energy from solar

radiation has become a prominent option for various residential and industrial heating applications.

1.1 Feasibility of solar heat for industrial processes (SHIP) in India

India is a highly fossil fuel-dependent nation for energy production and the excellent insolation the country receives will be very crucial in reducing the dependency on conventional energy sources. Because of its geographic position, India receives a higher value of direct normal irradiance which is equal to 5.5 kWh/m^2/day and is available for 250 to 300 days a year [3]. Though this value is not the same across the country, almost all the industrially developed states receive a fair amount of solar radiation.

Industrial sectors account for more than 50% of the country's energy needs [3] and there is a huge demand for heat energy in industrial processes. Many industrial processes in India require low to medium temperatures, especially below 100ºC. In this context, the processes and the required temperatures in very popular and widely spread industries across the country are listed in Table 1.1. From the table, it can be reckoned that a plethora of industrial processes can be supplemented with solar heat which is capable of producing the required temperature range. Because of the enormous availability of solar radiation and its potential to meet residential and industrial heat energy needs, India has been an early adopter of solar thermal technologies. The country is actively promoting SHIP technologies through the Solar Thermal Federation of India (STFI) and National Institute of Solar Energy (NISE).

1.2 General scheme of a SHIP plant and the need for thermal energy storage

Solar thermal technologies for water heating and space heating are very popular for many years. However, integrating these technologies for industrial heat energy demand is the pressing priority. Figure 1.1(a) shows the schematic of a simple solar integrated process heat cycle. The solar collector receives solar radiation and heats the thermal transfer fluid. This thermal transfer fluid can be directly supplied to production processes or transfer of heat to another medium is done via a heat exchanger. But the fluctuations and intermittency in solar radiation may not suffice the energy demand and hence an external heat source is provided. When solar radiation is not available, the required heat will be supplied by external heating equipment or by electricity.

When the energy demand is less the tapped solar radiation will be squandered and when there is no sunshine, dependency on conventional energy resources is inescapable. To bridge the gap between energy supply and demand, energy storage has become essential. The thermal energy harnessed from solar radiation is stored in a heat storage unit and when needed the working fluid is heated using the stored energy. Figure 1.1(b) shows a typical layout of the heat storage integrated plant which comprises of solar collector and heat storage unit.

Table 1.1: Various industrial processes and temperature ranges [4–7]

Industry	**Process**	**Temperature (°C)**
Dairy	Washing and cleaning	40-60
	Pasteurization	70
	Chemical processes	40
	Evaporation	100
Food processing and beverages	Pasteurization	80-100
	Washing	40-80
	Drying	70-90
	Heat treatment	40-60
	Cooking	60-90
Textile	De sizing	60-90
	Bleaching	90
	Mercerizing	60-70
	Dyeing	70-90
	Sizing	80-85
Pharmaceutical	Distillation	55-80
Automotive processing	Paint shop pre-treatment	40
	Paint shop evaporation and drying	80-100
Rubber, plastic and other chemical processing	Pre-heating	50-70

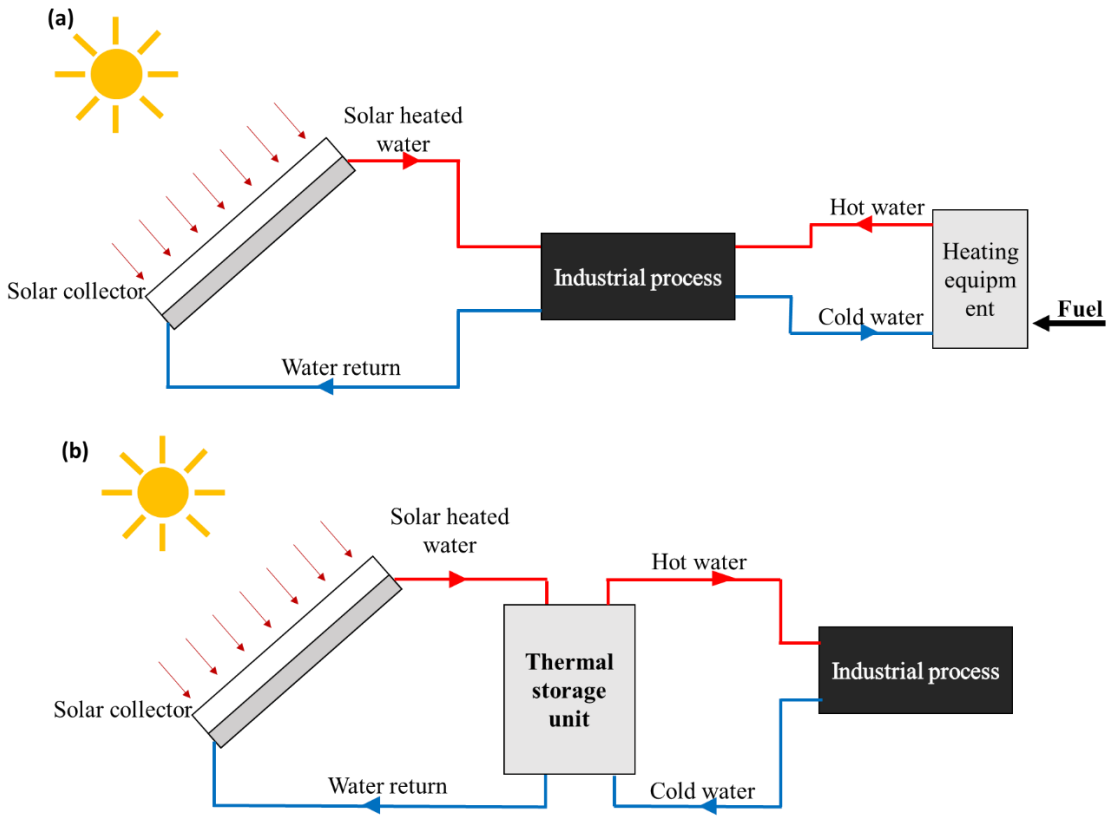

Figure 1.1: Schematic illustration of SHIP plant layout (a) without storage unit (b) with heat storage unit

Selection of an appropriate thermal energy storage technology and proper design of the energy storage unit plays a vital role in the efficient operation of the plant. The following are the desired characteristics of a thermal energy storage (TES) unit.

- High energy storage density (storage capacity per unit volume)
- High energy storage and retrieval rates
- Operating temperature should be close to the required process temperature
- Thermal stability over the number of charging and discharging cycles
- Minimal thermal losses to the surroundings
- Ease of fabrication and low cost

1.3 Energy storage technologies for low temperature applications

Thermal energy storage generally involves the temporary holding of thermal energy (at low or high temperatures) for later use. By process reversal, the stored energy can be retrieved back. TES is not new for the world, probably the oldest TES was harvesting ice from lakes and rivers,

storing it in well-insulated containers which are used for preserving food, cool drinks, and air conditioning [8]. TES involves heating/cooling, melting/solidification, or vaporizing a material to store the energy. The most prominent TES methods are sensible heat storage and latent heat storage.

Sensible heat storage is achieved by subjecting the storage material to a rise in its temperature. The efficiency and effectiveness of this system mainly depend on the specific heat of storage material. A wide variety of sensible heat storage materials are available which include water, rocks, liquid metals, etc. When the storage material needs to be pumped, water or liquid metals are used. On the other hand, solids have the advantage of higher specific heat capacity which allows compact storage units.

Latent heat storage involves the phase transition of a material which is termed as phase change material (PCM). As the phase transition needs latent heat to be supplied, higher amount of heat can be stored at a constant temperature. The storage capacity of a latent heat storage system largely depends on the latent heat of the PCM. Various types of PCMs are available in the market which include organic, inorganic and eutectic PCMs. The PCM can be chosen based on the required temperature range in the desired application. When compared to sensible heat storage latent heat storage has the following advantages [9–15]

- Latent heat storage capacity per unit volume is 5-14 times more in comparison with sensible heat storage.
- Nearly isothermal heat recovery is possible.
- Can be used in a wide temperature range.
- Compact energy storage systems can be made possible.

Another method of storing heat is through reversible endothermic chemical reactions which is known as **thermochemical energy storage**. This method involves energy storage by means of breaking and forming chemical bonds. For this purpose, a variety of chemical reactions are being explored such as catalytic reactions, thermal dissociation reactions, etc. However, these reactions take place at a higher temperature and for low temperature application (<300°C) this method is not proven to be promising [11].

Because of its diverse desirable advantages, PCMs have attracted various applications viz, heating and cooling in buildings [16–18] Trombe walls [19], PCM wallboards, PCM shutter, solar water heating [20,21], cold storages [22,23], solar cooker [24], to increase thermal

comfort in vehicles [25,26], insulating telecom shelters, transportation of pharmaceuticals and chemicals, electronic cooling [27–29] etc. In view of enormous applications, active research is being carried out on the development of different kinds of PCMs, and a few available PCMs are listed in Table 1.2. From the table, it can be reckoned that the PCMs are available in a wide range of temperatures and because of high latent heat values, heat storage using PCMs results in high energy storage density. Because of this, latent heat storage has grabbed the attention of researchers over the years and chosen as the area of research for the current study.

Table 1.2: List of PCMs [13,16,20,30,31]

		Melting point (°C)	**Latent heat (kJ/kg)**
Organic PCMs	N-pentadecane	10	205
	Propyl palminate	19	186
	Paraffin C18	28	244
	Capric acid	36	152
	Medicinal paraffin	40-44	146
	Lauric acid	49	178
	Myristic acid	58	199
	Stearic acid	69.4	199
	Acetamide	81	241
Inorganic PCMs	H_2SO_4	10.4	100
	P_4O_6	23.7	64
	$TiBr_4$	38.2	23
	$H_4P_2O_6$	55	213
	$SbCl_3$	73.4	25
Eutectics	$C_5H_5C_6H_5$+ $(C_6H_5)_2O$	12	97.9
	$C_{14}H_{28}O_2$+$C_{10}H_{20}O_2$	24	147.7
	Myristic acid + glycerol	31.96	154.3
	NH_2CONH_2+NH_4NO_3	46	95
	Palmitic acid + glycerol	58.5	185.9
	Stearic acid + glycerol	63.45	149.4
	$AlCl_3$+NaCl+KCl	70	209
	$LiNO_3$ + NH_4NO_3+$NaNO_3$	80.5	113

1.4 Various configurations of latent heat storage units

The performance of a latent heat storage unit (LHSU) primarily depends on the proper selection of the PCM and the container shape. Generally, PCM is selected based on the temperature range of the intended application and thermophysical properties of the PCM. Another important factor to be considered is the geometry of the PCM container. A thorough literature survey on latent heat storage systems revealed that the most commonly employed geometries are cylindrical and rectangular. In the cylinder model, three configurations are popular namely pipe model, shell and tube, shell and multi-tube model which are shown in Fig. 1.2. In the pipe model, PCM is placed in the tube and the HTF flows through the annulus. In shell and tube configurations HTF is passed through the tube and the PCM is placed in the annular space of shell and tube. A survey conducted by Agyenim et al. [31] disclosed that more than 70% of the previously published works employed shell and tube configuration. This is due to the fact that the heat loss from the shell wall to the surroundings is minimum when the cylindrical container is employed. Because of this advantage and ease of fabrication shell and tube configuration is chosen for the current research work.

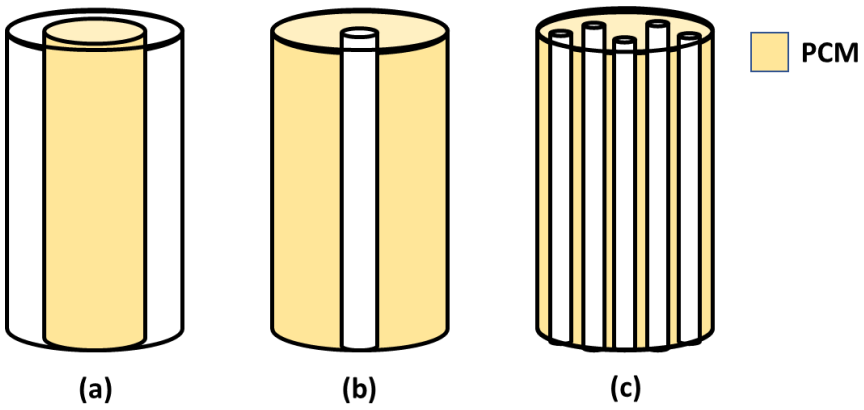

Figure 1.2: Various configurations of cylindrical model of LHSU (a) pipe model (b) shell and tube model (c) shell and multi-tube model

1.5 Scope of research work

Thermal energy storage is essential for the efficient utilization of solar heat for various industrial applications. In this regard, latent heat storage has many advantages over other heat storage methods. Hence there is a need for extensive research in maximizing the performance of the latent heat storage unit. Along with PCM's thermophysical properties, various operating and geometrical parameters of LHSU influence its performance. Owing to the low thermal conductivity of PCMs, heat transfer enhancement techniques should also be explored. Hence

the research should be aimed at maximizing the performance of the heat storage unit by optimizing various influential parameters along with incorporating heat transfer augmentation technique. In addition to energy analysis, exergy analysis should also be carried out as the ultimate aim of any energy storage unit is to extract and supply useful work. The current research work is focused on analyzing the effect of various operating, geometric parameters, and optimizing design parameters of fins to make LHSU both energy and exergetically efficient.

1.6 Organization of the thesis

In the thesis, experimental and numerical investigations on the influence of various parameters on the performance of shell and tube LHSU are discussed. The entire work is presented in 9 chapters.

Chapter 1 provides a brief introduction to the research topic – latent heat storage

Chapter 2 presents the literature review on parametric analysis on the heat transfer characteristics of shell and tube LHSU, heat transfer augmentation techniques being employed in LHSU, and the mathematical formulations to simulate the phase changing process of PCM.

Chapter 3 provides the details of the experimental setup and the numerical methodology adapted for the current research work.

Chapter 4 presents the non-dimensional parametric analysis on the melting behavior of PCM impregnated in a vertical shell and tube LHSU.

Chapter 5 deals with the effect of LHSU inclination on its thermal performance.

Chapter 6 provides the comparative analysis on the thermal performance of LHSU with solid fins and perforated annular fins for heat transfer intensification.

Chapter 7 presents the multi-objective optimization of fin parameters to make LHSU energy and exergetically efficient.

Chapter 8 provides numerical investigations on the performance of LHSU by employing a frustum shaped shell along with fins.

Chapter 9 provides the major findings of the current research work and the scope for future work.

1.7 Closure

In this chapter, the feasibility of adapting solar thermal technologies in India and the need for thermal energy storage are outlined. Advantages of latent heat storage over other methods of storage are discussed and a brief overview of the research scope pertaining to shell and tube latent heat storage unit is provided. As a concluding remark, thermohydraulic studies of latent heat storage unit need to be carried out and the optimization of various influential parameters should be carried out by conducting both energy and exergy analyses.

Chapter 2

Literature review

Thermal energy storage is essential to avail of the enormous solar radiation for various industrial and residential applications. In this regard, latent heat storage is proven to be superior to other methods of thermal energy storage. Out of various proposed configurations for latent heat storage units, shell and tube (S&T) configuration is widely used and very simple in construction. In a shell and tube configuration, heat transfer fluid (HTF) is passed through the tube, and PCM is placed in the annular space of shell and tube. The latent heat storage unit should be designed in a way that would exhibit higher energy charging/discharging rates. There are various parameters which influence the thermal performance of LHSU which need to be analyzed. For heat transfer intensification in LHSU employment of heat transfer enhancement technique is necessary. In this chapter, a thorough literature review pertaining to shell and tube LHSU is provided. Studies corresponding to the influence of various parameters and heat transfer augmentation techniques are discussed. A brief overview of various mathematical formulations to analyze the phase changing process of PCM is also provided.

2.1 Effect of operational and design parameters on the performance of latent heat storage unit

The design of the LHSU plays a crucial role in the heat transfer rate between heat transfer fluid and PCM, thereby influences total melting and solidification times. Various authors studied the effect of different operating and design parameters viz. mass flow rate, inlet temperature of HTF, orientation of LHSU, diameters of shell and tubes on the melting/solidification rates and energy storage/discharged rates of PCM.

2.1.1 Effect of mass flow rate

The mass flow rate of HTF which is directly related to velocity or Reynolds number of the flow has a significant influence on the heat transfer rate as it dictates the overall heat transfer coefficient between HTF and PCM. An increase in mass flow rate or inlet velocity of HTF enhances the heat transfer rate. However, the difference between the inlet and outlet temperature of the HTF reduces, which may not be desirable in some applications like water

heating. So, an optimum value of mass flow rate should be chosen which will be a compromise between heat transfer rate, energy stored, and temperature drop or rise of the HTF.

Cao and Faghri [32] was the first study where the parametric investigation on the performance of LHSU was carried out. They compared the melting front radius for different Reynolds numbers. It was observed that the melting front radius increased with the increase in Reynolds number which infers that the heat transfer rate increases with an increase in mass flow rate. Wang et al. [33] reported that mass flow rate has a negligible effect on the storage capacity, whereas heat transfer rate increased with the increase in mass flow rate thereby reducing the melting time and solidification time. Agarwal and Sarviya [34] designed LHSU for solar dryer in which paraffin was used as PCM and air as HTF. They concluded that discharging time reduced with an increase in HTF mass flow rate. Seddegh et al. [35] and Kibria et al. [36] carried out numerical studies to understand the effect of operating conditions on melting time. They reported that melting time decreased with the increase in mass flow rate. Esen et al. [37] numerically studied the melting behavior of 4 different PCMs under various operating conditions. For all the PCMs they found similar behavior i.e. decrease in melting time with the increase in the mass flow rate of the HTF. This was the consequence of the increase in heat transfer rate because of the increase in Reynolds number. Akgun et al. [38] experimentally investigated the effect of inlet velocity of HTF on transient temperatures of the PCM. They observed an increase in thermal transport with the increase in inlet velocity of HTF. Rathod and Banerjee [39] reported that the melting time of PCM increased with a decrease in mass flow rate. Similar kind of result was also obtained by Seddegh et al. [35]. All these works suggest that an increase in the mass flow rate of HTF causes a reduction in melting and solidification time of PCMs because of the enhancement in heat transfer.

Some authors ([40–42]) studied the effect of mass flow rate on stored energy. Fath [40] experimentally observed that an increase in flow rate resulted in an increase in heat transfer rate and accumulated energy. This work can be referred as the first experimental work related to the parametric study on the performance of the heat exchanger employing PCM. Gong and Mujumdar [41] compared the energy stored at different mass flow rates for the same period of charging and their results indicated an increase in energy stored with the increase in mass flow rate. Same results were also reported by Lacroix [42]. So, it is evident that the increase in mass flow rate increases the energy stored in LHSU.

The phase change rate is mainly influenced by the overall heat transfer coefficient, hence it is essential to study the effect of mass flow rate on the overall heat transfer coefficient. Wang et

al. [43] experimentally studied the mass flow rate effect on the overall heat transfer coefficient of LHSU in which erythritol was employed as PCM. Because of higher convective heat transfer rates at higher mass flow rates, the overall heat transfer coefficient increased with the increase in mass flow rate. Contrary to this, Seddegh et al. [44] reported that mass flow rate has a negligible effect on the overall heat transfer coefficient. This was because the heat transfer rate was dominated by the heat transfer coefficient between PCM and tube surface whereas mass flow rate affected the heat transfer coefficient between HTF and tube surface.

2.1.2 Effect of inlet temperature

The difference between the phase change temperature of the PCM and inlet temperature of HTF is the driving force of heat transfer between PCM and HTF. Hence, the HTF inlet temperature will have a significant effect on the heat transfer rate. As the temperature difference increases, the heat transfer rate increases, and hence total melting time reduces. For the optimization of HTF inlet temperature, the effect on energy charged or discharged and total melting or freezing time needs to be taken into consideration.

Fath [40] reported that there was an increase in accumulated energy and heat transfer rate by 90% with the increase in HTF inlet temperature from 65°C to 81°C. This was due to the higher temperature difference which is the driving force for heat transfer. Lacroix [42] performed numerical experiments and observed that the higher inlet temperature of HTF resulted in faster melting at any mass flow rate and it was also stated that total energy stored in PCM increased linearly with the increase in inlet temperature. They reported 1.53 times increase in accumulated energy when the difference in inlet temperature of HTF and melting temperature of PCM increased from 5 to 20. Results inline to this were obtained by Gong and Mujumdar [10]. Similar observations were also made from the experimental studies of Avci and Yazici [45]. Ezan et al. [46] carried out experimental studies on charging and discharging periods of water (water was used as PCM) in which they observed that inlet temperature of HTF has more effect on melting and solidification time than the mass flow rate. Esen et al. [37] reported that the total melting time of paraffin wax decreased by 1.4 times when the inlet temperature of the HTF increased from 50°C to 65° C. The same trend was reported by [47], who numerically studied the effect of Stefan number on melting and solidification times. This was attributed to the enhanced buoyancy effects which ensure strong convection currents. Trp et al. [48] analyzed the effect of HTF inlet temperature on total energy stored and storage density during charging. Both total energy stored, and storage density were observed to increase with the

increase in inlet temperature. On the similar lines, the thermal energy delivered increased with the increase in the difference between PCM solidification temperature and inlet temperature of HTF. Increase in the temperature difference between the inlet temperature and PCM melting temperature resulted in higher sensible heat storage occurring after complete melting, same was the case during discharging. Akgun et al. [38] carried out experimental studies and reported that a higher inlet temperature of HTF led to reduced melting times because of an increase in enthalpy flow. Rathod and Banerjee [39] experimentally analyzed the effect of HTF inlet temperature on melting and solidification times of paraffin wax. They reported that the inlet temperature of HTF has a significant effect on melting when compared to the effect of mass flow rate. In another work by the same authors [49], 44% decrease in melting time of paraffin wax was reported when inlet HTF temperature increased from 75°C to 85°C. Seddegh et al. [35], [44] also reported similar behavior.

Wang et al. [33], numerically analyzed the influence of HTF inlet temperature on heat transfer rate during charging and discharging. They stated that there exist three stages in the temperature of PCM before coming to the steady state: rapid rise, slow rise and slower rise in temperature periods. They observed that the duration of all the periods decreased with the increase in HTF inlet temperature during charging. Similarly, while discharging, the decrease in inlet temperature of HTF reduced the solidification time. Li and Kong [50] also observed the above mentioned three stages in their numerical study using air and water as HTFs.

2.1.3 Effect of shell and tube diameter ratio

The shell to tube diameter ratio "**λ**" is the most significant design parameter which affects the total melting time, solidification time and stored energy. As this ratio increases, the amount of PCM increases and hence stored energy can be increased. However, this leads to an increase in melting time and solidification time. Hence, there is a need to optimize 'λ' to obtain maximum energy storage density for lesser melting time.

Lacroix [42] presented a numerical model to analyze the heat transport characteristics of a TES. It was concluded that to optimize the design of TES, the radius of the shell should be taken into consideration along with the inlet conditions of HTF. Bellecci and Conti [51] used the enthalpy model to study the performance of TES. It was mentioned that the shell to tube diameter ratio (**λ**) and L/D ratio are the design parameters which need to be optimized. They observed that if the value of "**λ**" is greater than 4, some part of the PCM remained without undergoing phase change. Hence, the "**λ**" value was recommended to be less than 4. Ismail and Goncalves [52]

also suggested the ratio to be 4 after which the effectiveness of the TES reduced drastically. Numerical investigation was carried out on the performance of TES by Trp et al. [48]. Inline to Bellecci and Conti [51], it was highlighted that "**λ**" and length to shell diameter ratio need to be considered as the design parameters. They concluded that with the increase in both these parameters, the contribution of latent heat storage got reduced. This indicates that entire PCM is not undergoing phase change at higher "λ" and length to shell diameter ratio.

It is worth noting that, all the above-mentioned works optimized design parameters based on stored energy density. In addition to stored energy density, total melting time should also be considered to arrive at the optimum design of TES. This was done by Seddegh et al. [44] who experimentally analyzed the influence of "**λ**" on total melting time and energy stored. They suggested a value of 5.4 for "**λ**" which was obtained as a balance between stored energy and melting time.

From the above-mentioned works, it is clear that the major influencing operating parameter is HTF inlet temperature. The effect of HTF flow rate is not significant when compared to HTF inlet temperature, but the influence of the HTF flow rate cannot be completely disregarded. The design parameters that need to be considered are diameter of the shell and length of the system. Along with these, tube material and tube thickness should also be taken into consideration as it offers resistance to heat transfer [46]. As reported by Esen et al. [37], the effect of all these parameters will be different for different PCMs. Hence, by doing the parametric analysis in dimensional form, one cannot generalize the results. This necessitates the need for non-dimensional parametric analysis which is lacking in the literature.

2.1.4 Effect of orientation

During the charging process, PCM absorbs the heat from the HTF and gets melted. In the course of the melting phenomenon, both conduction and convection modes of heat transfer exist. Within the solid PCM, heat is transferred via conduction and natural convection prevails as the PCM starts to melt. This phenomenon was observed and documented by several authors [53–55] and it was reported that the natural convection plays a prominent role in the melting of PCM. Natural convection gets influenced by the orientation of LHSU and thus melting behavior of PCM also gets affected by the orientation. A great number of studies [56–62] are available pertaining to the influence of the orientation of a rectangular LHSU. All the studies

designated that the container should be oriented such that the heat source is at the bottom for faster melting. But in a S&T configuration, the melting behavior is completely different when compared to melting in a rectangular LHSU. This is because the heat source i.e. HTF tube is concentric to the shell and is surrounded by PCM. In the literature, very few works are available in this regard and the existing studies explored the performance of LHSU in terms of melting rate and energy stored.

Bejan [63] illustrated the influence of the tilting angle on the heat transfer mechanism in an enclosure and it was reported that the tilting angle significantly affected Nusselt number. Hence, the orientation of LHSU is expected to play a significant role on the heat transfer rate. However, less attention is given by the researchers in studying the effect of inclination on the melting behavior of PCM. Sharifi et al. [64] studied the melting behavior of PCM in a cylindrical enclosure. A heating rod was placed concentric to the cylindrical container. They observed that even modest tilting of the enclosure significantly affected the temperature evolution at various locations. They attributed this to the establishment of three-dimensional flow with tilting. this work signifies the need for a thorough investigation on the effect of the orientation of LHSU on the melting behavior of PCM. But very limited number of works are available on the effect of orientation. Out of the available works some authors [35,65] reported vertical configuration is the best and some authors [66] reported that the horizontal configuration exhibited better performance. Seddegh et al. [35] made a comparison among the total melting time of paraffin wax in horizontal and vertical configurations. During the initial stages of melting, the melting rate was observed to be higher in horizontal configuration which got reduced drastically with the progression in time. They stated that the natural convection created recirculation region in both the configurations, however, the recirculation was not effective in vertical configuration. Hence, they recommended horizontal configuration for the melting process. Same conclusion was given by Kousha et al. [65] who carried out experimental studies on the effect of orientation on the melting characteristics of RT35. Riahi et al. [67] also reported that the horizontal configuration provided higher effectiveness when compared with the vertical configuration.

On the other hand, Pahalmi et al. [66] reported that vertical orientation is best for the melting process. Siyabi et al. [68] performed numerical and experimental studies to analyze the effect of inclination of the cylindrical thermal energy storage system on its performance. Three different orientations were considered: 90° (horizontal), 45° and 0°(vertical). They observed that the PCM average temperature was not affected with the change in inclination angle,

however, the axial variation in temperature was observed to be less for horizontal configuration. Through the careful observation of melting profiles with respect to time, it was revealed that the PCM tend to melt faster in radial direction than in axial direction in case of vertical configuration. But the horizontal configuration exhibited opposite behavior. Moreover, in horizontal configuration PCM did not melt completely. By analyzing the flow of PCM, they concluded that 45° inclination provided more uniform flow in both the axial and radial directions and hence the melting rate was faster. In accordance with this result, Mehta et al.[69] also reported a higher melting rate in the case of 45° inclination. Mehta et al. [70] carried out a comparative study on the performance of a shell and tube LHSU in horizontal and vertical orientations. They suggested horizontal configuration for partial charging as 25% reduction in the time was observed to melt half of the PCM. For the solidification process, no significant variation was observed for the two configurations.

2.2 Correlations available for total melting time

The development of correlation for total melting time is needed as it helps in deciding the design and operating parameters. In the literature, few correlations were proposed and are listed below.

Solomon [71] presented a correlation for the total melting time of PCM in a cylindrical TES and is given in Eq. 2.1. It can be observed that the correlation was developed only as a function of Stefan number and they assumed that the PCM was initially at melting temperature. Riley et al. [72] also presented similar type of correlation for total solidification time.

$$Fo_{cm} = 0.11 + 0.25/St \tag{2.1}$$

Hasan [73,74] presented two different correlations for vertical and horizontal cylindrical TES given by Eqs. 2.2 and 2.3 respectively

$$Fo_{cm} = 0.25 + 0.134/St \tag{2.2}$$

$$Fo_{cm} = 0.14 + 0.15/St \tag{2.3}$$

Ho and Viskanta [75] included the effect of Rayleigh number and developed the correlation for melt fraction in terms of Ra, St and Fo given in Eq. 2.4

$$MF = 0.523(Ra^{0.25} \cdot St \cdot Fo)^{0.68} \tag{2.4}$$

On the similar lines, Katsman et al. [76] presented correlation for melt fraction in terms of Ra, St and Fo. The Rayleigh number was based on length of the TES. Various other authors [77–80] also developed correlations as a function of Ra, St and Fo.

Rathod and Banerjee [49] reported that the HTF flow rate influenced the total melting time and hence they presented correlation as a function of St and Re. The correlation is given in Eq. 2.5

$$Fo_{cm} = 0.515\, St^{-1.24} \cdot\ Re^{-0.133} \tag{2.5}$$

Later, they [81] developed another correlation by including the effect of initial temperature of the PCM and is given by Eq. 2.6

$$Fo_{cm} = 0.853 - 3.73 \times 10^{-5}\, Re - 0.04778\, St\, \frac{T_{inlet}}{T_{ini}} \tag{2.6}$$

From the above-mentioned works, it can be noticed that these correlations (Eqs.2.1-2.6) are applicable for fixed dimensions of the heat exchanger and tube material. It is necessary to have correlations for total melting time and melt fraction which can be used irrespective of PCM and heat exchanger dimensions. But high non-linearity in the melt fraction evolution and dependency on a large number of parameters makes it difficult to develop correlation.

2.3 Heat transfer enhancement techniques

The performance of LHSU depends on energy charging/discharging rates which are hindered due to lesser thermal conductivity of PCM. To overcome this issue various heat transfer enhancement techniques are available such as dispersion of nanoparticles, embedded metal foam, multiple PCM arrangement, and employment of fins. In this section, the works pertaining to all the heat transfer enhancement techniques are discussed. However, the review of literature is more focused on the employment of fins as fins are chosen as the heat transfer enhancement technique for the current research work.

2.3.1 Employment of fins

Among various enhancement techniques, employing fins is very efficient, least expensive and no fabrication complexity is involved [82]. In this respect, various designs of fins are proposed which include longitudinal fins, annular fins, and pin fins. In the shell and tube model,

longitudinal and radial fins are used widely, and subsequent discussion will be on studies pertaining to design parameters for these kinds of fins.

Longitudinal fins

Application of longitudinal fins for enhancing melting rate can be found in 1985 by Kalhori and Ramadhyani [83]. In this work, they experimentally studied the melting and freezing characteristics of n-eicosane paraffin placed around a vertical cylinder. They compared the heat transfer rate with respect to time with fins and without fins and observed significant enhancement in heat transfer rate by using longitudinal fins. Shokouhmand and Kamkari [84] considered longitudinal fins on the horizontal tube and studied the melting behavior of paraffin wax placed around the tube. By observing the melt fraction over time, they concluded that an increase in number of fins increased the melting rate. This was due to the increase in heat transfer area. Rathod and Banerjee [85] experimentally analyzed the effect of fins on the melting and solidification behavior of paraffin wax. They considered 3 longitudinal fins, and their results revealed that the effect of fins was more significant on solidification when compared to melting. They observed a reduction in melting time of 24.52%, whereas the reduction in solidification time was 43.6%. These works indicate that using longitudinal fins greatly enhances the heat transfer rate in melting as well as solidification process irrespective of the orientation of heat exchanger.

The fin parameters to be considered are number of fins, fin width, fin pitch, and fin thickness. Various authors have optimized these parameters to attain maximum enhancement in heat transfer. Ismail et al. [86] studied solidification characteristics of PCM placed around a vertical finned tube. They studied the effect of different design parameters of the fin: number of fins, fin length, and fin thickness. They observed that an increase in all these parameters resulted in lesser solidification time. However, the space available for PCM gets reduced and hence storage capacity got reduced. By optimizing these, they recommended fin thickness to be equal to tube wall thickness, radial length of the fin to be equal to twice the diameter of the tube and number of fins to be 4 or 5. Tao and He [87] carried out numerical analysis on melting characteristics of PCM around a horizontal finned tube. They also concluded that enhancement in melting rate by increase in number of fins, fin thickness, and fin height will be at the expense of storage capacity of the system. They suggested number of fins to be equal to 7 and to be placed in lower part of the shell. To compensate the reduction in heat storage capacity it was recommended to use compound enhancement technique i.e. a combination of fins and multiple

PCMs [88]. Along with conventional rectangular shaped fins, few authors [89–91] have proposed different shapes for longitudinal fins by carrying out topology optimization by which substantial performance enhancement was observed.

Annular/radial fins

A great number of studies, both experimental and numerical are available which documented the influence of different annular fin parameters on the thermal performance of LHSU. For the radial fins, the influencing geometric parameters are fin radius, fin thickness and fin pitch i.e, number of fins. An increase in fin number and fin radius increases the heat transfer area thereby enhances the heat transfer rate. However, this leads to reduction in the amount of PCM that can be placed due to which energy stored decreases. Hence, these parameters should be optimized by considering the heat transfer rate and stored energy.

Choi and Kim [92] experimentally investigated the solidification characteristics of $MgCl_2.6H_2O$ by employing circular fins. The temperature distribution was observed to be uniform in case of the finned tube and they observed an increment of 3.5 folds in the heat transfer coefficient with circular fins. Lacroix [93] conducted a number of numerical experiments to observe the effect of number of fins and noticed the rate of energy storage to be increasing as the number of fins increased. Wang et al. [94] considered energy efficiency ratio and energy storage rate as the performance parameters and examined the impact of fin parameters on these two parameters. They observed that the effect of fin thickness and fin diameter were insignificant if the dimensionless fin pitch (ratio of fin pitch to tube radius) is greater than 4. Hence, they suggested fin pitch to be small and higher fin diameter. On the other hand, Thirunavukkarasu et al. [95] insisted on optimizing number of fins with respect to the length of the heat exchanger. They reported that increasing number of fins after a certain value has no significant reduction in melting time. Owing to this fact, Yang et al. [96] optimized group fin parameters (number of fins, fin height, and fin thickness) for the maximum reduction in melting time of PCM around the vertical finned tube. The optimized parameters were observed to be: number of fins = 31, the ratio of thickness to length of the tube = 0.0248, the ratio of fin pitch to length of the tube = 0.0313.

Seeniraj et al. [97] carried out numerical studies on melting of PCM around a horizontal finned tube. The fins were extended up to the shell wall i.e. fins were placed such that whole space was divided into an equal number of divisions. They observed that after some time there was no radial variation in the temperature of the fin and temperature was equal to the HTF

temperature. This type of fin configuration also facilitates accommodating different PCMs. The same configuration was considered by Groulx and Ogoh [98], who also reported a decrease in melting time with the increase in number of fins.

Zhao and Tan [99] studied the effect of dimensionless fin height on various parameters such as charging rate and melt fraction. They did not observe any significant difference between the results when dimensionless fin heights of 0.66 and 0.99 were employed. Hence, they suggested optimizing fin diameter to balance system performance and material cost. Hosseini et al. [100] numerically studied the combined effect of fin height and Stefan number on melting and solidification time of PCM. They concluded that total melting time reduced with the increase in fin height which was much noticeable at higher Stefan numbers. They also reported that fin height has more influence on solidification time than that of melting time. Ismail and Lino [101] studied the effect of annular fin diameter on the total solidification time of PCM. They suggested an optimum fin diameter range to be 60-80 mm. Solidification time was observed to be increasing if fin diameter is beyond these limits. Jmal and Baccar [102] investigated the effect of fin number on heat transfer enhancement. They observed attenuation of convective motion of PCM with an increase in number of fins which led to reduction in heat transfer rate. Zhai et al. [103] employed both annular and longitudinal fins and analyzed the influence of different fin parameters viz, annular fin pitch, fin thickness, and the number of rectangular fins. They reported a reduction in solidification time of PCM with the reduction in annular fin spacing. However, the minimum fin pitch was restricted to 40 mm as further reduction of fin pitch increases the manufacturing complexity. On similar lines, Santos et al. [104] also recommended for optimization of fin diameter. They observed degradation in the performance of LHSU if the fin diameter was more than the optimized value. Kuboth et al. [105] came up with an idea of the uneven distribution of fins attached to the tube in a horizontal shell and tube model. They numerically analyzed the discharge power with respect to different arrangement of fins. Linear variation in fin density along the length of the tube and for a growth factor of 10 was considered. An increase in discharge power of 3% was observed. However, the reason for this increase was unclear and also the effect of uneven distribution of fins on the charging process was not discussed. Erek et al. [106] and Paria et al. [107] reported that energy stored increases with the increase in number of fins and fin radius which was observed to be insignificant after a Reynolds number of 5000.

From these works, it can be understood that the fins increase the heat transfer area leading to an increase in heat transfer rate but the fins also affect the natural convection by obstructing the flow of melted PCM which poses a negative impact on heat transfer rate.

The drawback of suppressing natural convection through annular fins can be addressed by providing perforations on the fins. Previous studies [108–110] demonstrated the advantage of perforated fins over solid fins in increasing the melting rate. Karami and Kamkari [108] provided circular perforations on the solid fins and experimentally examined the performance of LHSU. They observed that the time-averaged Nusselt number was 30% more in the case of perforated fins when compared to solid fins. Fin effectiveness of perforated fins was also found to be 13% greater than solid fins. Maji et al. [109] compared the performance of heat sink with solid pin fins and with perforated pin fins. Different shapes of the perforations such as circular, diamond, and elliptical were considered. They observed that the Nusselt number was more in case of perforated fins when compared to solid fins. Asl et al. [110] carried out numerical investigations on the effect of porous fins on the melting behavior of PCM in a rectangular enclosure. They reported that porous fins exhibited better performance at higher Rayleigh numbers. Specific to the application of perforated fins in shell and tube LHSU, [108] is the only available work. Perforations' size, shape, and number of fins also affect the LHSU's performance. Hence there is a need to further explore the performance characteristics of perforated fins.

Comparison of various types of fins

The role of various types of fins viz. longitudinal, annular and pin fins are extensively studied by numerous researchers and succeeded in achieving significant heat transfer enhancement. Though numerous studies were found on different kinds of fins, comparison among them is scarce. Agynenim et al. [111,112] in their works compared the performance of horizontal shell and tube type LHSU employing longitudinal and circular fins. Erythritol was used as PCM and the fin dimensions were chosen such that the same amount of PCM was available irrespective of the type of fin used. All the operating conditions were kept same, and they compared melting time and charged energy for a fixed duration of 8 hours. They observed that the charged energy was more for longitudinal fins. During the charged duration no complete melting was observed with circular fins. However, in the case of longitudinal fins, complete melting was observed and the rise in PCM temperature above melting temperature was also observed. Circular fins did not greatly enhance the convection and conduction heat transfer rates when compared to

longitudinal fins. Hence, they recommended longitudinal fins for a horizontal shell and tube LHSU.

On the other hand, Abdulateef et al. [113] made a comparative analysis on the performance of LHSU with longitudinal fins and annular fins. It was observed that the highest charging rate and melting rates were obtained by using annular fins. Similarly, Tay et al. [114] compared annular fins and pin fins and reported that annular fins resulted in 20-40% more effective when compared to pin fins. Hence it is proven that the annular fins are more effective for the heat transfer augmentation in LHSU.

2.3.2 Multiple PCM arrangement

To increase the heat transfer rate in a PCM based heat exchanger, one of the most efficient method is to use multiple PCMs placed layer by layer either in the direction of flow of heat transfer fluid or in the radial direction. This method was first proposed by Farid and Kanzawa in 1989 [115]. They studied the performance of the heat storage unit in which encapsulated PCMs were employed. Air was used as the heat transfer fluid which flows across the tubes containing PCMs. As the air traverse through the heat exchanger, it's temperature decreases. In order to have a uniform melting in all the capsules, it must be made to flow across the capsules containing PCMs in the order of decreasing melting temperature. When compared to a single PCM arrangement, in this type of arrangement significant reduction in the air outlet temperature was observed. Similarly, in the discharging process, the arrangement of PCMs in the increasing order of melting point temperatures yielded higher outlet air temperature. They reported an increase of 10% in heat transfer rate when multiple PCMs were used. This idea of using multiple PCMs gained the attention of the researchers when Adebiyi [116] reported that using single PCM may not be always superior to the use of sensible heat storage. Based on this conclusion, Lim et al. [117] did second law analysis to illustrate the relative merits of using multiple PCMs over single PCM. The allocation for the heat transfer area was optimized for two PCMs. Watanabe et al. [118], carried out experimental and numerical analysis of latent heat storage unit which was similar to that of the model suggested by Farid and Kanzawa [115] but the heat transfer fluid used was water. They observed a reduction in total melting time which was attributed to the constant temperature difference between water and the melting point of PCMs. Reduction in solidification time was also reported for multiple PCM arrangement. Seeniraj and Narasimhan [119] reported that multiple PCM heat exchanger gave nearly equal outlet temperature of the fluid for a very long time. The above-mentioned works

proved that the use of multiple PCMs enhances the heat transfer rate thereby reducing both melting time and freezing time.

The selection of PCMs is the most critical aspect which greatly influences the heat transfer enhancement. Numerous studies are available for choosing the suitable PCMs. Gong and Mujumdar [120] studied the influence of thermophysical properties of PCMs on energy discharge rates. They reported that lower thermal conductivity ratio (ratio of thermal conductivities of the two PCMs) and lower thermal diffusivity ratio gave more enhancement in energy discharge rate. In another work by the same authors [121], exergy analysis of the charging process for energy storage was presented. They concluded that, for a fixed inlet temperature and ambient temperature, to obtain maximum exergy output, melting points of the PCMs should be in geometric progression. In continuation to this work, they carried out exergy analysis for discharging process [122]. They re-confirmed that, to have maximum overall exergy efficiency melting temperatures of PCMs should be in geometric progression and the ratio was equal to 1.129. Ezra et al. [123] defined a new parameter called melting temperature span, which was given as the difference between the maximum melting temperature of the considered PCMs and their mean melting temperature. They optimized this value for any given number of PCMs.

From these works, it can be concluded that for the charging process the PCMs must be placed in the decreasing order of melting temperatures in the flow direction of HTF or in the radial direction and in the reverse direction for the discharging process.

2.3.3 Porous metal matrix

As mentioned earlier, the major drawback of the PCMs is their low thermal conductivity. To enhance the thermal conductivity of PCM, one of the methods is to employ PCM embedded in highly conductive porous metal foam like copper or aluminum. Various materials were proposed for the enhancement of thermal conductivity and the consolidated list taken from the literature is given in Table 2.1.

Due to the voids of the metal foam, the contact area of PCM and metal increases and hence heat transfer rate increases. But the metal matrix restricts the motion of melted PCM because of which buoyancy effect will be minimized. Hence the effect of porosity of metal matrix affects the heat transfer enhancement. Meshally et al. [124] numerically compared the time required to absorb a fixed amount of energy by using different porosities of the metal matrix. They concluded that storage response reduced with the reduction in porosity because of the

dampening of the natural convection effect. Hence, they recommended higher porosity and higher thermal conductivity metal matrix. Inline to this, Atal et al. [125] experimentally and numerically studied the effect of aluminum foam porosity on melting and solidification characteristics of paraffin wax placed in a horizontal shell and tube heat exchanger. Experiments were conducted on two types of aluminum foam having porosities of 95% and 77%. They reported that less porosity resulted in higher overall thermal conductivity and thus enhanced the heat transfer rate. Li and Wu [126] also observed similar kind of results in their numerical study in which the thermal behavior of sodium nitrate embedded in the copper matrix was studied.

Table 2.1: Various thermal conductivity enhancers used

Thermal conductivity enhancer	PCM	References
Graphite matrix	Paraffin wax	[127], [128], [129]
	Cyclohexane	[130]
	$MgCl_2$	[131]
Expanded graphite	Paraffin wax	[132], [133]
	$NaNO_3$	[134], [135]
	Binary molten salts	[136]
	Binary nitrate	[137]
	$CaCl_2.6H_2O$	[138]
Copper foam	Not available	[139]
	n-eicosane	[140]
	$NaNO_3$	[134], [135], [141]
	Paraffin wax	[142], [143], [144]
Aluminum foam	Paraffin wax	[145], [146]
	n-eicosane	[147]
	Water	[148]
High-density polyethylene	Paraffin wax	[149]
Steel alloys	$NaNo_3$	[134], [135]
β-aluminum nitride	Polyethylene glycol	[150]

Pore density which in turn is a function of pore size could also be an influencing parameter as the pore size is an essential parameter for the flow of melted PCM. By keeping porosity constant, Liu et al. [151] varied the pore density of the copper matrix and analyzed the thermal characteristics of paraffin wax. By reducing pore size from 10PPI to 30PPI, they observed an

increase in melting rate because of the increase in the contact area of PCM and metal matrix. Further reduction in pore size resulted in a substantial reduction in buoyancy effect i.e. the flow of the liquid PCM and hence melting rate reduced. Hence, it can be concluded that pore size should not be very less in order to enhance the melting rate.

By observing the melting behavior, it can be inferred that the melting rate of PCM is least at the bottom which increases vertically upwards. So, the metal foam structure should be such that the effective thermal conductivity is more at the bottom than at the top. This can be achieved by varying the porosity of the metal matrix in the vertical direction. Yang et al. [152] optimized the copper metal foam structure and numerically investigated the performance of vertical LHTES in which sodium nitrate was used as PCM. They considered linearly varying porosity of copper foam in the vertical direction. The comparison was made for the melting rates of PCM with three different cases: (i) uniform porosity, (ii) linearly increasing porosity in vertically upward direction and (iii) linearly decreasing porosity in vertically upward direction. They reported lesser melting time for the second case.

In the same way, for the horizontal configuration of shell and tube heat exchanger, it may be noted that the melting rate can be expected to be low at the bottom portion and high at the top portion. Instead of placing metal foam in the entire shell, placing the metal foam in the bottom half can extract the advantages of both enhanced thermal conductivity at the bottom and natural convection at the top. Xu et al. [153] studied the effect of partially filled metal foam in a horizontal shell and tube heat exchanger. Based on their study they concluded that filling metal foam in the entire cross-section of the shell did not greatly enhance the melting rate when compared with the case of half-filled metal foam at the bottom portion. Partial filling also aids in material saving and hence reduction in cost.

2.3.4 Dispersion of nano particles

Dispersing nanoparticles into the liquid enhances the thermal properties of liquid [154] and this new class of liquids with enhanced thermal properties are coined as nanofluids by Choi [155]. Nanofluids are being used in numerous applications for the enhancement of heat transfer. Similarly, adding nanoparticles to PCM can be treated as a considerable option to enhance its thermal conductivity. Khodadadi and Hosseinizadeh [156] documented the potential for the improvement in latent heat storage by nanoparticle dispersion in PCMs. These kinds of PCMs

are termed as Nanoparticle enhanced phase change materials (NEPCM). Several nanoparticles were dispersed in various PCMs and the consolidated list is provided in Table 2.2.

Table 2.2: Nanoparticle – PCM combinations for thermal conductivity enhancement

Dispersed nanoparticles	PCM	References
Single wall carbon nanotubes	Wax	[157]
Multi wall carbon nanotubes	Paraffin wax	[157],[158],[159],[160],[161]
	Palmitic acid	[162], [163], [164]
	Stearic acid	[165]
Carbon nanofibers	Wax	[157], [166], [167]
Graphite	Paraffin wax	[160]
	Stearic acid	[168]
Graphene platelets	Stearic acid	[168]
	Paraffin wax	[166],[161]
	Lauric acid	[169]
	Eicosane	[170]
	Hexadecanol	[171]
Aluminium powder	Paraffin wax	[172]
Al_2O_3	Paraffin wax	[173]
TiO_2	n-octadecane	[174]
Copper nanowires	Tetradecanol	[175]
Silver nanowires	Tetradecanol	[176]

NEPCMs have the advantage of enhanced thermal conductivity and hence melting and solidification rates of PCM increase. Xiao and Zhang [177] reported a reduction of 40.6% in the melting time by using paraffin/ 10 wt% EG composite in a vertical tube heat exchanger. Similarly, Das et al. [178] also observed a reduction in melting time of 41% when 2 vol% graphene was dispersed in n-eicosane.

By increasing the concentration of nanoparticles, thermal conductivity can be further improved. However, this addition increases the viscosity of the PCM which suppresses the natural convection phenomenon. Paraszadeh and Duan [179] numerically studied the thermal performance of paraffin-CuO NEPCM in a vertical shell and tube heat exchanger. They observed that the melting rate reduced for a nanoparticle concentration of over 4 vol%. It was

mentioned that the reduction in buoyancy effect overshadowed the enhancement in thermal conductivity.

2.3.5 Geometric modifications to shell or tube cross-sections

As mentioned earlier, the melting of PCM is mainly affected by natural convection. Based on this fact, many researchers have tried different shapes of shell and tube which can augment the convection currents thereby reducing the melting time. Fomin et al. [180] developed a mathematical model for contact melting in a horizontal elliptic cylinder. They reported that the elliptical cylinder requires lesser melting time when compared to a circular one. Even though this work was not a straightforward application for a PCM based heat exchanger, the optimization of the shape of the cylinder seemed to be a viable option to reduce the melting time. Alawadhi [181] reported that the solidification time can be reduced by using an elliptical tube and also observed that the aspect ratio of ellipse influences the solidification time. These two works proved that the shape of the cylinder is an important factor to arrive at the minimum melting and solidification times.

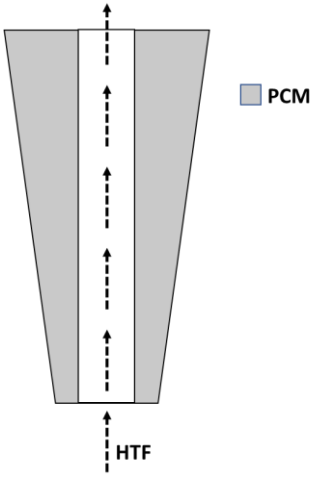

Figure 2.1: Vertical conical shell [182]

Akgun et al. [182] observed that in a vertical shell and tube heat exchanger, the melt region of PCM at intermediate stage was in conical shape. Hence, they suggested vertical conical shell model to enhance the heat transfer rate. They provided an inclination of 5° to the outer shell as shown in Fig. 2.1. They reported that conical shell requires less melting time with 20% reduction in melting time.

Hu et al. [183] considered frustum shaped tube and they investigated the effect of length ratio which is the ratio of top radius of the shell to bottom radius of the shell on melting time of

PCM. They found that for a length ratio of 5, the reduction in melting time was 33.1%. Further increase in length ratio did not affect the melting time. Hence, the optimized length ratio was taken as 5. Korawan et al. [184] proposed two models for the tubes namely nozzle-and-shell (same as frustum tube) and reducer-and-shell models and are shown in Fig. 2.2. Paraffin wax was taken as PCM. As the melt region expands from bottom to top of a truncated cone one can expect faster melting in nozzle-and-shell model and the same was reported by [184]. They also reported slower melting rate in reducer and shell model when compared to conventional shell and tube heat exchanger. In another work by the same authors [185], the design of the nozzle-and-shell model was modified slightly and named it as combined-and-shell model. Due to stronger convection, the higher melting rate was reported for combined-and-shell model when compared to the shell-and-tube model. However, comparison with nozzle-and-shell was not discussed.

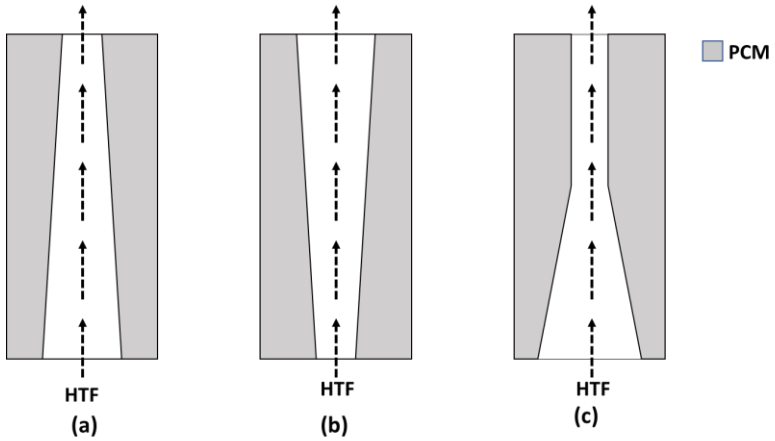

Figure 2.2: Proposed models (a) Nozzle-and-shell [184] (b) Reducer-and-shell [184] (c) Combined-and-shell [185]

Darzi et al. [186] numerically investigated the melting and solidification behavior of N-eicosane for various horizontal configurations of annulus such as concentric circular tube, vertically oriented elliptical tube, and horizontally oriented elliptical tube. Further, they investigated the effect of aspect ratio of the tube. As far as melting is considered vertically oriented elliptical tube with high aspect ratio gave lesser melting time, whereas for solidification elliptical tube was not efficient irrespective of orientation. Faghani et al. [187] considered 9 different configurations as shown in Fig. 2.3 resulting from the combination of elliptical and circular shapes. From Fig. 2.3, it may be noted that these shapes were employed for both the inner tube and the shell. Out of all the configurations, horizontally oriented elliptical annulus and vertically oriented elliptical tube combination (case g) gave the least

melting time. So, it is noteworthy to mention that both the shell and tube shapes are to be chosen carefully to obtain maximum melting rate.

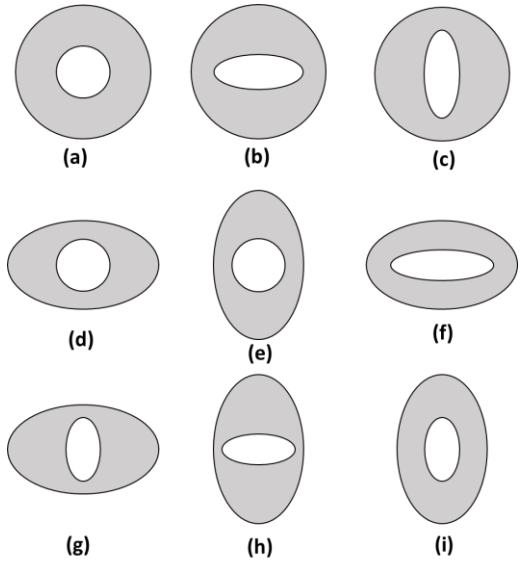

Figure 2.3: Different configurations for horizontal shell and tube heat exchanger [187]

2.4 Mathematical formulations

During the phase change phenomenon, the most critical part is to track the interface between solid and liquid as a function of time and space. Properties vary considerably between phases, which results in totally different rates of momentum and energy transport from one phase to another because of which mathematical modelling of this phenomenon becomes complex. As the boundary or the interface moves with respect to time, these kinds of problems are termed as moving boundary problems.

In the olden days, analytical methods with appropriate assumptions were the only means to understand and analyze the moving boundary phenomenon. Analytical methods offer exact solutions and are mathematically elegant. However, analytical methods are limited to simple initial and boundary conditions and mostly applicable to 1D or 2D cases. With the advent of higher computing facilities, numerical analysis gained a lot of interest which is capable of simulating moving boundary phenomenon in 3D and with any complex boundary conditions. In this section, various analytical and numerical models proposed for the analysis of phase change in PCM based heat exchangers are discussed.

2.4.1 Analytical models

In all the analytical models, conduction is assumed to be the only heat transfer mechanism in both the phases. Pioneering work in this regard was done by Stefan [188,189] is given below.

Stefan Problem

Stefan problem is the simplest one in which the problem is considered as one phase and convection in liquid phase is neglected. Here one phase designates that only one phase (liquid) is being active in the transformation while the other one (solid) is at its melting temperature. At the interface, by the conservation of energy, net heat transfer from solid and liquid phases will be equal to change in internal energy which in turn will be equal to latent heat release as represented by Eq. 2.7

$$k_s \frac{\partial T}{\partial x}\Big|_s - k_l \frac{\partial T}{\partial x}\Big|_l = \rho L u \tag{2.7}$$

This is known as Stefan condition. On non-dimensionalizing the above equation with appropriate scales, non-dimensional form of Stefan condition will be obtained as Eq. 2.8

$$\frac{\partial \Theta}{\partial \eta}\Big|_s - \frac{k_l}{k_s}\frac{\partial \Theta}{\partial \eta}\Big|_l = \frac{1}{St}\frac{d\delta}{d\tau} \tag{2.8}$$

Where 'St' is known as Stefan number and is given by $St = \frac{C_l\ \Delta T}{L}$

Here 'C_l' is the heat capacity of liquid PCM, L is latent heat and ΔT is the difference between surrounding temperature and melting temperature.

As mentioned earlier, Stefan's solution is applicable only to single phase which is impractical. Moreover, it assumes single moving boundary but there is a possibility of more than one interface locations [190]. In addition to this, interface location will be non-linear and along with conduction convection also should be considered. To address these issues, non-linearity in governing equations is introduced and the solution to these equations can be obtained for a very few scenarios [191].

Neumann's method

Neumann extended Stefan's solution to two phase scenario by solving non-linear governing equations using similarity approach [192]. The initial state of PCM was assumed to be solid which is at a temperature below its melting point ($T_s < T_m$) and the melting temperature is not a constant value. If melting is occurring in a semi-infinite slab ($0 < x < \infty$), a constant temperature is imposed on the face i.e. $x = 0$. By assuming constant thermo physical properties of PCM, the problem can be written mathematically as:

Heat conduction in solid or liquid region

$$\frac{\partial T}{\partial t} = \alpha \frac{\partial^2 T}{\partial x^2} \quad for\ 0 < x < \delta(t),\ \ t > 0 \tag{2.9}$$

Here 'α' is thermal diffusivity, 't' is time, 'x' is spatial coordinate and '$\delta(t)$' is the position of interface.

At the interface ($T(x = \delta(t), t > 0) = T_m$), Stefan condition should be imposed to track the interface

$$k_s \frac{\partial T}{\partial x}\Big|_s - k_l \frac{\partial T}{\partial x}\Big|_l = \rho L \frac{dx}{dt} \tag{2.10}$$

Initial condition is:

$$T(x > 0, t = 0) = T_s < T_m \tag{2.11}$$

Boundary conditions are:

$$T(x = 0, t) = T_l \tag{2.12}$$

$$T(x \to \infty, t) = T_s \tag{2.13}$$

Position of the interface and temperature with respect to time are the two variables to be solved, by using similarity approach two variables are clubbed into a single variable parameter known as similarity variable and is taken as $\eta = \delta(t)/2\sqrt{\alpha_l}$. The final solution can be written as

$$\delta(t) = 2\lambda\sqrt{\alpha_l t} \tag{2.14}$$

Temperature in liquid region:

$$T(x,t) = T_l - (T_l - T_m)\frac{erf\left(x/2\sqrt{\alpha_l t}\right)}{erf\ \lambda} \tag{2.15}$$

Temperature in solid region:

$$T(x,t) = T_s + (T_m - T_s)\frac{erf\left(x/2\sqrt{\alpha_l t}\right)}{erfc\left(\lambda\sqrt{\alpha_l/\alpha_s}\right)} \tag{2.16}$$

λ can be obtained by solving the equation

$$\frac{St_l}{exp(\lambda^2)\text{erf}\,(\lambda)} - \frac{St_s\sqrt{\alpha_s}}{\sqrt{\alpha_l}\exp(\alpha_l\lambda^2/\alpha_s)\,erfc\left(\lambda\sqrt{\alpha_l/\alpha_s}\right)} = \lambda\sqrt{\pi} \tag{2.17}$$

Where $St_l = \frac{C_l(T_l - T_m)}{L}$, $St_s = \frac{C_s(T_m - T_s)}{L}$

However, this solution is applicable to only rectangular domains (cartesian co-ordinate system) which is of rare practical relevance.

Heat balance integral method

Based on Karmann-Pohlhausen's method of the momentum integral in the boundary layer theory, Goodman developed an integral equation. This equation expresses the overall heat balance of the system by integrating the one-dimensional heat conduction with respect to the spatial variable. By assuming temperature distribution with respect to space variable, temporal temperature variation can be obtained. Proper assumption of the space wise temperature is almost impossible and hence application of this method to PCM based heat exchanger was not found in the literature.

2.4.2 Numerical models neglecting natural convection

In these methods, the energy equation is solved in each phase by finite difference or finite element method either by using fixed grid or adaptive grid. In fixed grid method, the grid is fixed, and interface is located between any two grid points. Interface is tracked by using suitable interpolation as a part of formulation. In adaptive grid method, the grid can be either interface fitting or dynamic. In interface fitting grids, a variable time step is used such that the interface coincides with the grid. But in dynamic grid, spatial intervals of the grid are adjusted so as to match the grid with the interface.

Two approaches are available for numerical modelling of phase change process namely, multi domain approach and single field approach. In multi domain approach, energy equation is written separately for liquid and solid phases and temperatures are coupled through interface energy balance. This gives rise to tracking the interface explicitly. Due to time dependent interface position multi domain approach requires continuous update of two domains. Alternative to this approach is incorporating latent heat effects (at the interface) in the governing equations implicitly gives rise to new form of equations which can be applied to entire domain. This approach is known as single field approach. The methods pertaining to single field approach are discussed in the following section.

Apparent heat capacity method

This method was first proposed by Hashemi and Sliepcevich in 1967. In this method, the latent heat is accounted by the increase in heat capacity of the PCM in the phase change temperature range. The apparent heat capacity is defined as

$$C_{app} = \begin{cases} C_s & T < T_s \\ C_{in} & T_s \leq T \leq T_l \\ C_l & T > T_l \end{cases} \quad (2.18)$$

Where $C_{in} = \frac{\int_{T_s}^{T_l} C(T)dT + L}{(T_l - T_s)}$

The energy equation can be written in terms of effective heat capacity in one dimension as

$$\rho C_{eff} \frac{\partial T}{\partial t} = \frac{\partial}{\partial x}\left(k \frac{\partial T}{\partial x}\right) \quad (2.19)$$

This equation can be discretized and solved numerically. Apparent heat capacity can be obtained explicitly or implicitly. The absorption or release of latent heat will not be accounted if a node temperature raises from solidus to liquidus temperature in single time step. Similarly, in case of isothermal phase change, an artificial phase change temperature should be assumed to incorporate latent heat effects. This leads to errors in solution. In order to eliminate the need of assuming artificial phase change, effective heat capacity method is proposed.

Effective heat capacity method

This method is an improvement of the apparent heat capacity method proposed by Poirier and Salcudean [193]. In this method, a temperature profile is assumed between the nodes and effective heat capacity is calculated through integration over control volume rather than in terms of nodal temperatures like in the case of the apparent heat capacity method. By evaluating effective heat capacity at each time step, the method correctly accounts for latent heat effect and the solution is independent of artificial phase change temperature range.

Enthalpy based method

The interface boundary condition is incorporated in the energy equation by establishing a relation between enthalpy and temperature. This method is capable of solving both isothermal and non-isothermal phase change.

The relationship between enthalpy and temperature can be defined in terms of latent heat characteristics of the PCM. The relationship is assumed to be a step function for isothermal phase change and a linear function for non-isothermal phase change. Pertaining to this method the following relations can be given.

For isothermal phase change

$$h = \begin{cases} C_s T & T \leq T_m \quad solid\ phase \\ C_l T + L & T > T_m \quad liquid\ phase \end{cases} \tag{2.20}$$

For non-isothermal phase change

$$h = \begin{cases} C_s T & T < T_s & solid\ phase \\ C_{in} T + \dfrac{L(T - T_s)}{(T_l - T_s)} & T_s \leq T \leq T_l & mushy\ zone \\ C_l T + L + C_{in}(T_l - T_s) & T > T_l & liquid\ phase \end{cases} \tag{2.21}$$

Energy equation can be written as

$$\rho \frac{\partial h}{\partial t} = \frac{\partial}{\partial x}\left(k \frac{\partial T}{\partial x}\right) \tag{2.22}$$

The above equation can be solved numerically to get temperature evolution.

2.4.3 Numerical models including effect of natural convection

All the above discussed models neglected the effect of natural convection. But Sparrow et al. [194] reported that convection could not be ignored in the analysis of the phase change phenomenon of a PCM. Yao and Chen [195] and Buddhi et al. [196] emphasized on including natural convection effects in the melting of PCM. Hasan [74], Lacroix [197] also reported that conduction alone will not describe the phase change process correctly. Hence, the mathematical formulation should also consider natural convection. Several methods are introduced for modelling phase change by considering convection effects. The most popular method is Enthalpy-Porosity method which will be discussed in the following section.

Enthalpy porosity model

As explained earlier, the enthalpy method is based on single field formulation. So, there is no need to track the boundary explicitly. But source terms have to be introduced in governing equations for accounting interfacial effects. While using fixed grids, one need to take care about the velocity as velocity boils down to zero as phase changes from liquid to solid. Different schemes are proposed to dampen the velocity in the cells of solid phase. Brent et al.[198] treated the mushy zone as a porous medium where Carman-Kozeny law applies. Gartling [199] assumed that the mushy zone is a non-Newtonian fluid with the viscosity as a function of the cell latent heat. IIegbusi and Mat [200] proposed a hybrid model by treating the mushy zone as semi-solid slurry and porous medium, which are determined by solid fraction.

Governing equations used in the enthalpy-porosity approach are:

Conservation of mass

$$\frac{\partial \rho}{\partial t} + \vec{\nabla}.\left(\rho \vec{V}\right) = 0 \tag{2.23}$$

x-momentum equation

$$\frac{\partial (\rho u)}{\partial t} + \vec{\nabla}.\left(\rho u \vec{V}\right) = \vec{\nabla}.\left(\mu \vec{\nabla} u\right) - \frac{\partial p}{\partial x} + Au \tag{2.24}$$

y-momentum equation

$$\frac{\partial (\rho v)}{\partial t} + \vec{\nabla}.\left(\rho v \vec{V}\right) = \vec{\nabla}.\left(\mu \vec{\nabla} v\right) - \frac{\partial p}{\partial y} + Av + S_b \tag{2.25}$$

Energy equation

$$\frac{\partial (\rho h)}{\partial t} + \vec{\nabla}.\left(\rho h \vec{V}\right) = \vec{\nabla}.\left(\frac{k}{C} \vec{\nabla} h\right) + S_h \tag{2.26}$$

By using Boussinesq approximation, natural convection effects can be accounted for on defining the buoyancy source term can be given as

$$S_b = \rho_{ref}\, \beta\, \Delta T \tag{2.27}$$

Source term in energy equation is defined as

$$S_h = \frac{\partial (\rho \Delta h)}{\partial t} + \vec{\nabla}.\left(\rho \vec{\nabla} \Delta h\right) \tag{2.28}$$

Here, latent heat content 'Δh' is defined as a function of temperature ($\Delta h = f(T)$). In the isothermal phase change $\vec{\nabla}.\left(\rho \vec{\nabla} \Delta h\right)$ vanishes. $f(T)$ is defined as follows

For isothermal phase change

$$f(T) = \begin{cases} L & T \geq T_m \\ 0 & T < T_m \end{cases} \tag{2.29}$$

For non-isothermal phase change

$$f(T) = \begin{cases} 0 & T < T_s \\ \dfrac{L(T - T_s)}{(T_l - T_s)} & T_s \leq T \leq T_l \\ L & T > T_l \end{cases} \tag{2.30}$$

The condition that the velocities in solid phase equal to zero is accounted by appropriate definition of A in the momentum equations. The basic principle is to gradually reduce the velocities from a finite value in the liquid phase to zero in solid phase over the computational

cells that are changing phase. This can be achieved by assuming the phase change cells behave as porous media with porosity ϵ which is equal to liquid fraction in that cell. A is defined such that the momentum equations are forced to mimic the Carman-Kozeny equations for flow in porous media and is given by

$$A = -C\frac{(1-\epsilon)^2}{\epsilon^3 + b} \tag{2.31}$$

Here, 'C' is a constant accounting for the mushy region which controls the penetration of the convection field into the mushy region and 'b' is a computational constant introduced to avoid the division by zero. Mushy zone constant 'C' needs to be carefully chosen as it influences the thermo-hydraulics of PCM [201], however, most of the studies used mushy zone constant value equal to 10^5 [202].

Effective thermal conductivity model

This model is a very simplified model which follows the philosophy of effective thermal conductivity by replacing the liquid PCM thermal conductivity in energy equation to include the effects of natural convection. This approach was proposed by Farid and Mohamed [203] for planar geometries and extended to cylindrical geometries by Farid et al. [204]. To incorporate the effect of natural convection the following correlation for effective thermal conductivity was given

$$\frac{k_{eff}}{k_l} = c\ Ra^n(^{\delta}/_{l}) \tag{2.32}$$

'k_{eff}'represents effective thermal conductivity, 'Ra' is Rayleigh number, 'δ' is thickness of the melted PCM and 'l' is length of the cylinder. Constants 'c' and 'n' depends on the geometry of LHSU.

2.4.4 Effectiveness NTU method

ε- NTU method is a well established method to characterize the conventional heat exchangers. It is extended to LHSU which helps in optimizing the design of heat exchanger without the need of cumbersome and tedious calculations. This method was first proposed by Belusko and Bruno [205] for the storage system with parallel plates, later it was extended to tube in tank LHSU by Tay et al. [206]. By using this method, it is not needed to solve for temporal evolution of interface and temperature to obtain performance of the heat exchanger. However, this method also associated with the major limitation of omitting the natural convection effect.

Other assumptions include one dimensional heat flow which is justified by the uniform phase change of the PCM, constant thermo physical properties of PCM and constant inlet velocity and inlet temperature.

Effectiveness and NTU in this case also have their usual definitions, as phase change is the point of interest it corresponds to the case of infinite sensible specific heat and effectiveness is represented in terms of NTU as

$$\varepsilon = 1 - \exp(-NTU) \tag{2.33}$$

NTU is given by the equation

$$NTU = \frac{UA}{\dot{m}c_p} = \frac{1}{R_T \dot{m} c_p} \tag{2.34}$$

Where 'U' is overall heat transfer co-efficient, '$\dot{m}$' is mass flow rate of HTF and 'c_p' is specific heat of HTF. 'R_T' is the total thermal resistance to the heat flow and is calculated by a simple thermal circuit as

$$R_T = R_{HTF} + R_{wall} + R_{PCM}$$

$$R_T = \frac{1}{2\pi r_i L h_f} + \frac{\ln(\frac{r_o}{r_i})}{2\pi k_{wall} L} + \frac{\ln(\frac{r}{r_o})}{2\pi k_{PCM} L} \tag{2.35}$$

Subscripts 'i, o' represents the inner and outer surfaces of the tube. 'L' is the length of the unit, 'k' is thermal conductivity and 'r' is the instantaneous radius of melting front which varies with time. Instead of representing 'r' as a time-dependent variable, it is written in terms of melt fraction (MF) which is given by

$$MF = \frac{A_r - A_o}{A_{max} - A_o} = \frac{r^2 - r_o^2}{r_{max}^2 - r_o^2}$$

$$\Rightarrow r = [M.F(r_{max}^2 - r_o^2) + r_o^2]^{0.5} \tag{2.36}$$

Here, 'r_{max}' represents radius of the shell. For obtaining heat transfer co-efficient appropriate correlations may be used. As the melt fraction changes over time, effectiveness also changes, and hence average effectiveness is calculated by

$$\bar{\varepsilon} = \int_0^1 \varepsilon \, d(M.F) \tag{2.37}$$

Integration can be performed numerically by taking appropriate melt fraction interval.

2.5 Observations from literature review

- There are several operating and design parameters that influence the thermal performance of shell and tube latent heat storage unit. The influence of inlet temperature, mass flow rate of HTF and shell to tube diameter ratio is extensively studied by the researchers.
- Inlet temperature of HTF is the major influencing factor on the melting/solidification time. As the inlet temperature of HTF depends on the available solar intensity and the efficiency of the solar collector, one cannot have any control over this parameter. Hence in the present study, the experiments are conducted at a constant inlet HTF temperature.
- Mass flow rate of HTF is not significant if the flow is in the turbulent regime. And various authors suggested that the flow should be in the laminar regime. Hence in the current research work, the flow rate is chosen such that it is in laminar regime.
- Various techniques are available for heat transfer intensification, each method has its own advantages and disadvantages. Majority of the works on multiple PCM arrangements employed numerical investigations and it may not be practically possible to have PCMs with optimized melting temperature values. Embedding the metal foam increases the weight and cost of LHSU, moreover the thermophysical properties of PCM when embedded in metal foam may get deteriorated. Similarly, nano enhanced PCMs' thermal stability needs a proper investigation. On the other hand, employing fins is very efficient and easy to fabricate. Hence for the current research work, fins are chosen for augmentation in heat transfer rate.

2.6 Research gaps

- Though the influence of various operating and design parameters on the melting characteristics of PCMs are vast, non-dimensional parametric analysis are scarce. Non dimensional analysis is must as the results corresponding to a particular PCM cannot be presumed for all the PCMs.

- A reliable correlation for total melting time in terms of all the influential parameters is not available which will be very much handy in deciding various design and operating parameters.
- Effect of inclination on the thermal performance of LHSU needs further investigation as the existing studies contradicting each other's results.
- Studies pertaining to the influence of orientation of finned LHSU on its performance are very few and no study is available on the effect of inclination when annular perforated fins are employed.
- Providing perforations for annular fins enhances the thermal performance of LHSU but very few studies are available in the literature in this regard.
- Exergetic performance should also be considered while optimizing the fin parameters, but the existing studies pertaining to optimization of fin parameters did not account entropy generation.
- Combination of active and passive heat transfer enhancement techniques are not properly investigated.

2.7 Objectives

Based on the above-mentioned research gaps, the following objectives are formulated.

1. To carry out non-dimensional parametric analysis on the melting characteristics of PCM and to develop a correlation for total melting time.
2. To carry out energy and exergy analyses of a shell and tube latent heat storage unit positioned at different orientations.
3. To employ solid and perforated annular fins for heat transfer intensification and to analyze the effect of orientation on the thermal performance of LHSU.
4. To optimize the fin parameters for attaining an energy and exergetically efficient LHSU.
5. To investigate the performance of the frustum shaped shell and tube heat storage unit and optimize the fin parameters to achieve a minimum total cycle time.

On the whole, the current research work is intended for the analysis and optimization of different parameters to maximize the thermal performance of a shell and tube latent storage unit.

2.8 Closure

A thorough literature survey pertaining to the influence of various parameters on the thermal performance of a shell and tube latent heat storage unit is provided. Various heat transfer augmentation techniques are explored and employing fins is the least expensive, reliable and no fabrication complexity is involved. By thoroughly identifying the research gaps, objectives for the current research work were framed. To achieve the proposed objectives both experimental and numerical experiments are needed, the details of which are discussed in the next chapter.

Chapter 3

Experimental setup and numerical methodology

In the previous chapter, numerous works pertaining to shell and tube latent heat storage unit were discussed and depending on the research gaps various objectives were framed. To accomplish these objectives an experimental test facility was designed and fabricated. Along with the experimental work, numerical simulations are also carried out for scrupulous analysis of the phase change behavior of the PCM. The details of the experimental setup and the numerical methodology adopted for the simulations are discussed in the current chapter. The methodology adopted for evaluating various performance parameters from the experimentally measured temperature values is also provided in this chapter.

3.1 Experimental setup

An experimental setup is designed and fabricated as shown in Fig. 3.1 to accomplish the objectives. To supply the heat transfer fluid at the desired temperature a hot water bath for charging and a cold water bath for the discharging process are equipped with PID controllers. To control the flow rate of water, needle valves are provided, and the flow rate is monitored by a turbine type digital flow meter. To facilitate the LHSU to be placed at different orientations, a tilt table is designed with which the LHSU can be positioned at any desired inclination. Heat transfer fluid is supplied to LHSU by pumping the water with a pump. The tube is made up of SS (stainless steel) and has an inner diameter of 16mm and a thickness of 1.5mm. Shell has an inner diameter of 100mm and is made of polycarbonate which facilitates the visualization of melting and solidification fronts. An added advantage of polycarbonate is that it has a very low thermal conductivity which results in minimal heat loss. To ensure minimum heat loss sufficient thickness of 5mm is provided for the shell wall. Hence the heat loss from the shell wall will be very less and can be neglected. The annular space of the shell and tube is filled with 1670 grams of lauric acid. The combination of lauric acid and SS is chosen because they do not undergo any type of corrosion [207,208]. K-type thermocouples are inserted in the PCM region at various locations to observe the temperature evolution of the PCM. Another two thermocouples are provided at the inlet and outlet of HTF. All these thermocouples are connected to “Keysight-34972A” data acquisition unit by which temperature can be recorded

at regular time intervals. The details regarding the location of the thermocouples are provided in the respective chapters.

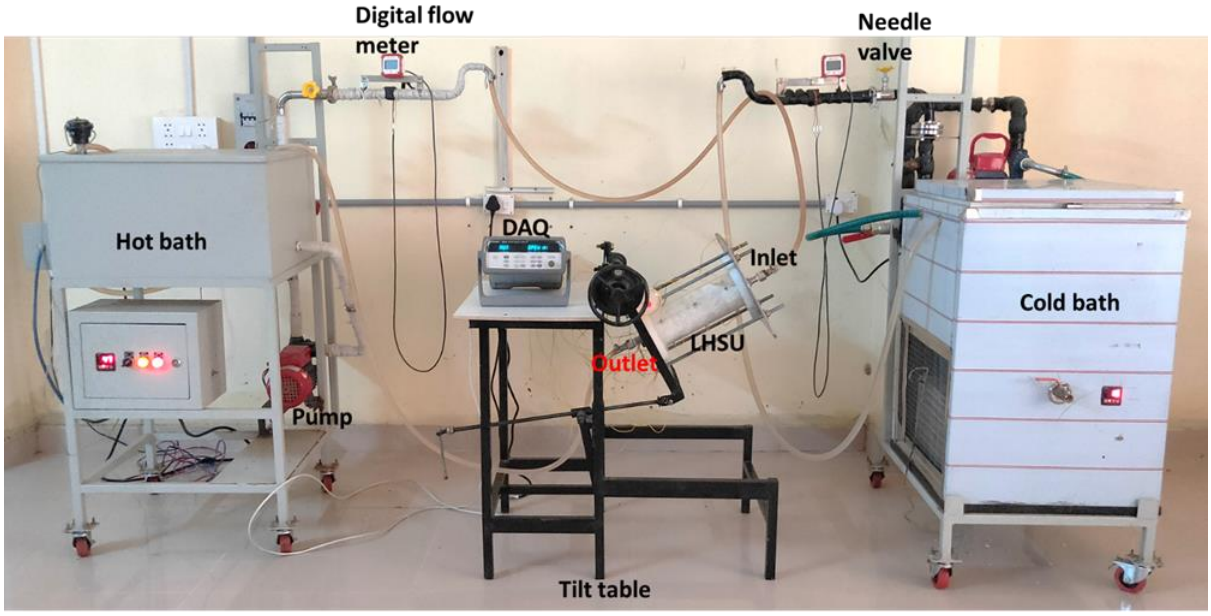

Figure 3.1: Photograph of the experimental test facility

3.2 Data reduction

From the recorded temperature data various other performance parameters are deduced. To calculate the average temperature, melt fraction, and energy stored/discharged weighing method proposed by Seddegh et al. [44] is adapted. Following this method, control volumes are created and weighing factor of a certain thermocouple is given by the ratio of surrounding control volume of that thermocouple and total volume of LHSU ($w_i = V_i/V_t$). Average temperature and melt fraction are given by Eqs. 3.1 & 3.2 respectively.

$$T_{PCM} = \sum w_i T_i \tag{3.1}$$

$$c = \sum w_i c_i \tag{3.2}$$

c_i is the melt fraction of ith thermocouple which is calculated as a function of temperature which is given by the following equation.

$$c_i = \begin{cases} 0 & T_i < T_s \\ \dfrac{T_i - T_s}{T_l - T_s} & T_s \le T_i \le T_l \\ 1 & T_i > T_l \end{cases} \tag{3.3}$$

Energy stored can also be calculated as a function of temperature and is given by Eq. 3.4. If the temperature is less than "T_s" the PCM experiences sensible heat gain alone, from solidus to liquidus temperature PCM takes the latent heat and above liquidus temperature again sensible heat gain will take place.

$$E_{st_i} = \begin{cases} mc_{p_s}(T_i - T_{ini}) & T_i < T_s \\ mc_{p_s}(T_s - T_{ini}) + mc_i L & T_s \le T_i \le T_l \\ mc_{p_s}(T_s - T_{ini}) + mL + mc_{p_l}(T_i - T_l) & T_i > T_l \end{cases} \tag{3.4}$$

Average energy stored is given by the following equation.

$$E_{st} = \sum w_i E_{st_i} \tag{3.5}$$

For the discharging process, energy discharged can be calculated as follows

$$E_{dis_i} = \begin{cases} mc_{p_l}(T_{ini} - T_i) & T_i > T_l \\ mc_{p_l}(T_{ini} - T_l) + mc_i L & T_s \le T_i \le T_l \\ mc_{p_l}(T_{ini} - T_l) + mL + mc_{p_s}(T_s - T_i) & T_i < T_s \end{cases} \tag{3.6}$$

Energy efficiency is defined as the ratio of energy stored to energy supplied by the HTF for the melting process and for the discharging process it is the ratio of energy retrieved by HTF to energy discharged by the PCM. The supplied energy can be calculated using Eq. 3.7. It is to be noted that in the solidification process this will be equal to energy retrieved by the HTF.

$$E_{in} = \int_0^{t_1} \dot{q}\ dt + \int_{t_1}^{t_2} \dot{q}\ dt + \int_{t_2}^{t_3} \dot{q}\ dt + \cdots \tag{3.7}$$

Where $\dot{q} = \dot{m}c_{p_{HTF}}(T_{in} - T_{out})$

Exergy efficiency is also defined similarly to energy efficiency which is equal to the ratio of exergy stored and exergy input whose definitions are given in Eqs. 3.8 & 3.9 respectively.

$$Ex_{st} = E_{st}\left[1 - \frac{T_o}{T_{PCM}}\right] \tag{3.8}$$

$$E\dot{x}_{in} = \dot{m_{HTF}} c_{p_{HTF}} \left[(T_{in} - T_{out}) - T_o \ln\left(\frac{T_{in}}{T_{out}}\right) \right] \quad (3.9)$$

Where T_o is the ambient temperature.

3.3 Numerical methodology

To get more insight into the PCM flow behavior and to obtain parameters like melt fraction and PCM average temperature, transient simulations are carried out. A finite volume based CFD tool Ansys-Fluent is used to carry out the numerical simulations. As discussed in the previous chapter, various formulations are available for the phase changing process of PCM. Out of all the methods, the enthalpy porosity technique is capable of solving phase change phenomenon accurately by including the effects of natural convection. Hence, the enthalpy porosity technique is employed for the simulation of PCM melting. The following assumptions are made to the above-mentioned physical model to simplify the analysis

- PCM in both the phases (solid and liquid) is considered homogeneous and isotropic
- Boussinesq approximation is considered to be valid for the density variation of the liquid PCM
- The flow of HTF is considered to be laminar
- Viscous dissipation effects are neglected
- Volume change when melting takes place is neglected

With these assumptions, the governing equations can be written as follows [96].

$$\nabla . \vec{V} = 0 \quad (3.10)$$

$$\rho \frac{\partial \vec{V}}{\partial t} + \rho\left(\nabla . \vec{V}\vec{V}\right) = -\nabla P + \mu \nabla^2 \vec{V} + \rho \vec{g} \beta \Delta T + A\vec{V} \quad (3.11)$$

$$\rho \frac{\partial h}{\partial t} + \rho\left(\nabla . \vec{V} h\right) = \frac{k}{c_p} \nabla^2 h + S_h \quad (3.12)$$

In the momentum equation (Eq. 3.11) “A” is defined such that the equation mimics the flow equation in porous media and is given below

$$A = -C \frac{(1-\epsilon)^2}{\epsilon^3 + b} \quad (3.13)$$

Here, "C" is mushy zone constant which influences the thermohydraulics of PCM [201] and should be carefully chosen. Most of the studies in the literature corresponding to numerical simulation of melting of PCM have taken the value of "C" as 10^5 kg/m^{3}s [209–218] and hence same is considered for the current study. "b" is a computational constant which is defined to avoid the division by zero. "ϵ" is porosity which is considered to be equal to the liquid fraction in the corresponding control volume.

The source term "S_h" in the energy equation (Eq. 3.12) is defined as follows

$$S_h = \frac{\partial(\rho \Delta h)}{\partial t} + \vec{\nabla}.(\rho \vec{V} \Delta h) \tag{3.14}$$

The first term in the above equation does not appear if phase change occurs isothermally and "Δh" is defined as given below.

$$\Delta h = \begin{cases} 0 & T < T_s \\ \dfrac{L(T - T_s)}{(T_l - T_s)} & T_s \leq T \leq T_l \\ L & T > T_l \end{cases} \tag{3.15}$$

SIMPLE algorithm is employed for pressure-velocity coupling. PRESTO scheme is used for the discretization of pressure, whereas the second-order upwind scheme is used for the discretization of momentum and energy equations. To ensure the exactness of the results, convergence criteria of 10^{-6} is set for momentum equations and 10^{-8} for energy equation. The simulations are carried out on a Workstation of 64GB RAM and 16 core CPU.

Chapter 4

Parametric investigation to assess the melt fraction and melting time for a PCM based vertical shell and tube latent heat storage unit

4.1 Introduction

The study pertaining to the influence of various design and operating parameters on the melting characteristics of a PCM is necessary for the understanding of thermal hydraulics. While designing a latent heat thermal storage system it is essential to analyze the effect of various parameters to arrive at the optimum melting time. Even though countless efforts have been devoted by the researchers on investigating the melting characteristics of PCM, a reliable correlation for the total melting time which can be applied in a wide range of parameters is not available. Moreover, the analysis should be in terms of non-dimensional parameters without which the insight of thermal transport cannot be presumed for different PCMs and different tube materials. A reliable correlation for total melting time will be very handy in deciding various parameters of LHSU. High non-linearity in the melt fraction evolution and dependency on a large number of parameters makes it difficult to develop correlation. Hence, the present work is aimed at developing correlations for melt fraction and total non-dimensional melting time by carrying out parametric investigation using numerical simulations. Enthalpy-porosity approach is adapted to discretize the governing equations and Boussinesq approximation is used to include the effect of natural convection. The parametric analysis has been carried out in terms of non-dimensional parameters such as Stefan number (0.2-0.6), Rayleigh number (2.04×10^5-2.32×10^6), Reynolds number (500-2000), L/D ratio (1-10), thermal diffusivity ratio (45.29-1500), and tube thickness to diameter ratio (0.036-0.113). A correlation is developed to determine the melt fraction evolution. Another correlation is developed to estimate the total melting time which will be useful in selecting various design and operating parameters while designing a shell and tube thermal storage unit.

4.2 Physical model

Longeon et al. [219] in their experimental analysis of annular PCM storage system compared the temperature evolution of PCM at various angular positions. They obtained similar curves

for all the angular positions, which indicates that the system can be modeled as a 2D axisymmetric domain. Based on this conclusion, a 2D axisymmetric domain is considered for the numerical simulations in the present study. Fig. 4.1 shows the physical model of the heat exchanger used for numerical investigations. It is composed of an inner tube for the flow of HTF and shell with the insulated outer wall. HTF is fed from the top as [219] recommended top charging for melting to obtain a higher melting rate.

Non dimensional parametric study is carried out by varying the operating parameters and geometric parameters of the heat exchanger. The details pertaining to the variation of these parameters to achieve the required non dimensional values are provided in the respective sub sections of results and discussions. It is to be noted that for all the simulations lauric acid is considered as PCM and the variation in non-dimensional parameters is achieved by varying operating and geometric parameters of the heat exchanger. Thermophysical properties of lauric acid are listed in Table 4.1. The thermophysical properties of the PCM and HTF are kept constant as the variation of these properties in the selected range of temperature is insignificant.

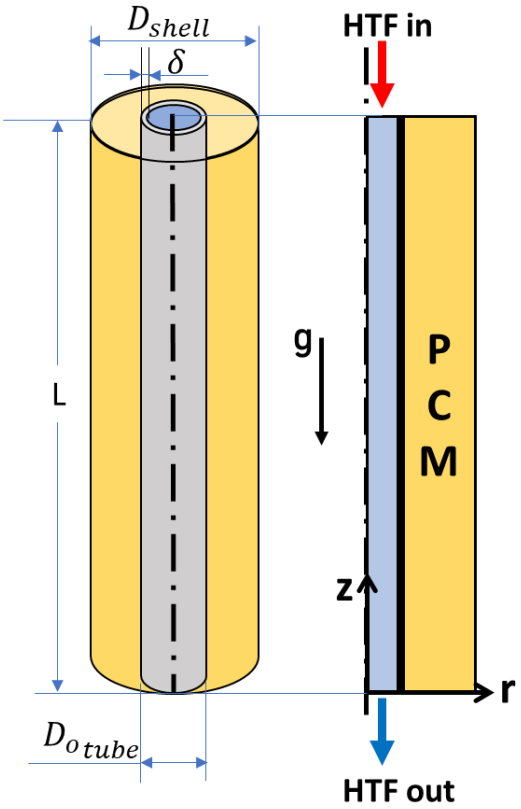

Figure 4.1: Physical model of the heat exchanger used for the numerical study

Table 4.1: Thermophysical properties of lauric acid [220]

Property	**Value**
Density	862.9 kg/m^3 at 60°C
Specific heat	1700 (s) /2300 (l) J/kg K
Latent heat	173800 J/kg K
Thermal conductivity	0.147 W/m K
Dynamic viscosity	0.005336 at 60°C, 0.004269 at 70°C, 0.003469 N s/m^2 at 80 °C
Thermal expansion coefficient	0.000615 K^{-1}
Melting point	317.22 K

4.3 Grid independence study and experimental validation

Grid independence study is carried out to choose the appropriate grid size. Uniform grid is chosen, and simulations are carried out using three element sizes for which number of nodes obtained are 16926, 23966 and 32482. Variation between the solutions obtained by employing grid sizes of 23966 and 32482 is observed to be less than 1% which is depicted in Fig. 4.2(a). Therefore, an element size corresponding to the number of nodes of 23966 is used for rest of the simulations. Similarly, to select the suitable time step size simulations are carried using three time step sizes: 0.2s, 0.1s and 0.05s and the melt fraction evolution is shown in Fig. 4.2(b). Total melting times observed are 4620s, 4675s and 4682s respectively. The percentage difference between the results of 0.1s and 0.05s is observed to be less than 0.2%. hence time step is taken as 0.1s.

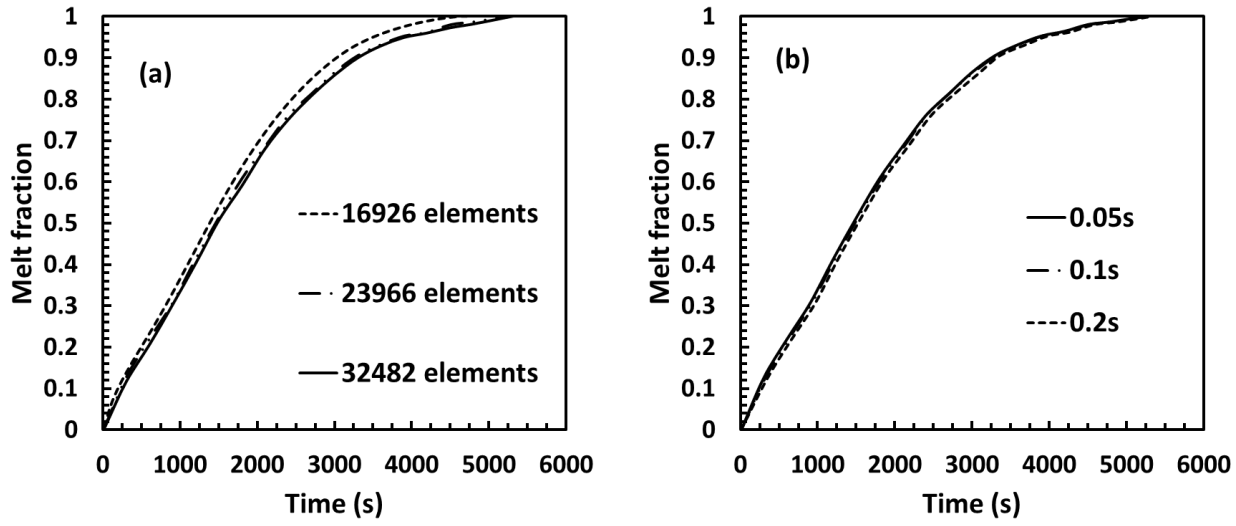

Figure 4.2: Plots showing (a) grid independence (b) time step independence

To verify the numerical procedure adapted in the present study, simulation results of the present study are compared with the experimental results of Longeon et al. [219]. RT35 was chosen as PCM in their study. All the operating parameters and PCM properties are kept same as that of Longeon et al. [219]. Temperature evolution of PCM at two different radial locations ‘a’ and ‘b’ is considered as shown in Fig. 4.3. It is to be noted that the geometry given in Fig. 4.3 is used only for validation. Fig. 4.4 gives the comparison of temperature evolution obtained from present work and the experimental results of Longeon et al. [219]. The variation between the experimental and the present study is observed to be less than 6%. This error can due to the assumption of the adiabatic wall which could not be the case in practical scenario. It is further validated by comparing the contours of melt fraction at different time levels with the instantaneous photographs taken while conducting the experiment by Longeon et al. [219]. Fig. 4.5 shows the comparison of the melt fraction contours of the present numerical work with snapshots of [219] at different time levels. From Fig. 4.4 and Fig. 4.5, it can be concluded that the present numerical methodology could satisfactorily predict the melting phenomenon and hence can be extended for further investigation.

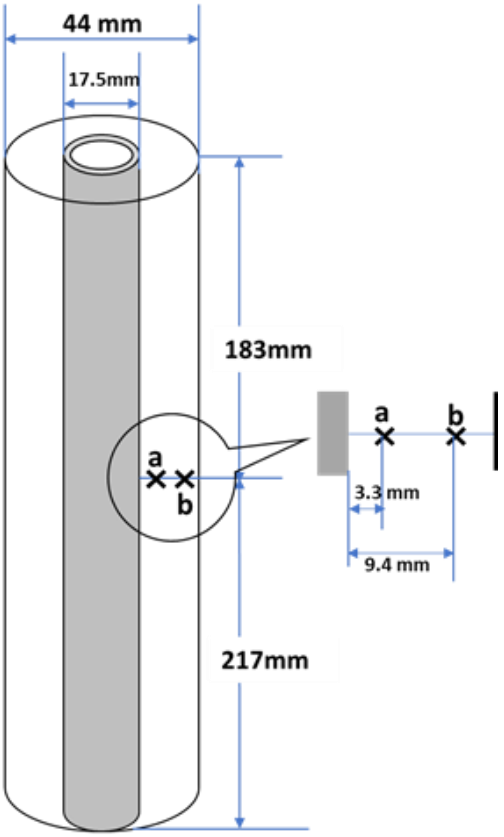

Figure 4.3: Geometry used for experimental validation

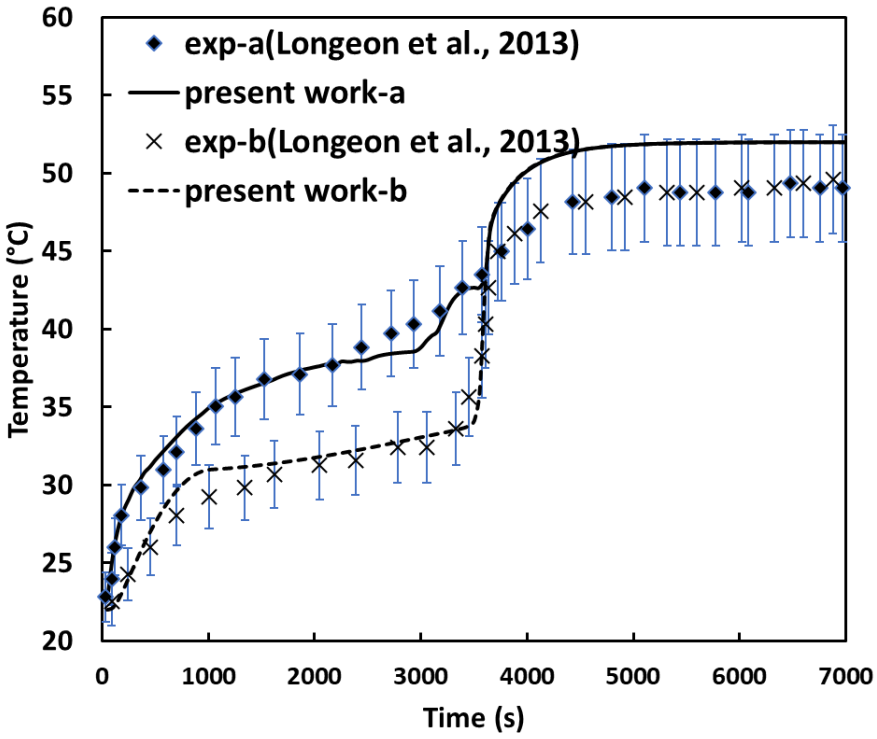

Figure 4.4: Comparison of temperature evolution at points ‘a’ and ‘b’ of present work with the experimental results [219]

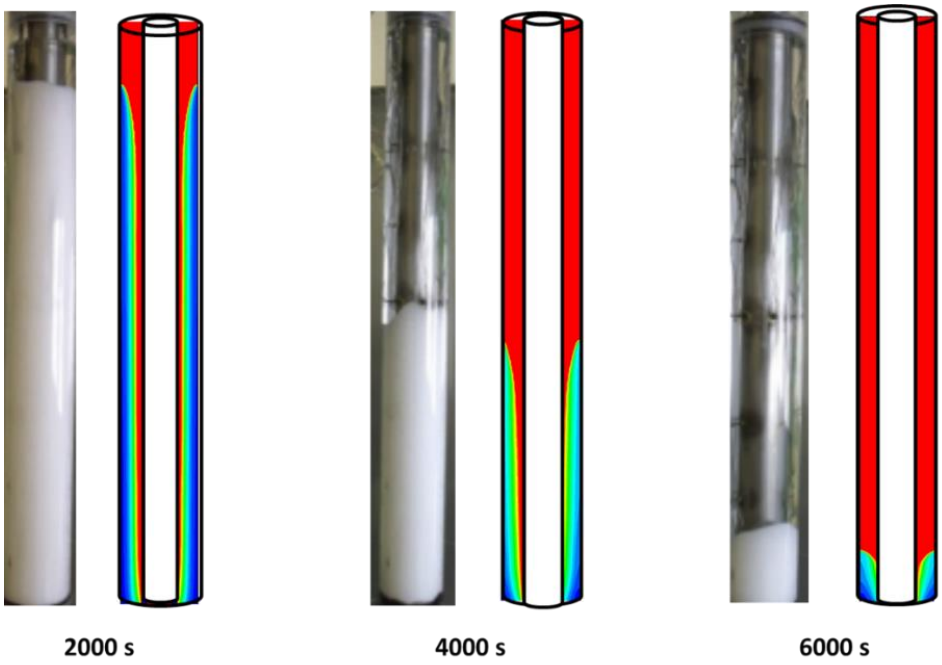

Figure 4.5: Comparison of melting fronts obtained from present work with the experimental results [219] at different time levels

4.4 Results and discussions

To understand the thermal hydraulics of a PCM based heat exchanger, 110 simulations are carried out by varying different parameters. The parameters considered for the study are Stefan number, Rayleigh number, Reynolds number of HTF, ratio of thermal diffusivities of PCM and tube material, ratio of tube thickness to shell diameter and L/D ratio. The definitions of all these non-dimensional parameters along with their ranges are provided in Table 4.2. For all the simulations, the initial temperature of the PCM is kept at 25°C. It can be noted that in the further discussions, unless and until specified the tube material is SS and the tube thickness is 2 mm.

Table 4.2: Definition and ranges of different dimensionless parameters

Dimensionless parameter	**Definition**	**Range**
Stefan number	$St = C_p(T_{inlet} - T_m)/L$	0.2 - 0.6
Rayleigh number	$Ra = g\beta(T_{inlet} - T_m)\left(R_{shell} - R_{o_{tube}}\right)^3/\vartheta\alpha$	2.04×10^5 - 2.32×10^6
Reynolds number	$Re = v\,D_{tube}/\vartheta_{HTF}$	500 - 2000
L/D ratio	$L/D = length/D_{shell}$	1 - 10
Ratio of thermal diffusivities	$\varphi = \alpha_{tube\ material}/\alpha_{PCM}$	45.29-1500
Tube thickness to diameter ratio	$\sigma = \delta/D_{shell}$	0.036-0.113
Fourier number	$Fo = \alpha t/(R_{shell} - R_{o_{tube}})^2$	---

4.4.1 Observations from the charging phenomenon

When the HTF is made to pass through the inner tube, the PCM which is adjacent to the tube takes the heat from the tube by conduction and starts melting. The melted PCM tends to move upwards due to natural convection. This natural convection causes recirculation in the melted PCM which accelerates the melting process. Due to the circulation of the fluid, the melting front propagates in a vertical conical shape. At the final stages of melting, i.e. at the bottom of the heat exchanger convection has a negligible role in melting which means that the mode of heat transfer at the bottom part of the heat exchanger is purely conduction. So, it can be said that melting is initiated by conduction and then accelerated by natural convection and at the final stage conduction is solely responsible for melting. Fig. 4.6 shows the melt fraction contours and streamlines colored according to velocity magnitude at different time levels.

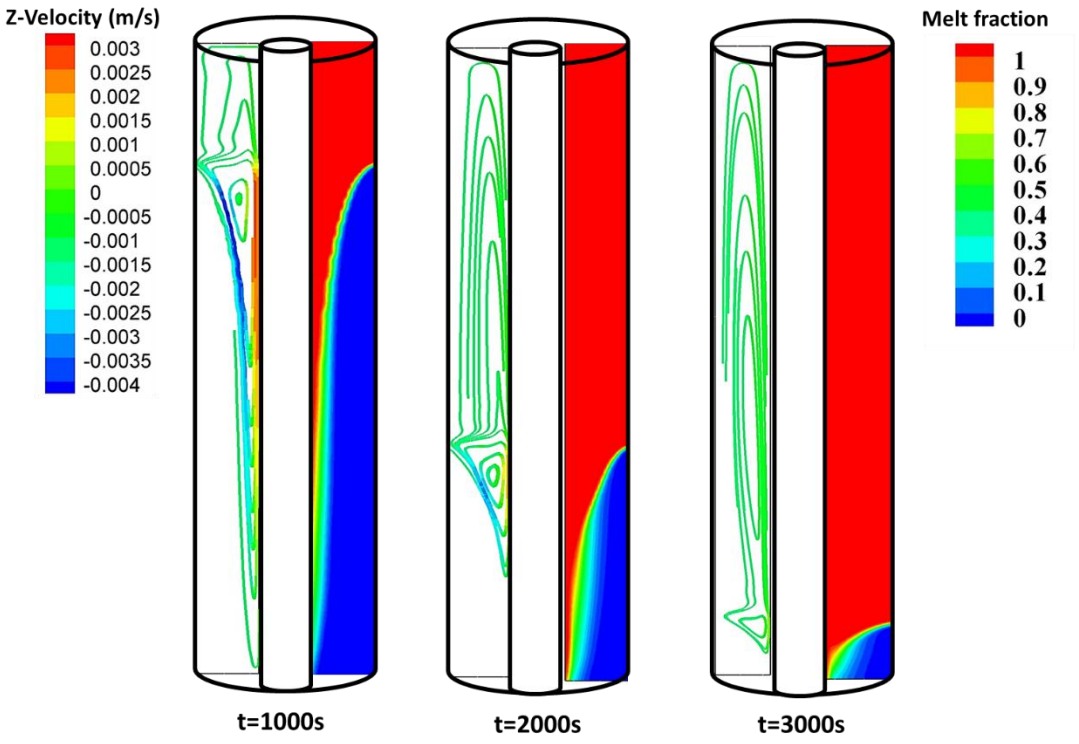

Figure 4.6: Streamlines (left), contours of melt fraction (right) at various time levels during melting of PCM (Re=1250, Ra=8.75×10^5, St=0.4, L/D=4)

In Fig. 4.6 the melting front propagation can be observed, and it is evident that the natural convection created recirculation in the melted PCM. It can also be observed that the velocity magnitude of the melted PCM decreased as the time progresses. Based on this behavior it can be inferred that the effect of natural convection tends to decrease towards the end of the melting process. As conduction is the only heat transfer phenomenon at the bottom of the heat exchanger, a duration of about 30% of the total melting time has been taken to attain a melt fraction from 0.9 to 1.

4.4.2 Effect of Rayleigh number

Rayleigh number can be defined as the ratio of buoyancy strength to that of viscous strength and it characterizes the heat transfer mechanism. In the melting of PCM, Rayleigh number is expected to play a dominant role as the melting is influenced by natural convection. To analyze the influence of Rayleigh number on the melting of PCM, *Ra* is varied from 2.04×10^5 to 2.32×10^6 by changing the diameter of the shell from 35mm to 55mm and by keeping tube diameter and other parameters constant (Re=1250, St=0.4, L/D=4). As the Rayleigh number increases, the buoyancy force can be noted to increase which results in faster melting rate. It is to be noted that the total melting time for different Rayleigh numbers should not be compared in terms of dimensional form. This is due to the fact that the amount of PCM to be melted

varies with the variation in shell diameter. Hence, to perceive the effect of Rayleigh number it is compared with the Fourier number which is the non-dimensional form of time. Fig. 4.7 shows the plot between Fourier number and melt fraction for different Rayleigh numbers. 36.37% reduction in total non-dimensional melting time is observed by increasing the Rayleigh number from 2.04×10^5 to 2.32×10^6. This is due to the increase in natural convection because of which the melting rate is enhanced.

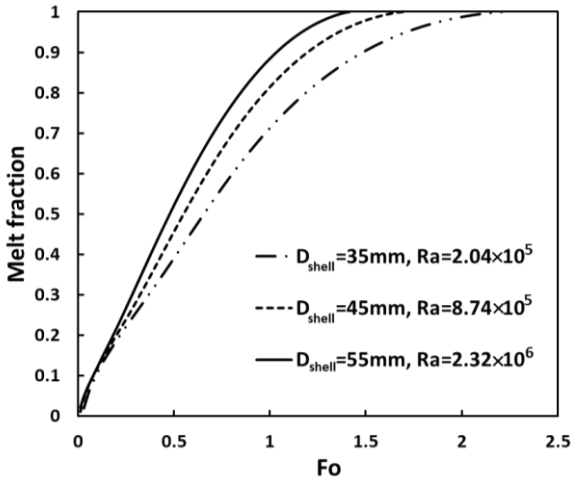

Figure 4.7: Fo vs Melt fraction plot for different Rayleigh numbers

4.4.3 Effect of Stefan number

Stefan number can be defined as the ratio of sensible heat to that of latent heat and is given in Table 2. Stefan number is varied from 0.2 to 0.6 by varying the inlet temperature of HTF from 59.17°C to 89.34°C. Other parameters are kept constant at Re=1250 and L/D=4. The driving force for thermal transport between HTF and PCM is the temperature difference between HTF and PCM. Hence, by increasing the HTF inlet temperature the heat transfer rate and thus melting rate increases. Fig. 4.8 shows the temporal evolution of melt fraction for various HTF inlet temperatures. Fig. 4.8 also shows the progression of melt fraction with Fourier number. With the increase in inlet temperature of HTF the total non-dimensional melting time is observed to decrease by 60.78%. By varying the inlet temperature of HTF, there will be a variation in Rayleigh number. Hence, this reduction is not entirely due to the increase in Stefan number. To obtain the sole effect of Stefan number, the effect of Rayleigh number should be neutralized. As shown in Fig. 4.9, it can be observed that the product of Fo_{cm} and $Ra^{0.185}$ is same for any value of Rayleigh number when other parameters are kept same. It indicates that the effect of Rayleigh number can be neutralized by multiplying Fourier number with $Ra^{0.185}$. Hence, the effect of Stefan number is analyzed by plotting melt fraction against $Fo.Ra^{0.185}$ as

shown in Fig. 4.10. From the figure, it can be noted that 51.95% of the reduction in melting time is obtained which is the sole effect of increase in Stefan number. Remaining 8.83% can be inferred due to the increase in Rayleigh number. Hence, it can be concluded that the increase in HTF inlet temperature has two consequences: increase in Stefan number and increase in Rayleigh number. Out of these two, Stefan number has more influence on melting time.

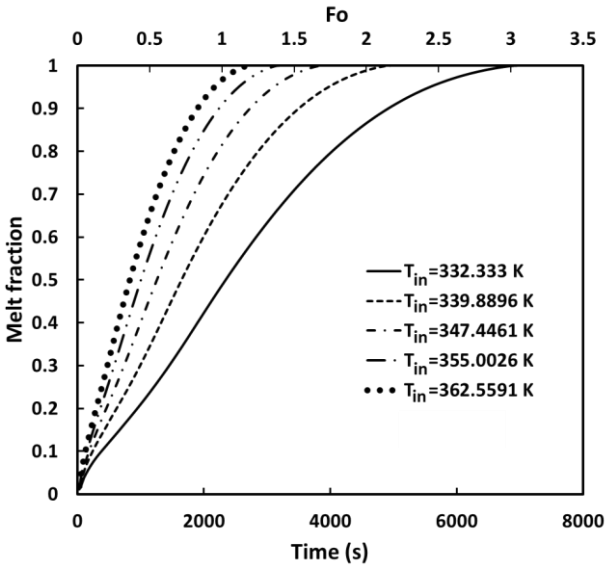

Figure 4.8: Evolution of melt fraction with respect to dimensional and non-dimensional time for various HTF inlet temperatures

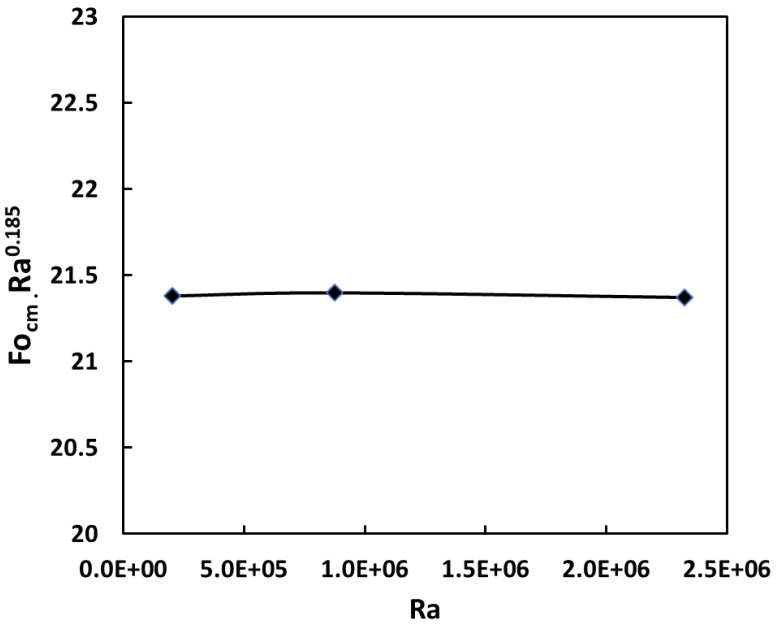

Figure 4.9: Neutralization of Rayleigh number effect

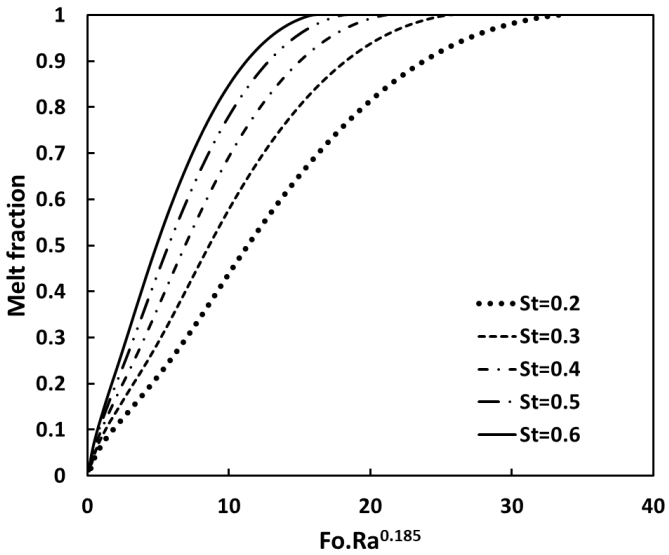

Figure 4.10: Effect of Stefan number on melt fraction evolution

4.4.4 Effect of Reynolds number

Reynolds number of HTF influences the heat transfer coefficient between HTF and tube. Hence, the increase in Reynolds number is expected to influence the melting rate as well. To investigate the effect of Reynolds number on total melting time, it is varied from 500 to 2000 in steps of 375 by keeping all other parameters constant at St=0.4, Ra=8.74×10^5, L/D=4. The Reynolds number is varied by varying the inlet velocity of the HTF from 0.03m/s to 0.118m/s. The effect of Reynolds is also studied for different Stefan numbers and different L/D ratios. But for brevity, results are presented only for a constant Stefan number of 0.4 and L/D ratio of 4.

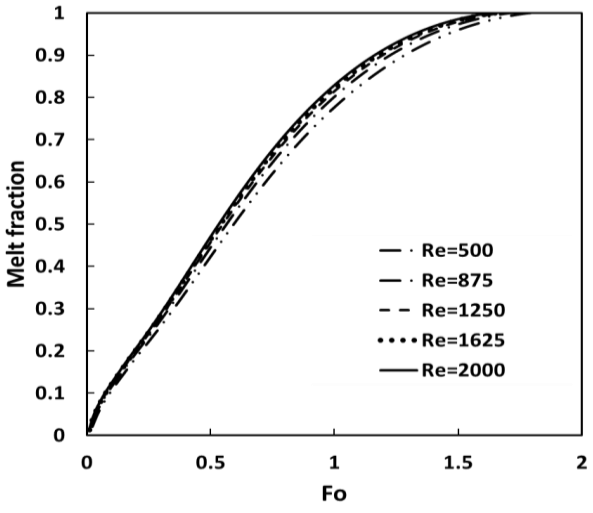

Figure 4.11: Effect of Reynolds number on melt fraction evolution

Fig. 4.11 shows the evolution of melt fraction for different Reynolds numbers. 9.03% reduction in total non-dimensional melting time is observed by varying Reynolds number from 500 to 2000. Hence, it can be said that Reynolds number is not a largely influencing parameter. This can be attributed to the fact that the effect of Reynolds number is very less on the overall heat transfer coefficient between HTF and PCM. It can be concluded that the melting rate is largely influenced by the heat transfer coefficient between tube and PCM but not on the heat transfer coefficient between HTF and tube.

4.4.5 Effect of tube material and tube thickness

Thermal conductivity and heat storage capacity of the tube material influence the heat transfer rate. Hence, the effect of thermal diffusivity (ratio of thermal conductivity and heat storage capacity) of the tube material is to be investigated. The ratio of thermal diffusivity of tube material to thermal diffusivity of PCM (φ) is considered as the non-dimensional parameter corresponding to tube material properties. Copper, Aluminum and SS are the most commonly used materials for tube and hence the effect of φ is investigated by considering these three materials. St, Ra, Re and thickness of tube are kept same at St=0.4, Ra=8.74×10^5, Re=1250, δ=2mm and the effect of φ on total melting time is analyzed. Fig. 4.12 shows the evolution of melt fraction for different values of φ. As can be observed from Fig. 4.12, there is hardly any variation in total melting time. So, it can be concluded that tube material has negligible effect on the total melting time. Hence, SS can be regarded as the recommended tube material as it is not susceptible to corrosion [207].

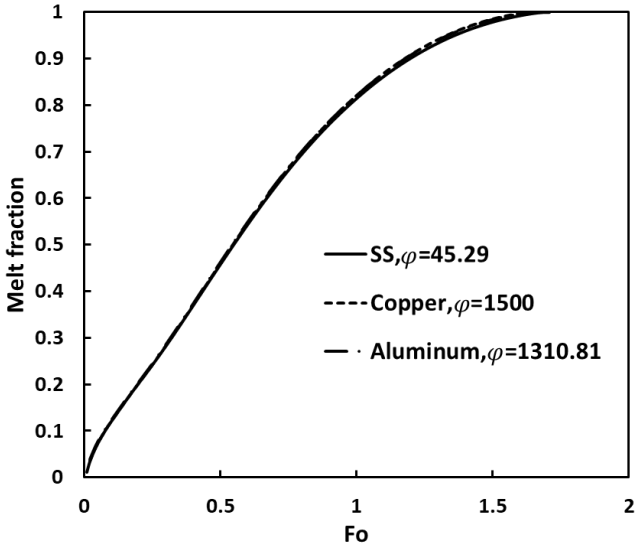

Figure 4.12: Evolution of melt fraction for different tube materials

Bechiri and Mansouri [221] analyzed the effect of φ on melting time of PCM inside a vertical cylindrical tube and concluded that melting time is not sensitive to variation in thermal diffusivity if $\varphi > 40$. For all the materials considered in this study, the value of φ is greater than 40. To have a value of φ less than 40, thermal diffusivity of tube material should be very low which is not the case for any metal. Hence the parametric study is not carried out for $\varphi < 40$. It is recommended to choose tube material such that φ value becomes greater than 40.

Increasing the tube thickness (δ) increases the resistance to heat transfer and thus influences the melting rate. Simulations are performed by varying thickness from 2mm to 6mm. Tube inner diameter and St are kept constant and the diameter of the shell is varied to keep *Ra* same for any thickness of the tube. As the thickness of the tube is increased, more time is required for the outer wall of the tube to reach a higher temperature. Hence, initially the melting rate got decreased with the increase in thickness. Once, the outer wall reached a higher temperature melting rate increased because of marginal increase in surface area available for heat transfer. Fig. 4.13 depicts the reduction in melting rate at the initial stage (up to $Fo = 0.3$) and increase in melting rate at the later stages. It can be said that the increase in thickness of the tube has two consequences: time required for the tube in attaining higher temperature is increased and heat transfer area increased due to which the melting time can be noted to decrease. Out of these two, the effect of increased heat transfer area is slightly more, and hence total melting time is reduced. However, the reduction in melting time is found to be very small and can be observed from Fig. 4.13 which shows the melting front evolution for different tube thickness. In this case, copper is chosen as the tube material. However, same kind of results are obtained for Al and SS as well.

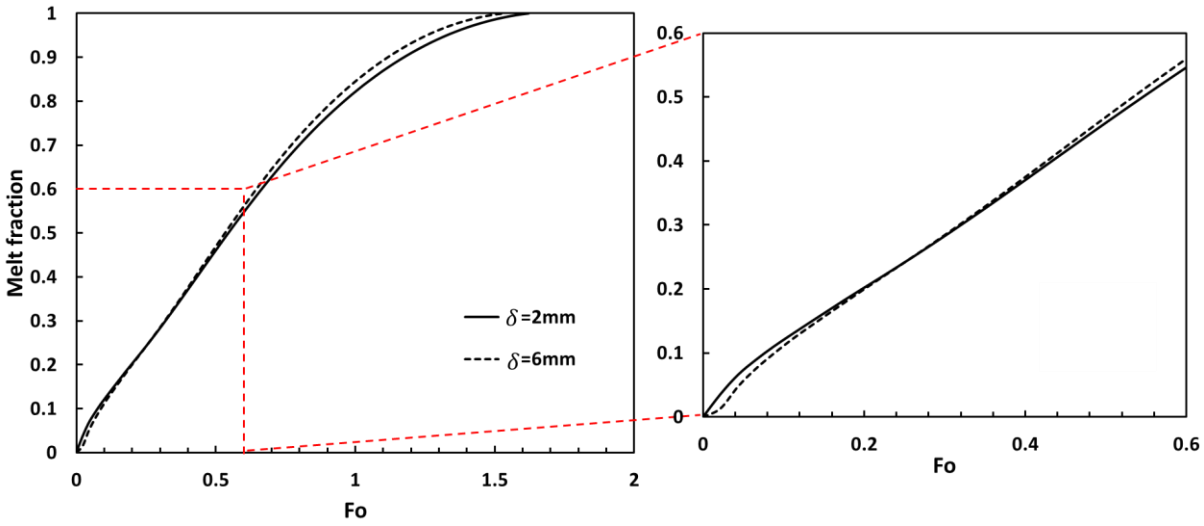

Figure 4.13: Melt fraction evolution for two different thickness of the tube

4.4.6 Effect of L/D ratio

The influence of L/D ratio is investigated by increasing the length of the heat exchanger and keeping diameter as constant. This leads to an increase in the amount of PCM to be melted and it causes no variation in Rayleigh number which means that there is no variation in convective strength. Hence, at constant Stefan number, increase in L/D ratio caused an increase in total melting time. By increasing L/D ratio from 1 to 4, total melting time increased by 1.75 times, similarly, increasing L/D ratio by 10 times, total melting time is observed to increase by 2.4 times. Fig. 4.14 shows the plot between L/D ratio and total non-dimensional melting time.

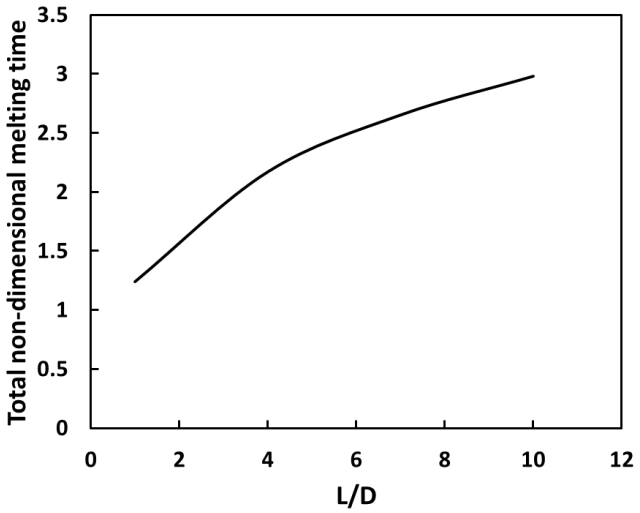

Figure 4.14: Effect of L/D ratio on total non-dimensional melting time

4.4.7 Correlation for melt fraction and total non-dimensional melting time

As discussed earlier in section 1.4.1, melting is initiated by conduction, and the effect of natural convection gradually increased up to some time and towards the end, the effect of natural convection gets diminished. Hence, the total melting phenomenon can be divided into three zones: conduction dominant zone, convection dominant zone, and convection diminishing zone. All the three zones exist irrespective of operating and geometric conditions. The existence of these zones cannot be generalized by plotting MF with respect to *Fo* alone [222]. To distinguish the three zones, $Fo.St^{0.6}$ denoted by "ω" is considered as the non-dimensional parameter whose value decides the zone. The product of *Fo* and *St* can generalize the results as it accounts for both conduction and phase change phenomenon [222]. When melt fraction is plotted against $Fo.St^{0.6}$, it is observed that, up to $\omega \leq 0.35$ melt fraction increased exponentially, if $0.35 < \omega \leq 0.74$ melt fraction increased in a linear manner and when $\omega >$

0.74 the rise in melt fraction is very low. This behavior can be observed in Fig. 4.15 which depicts the three zones. In all the three zones, the phenomenon which influences the melt fraction trend is natural convection. So, the contribution or effect of Rayleigh number to estimate the melt fraction will be different in different zones.

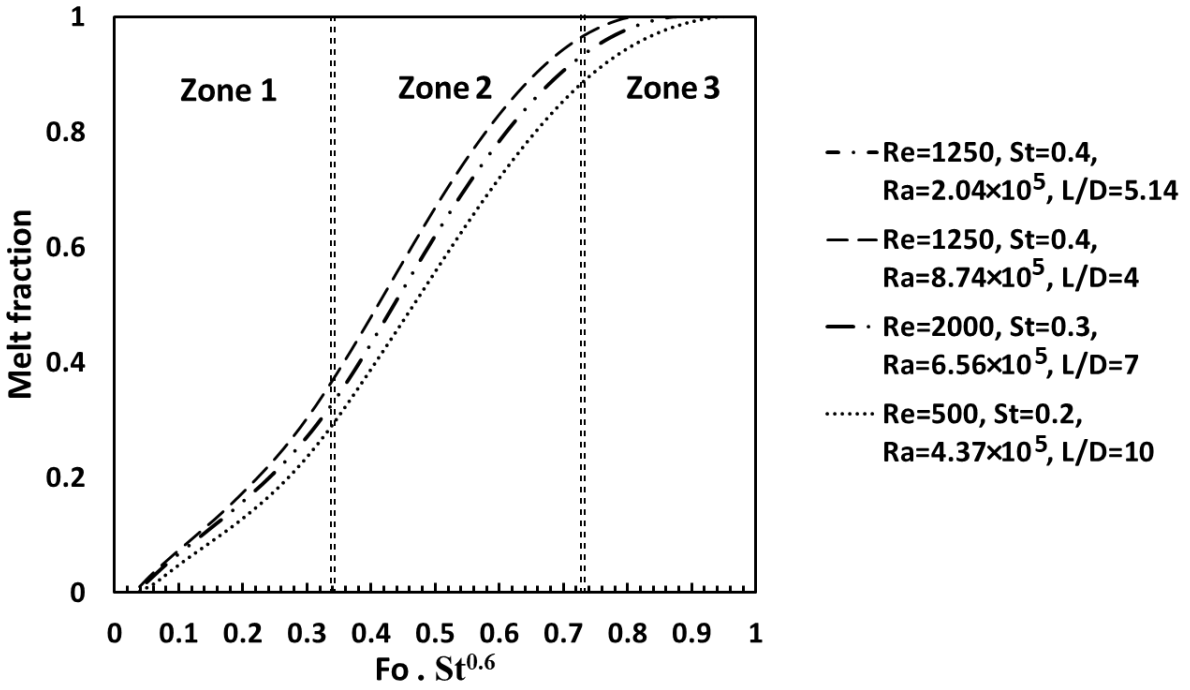

Figure 4.15: Three zones of melting phenomenon

The correlation for melt fraction is developed as a function of all the considered non-dimensional parameters. To incorporate the effect of the initial temperature of the PCM the Stefan number is slightly modified and is given by Eq. 4.1

$$St^* = \frac{C_{p_s}(T_m - T_{ini}) + C_{p_l}(T_{inlet} - T_m)}{L} \tag{4.1}$$

The correlation for melt fraction is developed by multiple regression analysis and is given by

$$MF = \left[\frac{0.1\, Fo\, Re^{0.064}\, Ra^{a}\, St^{*1.206}\, \varphi^{0.0106}\, \left(21.178\sigma + \frac{0.1}{\sigma}\right)}{(L/D)^{0.3795}}\right]^{0.7} \tag{4.2}$$

As mentioned earlier, the contribution of Rayleigh number in estimating melt fraction is different for different zones. Hence, the value of the co-efficient “a” given in Eq.4.3 depends on the zone and is given by

$$a = \begin{cases} \dfrac{e^{\omega\,(L/D)^{0.04}} - 1}{4.2} & if\ \omega \le 0.35 \\ 0.1\,(L/D)^{0.04} & if\ 0.35 < \omega \le 0.74 \\ \dfrac{0.08\,(L/D)^{0.025}}{\omega} & if\ \omega > 0.74 \end{cases} \tag{4.3}$$

The developed correlation for melt fraction (Eq. 4.2) is compared with the performed numerical simulations. As it is difficult to present the comparison for all the cases, 4 different cases are chosen such that a wide range of L/D ratios, Stefan number and Reynolds numbers are covered. The comparison is given in Fig. 4.16 from which it can be concluded that the developed correlation satisfactorily estimated the melt fraction with a maximum error of 10%.

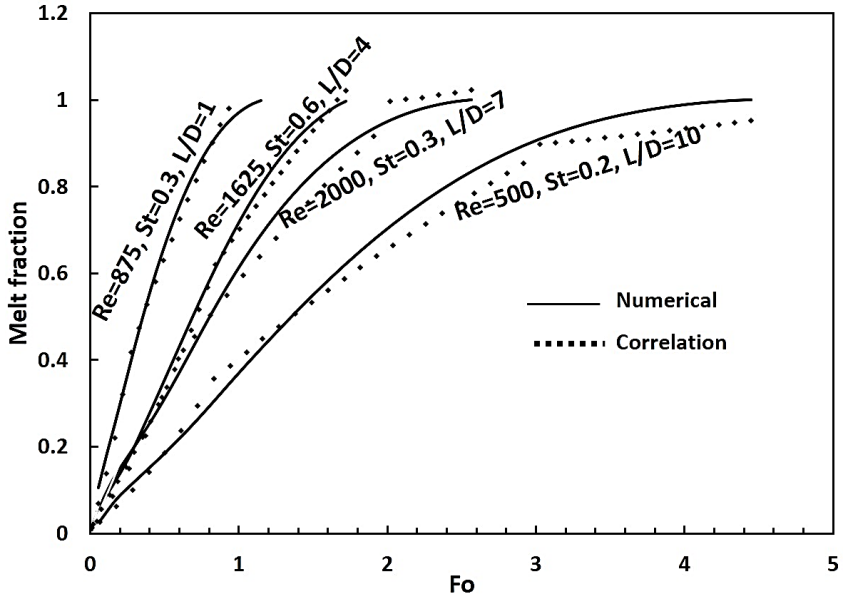

Figure 4.16: Comparison of correlation results with the numerical simulation results

From the developed correlation for melt fraction which is given in terms of Eqs. 4.2 and 4.3 it is difficult to deduce the *Fo* for complete melting due to the fact that the coefficient "a" is also a function of *Fo*. Hence, another correlation for the non-dimensional time required for complete melting is developed and is given by Eq. 4.4.

$$Fo_{cm} = \frac{0.6513\,(L/D)^{0.3795}}{Re^{0.06}\,Ra^{0.1455}\,St^{*1.111}\,\varphi^{0.0146}\,(0.7088\sigma + \frac{0.003}{\sigma})} \tag{4.4}$$

To check the accuracy of the correlation given in Eq. 4.4 parity plot is drawn between estimated complete melting time and numerically obtained results for all the 110 simulations and is shown in Fig. 4.17. The developed correlation accurately estimated the time required for complete melting with a maximum error of 5%.

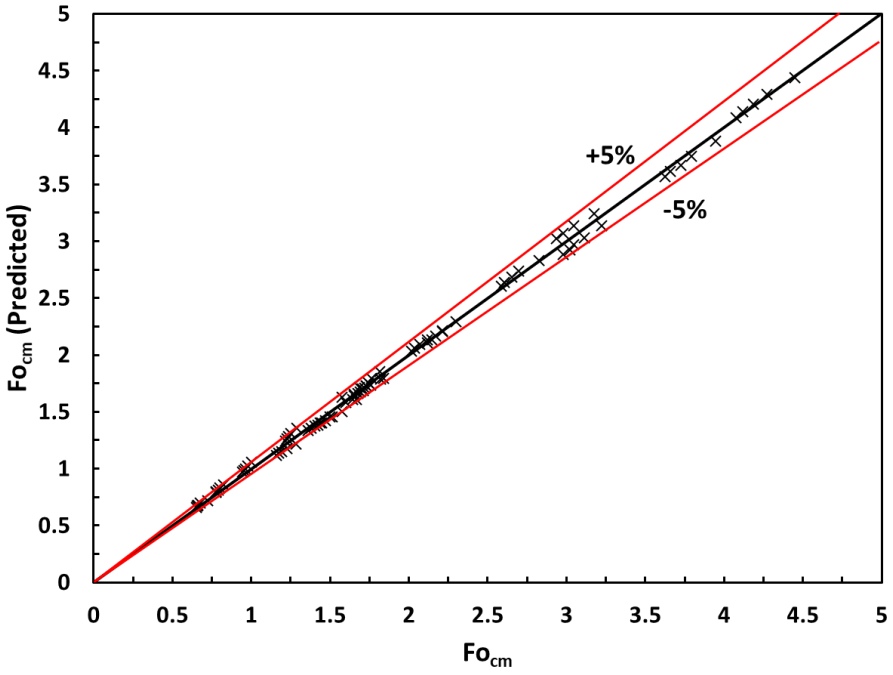

Figure 4.17: Parity plot for the developed non-dimensional melting time correlation

4.5 Closure

Numerical simulations have been performed to analyze the influence of different non-dimensional parameters on the melting characteristics of PCM placed in the annulus of shell and tube heat exchanger. The non-dimensional parameters considered for the study are Reynolds number (500-2000), Rayleigh number ($2.04 \times 10^5 - 2.32 \times 10^6$), Stefan number (0.2-0.6), L/D ratio (1-10), ratio of tube thickness to shell diameter ($0.036 - 0.113$) and ratio of thermal diffusivities of tube material and PCM (45.29-1500) . Axi-symmetric domain is considered, and the enthalpy-porosity approach is adapted to perform the simulations. Natural convection is accounted by Boussinesq approximation and the following conclusions can be drawn.

- Melting of PCM started initially by conduction and then accelerated by natural convection which created recirculation in the melted PCM. Towards the end of the melting process, the effect of convection got diminished

- With the increase in Rayleigh number, the buoyancy force increases which lead to the decrease in total non-dimensional melting time.
- Increase in the HTF inlet temperature caused an increase in Stefan number and Rayleigh number. Out of 60.78% of the decrease in total melting time due to an increase in inlet temperature, 51.95% is due to an increase in Stefan number and the remaining 8.83% is due to an increase in Rayleigh number.
- Reynolds number of the flow has less influence on the total melting time.
- Tube material and tube thickness in the considered range have negligible effect on the total melting time.
- The developed correlations satisfactorily estimated melt fraction with a maximum error of 10% and total non-dimensional melting time with a maximum error of 5%.

Chapter 5

Experimental investigations on the effect of inclination on the thermal performance of a latent heat storage unit

5.1 Introduction

In the previous chapter the influence of various non dimensional parameters on the melting characteristics of PCM was discussed. It was noted that Stefan number and Rayleigh number are the most influencing parameters. Along with these two parameters, the orientation of LHSU has a prominent role in the melting of PCM because of its influence on the natural convection phenomenon. After a thorough review of literature pertaining to the studies on the effect of inclination on the performance of a shell and tube LHSU, a contradiction among the results is noted. One of the reasons can be the difference in design parameters. In the horizontal configuration, the thermal transport by convection does not have any role during melting of PCM at the bottom half of LHSU. Hence, if the diameter of the shell is less, the amount of PCM to be melted by the conduction heat transfer will be less which leads to lesser melting time. On contrary, in the vertical configuration smaller diameter of the shell leads to lesser Rayleigh number which makes convection strength to be less. This results in higher melting time. Higher diameter of the shell may alter this trend which needs to be investigated.

There are two approaches available to evaluate the performance of LHSU: energy analysis and exergy analysis. As pointed out by Li [223], energy analysis alone is not enough to reveal thermal storage behavior. Energy analysis does not account for the internal irreversibilities which cannot be omitted in the analysis and design of LHSU. Hence in recent years, optimizing the design of LHSU based on exergy analysis is gaining a lot of interest. Exergy analysis serves as a measure to know the capability of LHSU for the storage or discharge of useful work. In other words, it quantifies the entropy generated due to which the earlier works [224–229] reported that the exergy efficiency is lower to that of energy efficiency. Table 5.1 provides the list of works which provided the comparison of energy and exergy efficiencies. From Table 5.1 it can be noticed that the exergy efficiency is 15% to 50% lesser than the energy efficiency which infers that the irreversibilities associated with energy storage and retrieval cannot be ignored. Therefore, the comparison for the performance of LHSU under different parameters

should be made in terms of exergy analysis. Hence, for the current study exergy analysis is chosen to compare the performance of LHSU at different orientations.

Table.5.1: Comparison of energy and exergy efficiencies

Ref	Mode of operation	Energy efficiency (%)	Exergy efficiency (%)
[224]	charging & discharging	55.20	34.83
[225]	Charging	40.4	4.2
[226]	Charging	80	40
[227]	Discharging	96	80
[228]	charging & discharging	62	9.5
[229]	charging & discharging	97	78

In the literature the effect of orientation is not thoroughly addressed and in most of the works, the exergetic performance was not taken into account. Hence, the present study is aimed at analyzing the effect of orientation of LHSU on the melting and solidification characteristics of PCM in terms of melting/solidification time, energy charged/discharged and exergy analysis.

5.2 Experimental procedure and temperature measurement

Experimental test facility, the description of which was given in chapter 3 (Fig. 3.1) is used to carry out the investigations on melting and solidification characteristics of PCM impregnated in a shell and tube LHSU at various orientations. lauric acid is chosen as PCM which has a melting point range of 43-50°C. Lauric acid is procured from HIMEDIA. The thermophysical properties such as melting point, latent heat, and specific heat are obtained using differential scanning calorimeter (DSC). All the measured properties of lauric acid are given in Table 5.2. Initially, the melted PCM is poured into the heat exchanger such that the PCM occupies the entire annular space of shell and tube. After solidification, an air gap is noticed because of the volume contraction of the PCM. Before the start of the experiments, it is ensured that there are no leakages in the entire setup. Longeon et al. [219] compared top and bottom injections for both melting and solidification processes. They observed that during the melting, the temperature adopted a thermocline profile in case of top injection whereas bottom injection homogenized the temperature along the tube. They obtained lesser melting time for top injection and solidification was unaffected by the injection side. Hence, the recommendation of top injection was made for melting process. Due to this reason HTF is fed from the top in

the present study. HTF is fed from the top of the heat exchanger. The charging process is initiated after the PCM come in equilibrium with the ambient temperature which is around 28°C. Discharging process is initiated by allowing the HTF from cold water bath to pass through the inner tube of the LHSU immediately after the PCM is completely melted.

Table 5.2: Thermophysical properties of lauric acid

Property	Value
Solidus temperature (T_s)	43.46°C
Liquidus temperature (T_l)	49.94°C
Latent heat (L)	156827 J/kg
Specific heat (C_p)	1390 J/kg K (s)/1570 J/kg K (l)

As shown in Fig. 5.1, 24 K-type thermocouples are placed to analyze the temperature distribution of the PCM. Thermocouples are placed such that the axial, radial and angular distribution of the temperature is recorded. At a given axial location, thermocouples are placed at two radial locations (one is near to tube, another one is near to shell) and three angular locations (120° interval). Another two thermocouples are provided at the entry and exit of the HTF. The location of thermocouples is shown in Fig. 5.1. "A, B, C, D" represents axial locations, "a, b, c" represents angular locations and "1, 2" denotes radial locations. The temperature at all the locations is recorded for every 2 minutes using a "Keysight-34972A" data acquisition unit with two 20-channel multiplexers. The data acquisition unit is connected to the desktop by which the recorded data can be viewed and analyzed.

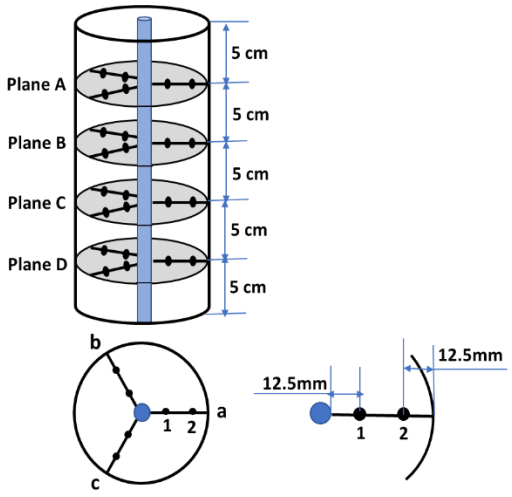

Figure 5.1: Location of thermocouples

5.3 Uncertainty analysis

All the thermocouples used for the temperature measurement are of K-type and are calibrated using "Julabo SL-8K" calibration bath. The uncertainty associated with temperature measurement is found to be ±0.2°C. Flowmeter has an uncertainty of ±0.1LPM. The energy stored or discharged by the PCM is a function of specific heat, latent heat, mass and temperature of the PCM. The uncertainties associated with specific heat and latent heat is 1% (uncertainty of the instrument (DSC) used for the measurement of these properties) and the uncertainty in measuring the mass of the PCM is 1%. Uncertainty in energy stored or discharged can be calculated using the root-sum-square method [230] and is given by Eq. 7. Using this equation, the uncertainty in energy stored is calculated to be 6%.

$$\delta E_{st} = \sqrt{\left(\frac{\partial E_{st}}{\partial m_{PCM}} \times \delta \mathrm{m}_{PCM}\right)^2 + \left(\frac{\partial E_{st}}{\partial C_p} \times \delta C_p\right)^2 + \left(\frac{\partial E_{st}}{\partial L} \times \delta L\right)^2 + \left(\frac{\partial E_{st}}{\partial T} \times \delta T\right)^2} \quad (5.1)$$

The energy supplied to the PCM is a simple product of mass flow rate, specific heat and temperature difference between inlet and outlet of the HTF. Hence, the percentage uncertainty can be easily calculated using Eq. 5.2

$$\frac{\delta E_{in}}{E_{in}} = \sqrt{\left[\left(\frac{\delta \dot{m}}{\dot{m}}\right)^2 + \left(\frac{\delta T}{T}\right)^2\right]} \quad (5.2)$$

By considering the HTF flow rate to be 2.0 LPM and inlet temperature of 80°C, the uncertainty in energy supplied is equal to 5%.

5.4 Results and discussions

5.4.1 Melting process

The melting characteristics and the performance of the LHSU under different orientations are investigated using different performance indicators like stored energy, energetic and exergetic efficiencies, and effectiveness of the heat exchanger. Four different orientations 0°, 30°, 60°, and 90° are considered. 0° and 90° corresponds to vertical and horizontal configurations respectively. As the effect of HTF inlet temperature and HTF flow rate are well documented in the literature, the discussion is focused on the analysis of the effect of orientation. It may be noted that the presented results in this section are for an inlet HTF temperature of 80°C and a flow rate of 2.0 LPM.

5.4.1.1 Effect of inclination on radial, angular and axial temperature distribution

Immediately after the starting of charging process, the tube takes the heat from HTF, and then the heat flows from the tube wall to solid PCM. Hence, the temperature at a location near to the tube wall rises rapidly when compared to the location near to the shell. Irrespective of the inclination angle, this behavior is going to be the same. This can be noted from Fig. 5.2 which depicts the temperature evolution of PCM at two radial locations of plane "B" for all the inclinations. The time taken to attain the liquidus temperature is also provided in the figure. In all the inclinations except horizontal configuration, outer radial location needed approximately 40 minutes more time when compared to the inner radial location to reach liquidus temperature. In the horizontal configuration, natural convective flow is more intense in the upper half of LHSU. Hence, it took a relatively lesser time to reach liquidus temperature at all the radial locations.

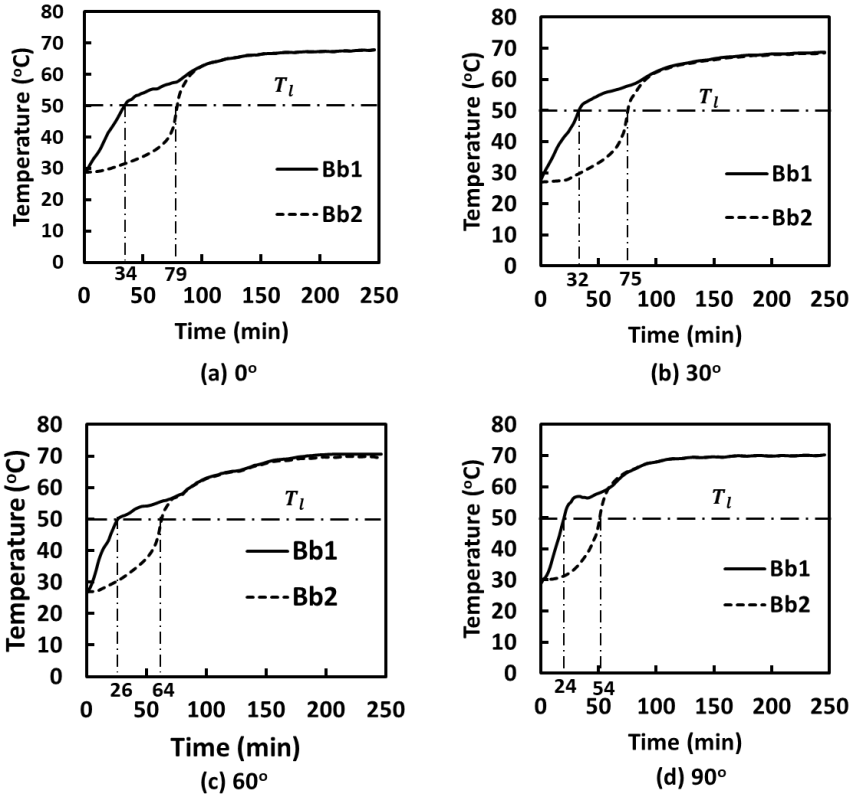

Figure 5.2: Temperature evolution in the radial direction at different inclinations

Once the PCM starts melting, because of the natural convection phenomenon the melted PCM tends to move upwards which creates recirculation in the melted PCM. In the vertical configuration, the flow of melted PCM and the melting front are observed to be following axisymmetric nature. On the other hand, for remaining inclinations, axisymmetric nature is not followed as the buoyancy force is at an angle with the axis of the heat exchanger. It may be

noted that as buoyancy induced flow significantly influences thermal transport during melting phenomenon the consideration of natural convection should not be ignored. The transient variation in temperature of the PCM at the same radial and axial location but at different angular locations is presented in Fig. 5.3. When the LHSU is oriented in the horizontal direction (90°) one of the angular location "a" is exactly at the bottom of the tube, while other two ("b" and "c") are above the tube. For the vertical orientation, as the locations "a, b and c" lie in the same horizontal plane, all the three curves coincide with each other which can be observed in Fig. 5.3. It can also be noted that the temperature difference between lower and upper portions of the heat exchanger increased with the increase in inclination angle. With the increase in inclination angle, the amount of PCM that has to be melted by conduction alone increases. In horizontal configuration entire PCM in the bottom half of the LHSU has to be melted by conduction alone. Hence, the temperature rise is observed to be minimum at the bottom portion.

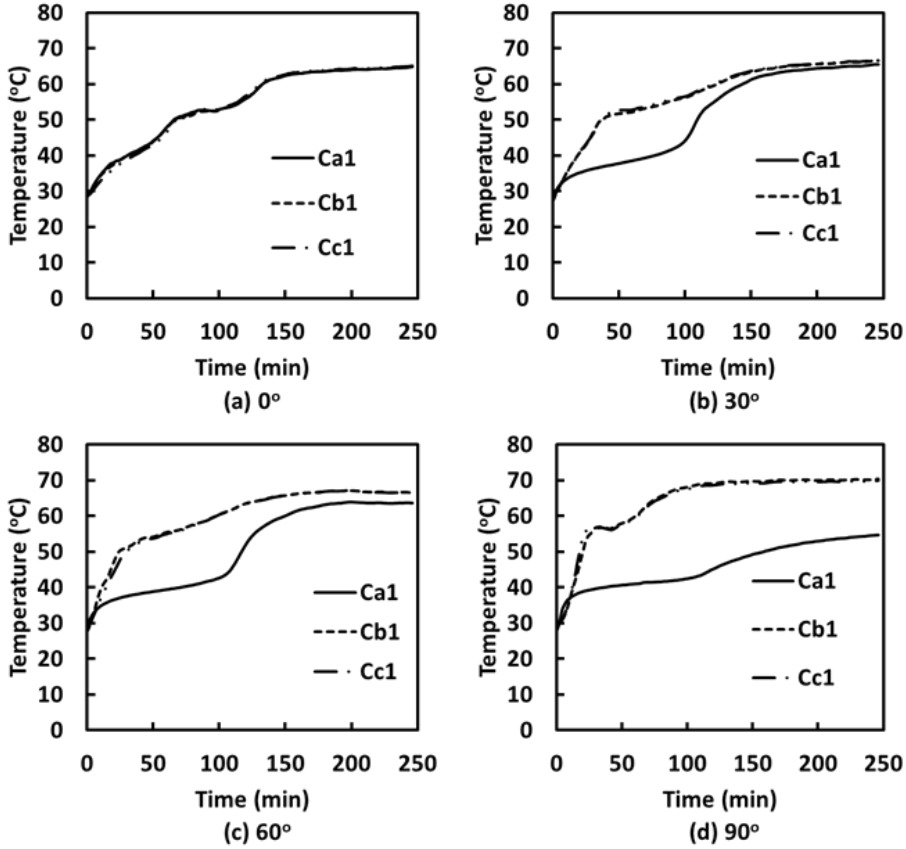

Figure 5.3: Temperature evolution in three angular positions for different inclinations

Another interesting feature is observed by analyzing temperature distribution in the axial direction. Fig. 5.4 shows the axial temperature distribution after 240 minutes of charging with different inclinations at two angular locations "a" and "b". From Fig. 5.4, it can be observed that there is no axial variation in temperature in case of horizontal configuration (90°

inclination). Similar trend is also observed for other angular location. Thereby, it can be stated that the temperature gradient in the axial direction gets diminished with an increase in the inclination angle. By analyzing the temperature distributions in axial, radial and angular locations, it can be inferred that in the vertical configuration (0° inclination), the flow gets induced by natural convection and gradually intensifies in the radial direction. Whereas in horizontal configuration (90°) natural convection is more intense in the upper half of LHSU and hence upper half portion takes lesser time to reach liquidus temperature. Based on the temperature distribution alone, one cannot conclude on the optimum orientation of the heat exchanger. To determine the better orientation, average temperature of the PCM should be looked into which is discussed in the next section.

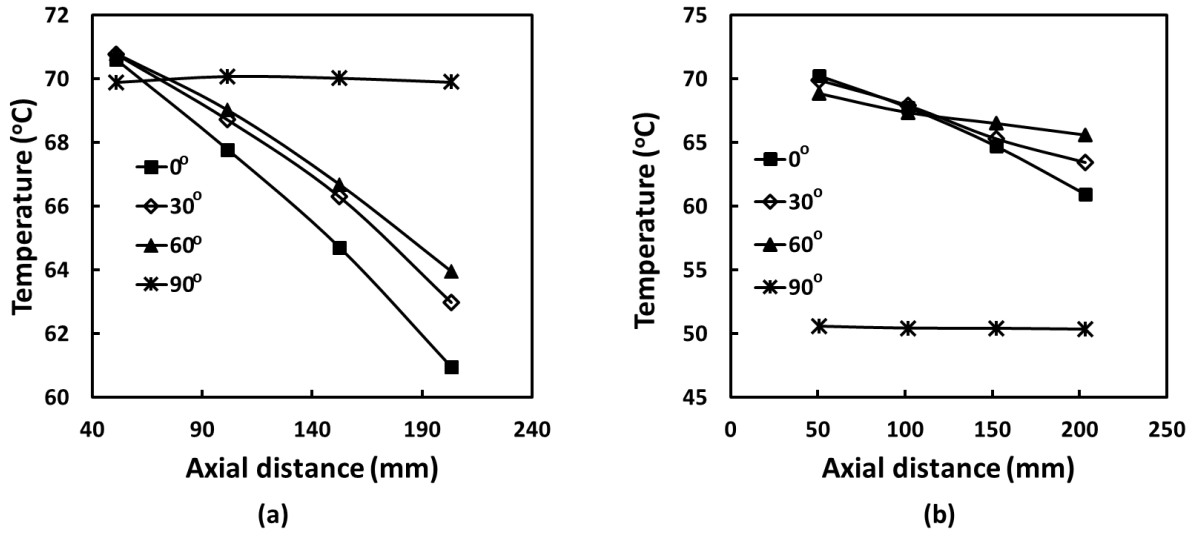

Figure 5.4: Axial temperature distribution after 240 minutes of charging at radial location "1" and (a) at angular location "b" (b) at angular location "a"

5.4.1.2 Comparison of average temperature of PCM

Comparing average temperature after complete melting will not be appropriate as the melting times are different for different configurations. Transient variation in the PCM average temperature should be analyzed. Fig. 5.5(a) shows the temporal variation in PCM average temperature up to a charging time of 240 minutes. From the Fig.5.5(a) it can be observed that the rate of rise in temperature is almost uniform in case of vertical configuration (0° inclination). In horizontal configuration (90° inclination), the temperature rise is observed to be more rapid up to 100 minutes of charging. After 100 minutes of charging the rise in temperature is very less which can be attributed to the decrease in natural convection effect by

that time. In case of vertical configuration, natural convection continues to aid the melting of PCM till the entire PCM got melted. Not much variation is observed for 30° inclination when compared to vertical configuration. Inline to horizontal configuration, the rise in average temperature for 60° inclination is observed to be decreasing towards the completion of the melting process. It is observed that the horizontal configuration took 60 minutes of charging time for the PCM average temperature to attain liquidus temperature which is 25 minutes lesser than the time required for vertical configuration. On the other hand, to reach 65°C of PCM average temperature the vertical configuration took lesser time (242 min).

Fig. 5.5(b) provides the comparison among PCM average temperature for different orientations at various time levels. From the figure, it can be observed that in horizontal configuration (90°) the rise in temperature is mere 3.61°C from 100 to 250 minutes of charging process. In the same period the average temperature of PCM is increased by 12.81°C in vertical configuration (0°), 9.42°C in 60° and 13.84°C in 30° inclination. This indicates that, in vertical and 30° configurations, the natural convection effect remained effective throughout the melting process. Whereas in other configurations, the natural convection is more intense at the initial stages which got reduced towards the end of the melting process.

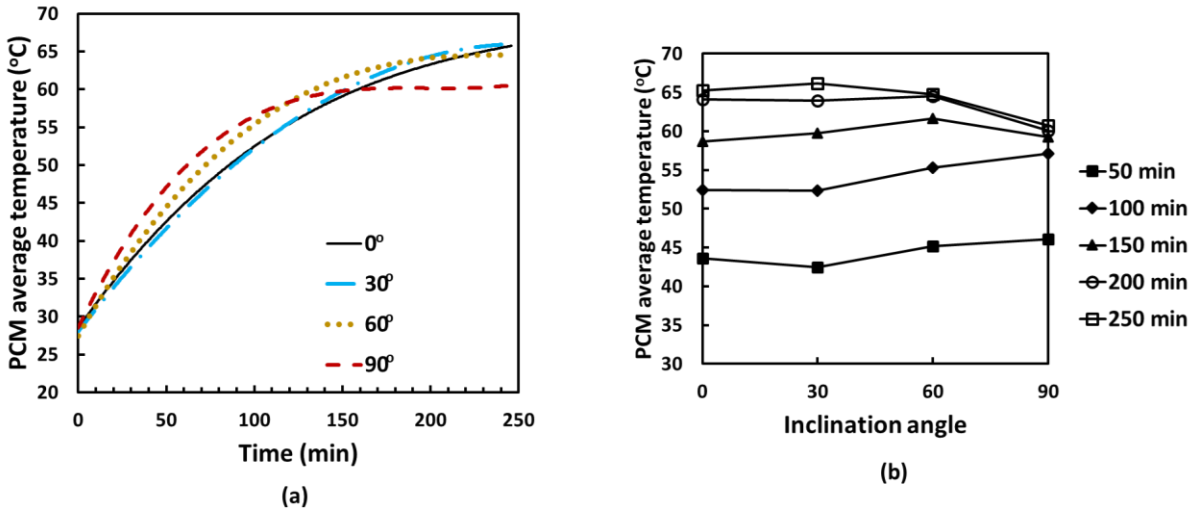

Figure 5.5: (a) Temporal variation of PCM average temperature (b) PCM average temperature at various time levels

5.4.1.3 Comparison of melting profile and melt fraction

Visualization of the melting profile is very much necessary for the better understanding of the melting behavior [201,231]. Photographs are taken while conducting the experiment at fixed

intervals of time and the melting of PCM is continuously monitored to record the complete melting time.

Fig. 5.6 shows the experimental photographs taken at various time levels during melting for all the considered inclinations. Irrespective of the inclination, during the initial period of melting, a thin layer of melted PCM circumvent the tube. Then the melt layer expands in a direction which depends on the orientation of the LHSU. In the vertical configuration, the melt layer expands radially and because of the natural convection, the melted PCM gets accumulated at the top of the LHSU. Hence, the melted PCM is first seen at the top of the LHSU. As time progresses a gradual increment of the melted PCM can be observed as shown in the Fig.5.6. In other inclinations, the recirculation caused by natural convection is profound in the upper half of the LHSU. Hence, more amount of melted PCM is seen at the upper half of the LHSU. Irrespective of orientation, the solid-liquid interface is observed to be a straight horizontal line because of gravity which can be noticed in Fig. 5.6. Also, the figure infers the amount of PCM which is yet to get melted. After 240 minutes of charging, the amount of PCM remained in the solid phase is more for the horizontal configuration followed by 60° inclination. It can also be observed that the increase in melt layer from 120 minutes to 240 minutes is minimum for horizontal configuration. This is because natural convection does not have any role in melting the PCM at the bottom portion of LHSU. It is possible to get more insight on the melting behavior by quantitative comparison of melt fraction.

To calculate the melt fraction, the procedure explained in section 3.2 is adapted. Fig. 5.7(a) shows the melt fraction evolution of various inclinations. The melt fraction evolution is observed to be similar to the evolution of PCM average temperature. At the initial stages, the rate of melting is higher for horizontal configuration which drastically reduced after 80 minutes of charging time. In the vertical configuration, the recirculating flow caused by natural convection is effective in all the directions. Whereas in other inclinations, natural convection is eloquent in the upper half of the LHSU. In 30° and 60° inclinations, a weak recirculating flow is present on the other half of the heat exchanger, whereas in horizontal configuration the flow is restricted to the upper half of the heat exchanger. Because of this, the PCM at the bottom half of the LHSU has to depend on conduction heat transfer for melting. As the PCM possess very low thermal conductivity, more time is required by the horizontal configuration for complete melting.

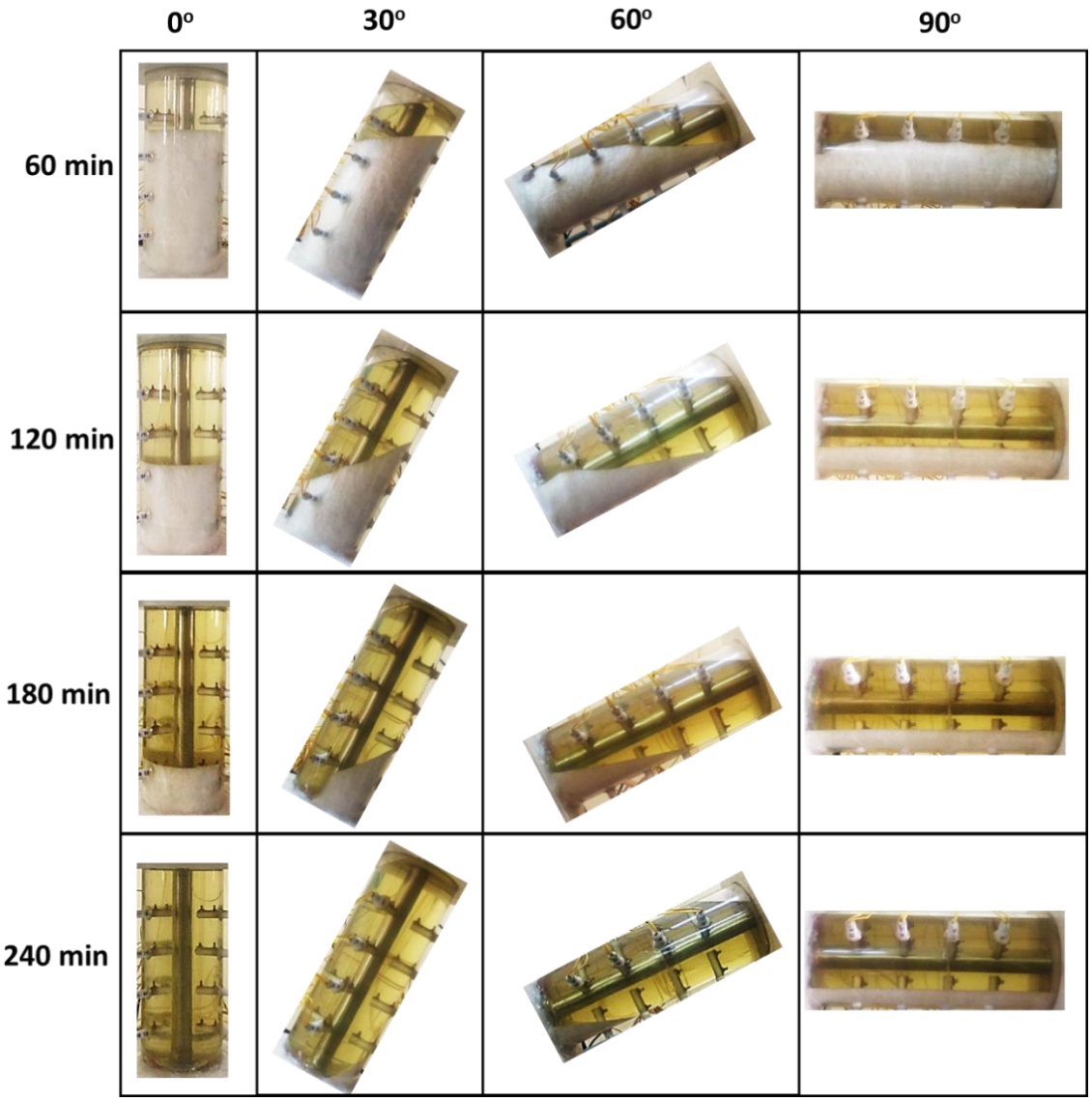

Figure 5.6: Experimental photographs taken during charging process at various time levels

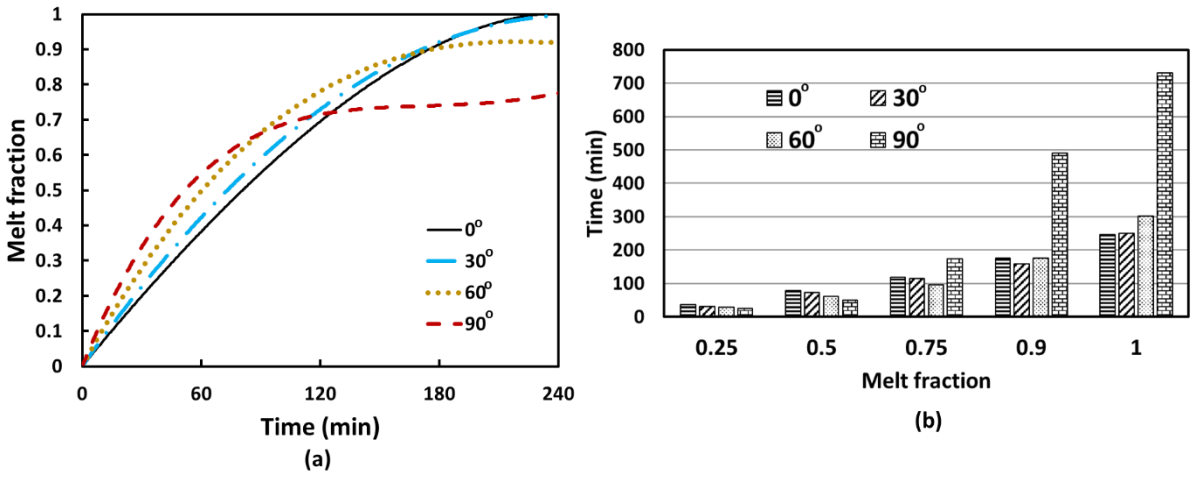

Figure 5.7: (a) Melt fraction evolution for various inclinations (b) Comparison of time required to reach various melt fractions

Fig. 5.7(b) provides the comparison of time required by the PCM at different inclinations to reach the melt fraction of 0.25, 0.5, 0.75, 0.9 and 1(complete melting). For melting half of the PCM i.e, to reach a melt fraction of 0.5, horizontal configuration took 37.17% lesser time when compared to vertical configuration. For a melt fraction of 0.75 lesser time is taken by 60° inclination and for 0.9 melt fraction, 30° inclination has taken lesser time. From Fig. 5.7(b) it is clear that for complete melting of PCM vertical configuration took lesser time. With the increase in inclination angle, natural convection got intensified at the initial period. As the time progresses conduction becomes predominant and this transition occurred very quickly in horizontal configuration followed by 60° and 30° inclinations. For horizontal configuration, after reaching a melt fraction of 0.5, conduction became dominant and hence required more time in the later stages. Similar behavior can be observed for 60° inclination angle after reaching a melt fraction of 0.75.

5.4.1.4 Effect of inclination on energy stored, efficiency and effectiveness

It can be noted that the stored energy depends on melt fraction and PCM average temperature. Hence, the stored energy is expected to follow the same trend as that of melt fraction and PCM average temperature. Fig. 5.8 shows the cumulative energy stored with respect to time for various inclinations. As expected, the rate of energy stored is higher for horizontal configuration at the initial stages. After 50 minutes of charging time, LHSU positioned in horizontal direction stored 38.48% more energy when compared to vertical configuration. While at the end of 240 minutes of charging time the energy stored is 20.01% lesser than that of vertical configuration.

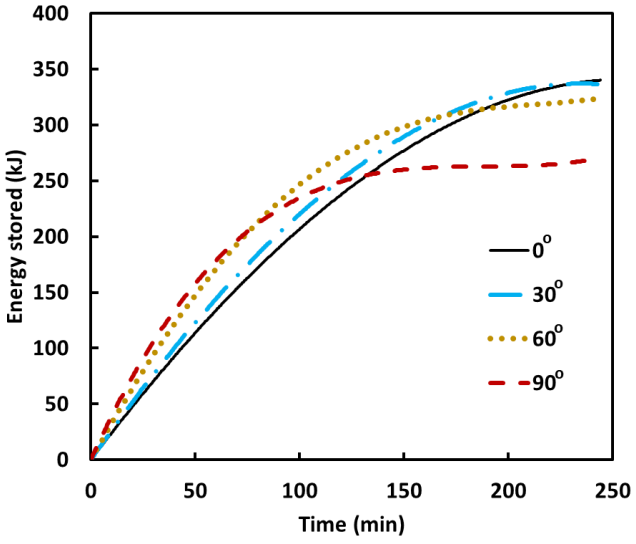

Figure 5.8: Cumulative energy stored with respect to time

The efficiency of any system is defined as the ratio of output to input. In this case energy input is the energy supplied by the HTF, and output is nothing, but the energy stored by the LHSU. The energy supplied is obtained using the below equation

$$E_{in} = \int_0^{t_1} \dot{q}\ dt + \int_{t_1}^{t_2} \dot{q}\ dt + \int_{t_2}^{t_3} \dot{q}\ dt + \cdots \tag{5.3}$$

Where $\dot{q} = \dot{m}C_p(T_{in} - T_{out})$

Energy efficiency is calculated by

$$\eta = \frac{E_{st}}{E_{in}} \tag{5.4}$$

Fig. 5.9(a) shows the energy efficiency with respect to time for all the inclinations. It is observed that the efficiency increased up to a certain time to reach a maximum value and then started to decrease. At the initial stages, conduction is solely responsible for heat transfer because of which efficiency is less at the starting of the charging process. Once the PCM starts melting, natural convection emanates due to which the heat transfer rate enhances and hence efficiency tend to increase. In the later stages, the effect of natural convection diminishes and again conduction heat transfer prevails. This causes a reduction in efficiency. Vertical configuration has achieved a maximum efficiency of 43% which is highest among all the inclinations. Out of all the configurations, the horizontal configuration is observed to have the least efficiency which is justified because of the dominance of conduction for most of the period during charging.

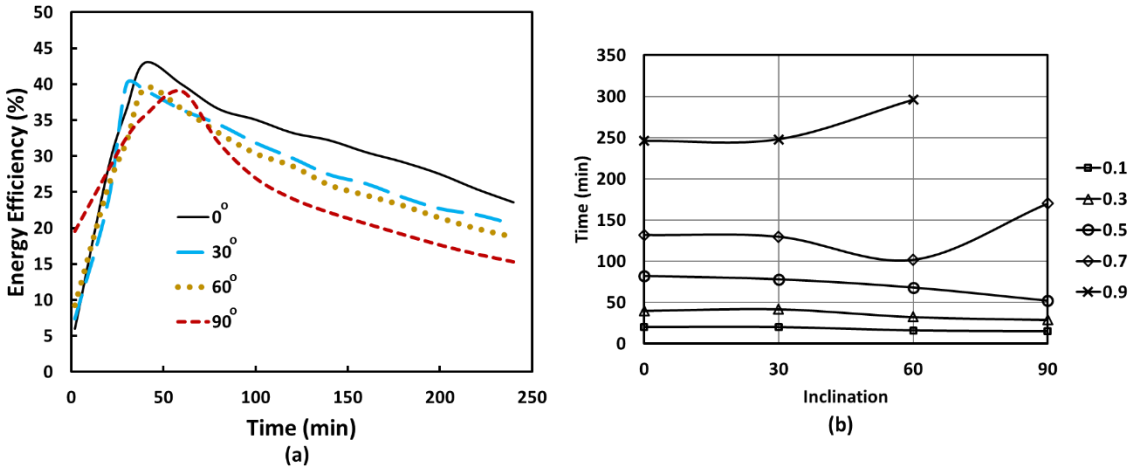

Figure 5.9: (a) Effect of inclination on the energy efficiency (b) Comparison of time required to attain effectiveness of 0.1,0.3,0.5,0.7 and 0.9

Erek and Dincer [226] introduced the parameter energetic effectiveness to investigate system effectiveness. It is a measure for the level of energy stored and is defined as the ratio of energy stored to maximum energy that can be stored and can be given by Eq. 5.5.

$$\varepsilon_{En} = \frac{E_{st}}{E_{st_{max}}} \tag{5.5}$$

Maximum energy can be stored when the PCM average temperature becomes equal to the inlet temperature of HTF. Practically an effectiveness of 1 cannot be achieved. So, LHSU should be designed such that at the end of the charging process, higher effectiveness is achieved. Fig. 5.9(b) shows the time required to reach various values of the effectiveness for the LHSU under different inclinations. Since maximum possible energy stored is equal for all configurations, energy effectiveness will be proportional to energy storage. Same is observed from the figure by which it can also be noticed that to reach effectiveness of 0.5 horizontal configuration needs lesser time. However, the PCM in horizontal configuration is not observed to attain an average temperature of more than 63°C even after complete melting. This limits the energy stored in LHSU and hence the effectiveness of 0.9 is not achieved in horizontal configuration. Maximum effectiveness achieved in the horizontal configuration is 0.79 and 0.9 in other inclinations. To attain effectiveness of 0.9, vertical configuration took lesser time.

5.4.1.5 Exergy analysis of charging process

Bejan [232] has given a beautiful quote regarding the thermal energy storage which says that

"the primary purpose of a thermal energy storage system is not, as the name implies, to store the energy, rather, to store useful work"

This quote signifies the importance of exergy analysis for thermal energy storage systems. There are various expressions available for calculating exergy efficiency which were consolidated by Jegadheeswaran et al. [233] in their review article. The methodology followed in the present work is explained below.

Rate of exergy input given by HTF can be calculated by Eq. 5.6

$$\dot{Ex}_{in} = \dot{m_{HTF}} C_{p_{HTF}} \left[(T_{in} - T_{out}) - T_o \ln\left(\frac{T_{in}}{T_{out}}\right) \right] \tag{5.6}$$

The exergy input over a period of time can be calculated by integrating the above equation over that time.

Exergy stored is calculated by Eq. 5.7

$$Ex_{st} = E_{st}\left[1 - \frac{T_o}{T_{PCM}}\right] \tag{5.7}$$

Where T_o is the ambient temperature.

Similar to energetic efficiency and effectiveness, exergetic efficiency and exergetic effectiveness are defined as follows

$$Exergy\ efficiency \quad \psi = \frac{Ex_{st}}{Ex_{in}} \tag{5.8}$$

$$Exergetic\ effectiveness \quad \varepsilon_{Ex} = \frac{Ex_{st}}{Ex_{max}} \tag{5.9}$$

Here Ex_{max} can be calculated by $Ex_{max} = E_{st_{max}}\left[1 - \frac{T_o}{T_{in}}\right]$. Fig. 5.10(a) shows the exergy efficiency of LHSU when placed at different inclinations. For the vertical configuration (0° inclination) maximum exergy efficiency is observed to be 20.09% while the maximum energy efficiency is 43%. Because of the increase in PCM average temperature, exergy efficiency increased in the initial stages. Later, because of the predominance of conduction mode of heat transfer efficiency decreased. It can be observed from Fig. 5.10(a) that the reduction in exergy efficiency started much earlier in horizontal configuration (90° inclination) when compared to vertical configuration (0° inclination). Once the PCM gets melted in the upper portion, conduction becomes the dominant mode of heat transfer in the later stages of charging. Hence, it can be stated that the zone of reduction in exergy efficiency can be treated as convection diminishing zone. This zone is observed to be less for vertical configuration and hence the vertical configuration is preferable for the charging process.

Fig. 5.10(b) shows the exergetic effectiveness of LHSU placed at different inclinations with time intervals of 50 minutes. Up to 100 minutes of charging time, 60° inclination has the maximum exergetic effectiveness. At the end of 250 minutes of charging time, vertical configuration (0° inclination) has the maximum effectiveness which is equal to 0.7. On the other hand, the maximum exergetic effectiveness achieved in horizontal configuration is only 0.5. Hence, it is recommended to employ horizontal configuration only for partial melting.

From the analysis of the charging process, it can be concluded that the design of LHSU and heat transfer intensification techniques should be aimed at reducing the conduction dominant period. The performance of the horizontal configuration is superior to the other configurations

in the initial periods. By employing any heat transfer enhancement technique at the bottom half of the LHSU, efficiency and effectiveness can be improved.

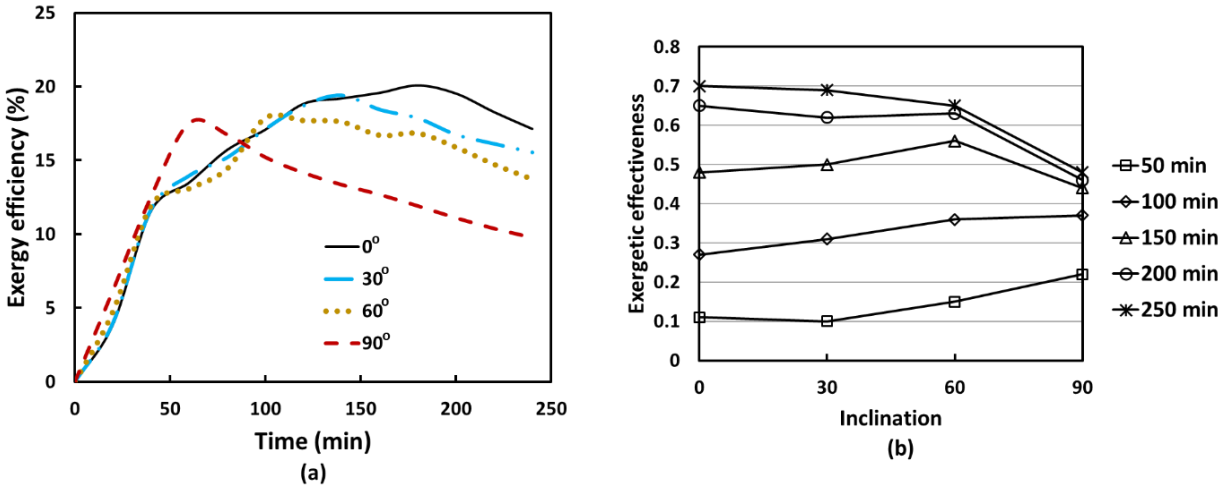

Figure 5.10: (a) Comparison of exergy efficiency at different inclinations (b) Exergetic effectiveness of LHSU at various time levels

5.4.2 Solidification process

Solidification process is initiated by allowing the HTF from cold water bath to pass through the inner tube of the LHSU. Experiments have been conducted at various mass flow rates and different inlet temperatures. The mass flow rate of HTF is observed to have a negligible effect on the performance of LHSU. Total solidification time increased with the increase in inlet temperature. Analyzing the effect of orientation is the prime objective of the current study. Therefore, the results are discussed for a constant flow rate of 2.0 LPM and 15°C inlet temperature of HTF.

Immediately after the cold water is introduced, the formation of a thin layer of solid PCM is observed around the tube. This layer of solid PCM causes thermal resistance and the entire solidification process will be conduction dominant. It is to be noted that the temperature profile of the melted PCM after the charging process is different for different orientations of LHSU. It is very difficult to attain uniform temperature throughout the PCM and temperature gradient is noted to exist even after 12 hours of charging under any inclination. As the initial temperature at any particular location is different for different inclinations, temperature evolution cannot be compared during the discharging process. However, it is made sure that before the start of the solidification process the PCM attains the same average temperature. Hence, the analysis is

made in terms of PCM average temperature, variation in melt fraction, energy and exergetic performance.

5.4.2.1 Comparison of PCM average temperature and melt fraction

Fig. 5.11 shows the timewise variation of PCM average temperature and melt fraction for various inclinations. It can be observed that there is no significant effect of orientation on both the parameters. This behavior is justified because convection does not have any role during the discharging process and conduction is solely responsible for the solidification of PCM. Conduction heat transfer does not get affected by the inclination of LHSU. It is also observed that within 60 minutes of discharging time, the average temperature reduced to solidus temperature which means that a major part of the latent heat stored in the PCM is retrieved. From there onwards, sensible heat needs to be extracted which takes longer time and hence the rate of temperature reduction is decreased.

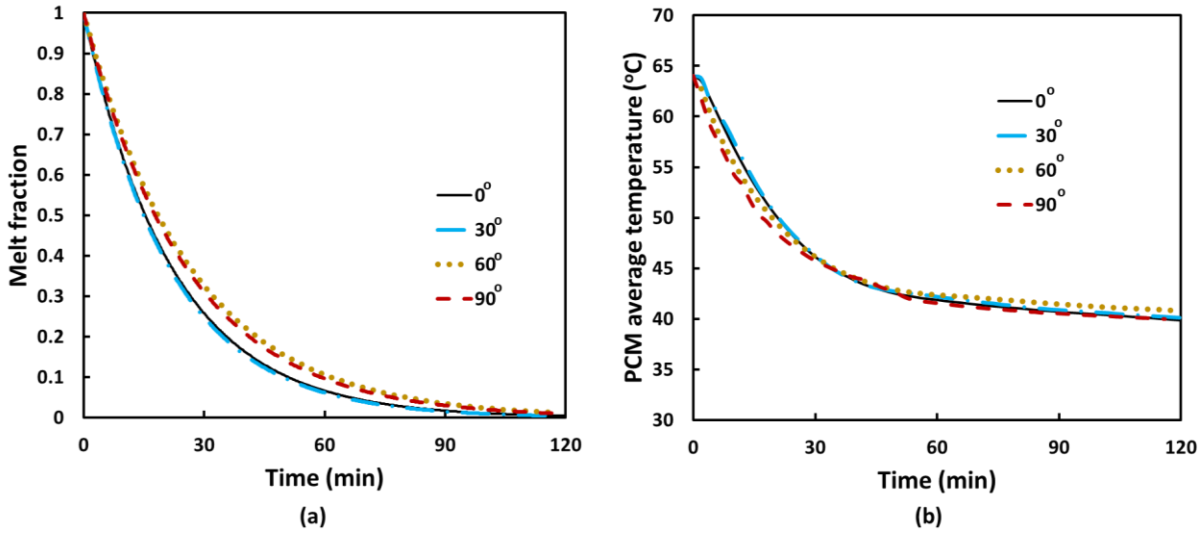

Figure 5.11: Comparison of (a) melt fraction and (b) PCM average temperature during discharging

5.4.2.2 Comparison of energy discharged, efficiency and effectiveness

For the discharging process, the expression for energy discharged in each control volume need to be slightly changed and is given as follows

$$E_{dis_i} = \begin{cases} mC_{p_l}(T_{ini} - T_i) & T_i > T_l \\ mC_{p_l}(T_{ini} - T_l) + mc_i L & T_s \leq T_i \leq T_l \\ mC_{p_l}(T_{ini} - T_l) + mL + mC_{p_s}(T_s - T_i) & T_i < T_s \end{cases} \quad (5.10)$$

Total energy discharged is calculated as

$$E_{dis} = \sum w_i E_{dis_i} \tag{5.11}$$

Fig. 5.12 shows the energy discharged with respect to time for various inclinations. Similar to the energy stored, energy discharged also depends on PCM average temperature and melt fraction. As there is no significant variation in both these parameters with the variation in inclination angle, energy discharged also does not get affected much with the variation in inclination angle.

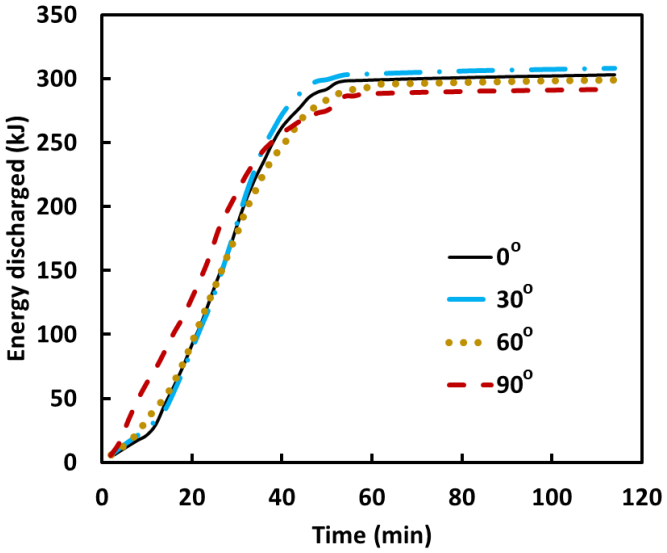

Figure 5.12: Energy discharged with respect to time

Energy efficiency for the discharging process can be defined as the ratio of energy discharged by the PCM to the energy retrieved by the HTF. Energy retrieved by the HTF can be obtained using Eq. 5.12

$$E_{ret} = \int_0^{t_1} \dot{q}\ dt + \int_{t_1}^{t_2} \dot{q}\ dt + \int_{t_2}^{t_3} \dot{q}\ dt + \cdots \tag{5.12}$$

Where $\dot{q} = \dot{m} C_p (T_{out} - T_{in})$

Unlike in the charging process, the efficiency during the discharging process is observed to decrease with respect to time and it remained almost constant after 45 minutes of discharging process. As can be observed from Fig. 5.13, the energy efficiency gradually decreased from 93% to 42% and remained constant.

Energy effectiveness for discharging process is defined as the ratio of energy retrieved by the HTF to the maximum possible energy that can be retrieved. Maximum retrievable energy will

be in turn equal to the maximum energy that can be discharged by the PCM. This is possible when average temperature of the PCM becomes equal to the inlet temperature of HTF. As the energy retrieved and maximum retrievable energy is same for each inclination, effectiveness also did not vary with inclination angle. The effectiveness after 120 minutes of discharging period is observed to be the same for all the inclinations and is equal to 0.63.

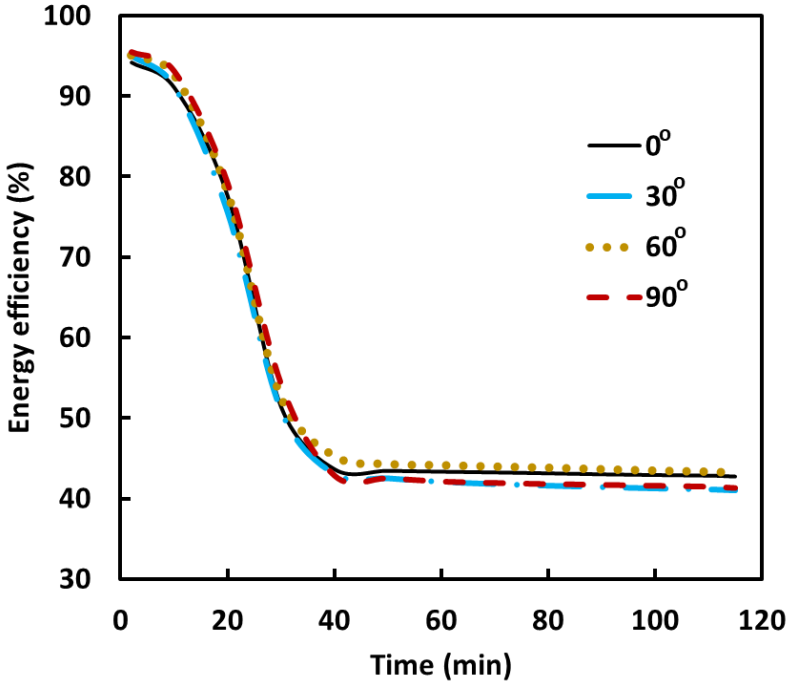

Figure 5.13: Comparison of energy efficiency during the discharging process

5.4.2.3 Exergy analysis of discharging process

Exergy analysis for discharging process is also carried out to quantify the exergetic efficiency and exergetic effectiveness. Exergy retrieved and exergy discharged can be calculated using the same expressions as that of Eqs. 5.6 and 5.7 respectively but with the change in sign. Exergetic efficiency is also observed to follow the same trend as that of energetic efficiency. However, the exergetic efficiency got decreased from 85% to 29% before it becomes constant. For all the inclinations, the exergetic effectiveness after 120 minutes of discharging period is observed to be 0.48 which means that only 48% of the maximum possible retrievable exergy is extracted by the HTF.

By the analysis of the solidification process, it can be concluded that the discharging process is unaffected by the orientation of LHSU. There is a scope for improvement in efficiency and effectiveness which can be achieved by employing heat transfer enhancement techniques.

5.5 Closure

The effect of orientation on the thermal performance of LHSU is investigated by means of energy and exergy analyses. Major conclusions drawn from the study are as follows

- The temperature evolution during the melting process followed axisymmetric nature in vertical configuration and asymmetric in other inclinations. This nature is mainly due to the variation in the angle of buoyancy force with the axis of the LHSU.
- The melting process can be broadly categorized into three zones: **I**. conduction dominant at the early stages of melting, **II**. convection dominant zone and **III**. convection diminishing zone. The occurrence of the third zone is delayed in vertical configuration, on the other hand, it occurred much early in horizontal configuration.
- Melting rate, rate of rise in PCM average temperature and rate of energy storage are observed to be higher at the initial stages in case of horizontal configuration. However, with the progression in time, vertical configuration showed better performance in all the aspects.
- Irrespective of orientation, energy efficiency is observed to be increasing up to some time and then energy efficiency started to decrease. Maximum efficiency is observed for vertical configuration which is equal to 43%.
- Exergy efficiency provided more insight on the thermal behavior of the LHSU. The zone of reducing exergy efficiency can be considered as convection diminishing zone and the LHSU should be designed in such a way that this convection diminishing zone is minimized.
- Entire solidification process is observed to be conduction dominant and hence solidification process is unaffected by the orientation of the LHSU.

Chapter 6

Effect of solid and perforated annular fins on the heat transfer characteristics in a shell and tube latent heat storage unit

6.1 Introduction

The performance of LHSU depends on energy charging/discharging rates which are hindered due to lesser thermal conductivity of PCM. To overcome this issue various heat transfer enhancement techniques are available such as dispersion of nanoparticles [234], embedded metal foam [152,153], heat pipe, and employment of fins [91,94]. Among various enhancement techniques, employing fins is very efficient, least expensive and no fabrication complexity is involved [82]. It is a well known phenomenon that adding fins increases the heat transfer area and thus increases the heat transfer rate. LHSU is also not an exception to this, by adding fins to the tube considerably augments the heat transfer rate. When HTF at a higher temperature is flowed through the tube, the temperature of the fins get increased quickly and the PCM surrounding the fin immediately melts. So the melting intiates from tube surface and fin surface as well. Similarly during discharging process also, solidification starts from fin surfaces. Hence, it can be said that employing fins can be considered as a prominent method to augment the heat transfer in LHSU. In this respect, various designs of fins are proposed which include longitudinal fins, annular fins, and pin fins. Abdulateef et al. [113] made a comparative analysis on the performance of LHSU with longitudinal fins and annular fins. It was observed that the highest charging rate and melting rates were obtained by using annular fins. Similarly, Tay et al. [114] compared annular fins and pin fins and reported that annular fins resulted to be 20-40% more effective when compared to pin fins. Hence it is proven that the annular fins are more effective for the heat transfer augmentation in LHSU. Annular fins enhance the heat transfer rate but there is a possibility of suppressing the natural convection. Providing perforated fins could be one option to address this issue. Hence in the current study a comparative analysis on the thermal performance of a LHSU with solid and perforated fins.

Previous chapter provided the effect of inclination on the thermal performance of a LHSU in which no heat transfer enhancement technique was employed. Owing to the lower thermal conductivity of PCMs, unfinned LHSU is unrealistic. But the effect of inclination could be different if any heat transfer augmentation technique is employed which needs to be thoroughly

investigated. However, minimal research is done on the effect of orientation on the thermal performance of LHSU in which fins are employed. Mahdi et al. [235] investigated the effect of orientation of LHSU with and without fins. Longitudinal fins were employed in their study. It was observed that the orientation has an insignificant impact on the LHSU performance when fins were employed. Borhani et al. [236] made use of a spiral fin structure for the enhancement of heat transfer and the influence of orientation was analyzed. 56% reduction in melting time was reported when LHSU was oriented vertically. Recently Zhang et al. [237] compared melting characteristics of PCM in vertical and horizontal orientations of LHSU with different types of fins viz. radial fins, longitudinal fins, double-helical fins, and quadruple helical fins. In the case of longitudinal and quadruple helical fins, horizontal configuration exhibited a higher heat transfer rate. On the other hand, vertical orientation was found to be superior when radial and double-helical fins were employed. Hence it can be stated that the effect of orientation could be different for different kinds of fins.

Annular fins divide the LHSU into a number of divisions and the presence of annular fins alters the flow of melted PCM. Hence the flow behavior will be completely different when compared with the flow in a LHSU with no fins or with any other kind of fins. Moreover, the effect of annular fins will be different in different orientations. Hence a detailed comparative analysis among different inclinations with annular fins is necessary to decide the optimum orientation of LHSU when annular fins are employed. Hence, in the present study, LHSU with solid annular fins and perforated fins are considered and the effect of inclination on its performance is examined. Both melting and solidification processes are analyzed using experimental investigations. The comparison among solid and perforated fins is presented in terms of temperature evolution, visualization of melt front, energy charging/discharging rate, energy efficiency, and exergetic performance.

6.2 Experimental procedure and temperature measurement

Experimental test facility, the description of which was given in chapter 3 (Fig. 3.1) is used to carryout the investigations on melting and solidification characteristics of PCM impregnated in a shell and tube LHSU at various orientations Shell and tube LHSU is made up of stainless steel (SS) tube and polycarbonate shell. The shell material is chosen so as to minimize the heat loss to the surroundings. Fins of thickness 0.8 mm are welded to the tube and SS is chosen as fin material. The dimensions of LHSU and fins are given in Fig. 6.1. Annular space of shell and tube is filled with 1670 grams of lauric acid whose thermophysical properties are given in

Table 6.1. The combination of lauric acid and SS is chosen because they do not undergo corrosion [207,208]. When the PCM temperature comes in equilibrium with the surrounding temperature (28ºC) the charging process is initiated. Longeon et al. [219] recommended top injection for the melting process. Hence, HTF from the hot water bath is fed from the top of the LHSU and from the bottom of LHSU water is pumped back to the hot water bath. After confirmation of complete melting through visual inspection, the charging process is terminated, and the discharging process is started by pumping cold water from the cold water bath. As the complete solidification cannot be confirmed by visual inspection, the discharging process is continued till all the thermocouples read solidus temperature. This procedure is repeated by placing the LHSU at 0º (vertical), 30º, 60º, and 90º (horizontal) inclinations. The experiments are initially conducted with unfinned LHSU, then LHSU with solid fins, and finally LHSU with perforated fins and comparison is made. It is to be noted that HTF inlet temperature is 80ºC for discharging process and 15ºC for discharging process. For both the processes HTF flow rate is taken as 1.4 litres per minute (LPM) which ensures laminar flow of the HTF.

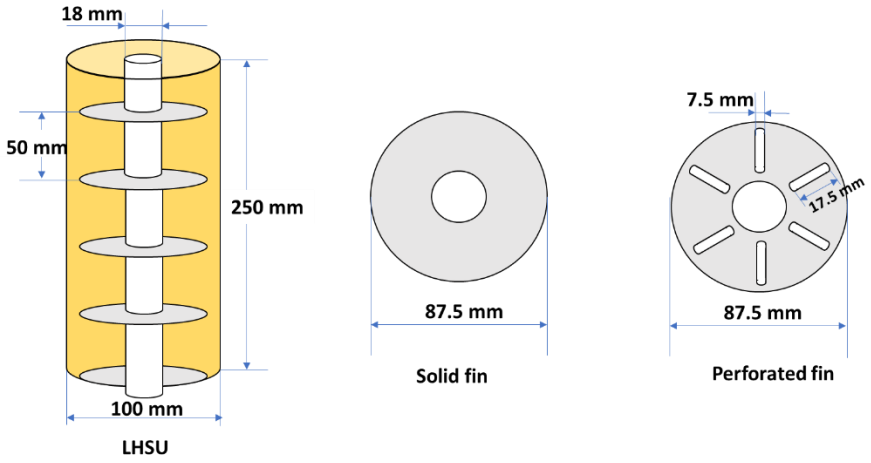

Figure 6.1: Dimensional details of LHSU, solid fin and perforated fin

Table 6.1: Thermophysical properties of PCM along with the uncertainty in measurement

Property	**Device used for the measurement**	**Value**	**Uncertainty**
Melting point	DSC	43.46ºC - 49.94ºC	±1%
Latent heat		156827 J/kg	
Specific heat		1390 J/kg K (s)/1570 J/kg K (l)	
Thermal conductivity	HotDisk thermal constants analyzer	0.227 W/m K (s)/0.388 W/m K (l)	±5%

To analyze the temperature distribution within the PCM, 9 k-type thermocouples are placed in the LHSU as shown in Fig.6.2 and two other thermocouples are provided to measure inlet and outlet HTF temperatures. The thermocouples are positioned in such a manner to record axial and angular temperature evolutions. In axial direction three thermocouples are provided, one is placed near to the top of LHSU, another one is at middle and the last one is placed near to the bottom of LHSU. In the angular direction, thermocouples are placed at 120º intervals. It is to be noted that the locations of thermocouples shown in Fig. 6.2 are for vertical orientation. When the LHSU is tilted, the plane A will be exactly below the tube i.e. in the lower half of LHSU, while the other two planes are in the upper half of LHSU. The thermocouple readings are recorded every two minutes using the data acquisition unit which is connected to a desktop.

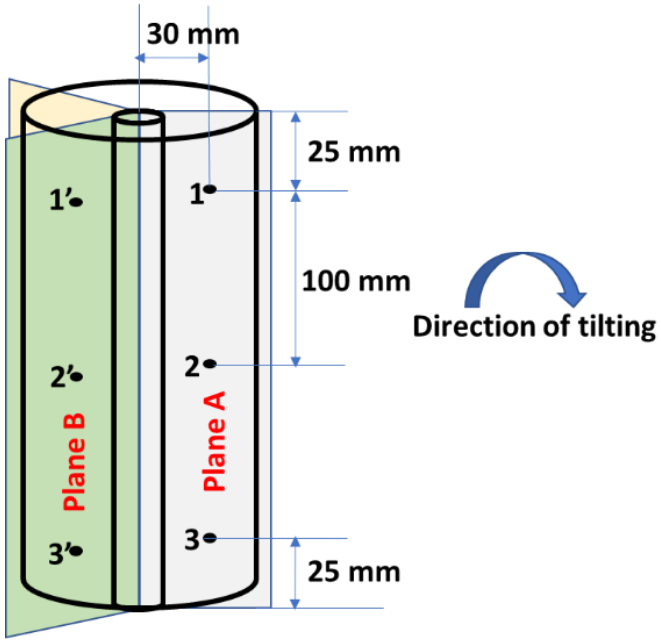

Figure 6.2: Location of thermocouples in vertical orientation

6.3 Results and discussions

6.3.1 Charging process

The charging process is initiated once all the thermocouples read the same temperature i.e., surrounding temperature which is equal to 28ºC. Upon receiving the heat from hot water the PCM starts to melt and through visual inspection complete melting of PCM is confirmed and then the charging process is terminated. Comparison of heat transfer characteristics of LHSU at different orientations with solid and perforated fins is presented by analyzing various

parameters viz. temperature evolution, melt profile, energy stored, exergy stored, and efficiency.

6.3.1.1 Temperature evolution

The temperature evolution at points 1, 2, 3 which are positioned in plane A (which can be considered as lower portion of LHSU in tilted position) is shown in Fig. 6.3. Irrespective of the type of fin used and the orientation except 90º (horizontal position), the thermocouple which is near to the top of the LHSU showed a higher rate of rise in temperature. This is attributed to the fact that the melted PCM flows towards top of LHSU because of buoyancy. In the case of 90º inclination (horizontal), all the thermocouples are positioned at the same level and hence no axial variation in the temperature is observed. With the increase in inclination the rate of rise in temperature at all the locations are observed to decrease. This is justified because of the ascendancy in conduction in the lower half of LHSU with the increase in inclination.

When perforated fins are employed, the thermocouples at points 1 and 2 exhibited higher temperature rise when compared to solid fins. Except in horizontal configuration, the thermocouple at 1 took 20 minutes lesser time to reach liquidus temperature when perforated fins are used. On the other hand, at point 2 the difference in time required to reach liquidus temperature is 14 minutes in case of vertical configuration and 6 minutes in 60º inclination. This indicates that employing perforations helped an increase in natural convection. But as the inclination is increased, the positive impact of the perforation is reduced and in horizontal configuration, the effect of perforations is completely nullified. It can also be observed that at the bottom thermocouple (at point 3), solid finned LHSU exhibited higher temperature rise in comparison with perforated fins. Providing annular fins can be considered as identical to dividing the LHSU into a number of segments. When perforations are not present the melted PCM is forced to circulate in the small segment whereas perforations cause the melted PCM to flow freely towards the top. This resulted in mild circulation in the bottom-most division of LHSU because of which the temperature rise at the bottom position is slower with perforated fins when compared to solid fins. Hence, it can be concluded that providing perforations on the fins resulted in a higher temperature rise at the top of the LHSU, and at the bottom of LHSU the rate of temperature rise is reduced.

Figure 6.4 shows the temperature evolution at the points 1′, 2′ and 3′ positioned at plane B (which is present in the upper half of LHSU in tilted position of LHSU). From the figure, it can be noticed that providing perforations in the vertical configuration is more beneficial as the rate

of temperature rise is more when compared to solid fins. At other orientations, not much difference in temperature rise is noted. As observed at point 3 of plane A, the point 3′ of plane B also exhibited lesser temperature rise when perforated fins are employed. To realize the cumulative effect of enhanced circulation at the top portion of LHSU and reduced circulation at the bottom portion, average temperature of PCM is analyzed and is presented in Fig. 6.5. As can be seen from the figure, irrespective of the fin type, with the increase in inclination the rate of rise in temperature is increased up to sometime after which it got reduced. As the LHSU is tilted from vertical to horizontal, natural convection in the upper half got intensified which resulted in a higher rate of temperature rise. As time progressed conduction became more dominant leading to the reduction in rate of temperature rise. It can also be observed that employing perforations is more advantageous in vertical configuration. At 30º and 60º orientations increase in the rate of temperature rise is very marginal and in horizontal configuration, perforations showed a negative impact due to lesser heat transfer area. Although in vertical configuration, perforated fins exhibited a rise in temperature during initial stages, the average temperature is more in the case of solid fins at the end of 180 minutes of charging. This is because at the bottom most part of LHSU the temperature rise is very low in case of perforated fins owing to diminished circulation at that portion.

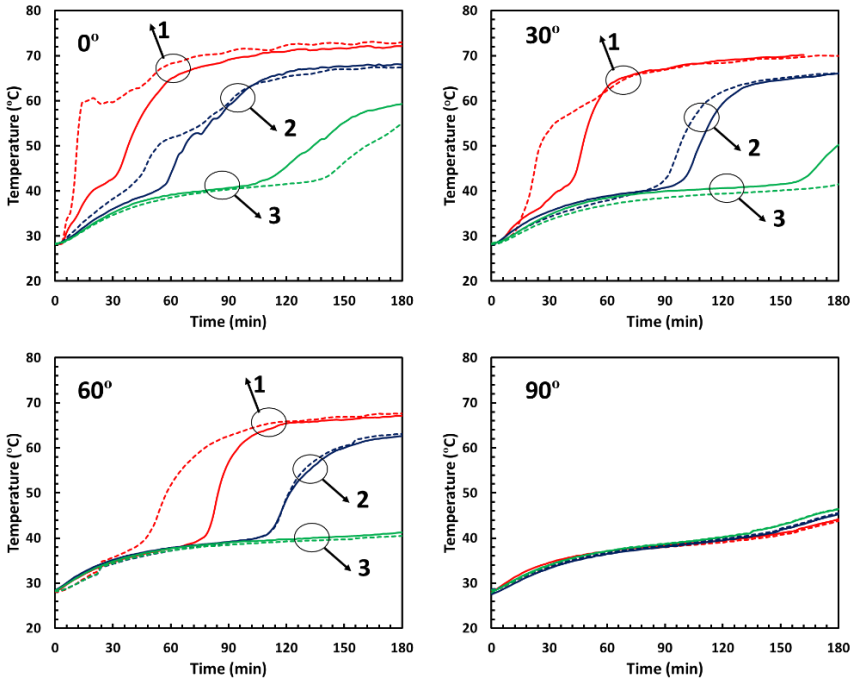

Figure 6.3: Temperature evolution at points 1,2 and 3 in solid finned (solid line) and perforated finned LHSU (dotted line)

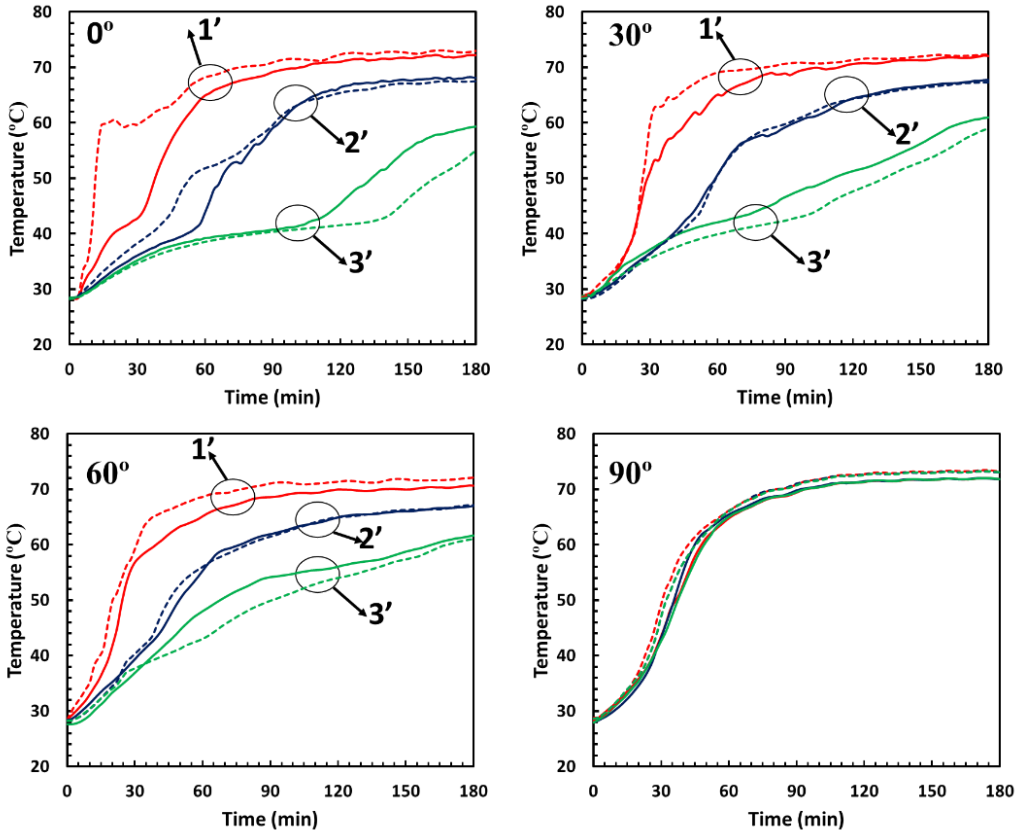

Figure 6.4: Temperature evolution at points 1',2' and 3' in solid finned (solid line) and perforated finned LHSU (dotted line)

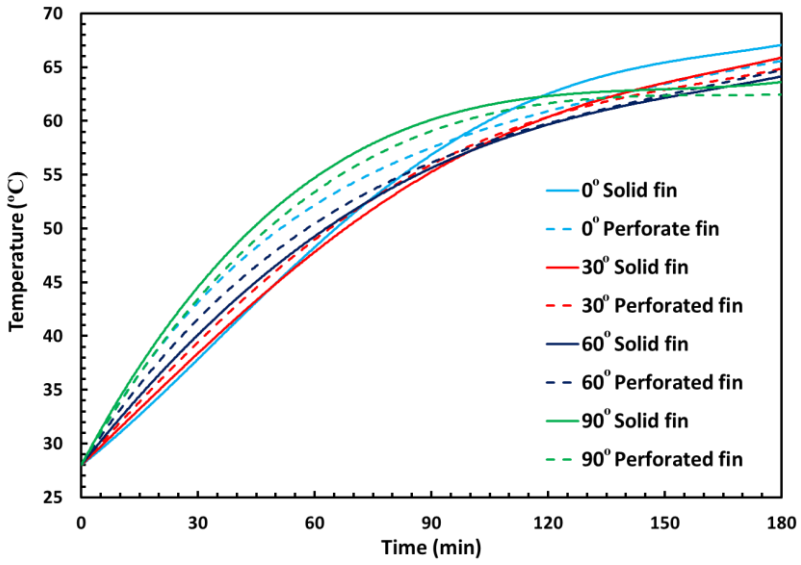

Figure 6.5: Comparison of average temperature of PCM at different inclinations

6.3.1.2 Comparison of melt profile

Melting behavior of the PCM can be well understood by analyzing the melt profile [201,231] and hence the experimental test section was designed so as to facilitate the visual inspection. To analyze and compare the melt profiles with different fins, photographs were taken at regular intervals of time and is presented in Fig. 6.6. The figure shows the instantaneous photographs of LHSU without fins, with solid fins and perforated fins taken at 60, 120, and 180 minutes of the charging process. The advantage of adding fins can be clearly seen from the figure and irrespective of the inclination both the types of fins helped in faster melting of PCM when compared to unfinned LHSU.

At 0º inclination (vertical configuration), the melted PCM is observed to exist adjacent to fins in the case of solid fins, whereas no such phenomenon is noted when perforated fins are employed. When perforations are not provided, the melted PCM is forced to flow along the fin and then it tends to flow upwards through the gap between fin and shell. On the other hand, perforations do not cause any obstruction to the flow of PCM and hence the melting is more pronounced in the axial direction. However, at the end of 180 minutes of the charging process, more unmelted PCM can be noticed in the case of perforated fins when compared to solid fins. Even though solid fins caused a restriction to the flow of melted PCM, it resulted in accelerated melting in the radial direction and also lead to circulation in the bottom-most division of LHSU (the division below the bottom-most fin). Hence, it can be stated that the providing perforations on the annular fins accelerated the melting process during initial stages, but at the bottom of LHSU, the melting rate is deteriorated in case of vertical orientation. When 30º and 60º orientations are analyzed, at 60 and 120 minutes of charging slightly more amount of melted PCM is observed in case of perforated fins. But to melt the PCM which is at the bottom of the LHSU, more amount of time is taken by perforated fins. In the case of horizontal orientation, the difference between solid and perforated fins is negligible with respect to melt profile, and the amount of PCM melted. This is justified as the perforations in horizontal orientation do not alter the flow of melted PCM.

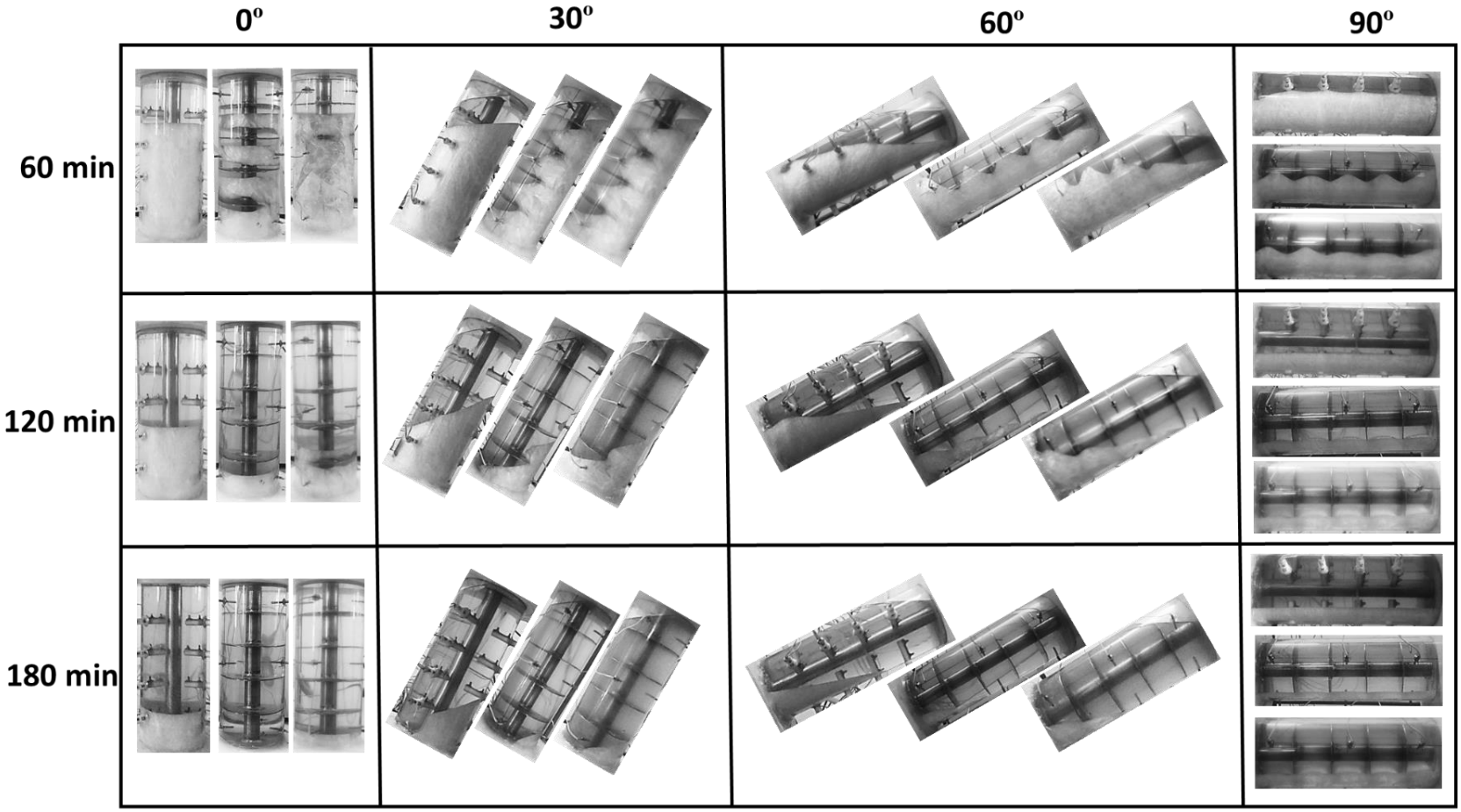

In each set of photographs first one corresponds to unfinned LHSU, middle one corresponds to solid finned LHSU and the last one corresponds to LHSU with perforated fins.

Figure 6.6: Instantaneous photographs of the melt front at various time levels

Comparison for the duration required by solid fin, and perforated finned LHSU to attain melt fraction values of 0.25, 0.5, 0.75, and 1 at different orientations are presented in Fig. 6.7. To reach 0.25 and 0.5 melt fractions horizontal configuration took lesser time in both types of LHSUs, whereas the least duration for complete melting is obtained in vertical configuration of both the LHSUs. With the increase in inclination, the total melting time is increased because of the predominance of conduction. When solid and perforated fins are compared, perforated fins are found to be superior in vertical configuration up to 0.75 melt fraction. To melt 75% of the PCM perforated fins took 10% lesser time in comparison with solid fins, but for complete melting 10.5% more time is required by perforated fins. At other orientations, more time is required by the perforated fins to reach melt fractions of 0.75 and 1 when compared to solid fins. Hence, irrespective of the inclination for complete melting solid fins are preferred as it exhibited a lesser melting time. On the other hand, for partial melting (up to 0.5 melt fraction) perforated fins are beneficial except for horizontal orientation.

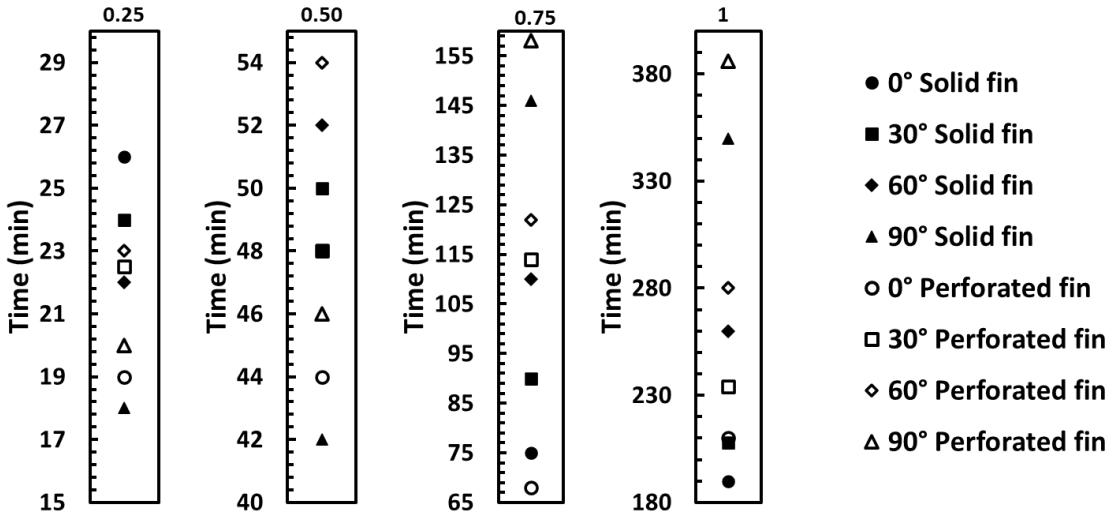

Figure 6.7: Time taken by solid finned and perforated finned LHSU to reach melt fraction of 0.25, 0.5, 0.75 and 1

6.3.1.3 Energy storage characteristics

Figure 6.8 illustrates the comparison of cumulative energy stored in solid finned and perforated finned LHSU at various orientations. Till the PCM starts melting the energy stored will be in the form of sensible heat and then latent heat gain will take place. After complete melting, sensible heat gain will occur. Majority of the heat stored is through latent heat and hence the LHSU which exhibits a higher melting rate will absorb the heat more quickly. As the natural

convection accelerates the melting process, the configuration of LHSU which enhances the natural convection is expected to store more heat in lesser time. After 60 minutes of charging, energy stored is found to be highest for vertical perforated finned LHSU followed by horizontal solid finned LHSU. In both these configurations, the natural convective flow is more pronounced during the early phase of melting and hence this behavior is justified. At 120 minutes, horizontal configuration with both types of fins has the lowest cumulative energy stored. This indicates that the natural convection is diminished very quickly in the horizontal configuration. After 180 minutes of the charging period, vertical solid finned LHSU attained the highest energy storage. It is worth noting that providing perforations in vertical configuration did not result in increased energy storage. Also, at other inclinations perforated LHSU has lesser heat storage when compared to solid finned LHSU. More insight on this behavior can be obtained by analyzing the rate of energy storage.

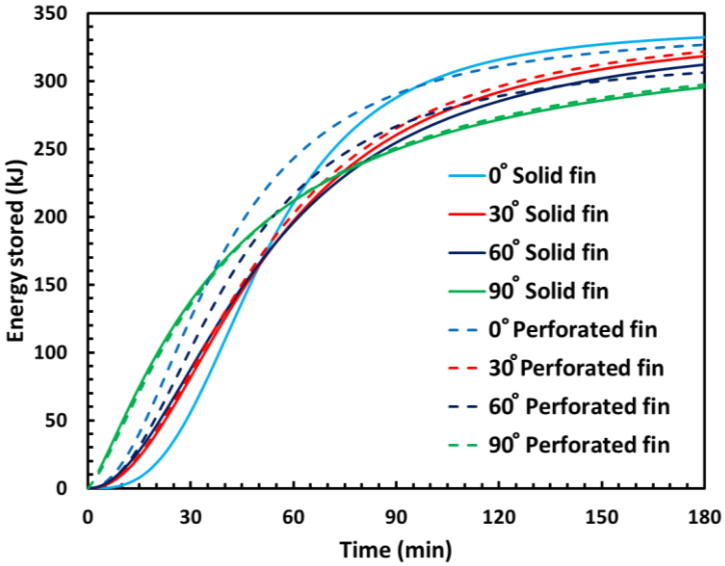

Figure 6.8: Plot showing time vs cumulative energy stored

Figure 6.9 shows the time-wise variation in the rate of energy stored at all the considered orientations. A general overview of the figure shows that the rate of energy storage is less at the staring of melting which got increased as the melting progresses. After a certain period, the rate of energy storage showed a decreasing trend and became nearly constant towards the end of melting. This behavior can be inferred to different stages in the melting process: conduction at initial stages, onset, and intensification of natural convection, diminishing convection, and conduction dominant at the end of the charging process. Initially, heat is transferred to the PCM via conduction because of which energy storage rate is less. As the PCM starts to melt, natural convection prevails which caused a rise in energy storage rate. With the progression in time

convection currents diminish, at the final stages melting takes place by taking heat via conduction, and hence the rate of energy storage is very less at the final stages of the charging process.

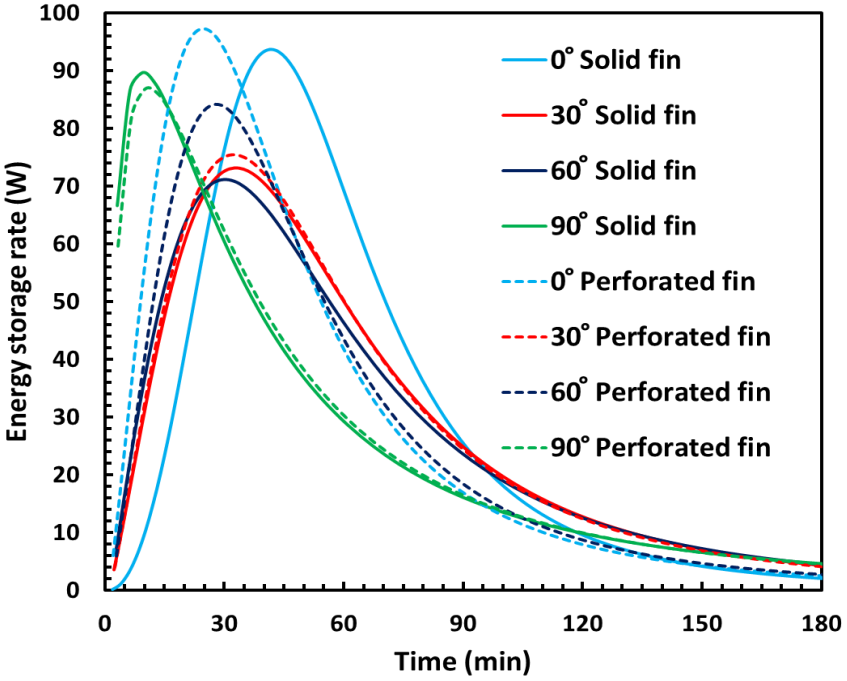

Figure 6.9: Variation in energy storage rate with respect to time

Horizontal configuration with both the types of fins has the highest energy storage rate at the starting which indicates that the natural convection prevailed more quickly when compared to other configurations. But the rate of energy stored started decreasing much earlier indicating that the natural convection diminished very quickly. Similar to the horizontal configuration, vertical configuration with perforated fins has a higher energy storage rate during initial stages and natural convection remained effective for more time when compared to horizontal configuration. Providing perforations on the fins helped in intensifying natural convection during initial stages and hence the higher energy storage rate is noted during initial period. On the other hand, the rise in the energy storage rate is found to be least for vertical configuration with solid fins. But the decrement in the rate of energy stored is also found to be less for this configuration.

Figure 6.10 shows the time-averaged energy storage rate for different configurations. When the effect of inclination is compared, with the increase in inclination (from vertical to horizontal) time-averaged energy storage rate got decreased irrespective of the type of fin. Providing fins increased the time-averaged energy storage rate at all the inclinations. Time-

averaged energy storage rate is highest for vertical configuration with solid fins and lowest for horizontal configuration with perforated fins. Vertical configuration with perforated fins has the second highest value of energy storage rate of 26.7W.

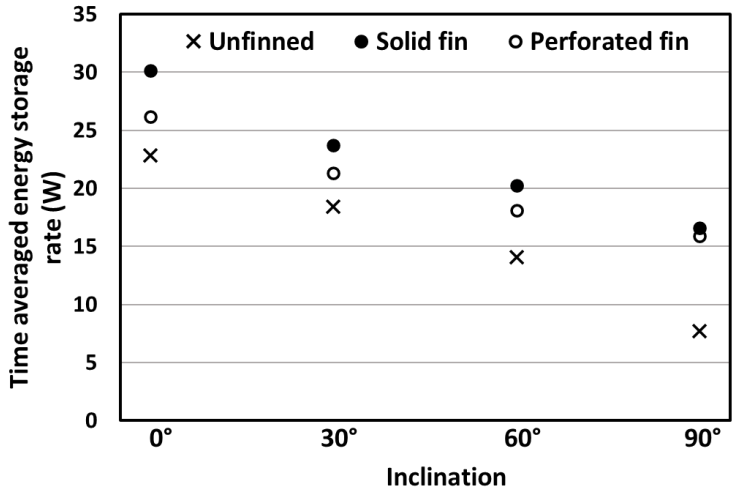

Figure 6.10: Time-averaged energy storage rates for unfinned, solid finned and perforated finned LHSU at different inclinations

Energy efficiency of LHSU with solid and perforated fins is presented in Fig. 6.11(a). Similar to the rate of energy storage trend, energy efficiency also increased up to some time and then decreased. When solid fins are employed, LHSU at horizontal configuration quickly attained a higher value of energy efficiency and immediately started to decrease. On the other hand, vertical configuration slowly attained a higher value of energy efficiency, and then the decrement in energy efficiency is lesser in comparison with other inclinations. This is because the natural convection remained effective throughout the charging process in vertical configuration but in horizontal configuration, conduction becomes more dominant for most of the time. When perforations are provided on the fins, the rate of increment in energy efficiency is observed to increase for all the inclinations except for horizontal orientation. In the same way, the decrement in energy efficiency after attaining peak energy efficiency is also noticed to be higher when perforations are provided. This indicates that the perforations intensified the natural convection in the early stages of melting but towards the end, the heat transfer became more conduction dominant. In the horizontal configuration, perforations has a negligible effect on energy efficiency.

Exergy efficiency is defined as the ratio of exergy stored to exergy input. Figure 6.11(b) shows the comparison of exergy efficiency among solid fins and perforated fins at various orientations. From the figure, it can be noticed that LHSU with solid fins has relatively higher

exergy efficiencies for majority of the charging process at all the orientations. During the early stages of melting, perforated fins showed slightly higher exergy efficiency, but it reduced significantly in the later stages of melting. Exergy stored mainly depends upon the average temperature of the PCM which was observed to be less in case of perforated fins in the latter stages of melting. This could be the reason for the reduction in exergy efficiency when perforations are provided on the fins.

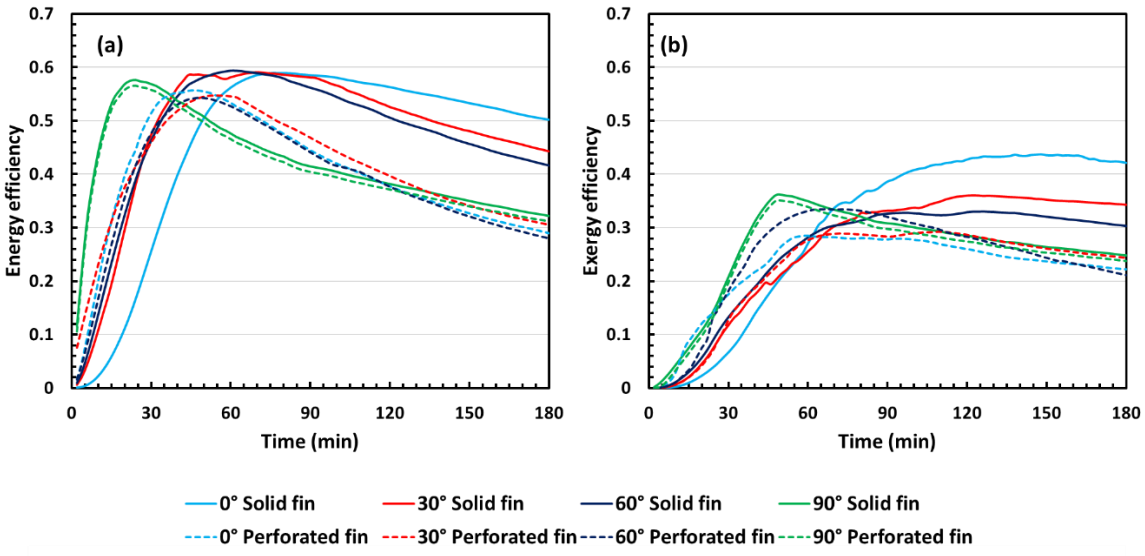

Figure 6.11: (a) Energy efficiency (b) exergy efficiency of LHSU with different fins

6.3.1.4 Fin effectiveness

The main purpose of a heat storage unit is to store the energy and hence the definition of fin effectiveness is slightly modified and is given in terms of energy storage rate. Fin effectiveness is defined as the ratio of time-averaged energy storage rate of LHSU with fin to that of unfinned LHSU. Figure 6.12 shows the comparison of fin effectiveness at various orientations. Employing fins in horizontal configuration exhibited the highest effectiveness as the fins substantially improved the melting rate at the bottom half of LHSU. It can also be noted that perforated fins have slightly lesser effectiveness when compared to solid fins at all the orientations. In the present study, the number of fins employed is 4, and thus it might not have a considerable effect on the circulation of melted PCM. Hence providing perforations did not result in higher effectiveness. When higher number fins are used perforations could be more effective which can be investigated further.

The analysis of the melting process revealed that the inclination has a considerable effect on the charging process. Melting rate and energy storage rate are higher for horizontal configuration in the initial stages which got reduced in the later stages. The diminishing of natural convection during the latter stages of melting in the horizontal configuration is the prime reason for this behavior. By providing the perforations the natural convection is intensified and hence melting rate is increased in the initial stages at all the orientations except in horizontal configuration. But towards the end of melting, conduction became dominant and due to the fact that the perforated fins have lesser heat transfer area, solid fins are found to be superior. Perforated fins can be a promising option to intensify the natural convection, but the optimization of various fin parameters and shape of perforations need to be carried out in order to make them effective for the entire period of charging process.

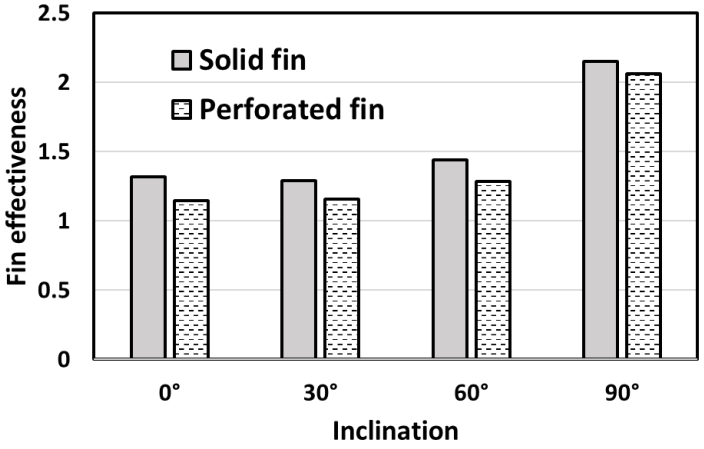

Figure 6.12: Comparison of fin effectiveness

6.3.2 Discharging process

After complete melting, the discharging process is initiated by pumping water from the cold bath through the tube. It is to be noted that before starting the discharging process i.e. at the end of melting the temperature of the PCM is not uniform. The temperature gradient within the melted PCM continued to be existing even after 20 hours of charging. Hence to compare the performance of LHSU at various orientations and with different fins, it is made sure that the average temperature of the PCM at the starting of the discharging process is same. Unlike the melting process, complete solidification cannot be confirmed by visual inspection as some voids may be present within the solid PCM. Hence the performance comparison is presented only in terms of average temperature and energy discharge characteristics.

Figure 6.13(a) presents the transient variation in the average temperature of PCM and energy discharged during the solidification process at all the orientations and with both the types of fins. As can be seen from the figure all the curves are close to each other which indicates that orientation did not have any influence on the solidification process. This is because the solidification process mainly depends upon conduction which is independent of orientation. Natural convection has a minor effect on solidification and hence providing perforations also did not show an ample impact. Similar to the average temperature, energy discharged also did not get affected by the orientation. The rate of energy discharged is slightly slower when perforated fins are employed. It is also observed that within 40 minutes of discharge, the temperature reached solidus temperature which indicates that the latent heat stored has already been retrieved by that time. Hence, the rate of decrease in average temperature also reduced after 40 minutes of discharging. Figure 6.13(b) shows the energy and exergy efficiencies of LHSU for the discharging process. It can be observed that both the efficiencies started from a higher value and gradually decreased, and finally it became constant. Immediately after introducing the cold fluid, a thin layer of solid PCM is observed around the tube. This acts as thermal resistance and with the increase in solid layer thermal resistance increases. Hence the efficiency is decreased with the progression in time.

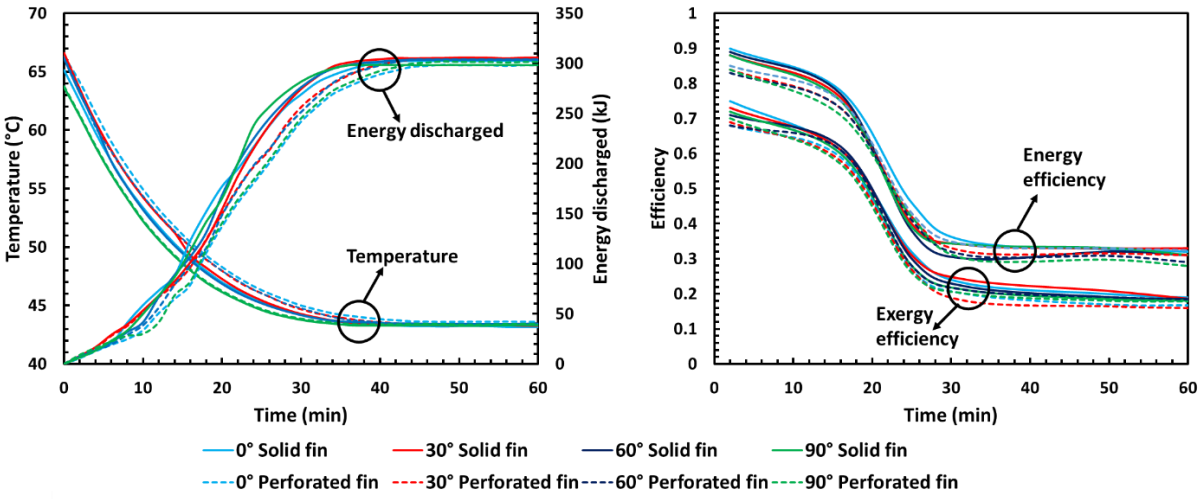

Figure 6.13: (a)Time wise variation in average temperature and energy discharged by the PCM in various configurations of LHSU (b) Energy and exergy efficiencies

6.4 Closure

Experiments are carried out to compare the performance of LHSU with solid fins and perforated fins. Effect of inclination is also studied using both the fins and comparison is made

in terms of temperature evolution, melt profile, energy storage characteristics. The following conclusions are drawn from the current study.

- By varying the orientation of LHSU from vertical to horizontal, natural convection in the upper half became intense, and at the same time conduction became more dominant in the lower half of LHSU. This behavior is observed to be the same for both solid and perforated annular fins.
- In vertical orientation, providing perforations to the fins caused the rate of temperature rise to be higher in the initial stages of charging. This effect gradually got nullified with the increase in inclination.
- Total melting time is observed to be lower for vertical orientation with solid fins. However, to reach 0.5 and 0.75 melt fractions horizontal configuration with solid/perforated fins and vertical configuration with perforate fins are found to be superior.
- Time-averaged energy storage rate is approximately 10% more in the case of solid fins when compared to perforated fins for all inclinations except in horizontal configuration.
- Time-wise energy and exergy efficiencies are maintained at a higher level for a longer period of time in the case of vertical LHSU with solid fins.
- For solid finned LHSU fin effectiveness is observed to be nearly 5% more than the perforated fins at all the inclinations.
- During the solidification process, inclination did not show any impact as the thermal transport is conduction dominant.
- Perforations on fins do not have ample effect on the discharging process.

Perforated fins in the vertical configuration showed better heat transfer characteristics in the initial stages of melting. But towards the end of melting solid fins are found to be superior. Certainly, perforated fins could be a promising option to augment the melting rate but optimization of perforated size, shape, and number of fins should be carried out.

Chapter 7

Optimization of fin parameters to reduce entropy generation and melting time of a latent heat storage unit

7.1 Introduction

One of the challenges in the design and development of a latent heat storage unit (LHSU) is to increase the charging and discharging rates which are inherently low because of low thermal conductivity of phase change materials (PCM). To overcome this issue, two types of fins (solid and perforated fins) were employed and it was observed that solid fins are preferable for complete melting. Fin parameters (fin size and number of fins) significantly influence the enhancement in heat transfer rate. Hence, optimization of fin parameters is necessary for the efficient design of a LHSU.

In the literature optimization of fin parameters was done to maximize the melting rate and energy storage rate. But, as indicated by Bejan [117] the purpose of the thermal energy storage system is not to store the energy but to store the useful work. Hence, the exergy analysis must be done while designing LHSU. Various authors [224–226,228,229,238] carried out the second law analysis of LHSU and reported a significant difference (15%-50%) between energy and exergy efficiencies. Hence, it can be stated that the irreversibilities associated with energy storage must be accounted. In the literature, various expressions are available for calculating exergy efficiency for the charging and discharging process which were consolidated by Jegadheeswaran et al. [233]. However, by calculating the exergy efficiency one can only get the information about how much exergy is being destroyed. But to optimize the design, one should have an idea about the distribution of the entropy generation which is scarce in the literature. Bejan [239] has stated that optimization of LHSU through exergy analysis is different from optimization through entropy generation analysis. Hence, an attempt is made in the current study to demonstrate the methodology to calculate local entropy generation and to analyze the entropy generation distribution.

Guelpa et al. [227] carried out entropy generation analysis and proposed new fin arrangements to minimize the total solidification time of the PCM. An interesting feature was reported by the authors in this work. With the increase in number of fins, solidification time was reduced but the global entropy generation was increased. Hence, it can be concluded that the fin configuration which results in higher solidification rate may not reduce the entropy generation.

This aspect needs to be investigated for the melting process which is yet to appear in the literature. Rathod and Banerjee [240] carried out entropy generation analysis of LHSU for melting process, but no fins were employed. Li [241] documented various works available on the energy and exergy analysis of LHSUs. From his extensive literature survey, it was concluded that the exergy performance evaluation with the effect of fins was lacking. Hence, the present study deals with the exergy analysis with various fin parameters and optimization is carried out to make LHSU efficient in terms of energy and exergy.

The optimization of fin design should be done to achieve two objectives: to minimize melting time and to minimize entropy generation. Hence, multi-objective optimization has been carried out in the present study. This work presents a detailed investigation of time-wise entropy generation distribution along with the multi-objective optimization of fin parameters. The present study is the first-ever work in this regard and the analysis will be helpful for the design improvement of LHSU.

7.2 Model description

Fig. 7.1 depicts the physical model and computational domain considered for the current study. A vertical shell and tube LHSU of length 250 mm is considered with a shell diameter of 100 mm and the inner diameter of the tube is 15 mm. The tube is considered to be made of stainless steel (SS) because of its anti-corrosive nature [207] and has a thickness of 1.5 mm. Annular fins made of stainless steel with a diameter "D_f" and thickness "t_f" are attached to the tube for heat transfer intensification. The fins are equally distributed with a pitch (center to center distance) of "p_f". Water is chosen as heat transfer fluid (HTF) and is fed from the top as recommended by Longeon et al. [219]. The inlet temperature of HTF is kept constant at 80°C and the flow rate of the HTF is 1.4 LPM. Flow rate is chosen so as to make the flow to be in the laminar regime. The Reynolds number for the considered flow rate is 1950. The employed flow rate ensures high transit time of HTF so that the temperature difference between inlet and outlet of LHSU will be more which is desired in the practical scenario. The entire annular space is filled with lauric acid. Lauric acid is chosen due to its stable properties and it does not corrode with stainless steel [208]. Melting point, latent heat and specific heat of lauric acid are measured using Differential scanning calorimeter (DSC). Thermal conductivity is measured using Hot Disk-TPS 500 thermal conductivity analyzer. Viscosity and density are measured with RheolabQc rheometer and pycnometer respectively. Thermal expansion coefficient is calculated by measuring the expanded liquid PCM volume in a thin long borosil cylinder of 3

mm diameter over a temperature rise. Calibration of thermocouples is carried out with "Julabo SL-8K" calibration bath and the uncertainty is observed to be ±0.3ºC. The uncertainty associated with the flow meter is 1%. To determine the measurement uncertainty of thermophysical properties a statistical approach as mentioned by Khan et al.[242] is used. Each property was measured three times and the uncertainty is evaluated from standard deviation. To calculate the uncertainty of thermal expansion coefficient, the method of propagation of errors is employed as it is a dependent variable. The uncertainties in measuring various thermophysical properties are provided in Table 7.1. For all the numerical simulations, initial temperature of the PCM is taken as 303.16 K. The simulations are performed on an axi-symmetric domain in order to reduce computational time and the computational domain is shown in Fig. 7. 1(b).

Table 7.1: Properties of lauric acid

Property	**Instrument used**	**Value**	**Uncertainty in measurement(%)**
Solidus temperature (T_s)	Differential scanning calorimeter (DSC)	43.46°C	0.32
Liquidus temperature (T_l)		49.94°C	0.25
Latent heat (L)		156827 J/kg	0.43
Specific heat (c_p)		1390 J/kg K (s)	1.07
		1570 J/kg K (l)	0.78
Density (ρ)	Pycnometer	1051.20 kg/m^3 (s)	0.8
		885.04 kg/m^3 (l)	0.82
Thermal conductivity (k)	HotDisk thermal constants analyzer	0.227 W/m K (s)	0.5
		0.388 W/m K (l)	0.93
Thermal expansion coefficient (β)	Calculated by measuring expanded liquid volume in a borosil cylinder	9.25×10^{-4} K^{-1}	0.85
Dynamic viscosity (μ)	Rheometer	4.35×10^{-3} Pa s	0.48

.

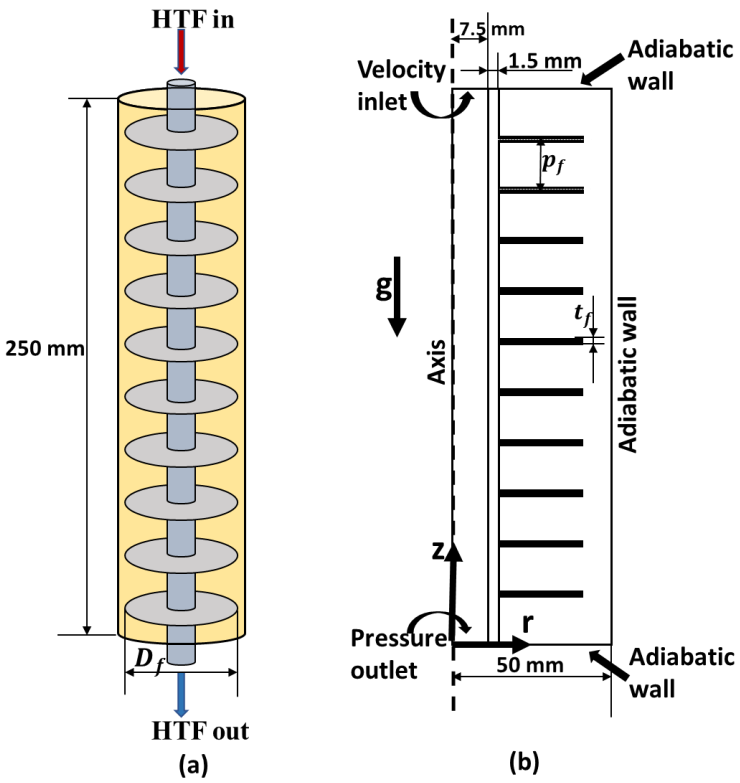

Figure 7.1: (a) Schematic of LHSU with annular fins (b) computational domain

For the numerical simulations, enthalpy porosity approach is adapted details of which are given in chapter 3 (section 3.3).

7.3 Parameters definition

Various parameters are used to compare the performance of LHSU with annular fins of different dimensions (fins diameter, thickness, and pitch) details of which are provided in this section. As explained in section 1, entropy generated during energy storage is one of the key parameters to be analyzed. There are two contributors to entropy generation: one is fluid friction and the second one is heat transfer or temperature gradient. The entropy generation in a control volume is given by the following equation [227].

$$s_p = \frac{-\overrightarrow{J_q}.\nabla T}{T^2} + \frac{\Delta : \tau}{T} \tag{7.1}$$

Here, $\overrightarrow{J_q}$ is the heat flux which can be obtained by Fourier's law ($\overrightarrow{J_q} = -k\nabla T$), Δ and τ are stress and strain tensors respectively which are given by Eqs. 7.2 and 7.3.

$$\Delta = \frac{1}{2}\left(\frac{\partial v_i}{\partial x_j} + \frac{\partial v_j}{\partial x_i}\right) \tag{7.2}$$

$$\tau = \mu\left(\frac{\partial v_i}{\partial x_j} + \frac{\partial v_j}{\partial x_i}\right) \tag{7.3}$$

Integrating local entropy generation over the entire volume gives the entropy generated in the entire LHSU.

$$S_p = \int s_p \, dV \tag{7.4}$$

For comparing heat transfer rate between HTF and PCM, the average Nusselt number is defined as follows [243]

$$\overline{Nu} = \frac{W}{k}\frac{q''}{(T_w - T_m)} \tag{7.5}$$

Where 'W' is the characteristic dimension of LHSU which is taken as the outer diameter of the tube, q'' is the average heat flux on the tube wall, 'k' is the thermal conductivity of the PCM, 'T_w' is the tube wall temperature and 'T_m' is the melting temperature of the PCM.

7.4 Grid independence and validation

7.4.1 Grid independence and time-step independence

For any transient problem, the results are significantly influenced by the mesh quality and the time step. Hence, both grid independent study and time step sensitivity studies are carried out to arrive at the appropriate combination of mesh size and time step. Simulations are carried out by employing different mesh sizes and time steps for a LHSU with 5 annular fins. Melt fraction evolution is compared to decide the mesh size and time step. Fig. 7.2(a) depicts the melt fraction evolution for different mesh sizes with a time step of 0.1s. It can be noticed that the melt fraction evolution curves corresponding to 66734 and 80297 number of elements coincided with each other. Hence, an element size corresponding to 66734 elements is chosen for the study. By using this element size, three different time steps 0.2s, 0.1s and 0.05s are employed and the melt fraction evolution is compared. Fig. 7.2(b) shows the results pertaining to time step independence. It can be noted that a time step of 0.1s is sufficient enough as there

is no significant difference in the results by employing a lesser time step (0.05 s). Hence, a time step of 0.1s is employed to perform the numerical experiments.

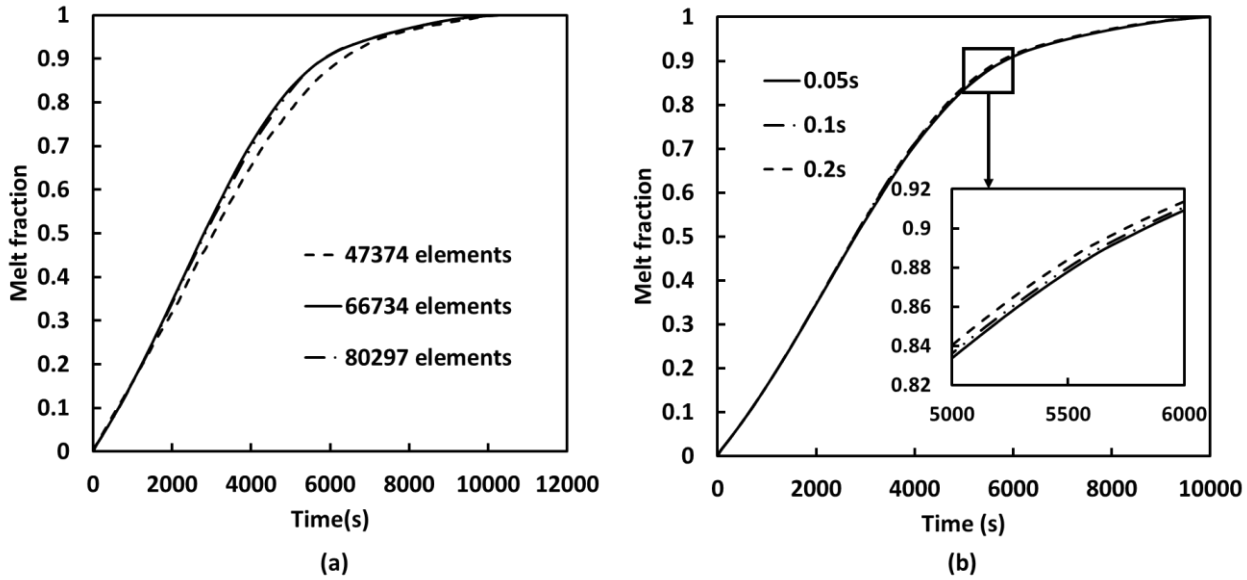

Figure 7.2: Plots showing (a) grid independence (b) time step independence

7.4.2 Experimental validation

To validate the adapted numerical methodology, the temperature evolution obtained from numerical simulation is compared with the previously conducted experimental readings. Comparison is made among Temperature evolution of PCM at a point location of which is shown in Fig. 7.3. the dimensional details of LHSU and fins are same as that of LHSU considered in the previous chapter. Though the thermal conductivity of shell material is very low, some heat loss to the surroundings takes place. To account for this heat loss, the convective boundary condition is given on the shell wall and the heat transfer coefficient is calculated by the following empirical correlation [96].

$$h = \frac{0.59k}{D}(Gr\ Pr)^{0.25} \tag{7.6}$$

Where 'D' is the shell diameter, Gr and Pr are Grashof number and Prandtl number of air respectively.

Figure 7.4 shows the comparison of numerical results with experimental results via temperature evolution at a given point. Error bars show the deviation of ±5%. With the uncertainty associated with experimental measurements, 5% deviation is acceptable. This indicates the feasibility of adapted numerical methodology to be extended for further study.

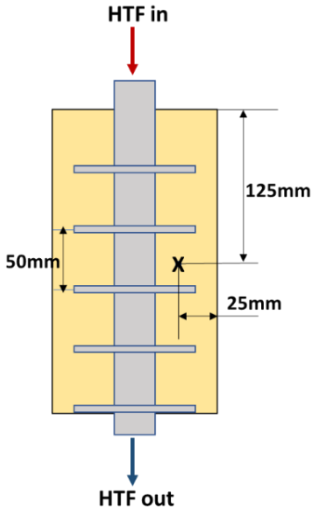

Figure 7.3. Location of thermocouple

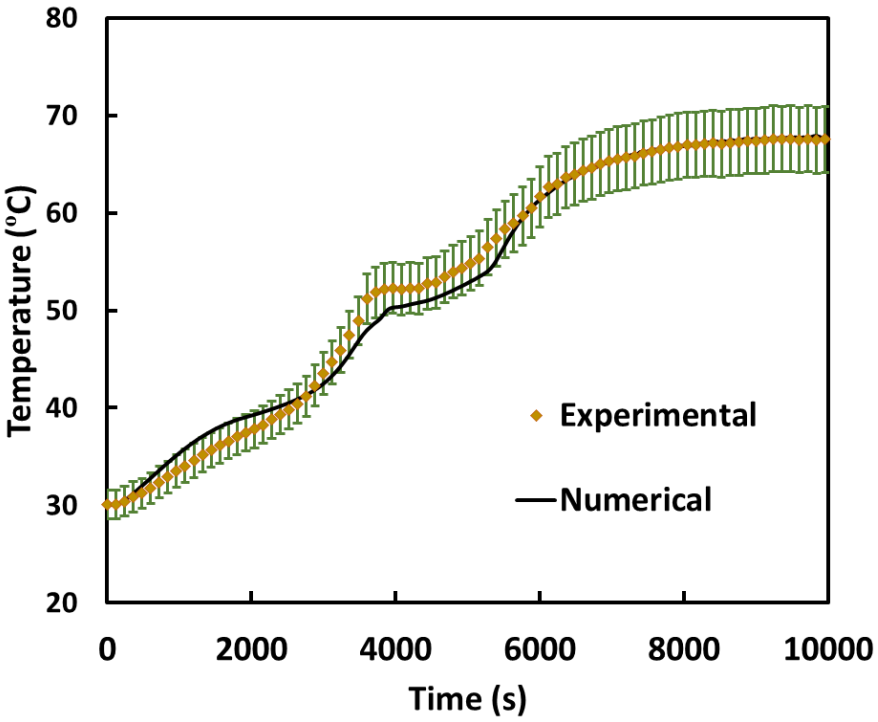

Figure 7.4: Comparison of numerical results with the experimental results

7.5 Results and discussions

It is a proven fact that the heat transfer enhancement is possible by adding fins and LHSU is no exception for this. However, in a thermal energy storage system natural convection plays a crucial role during the melting process. By adding a greater number of fins, there is a possibility of suppression of natural convection currents thereby it poses a negative impact on the melting

rate. Entropy generated is another important factor to be considered while designing LHSU. Entropy generation gets largely influenced by temperature gradient which in turn affected by different fin parameters. Hence, optimization of fin parameters is necessary for the optimum performance of a LHSU.

By keeping the ratio of fin volume to total annular space fixed at 1.25%, fin parameters are varied. Fin diameter and number of fins are taken as the variables. Fin thickness and fin pitch become dependent on fin diameter and number of fins. Table 7.2 provides the details of various cases considered for optimization. It is to be noted that the number of fins can be increased further but it results in fin thickness to be very low for which fabrication becomes extremely difficult. Hence, 0.25 mm is kept as the lowest thickness of the fin and accordingly maximum number of fins for different fin diameters is calculated.

Table 7.2: Fin parameters for different cases

D_f (mm)	N	t_f(mm)	p_f(mm)
100	5	0.628	41.67
	10	0.314	22.72
90	5	0.781	41.67
	10	0.39	22.72
	15	0.26	15.62
80	5	1.0	41.67
	10	0.5	22.72
	15	0.333	15.62
	20	0.25	11.90
70	5	1.328	41.67
	10	0.664	22.72
	15	0.442	15.62
	20	0.332	11.90
	25	0.265	9.61

7.5.1 Effect of number of fins

The effect of number of fins is analyzed at all the considered fin diameters, but for brevity, the results corresponding to a fin diameter of 80 mm are presented in this section. Initially melt fraction evolution is analyzed for different number of fins. Fig. 7.5 shows the contours of melt fraction at different time levels for 5,10,15 and 20 number of fins. Irrespective of the fin number, the melting of PCM is initiated from the tube wall and then melt front propagated to

other parts of the LHSU. With the progression in time the melting phenomenon is favored by two mechanisms. Because of the temperature rise in annular fins the PCM in the vicinity of fins started melting by taking heat from the fins via conduction. The second one is free convection because of which the melted PCM proceeds towards the top portion of the LHSU. Annular fins divide the energy storage unit into number of divisions and act as obstruction for the PCM to flow towards top. This causes the melted PCM to accumulate at the bottom portion of the fin and the PCM is made to circulate in the space between two fins. Hence, the LHSU with annular fins is similar to number of unfinned LHSUs with a smaller length.

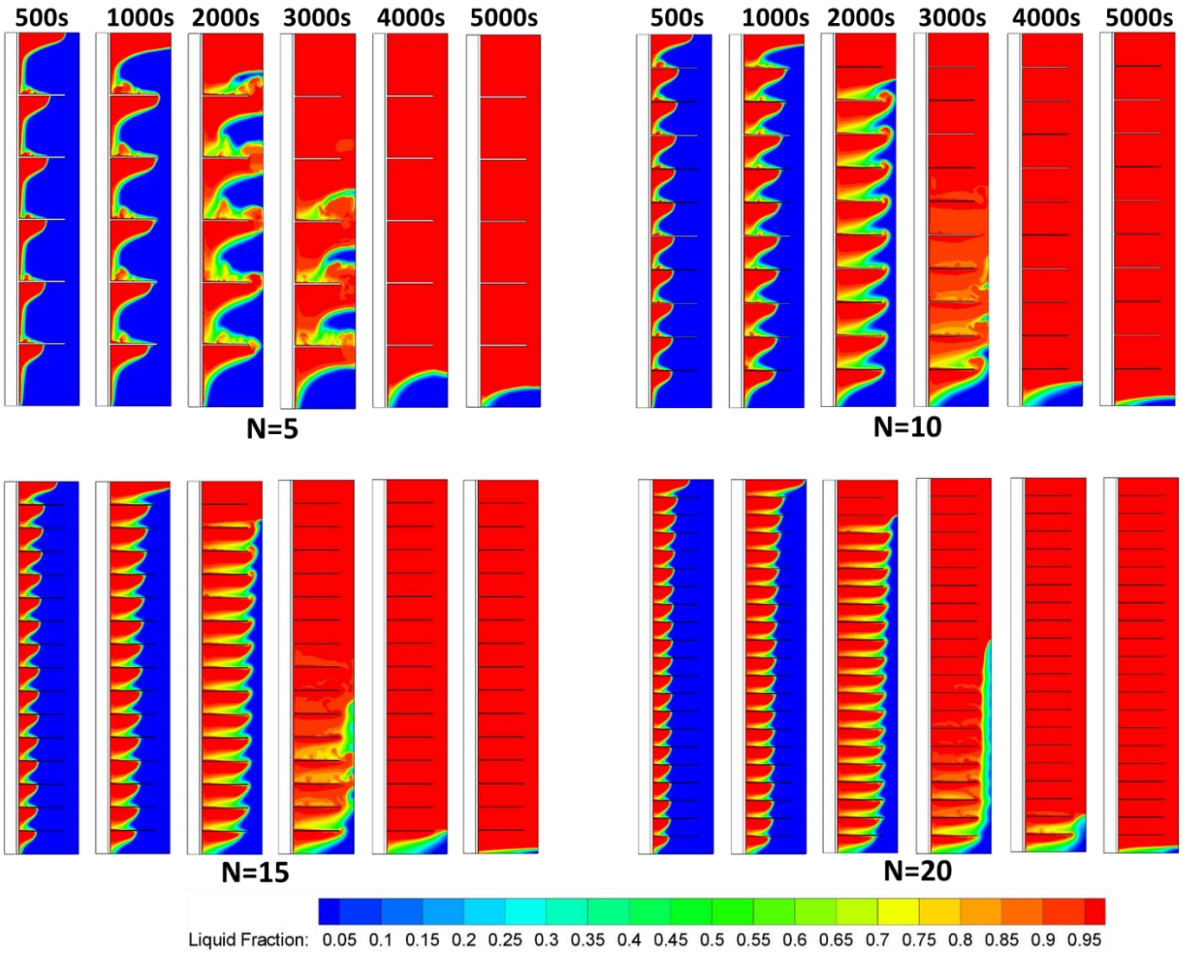

Figure 7.5: Contours of melt fraction at different time levels

The thermal transport in the PCM takes place by means of conduction and convection. It may be noted that for N=20 case, the last fin (bottom most fin) is present closer to the bottom of LHSU when compared to N=15 case. The increase in surface area with the increase in fin number increases the thermal transport by conduction due to which larger liquid fraction can be noted at the bottom. But for N=20 case, space between the two consecutive fins reduces leading to the decrease in convective strength which in turn increases the melting time. A

quantitative comparison of melt fraction is made to analyze the combined effect of increase in conduction mode heat transfer and suppression in free convection. Fig. 7.6(a) shows the melt fraction evolution for different fin number. It is observed that the slope of melt fraction curve changed abruptly after a point which is indicated as inflection point in Fig. 6(a). The slope of the curve after the inflection point is observed to be almost equal for any number of fins. This indicates that after inflection point, the enhancement in heat transfer is hindered and the melting rate is same. This inflection point is observed to exist irrespective of fin number. The earlier (at a lower melt fraction) the occurrence of inflection point, the worse the performance of LHSU. Out of all the fin numbers considered, the inflection point has occurred at a higher melt fraction for a fin number of 15. Fig. 7.6(b) shows the total melting time under different number of fins. From Fig. 6 it can be concluded that among considered fin number, 15 number of fins is optimum to have a lesser melting time.

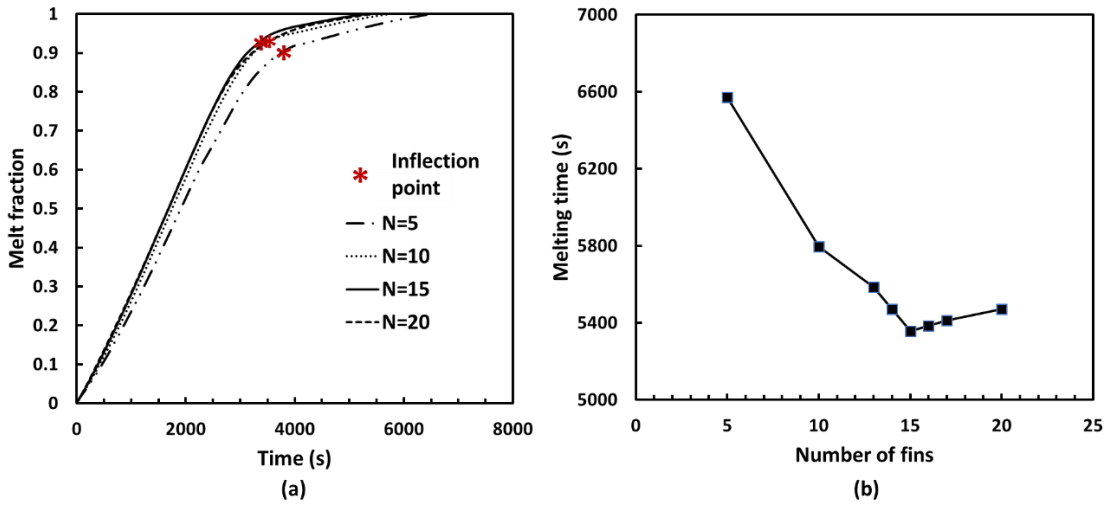

Figure 7.6: (a) Melt fraction evolution (b) Effect of number of fins on total melting time

Fig. 7.7 shows the transient variation in average Nusselt number for different number of fins. Immediately after the HTF is introduced the PCM adjoining the tube easily absorbs the heat and a thin layer of melted PCM is observed to be formed around the tube. The formation of liquid PCM layer acts as resistance to heat transfer which caused a sudden reduction in Nusselt number during the initial period of melting. Then the onset of natural convection caused the Nusselt number to increase again. As time progresses, the intensity of natural convection gradually diminishes and hence a reduction in Nusselt number has occurred. Towards the end of the melting process, the temperature of the liquid PCM becomes uniform because of which circulation inside the liquid PCM will be almost negligible. This caused a very low Nusselt number at the final stages of melting. As can be noticed from Fig. 7.7 increase in the number

of fins caused an increase in the average Nusselt number. For N=20, though the average Nusselt number is more at the beginning, it did not sustain for a longer time. This can be inferred to the insufficient space available for the liquid PCM to circulate freely. Time-averaged Nusselt number is found to be higher for N=15 followed by 20,10 and the least being N=5 which is in line with the total melting times.

Fig. 7.8 shows the plot between time and energy stored by the PCM. As can be noted from the figure, the energy storage rate is improved with the increase in number of fins up to 15. For N=20, no significant enhancement in heat storage rate is observed. It can also be noted that the energy stored at the end of the melting process is unaffected by number of fins. It is due to the fact that the average temperature of the PCM at the end of the charging process is same for all the cases. Hence, it can be stated that the number of fins affects the energy storage rate and it does not have influence on the maximum energy stored.

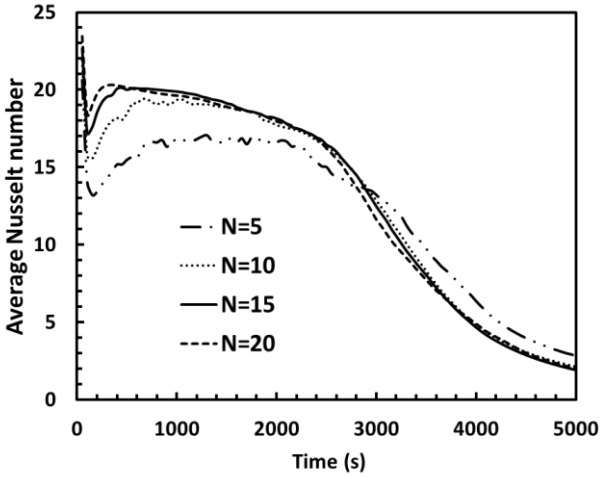

Figure 7.7: Transient variation in average Nusselt number

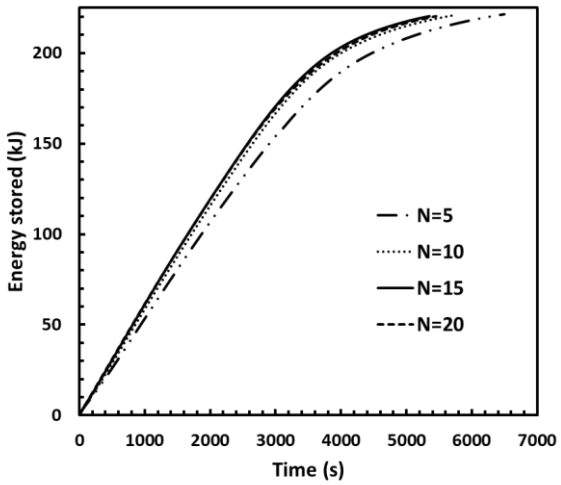

Figure 7.8: Effect of number of fins on energy stored

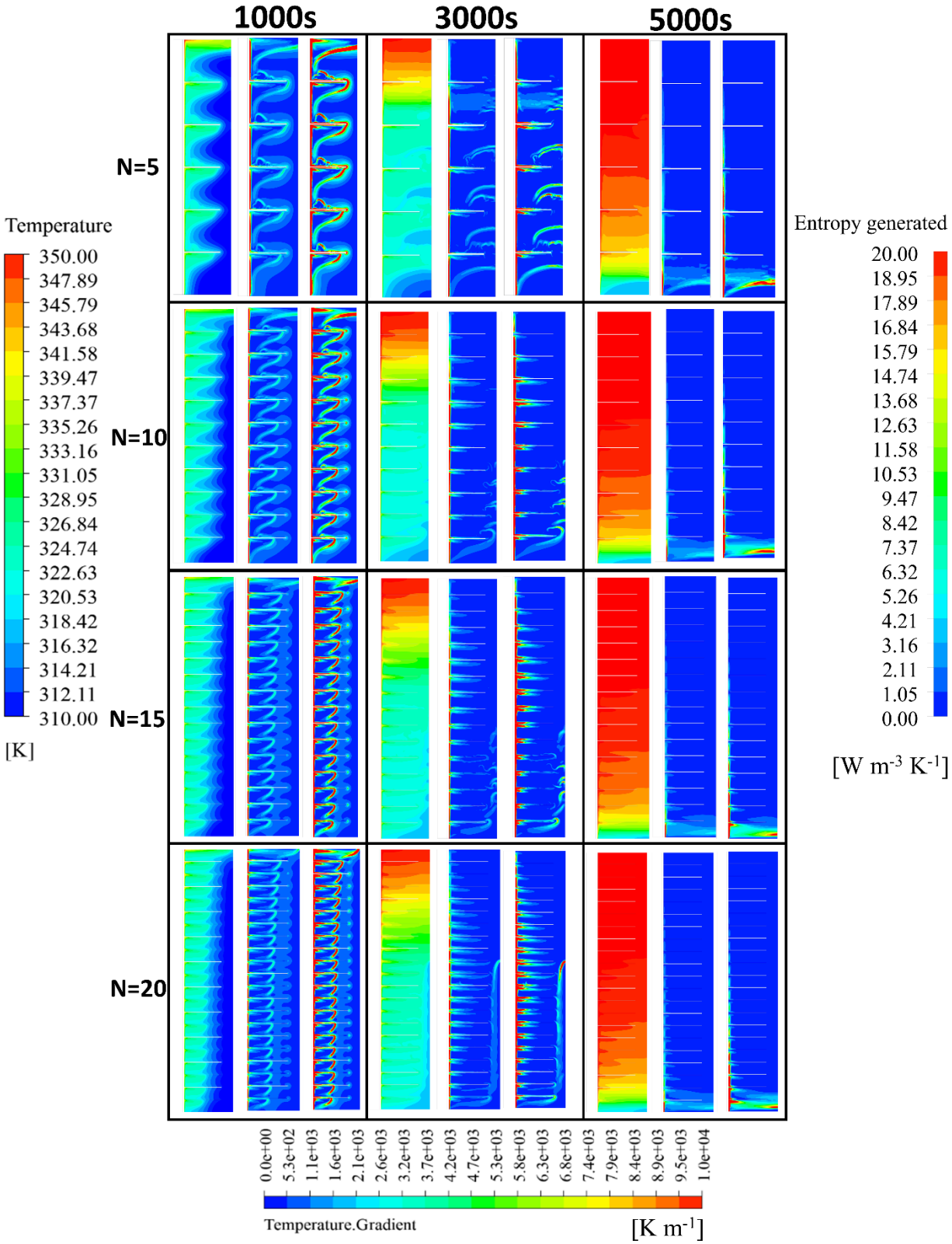

Figure 7.9: Contours of temperature (left), temperature gradient (middle) and entropy generated (right) at different time levels

The distribution of entropy generation and the effect of the number of fins on the global entropy generation is discussed here. Fig. 7.9 shows temperature contours (left), temperature gradient contour (middle) and the contours of entropy generated (right) at different time levels for N=5,10,15 and 20. As per Eq. 10, the entropy generation is caused because of temperature gradient and viscous stresses. But the flow field in LHSU is laminar and viscous stresses are negligible. For the quantitative comparison of both these contributors, Bejan number is calculated which is defined as the fraction of entropy generated due to heat transfer to the total entropy generated. It is found that the Bejan number is approximately equal to 1. Hence, it can be stated that the temperature gradient is mainly responsible for entropy production. It can be noticed from Fig. 7.9 that the temperature gradient and entropy generated contours are identical but varied in magnitude. The temperature gradients are more near the tube wall and fin surfaces and hence larger entropy generation can be observed near the walls. Apart from the wall surface, higher temperature gradients are observed at the interface of the solid and liquid PCM. As the entropy production near the fin surface is more, the entropy generation near the fin surface increased with the increase in number of fins. However, increase in number of fins aids in achieving uniform temperature within the PCM by increasing the thermal transport by conduction. This helps in reducing entropy generation within the PCM. Hence, it can be stated that the increase in number of fins has two effects on entropy generation: increase in entropy generated near the walls due to an increase in fin surface area, reduction in entropy generation within the PCM because of uniform temperature distribution. To analyze the combined effect of these two, a quantitative comparison is made via global entropy generation and is shown in Fig. 7.10. From the figure it can be inferred that the entropy generated decreased by increasing the fin number.

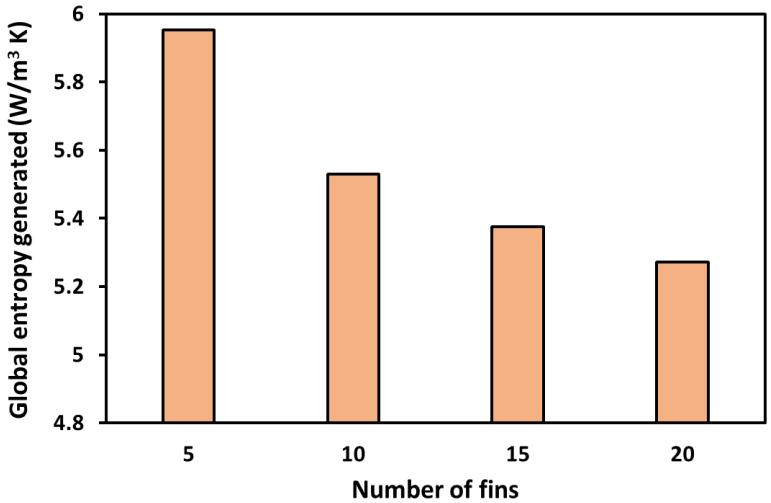

Figure 7.10: Effect of number of fins on global entropy generation

7.5.2 Effect of fin diameter

The effect of fin diameter is analyzed by keeping number of fins fixed and fin diameter is changed from 70 mm to 100 mm in steps of 10 mm. The results presented in this section correspond to a fin number of 10. By increasing the fin diameter, fin surface area increases which lead to higher heat transfer rate. Hence, the melting rate is increased thereby total melting time got decreased with the increment in fin diameter. Fig. 7.11 shows the melt fraction evolution and total melting times at various fin diameters. 12.71% reduction in melting time is noticed by increasing the fin diameter from 70 mm to 100 mm. No significant enhancement in melting rate is observed from 90 mm to 100 mm increase in fin diameter. Employing 100 mm fin diameter divides the entire LHSU into number of compartments. This restricts the PCM to flow towards top of the LHSU and hence proper thermal mixing did not take place. This shadowed the effect of increase in heat transfer surface area and hence no significant increase in melting rate is noticed. The results corresponding to time-averaged Nusselt number are also observed to be following the similar trend. It can be observed from Fig.7.12 that the time-averaged Nusselt number for 100 mm fin diameter is almost equal to the Nusselt number for 90 mm fin diameter. It is noticed that the effect of fin diameter on energy stored is similar to the effect of number of fins. Fin diameter is observed to have negligible effect on the average temperature of PCM at the end of melting process. Hence, maximum energy stored is observed to be same for all the fin diameters and is equal to 220 kJ/kg.

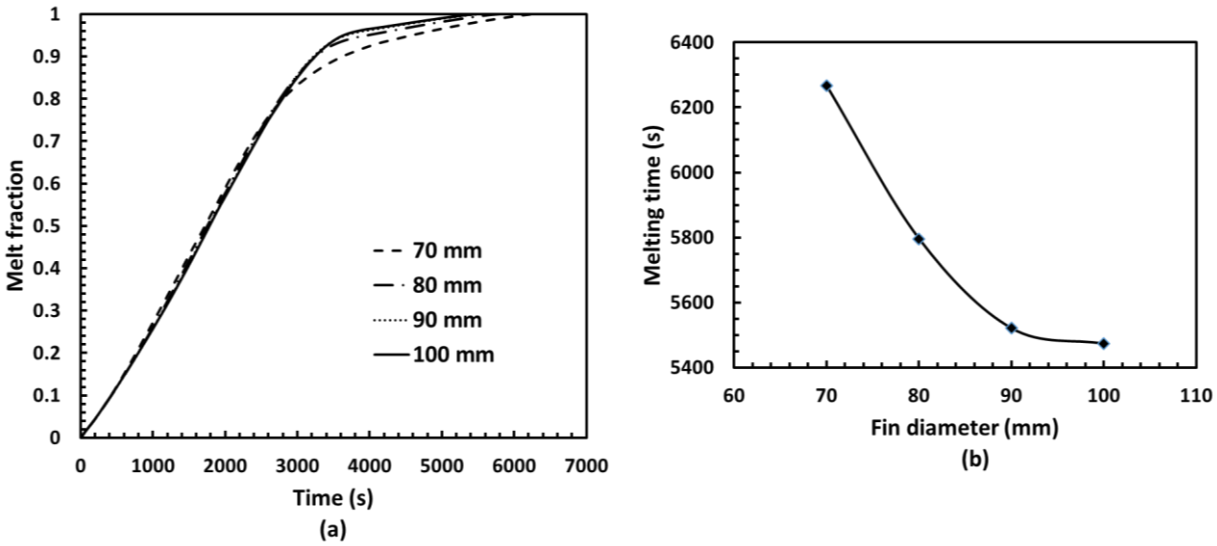

Figure 7.11: Effect of fin diameter on (a) melt fraction evolution (b) total melting time

Temperature gradients are more near the fin surface and hence entropy generation is more near the fin surface. Hence, with the increase in fin diameter entropy generation got increased as the

fin surface area is increased. Increase in fin surface area should also result in the more uniform temperature of PCM which should minimize the entropy generated in the PCM region. But this reduction is not sufficient enough to nullify the effect of the increase in entropy production near the fin surface. Hence, with the increase in fin diameter global entropy generation is increased and the comparison is shown in Fig. 7.13.

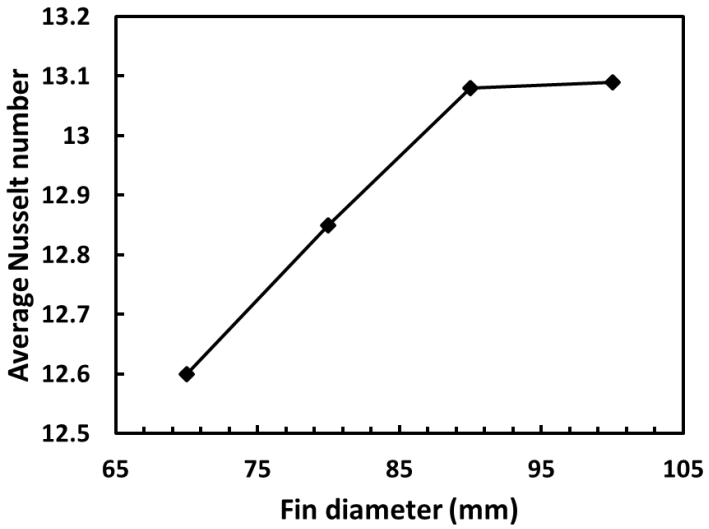

Figure 7.12: Variation in time-averaged Nusselt number with fin diameter

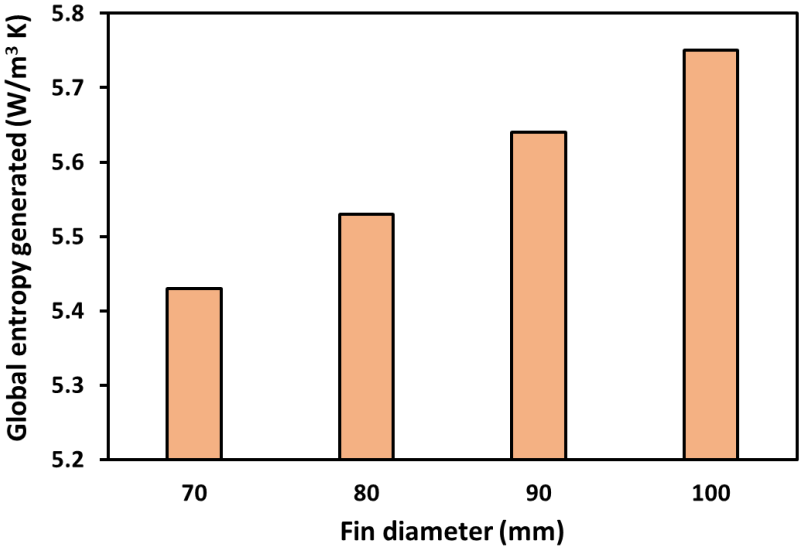

Figure 7.13: Effect of fin diameter on global entropy generation

At this juncture, it can be concluded that the increase in fin diameter has a positive impact on total melting time and a negative impact on entropy generation. Similarly, an increase in number of fins has a favorable effect on entropy production and beyond certain number of fins, the total melting time is observed to be increasing. This indicates the need for adapting the multi-objective optimization technique to optimize the fin parameters in order to make LHSU

both energy and exergetically efficient. The details of multi-objective optimization are discussed in the next section.

7.5.3 Multi-objective optimization

As mentioned above, the design of LHSU should be aimed at two objectives: to achieve higher melting rate and lesser entropy production. Multi-objective optimization based on ratio analysis (MOORA) is chosen for the current study to decide optimized fin parameters based on these two objectives. MOORA technique is very simple to implement and does not involve any laborious calculations. This method has been successfully applied to various complex decision-making problems in the manufacturing environment and reported to be very robust for quantitative attributes [244]. As the present multi-objective decision making involves only the quantitative comparison, the MOORA technique can be applied to the present problem.

The MOORA method was first proposed by Brauers [245] and the method starts with a decision matrix as given below

$$X = \begin{bmatrix} x_{11} & x_{12} & \cdots & \cdots & x_{1n} \\ x_{21} & x_{22} & \cdots & \cdots & x_{2n} \\ \vdots & \vdots & \ddots & \ddots & \vdots \\ \vdots & \vdots & \ddots & \ddots & \vdots \\ x_{m1} & x_{m2} & \cdots & \cdots & x_{mn} \end{bmatrix} \tag{7.7}$$

x_{ij} is the performance value with ith alternative corresponding to jth attribute. m and n are the number of alternatives and number of attributes respectively. For the present work number of attributes is equal to 2. The next step is to normalize the performance values using an appropriate ratio system. Various ratio systems were considered by Brauers et al. [246] and concluded that the normalization using square root of sum of squares is the best. Normalized performance value is given as follows.

$$x_{ij}^{*} = \frac{x_{ij}}{\left[\sum_{i=1}^{m} x_{ij}^{2}\right]^{0.5}} \tag{7.8}$$

These normalized performance values will be within the limits of [0, 1]. The next step involves adding normalized performance values of all attributes for each alternative and is given as Eq. 7.9. This results in a single assessment value for each alternative.

$$y_i = \pm x_{i1}^{*} \pm x_{i2}^{*} \pm \cdots\cdots\cdots \pm x_{in}^{*} \tag{7.9}$$

It is to be noted that in Eq. 19 positive or negative sign should be decided by the nature of the attribute. If the attribute is a beneficial one, in other words, if the objective is to maximize, performance value corresponding to that attribute is to be added. If the objective is to minimize, that performance value is to be subtracted. Sometimes one attribute might be more important than the other attributes. In those cases, a proper weighting factor can be given to each attribute and Eq. 7.9 can be modified as follows

$$y_i = \pm w_1 \, x_{i1}^* \pm w_2 \, x_{i2}^* \pm \cdots\cdots\cdots\cdots \pm w_n \, x_{in}^* \tag{7.10}$$

For the present multi-objective problem, both melting time and entropy production are equally important and hence a weighing factor of 0.5 is employed to both the attributes. Depending on the y_i values ordinal ranking can be given to the alternatives. The alternative with the highest y_i value will be the best choice and the one with the lowest y_i value will be the least preferred alternative.

Using the above explained MOORA technique optimization of fin parameters is carried out and is given in Table 7.3. Total melting time and global entropy generated are taken as the attributes and 14 alternatives are taken into account for the ranking. Both the attributes are to be minimized and hence negative sign is used for both the attributes in Eq. 7.10. As can be observed from Table 7.3 and Fig. 7.14 highest performance assessment value (y_i) is obtained for a fin diameter of 80 mm and the number of fins is equal to 15. As both the melting time and entropy production are more for lesser number fins, 5 number of fins stood as the least preferred. It is to be noted that higher diameter of the fins is not found to be optimum which is not in accordance with the previous published works. In the literature entropy generation was not taken into account and the optimized values of fin diameter were reported by considering only total melting time. In this work, both melting time and entropy generation are taken into account. Hence, the present optimized parameters will make LHSU efficient in terms of both energy and exergy.

Table 7.3: Ranking of set of fin parameters using MOORA technique

Fin diameter (mm)	**Number of fins**	**Fin pitch (mm)**	**Fin thickness (mm)**	**Total melting time (s) x_{i1}**	**Global entropy generated (W/m^3 K) x_{i2}**	x_{i1}^*	x_{i2}^*	y_i	**Rank**
100	5	41.67	0.62	6442	6.160	0.2856	0.2942	-0.2899	13
100	10	22.72	0.31	5473	5.750	0.2427	0.2746	-0.2586	5
90	5	41.67	0.78	6495	6.090	0.2880	0.2908	-0.2894	12
90	10	21.72	0.39	5521	5.640	0.2448	0.2693	-0.2571	4
90	15	15.62	0.26	5337	5.480	0.2366	0.2617	-0.2492	3
80	5	41.67	1.00	6574	5.953	0.2915	0.2843	-0.2879	11
80	10	21.72	0.50	5796	5.530	0.2570	0.2641	-0.2605	7
80	**15**	**15.62**	**0.33**	**5351**	**5.375**	**0.2373**	**0.2567**	**-0.2470**	**1**
80	20	11.90	0.25	5478	5.272	0.2429	0.2518	-0.2473	2
70	5	41.67	1.33	7013	5.834	0.3110	0.2786	-0.2948	14
70	10	21.72	0.66	6266	5.430	0.2778	0.2593	-0.2686	10
70	15	15.62	0.44	5995	5.264	0.2658	0.2514	-0.2586	6
70	20	11.90	0.33	6142	5.230	0.2723	0.2497	-0.2610	8
70	25	9.61	0.26	6203	5.226	0.2750	0.2496	-0.2623	9

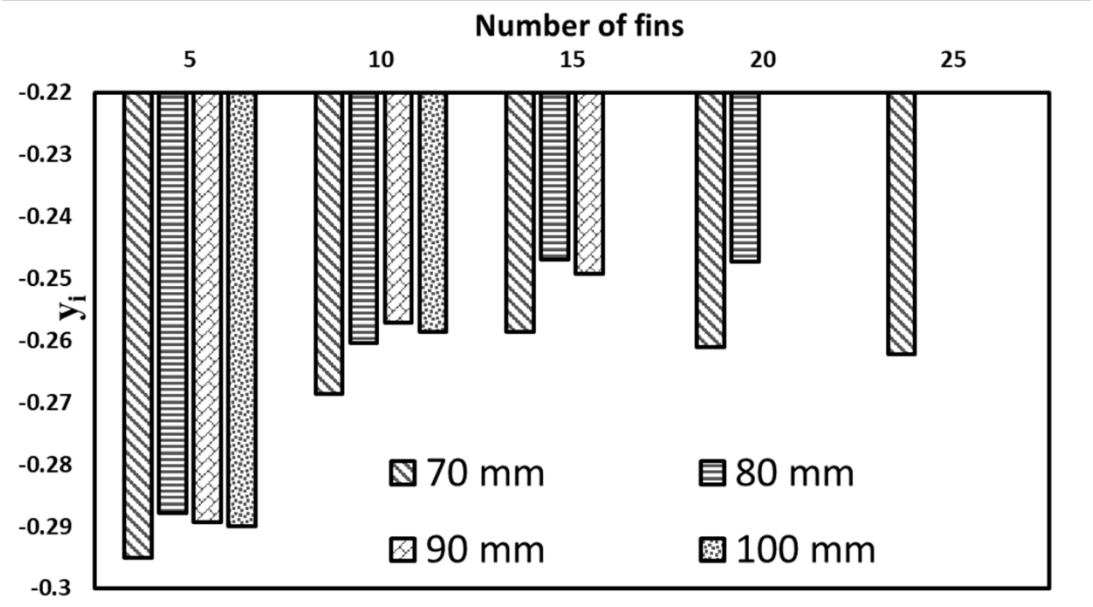

Figure 7.14: Plot showing y_i values for various fin diameters and number of fins

7.5.4 Optimized fin parameters in non-dimensional form

As discussed in section 7.5.3, the optimized fin parameters are: fin diameter = 80 mm, number of fins = 15. These parameters are to be represented in non-dimensional form to make them applicable for any dimensions of the LHSU. Fin diameter is non-dimensionalized by dividing it with shell diameter. This is more appropriate as it represents the amount of space available (space between fin and shell wall) for the melted PCM to move towards the top which is crucial for proper thermal mixing. Hence, the optimized fin diameter in non-dimensional form turned out to be 0.8. Though the number of fins is a non-dimensional parameter, the optimized number of fins cannot be same for any length of the LHSU. With the variation in number of fins, the space between two fins gets affected which in turn affects the intensity of natural convection. Along with the space between two fins, annular space also affects the circulation which is responsible for heat transfer rate. These two parameters are converted into a single non-dimensional parameter as per Eq. 7.11 and is termed as non-dimensional fin spacing.

$$Non\ dimensional\ fin\ spacing = \frac{2(p_f - t_f)}{D_{shell} - D_{tube}} \tag{7.11}$$

Depending on the fabrication viability, thickness of the fin can be decided and optimum pitch of the fin can be calculated for the given shell and tube diameters using the optimized value of non-dimensional fin spacing. The number of fins will be a function of optimum fin pitch and length of the LHSU.

Optimized values of the fin parameters in the non-dimensional form are as follows:

- Non dimensional fin diameter (D_f / D_{shell}) = 0.8
- Non dimensional fin spacing ($\frac{2(p_f - t_f)}{D_{shell} - D_{tube}}$) = 0.373

7.6 Closure

Optimization of annular fin parameters is carried out using the MOORA technique to meet two objectives: to minimize the total melting time and to minimize the entropy generation. Fin diameter, number of fins are taken as fin parameters and the following conclusions can be drawn.

Increasing fin number beyond a certain limit deteriorated the melting rate because of the suppression of natural convection currents. For the considered dimensions of the LHSU and fin diameter of 80 mm, 15 number of fins are found to be optimum to have a lesser melting time. The increase in fin diameter favored the melting rate. The values of time-averaged Nusselt number are in line with the melting times. By analyzing the entropy generation distribution, it is found that the value of entropy generation is higher near the tube, fin surfaces and at the interface of liquid and solid PCM. The increase in number of fins resulted in a uniform temperature distribution within the PCM and hence global entropy generation decreased. On the contrary to this, increase in fin diameter increased the global entropy generation. The optimized fin parameters are: Fin diameter = 80 mm; Number of fins = 15; Fin pitch = 15.62 mm and fin thickness = 0.33 mm. The optimized parameters are then converted in to non-dimensional form to make them applicable for any size of the LHSU and the optimized parameters in non-dimensional form are: non dimensional fin diameter = 0.8, non dimensional fin spacing = 0.373.

Chapter 8

Influence of fin parameters on melting and solidification characteristics of a latent heat storage unit with a conical shell

8.1 Introduction

In the previous chapter, the results corresponding to the optimization of annular fin parameters to maximize the performance of shell and tube LHSU were discussed. Employing fins can be categorized as an active enhancement technique which infers that some material is added to enhance the thermal conductivity or heat transfer surface area. Another category of heat transfer augmentation technique is passive techniques in which the geometry of the container is modified in such a way the rate of heat transfer is maximized. A close examination of melting behavior of PCM in a vertical shell and tube LHSU revealed that the melt front proceeds in a conical fashion. Hence conical shell design is expected to enhance the melting rate. various authors [182,247–250] reported that a conical shell is a promising option for effective utilization of natural convection and combining active enhancement technique (fins) with a conical shell can further increase the performance of LHSU. As discussed in the previous chapter, fin parameters (fin number and fin diameter) have a significant influence on heat transfer characteristics of LHSU. Hence, the current work is aimed at analyzing the effect of annular fin parameters on the thermal performance of the conical shell and tube LHSU. Both melting and solidification processes are analyzed, and the performance comparison is made in terms of melting/solidification time, energy stored/discharged, energy efficiency and exergy efficiency.

8.2 Model description

Initially, thermal performance of cylindrical and conical shell LHSU without fins is compared by considering quasi three dimensional i.e. axi-symmetric domain. For this purpose, dimensions of LHSUs are chosen such that the PCM volume remains the same. Dimensional details of cylindrical and conical shell LHSU are shown in Fig. 8.1. In both the cases, diameter and thickness of the tube are kept constant. For the conical shell, the diameter at the bottom is made equal to the tube outer diameter and the shell diameter at the top is deduced based on

PCM volume. Stainless steel (SS) is considered as the tube material and lauric acid is chosen as the PCM. The thermophysical properties of lauric acid are provided in the previous chapter (Table. 7.1). The combination of SS and lauric acid does not show any kind of corrosion because of which this combination has practical relevance. After comparing unfinned LHSUs' performance, simulations are carried out on conical shell LHSU with different fin parameters. Fins are evenly distributed along the length and the fin diameter (D_f) is varied along the length of LHSU such that the ratio of fin diameter to shell diameter (λ) at the fin location is the same. Depending on the number of fins and fin diameter thickness of the fin is determined. Fabricating a fin of thickness less than 0.2 mm is impractical and hence the number of fins are increased only till the fin thickness remained greater than 0.2 mm.

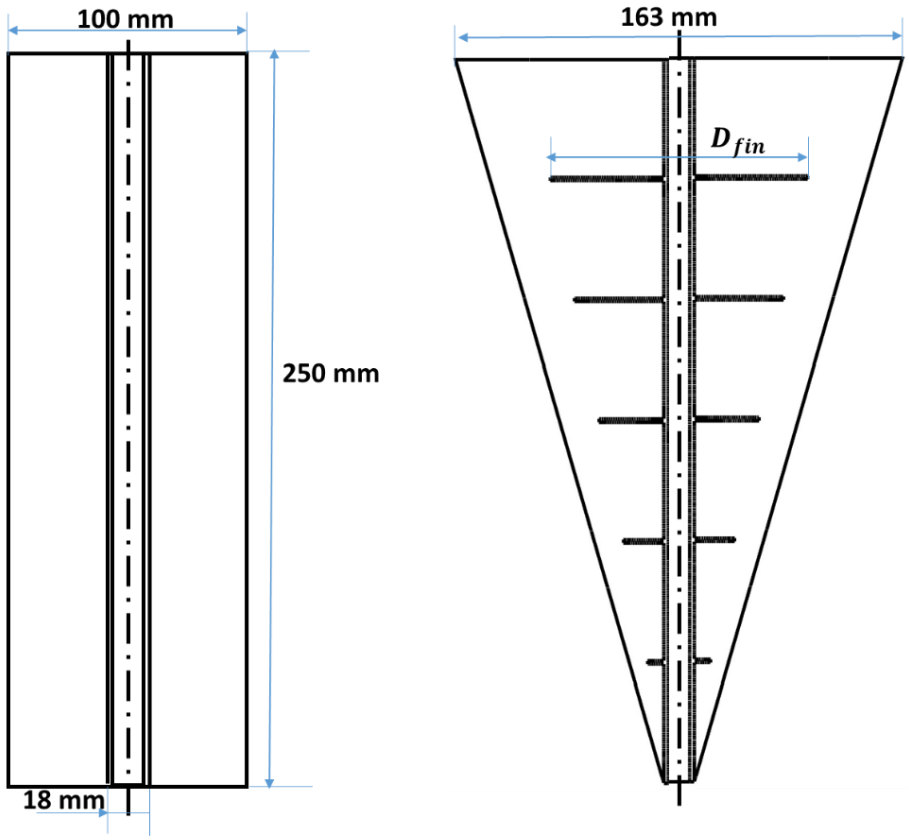

Figure 8.1: Schematic of cylindrical shell and conical shell LHSU

8.3 Initial conditions and boundary conditions

All the walls are treated as adiabatic with the no-slip condition. Velocity inlet and pressure outlet are chosen as the boundary conditions for HTF inlet and outlet respectively. HTF is introduced at a temperature of 80°C for the charging process and 15°C for the discharging process. Flow rate of the HTF is 1.4 LPM for both the processes and this flow rate ensures that

the flow is in the laminar regime. For the charging process, HTF is introduced from the top and for the discharging process, HTF is fed from the bottom. Initially, the PCM is considered to be at a temperature of 30° C for the charging process and for the discharging process initial temperature is kept as 60°C.

8.4 Grid independence and validation

8.4.1 Grid independence and time step independence

To ensure the correctness of the solution grid independence and time step independence studies are very much necessary for each computational domain. Hence these studies were carried out on unfinned cylindrical, conical LHSU and also for finned conical LHSU. But for brevity, the details pertaining to the melting of PCM in a finned conical shell are presented in Fig. 8.2. Initially with a time step of 0.1s simulations are carried out for different grid numbers for a LHSU with 5 number of fins and the ratio "λ" 0.8. As can be seen from the figure the melt fraction curve corresponding to 91528 number of elements did not deviate much from the curve corresponding to 116039 elements. Hence the element size corresponding to 91528 number of elements is considered for all the simulations. Using this element size, time step independence study is carried out at different time steps of 0.2s, 0.1s and 0.05s. Reducing time step beyond 0.1s did not result in significant difference in the results as shown in Fig. 8.2(b) and hence 0.1s is chosen as the time step for all the simulations. On the similar lines, for unfinned cylindrical and conical LHSU also, optimum time step is observed to be 0.1s.

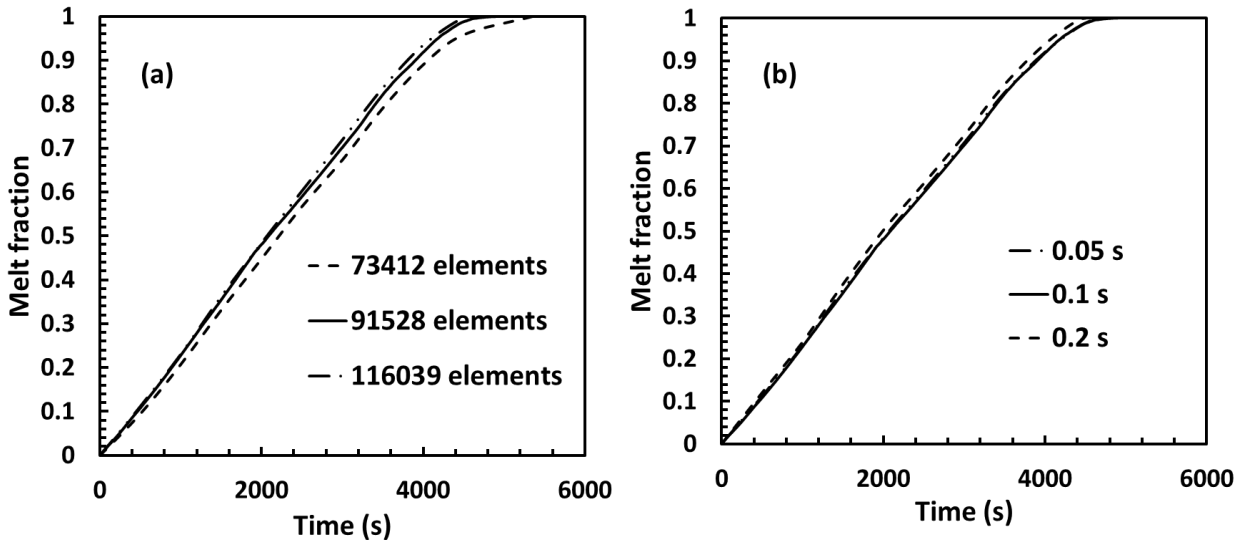

Figure 8.2: Plots showing (a) grid independence (b) time step independence

8.4.2 Experimental validation

The accuracy of the numerical methodology is ensured by validating the simulation results with the experimental findings of Longeon et al. [219]. All the boundary conditions and properties of PCM are kept same as that of experimental work. Though the outer wall of the shell is insulated while conducting the experiments it is impossible to completely avoid the heat loss. Hence, convective boundary condition is applied on the outer shell wall and the heat transfer coefficient is calculated by the correlation $h = 0.59k(Gr\ Pr)^{0.25}/D$ [96]. Figure 8.3 shows the comparison of temperature evolution of PCM at two locations during solidification processes. As far as the melting process is considered, details pertaining to experimental validation are already provided in chapter 7. Hence in this chapter validation is shown only for the solidification process. From Fig.8.3 it can be stated that the adapted numerical procedure accurately predicting phase changing behavior of PCM in a LHSU.

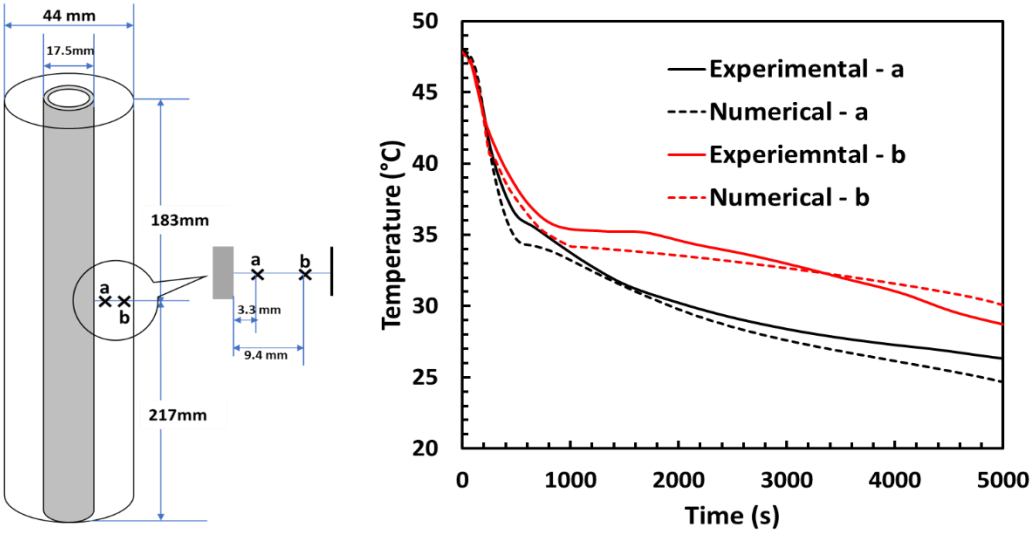

Figure 8.3: Comparison of numerical results with the experimental results of Longeon et al. [219] during solidification process

8.5 Results and discussions

8.5.1 Charging process

Initially, the melting characteristics of PCM in the cylindrical shell and a conical shell are compared without employing fins. The comparison is made in terms of melt fraction, average temperature evolution, and energy storage characteristics. For both the cases, the amount of PCM and tube diameter are kept constant. HTF inlet temperature and mass flow rates are 80°C and 1.4 LPM respectively.

8.5.1.1 Comparison of the cylindrical and conical shell without fins

Figure 8.4 shows the melt fraction and temperature contours at various time levels for both cylindrical and conical shells. By observing the melt fraction contours one can notice that in the case of a cylindrical shell melt front is not propagated in the radial direction at the bottom of LHSU even at 6000s time level. The design of conical shell is such that lesser amount of PCM is present at the bottom so that it does not require melt front propagation in the radial direction at the bottom. This kind of design resulted in effective utilization of natural convection at the top and hence in the conical shell model, the melt front propagates faster in radial direction at the top rather than in axial direction. It can be observed that at 2000s time level, melt front has moved farther in the axial direction in case of cylindrical shell when compared with conical shell. But in the conical shell more amount of PCM is located at the upper portion of LHSU and hence melt faction will be higher in case of conical shell. Similar thing can also be observed at 4000s and 6000s time levels. The amount of PCM unmelted is less in conical shell at all the shown time levels. This is because the conical shell model utilizes the natural convection more effectively thereby reduced the conduction dominance for the PCM to melt. In cylindrical shell the dominance of conduction at the bottom of LHSU can be realized by observing temperature contours which reveals that the rise in temperature is very less at the bottom of LHSU. Conical shell resulted in avoiding this phenomenon by packing lesser amount of PCM at the bottom. Hence the temperature of PCM will be more uniform in case of conical shell.

Figure 8.5 shows the evolution of melt fraction and average temperature of PCM. Up to 1000s no difference in melt fraction is observed as by that time natural convection effect has not prevailed. In the latter stages of melting natural convection is more effective in conical shell and hence melting rate is noted to be more when compared to cylindrical shell. It can also be observed that the melting rate is uniform throughout the charging process in case of conical shell. On the other hand, melting rate got reduced towards the end of charging process in cylindrical shell due to dominance of conduction heat transfer. For complete melting conical shell took 34.46% lesser time as compared to cylindrical shell.

Though the melt fraction is higher for conical shell throughout the charging process, average temperature of PCM is slightly less up to 5000s time level. In conical shell, due to effective utilization of natural convection more thermal mixing will takes place which results in uniform temperature distribution. In cylindrical model, temperature gradients will be more which means that the temperature of PCM at upper portion will be more and at the bottom the temperature

will be less. Due to higher rise in PCM temperature at the top of LHSU might have resulted in higher PCM average temperature. It can also be noted that at the end of melting process average temperature of PCM is higher in case of cylindrical shell when compared to conical shell. But rate of temperature rise is noted to be 47.62% higher by employing conical shell. Inline to average temperature, energy stored is also marginally higher for cylindrical shell up to 5000s time level which is depicted in Fig. 8.6. However, average energy storage rate is higher for conical shell.

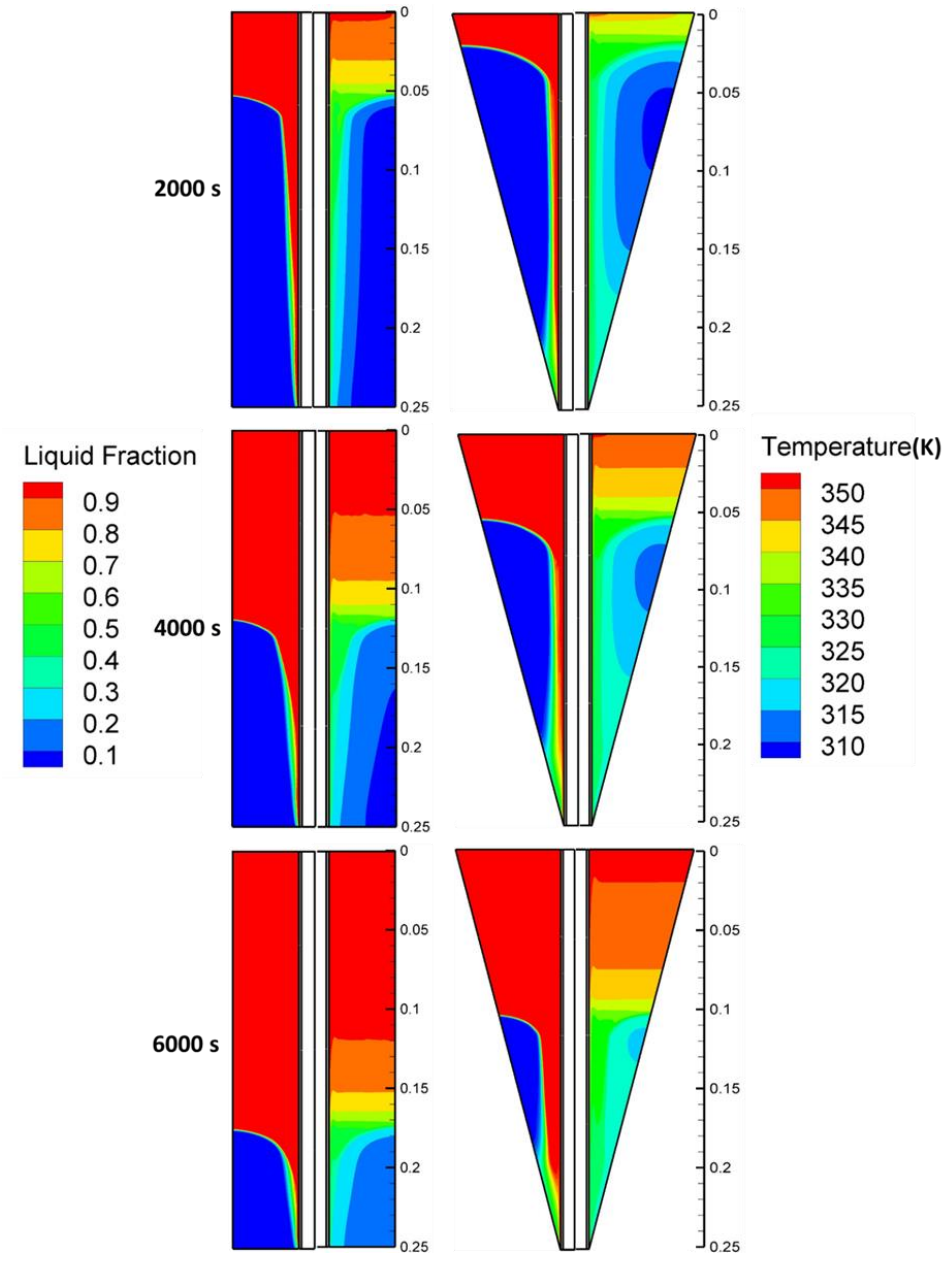

Figure 8.4: Contours of melt fraction and temperature at various time levels (In each figure melt fraction contours are shown in left half and the right half corresponds to temperature contour)

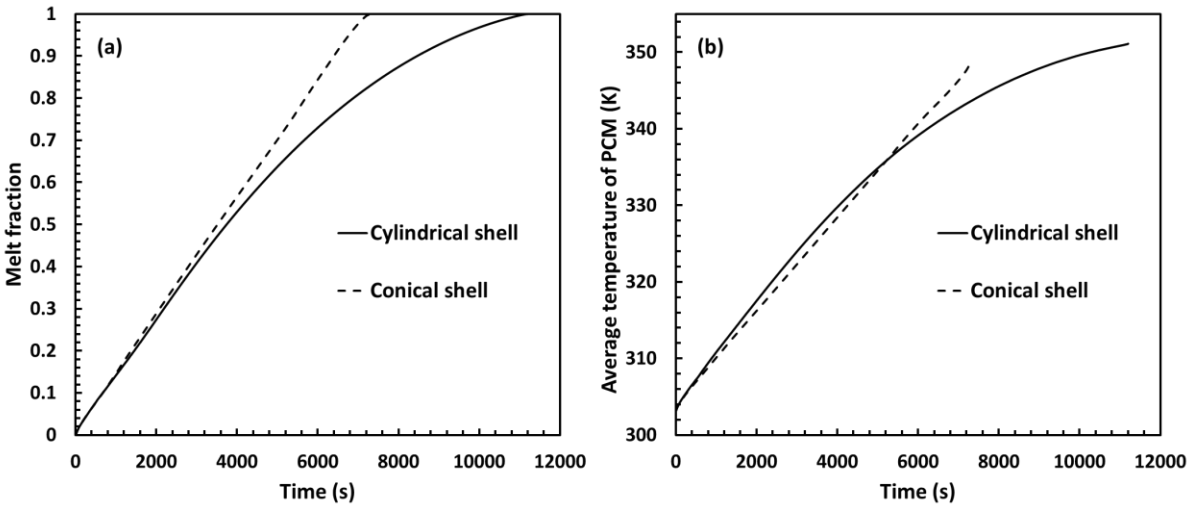

Figure 8.5: Comparison of (a)melt fraction evolution (b) average temperature of PCM

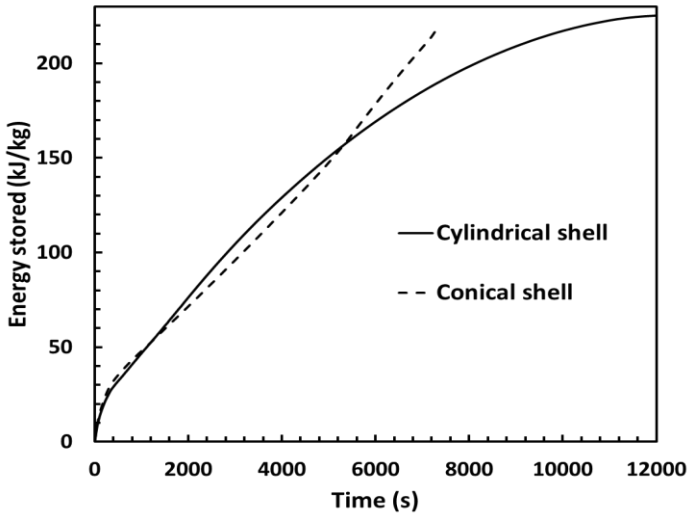

Figure 8.6: Transient variation in energy stored

Figure 8.7 shows the transient variation in energy and exergy efficiencies of both cylindrical and conical shell. It is observed that the energy efficiency started from a higher value and decreased as the time progressed, after some time energy efficiency almost became constant. When the flow of HTF is initiated the PCM adjacent to the tube immediately absorbs the heat because of which energy efficiency is higher. Upon melting formation of a thin layer of melted PCM acted as a resistance to heat transfer which caused reduction in efficiency. Afterwards the onset of natural convection did not cause further reduction in efficiency. As far as exergy efficiency is considered, it started from a lower value and then increased over time. This behavior is justified because at the starting of charging process average temperature of the PCM is almost close to ambient temperature which results in very less exergy stored and exergy efficiency. With the rise in average temperature of the PCM exergy efficiency increased. It is

also observed that the exergy efficiency is higher for cylindrical shell when compared to conical shell. This is due to higher PCM average temperature, lesser temperature difference between HTF inlet and outlet temperatures in case of cylindrical shell.

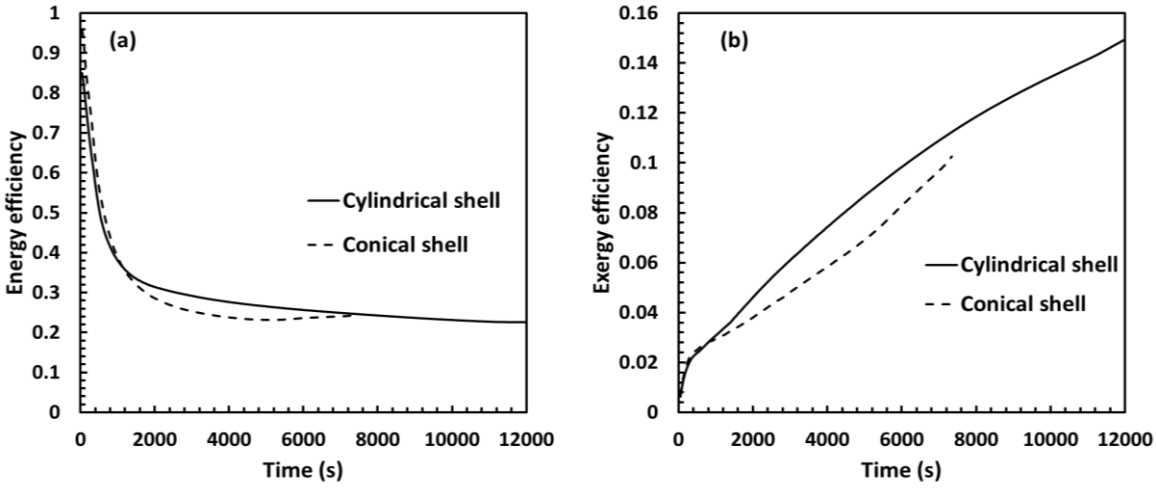

Figure 8.7: Comparison of (a) energy efficiency (b) exergy efficiency with respect to time

At this juncture it can be concluded that the conical shell resulted in lesser melting time, higher rates of temperature rise, and energy stored. However, energy efficiency and exergy efficiencies are slightly lesser when compared to cylindrical shell. Further reduction in melting time and augmentation of heat transfer is possible by employing fins which is discussed in the next section.

8.5.1.2 Effect of fin parameters on melting process

Employing fins is a very well known, simple yet efficient method of heat transfer augmentation. In this regard, fin parameters play a vital role in the extent of heat transfer augmentation. Especially during melting of PCM in a LHSU, natural convection is the most influencing phenomenon which gets affected by employing fins. Hence analysis of melting process by varying various fin parameters is necessary. This section provides the analysis of influence of fin parameters on the charging phenomenon in a conical shell LHSU. Fin diameter and number of fins are taken as variables and Table 8.1 provides the dimensional details of fins for various cases. As conical shell is considered, fin diameter is not considered as same throughout the length of LHSU. Fin diameter is varied in proportion to the shell diameter along the length. Hence for easy understanding, fin to shell diameter ratio (λ) is taken as the variable to realize the effect of fin diameter. Maximum number of fins is decided by the thickness of the fin which is practically feasible to fabricate. It is to be noted that the PCM volume, initial and boundary conditions are same for all the cases.

Table 8.1. Dimensional details of fins

D_{fin}/D_{shell}	Number of fins	Fin thickness (mm)	Fin pitch (mm)
0.9	5	0.663	41.67
	10	0.322	22.727
	15	0.212	15.625
0.8	5	0.85	41.67
	10	0.413	22.727
	15	0.272	15.625
	20	0.203	11.904
0.7	5	1.133	41.67
	10	0.55	22.727
	15	0.362	15.625
	20	0.27	11.904
	25	0.215	9.615
0.6	5	1.59	41.67
	10	0.77	22.727
	15	0.508	15.625
	20	0.378	11.904
	25	0.301	9.615

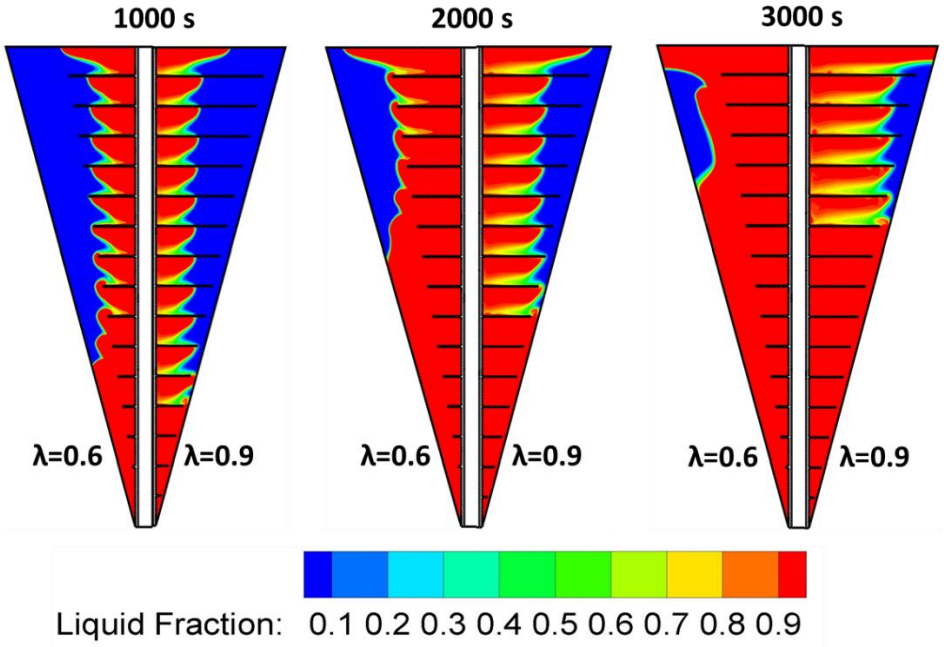

Figure 8.8: Comparison of melt fraction contours with λ=0.6(left) and λ=0.9 (right)

As previously mentioned, effect of fin diameter is analyzed by varying ratio of fin to shell diameter by keeping same number of fins. Fin diameter to shell diameter is varied from 0.6 to 0.9 in steps of 0.1. However, for perspicuous representation of figures, results corresponding to $\lambda = 0.6$ and 0.9 are presented in Figs. 8.8 and 8.9. Figure 8.8 shows the melt fraction contours of PCM with 15 number of fins at 1000s, 2000s and 3000s time levels. It can be observed that at all the time levels because of higher diameter of fins, at $\lambda = 0.9$ melt front has propagated more in the radial direction when compared to $\lambda = 0.6$. However, in the axial direction melt front propagation is faster when the fin to shell diameter ratio is 0.6. With the increase in fin diameter, the space available between fin and shell wall is reduced which restricted the flow of melted PCM to move upwards. When the fin diameter is less, the melted PCM proceeded upwards and hence thermal mixing takes place in the axial direction. In case of higher fin diameter, the flow is confined in the space between two fins. This phenomenon is represented in Fig. 8.9 in which streamlines are shown and the streamlines are colored according to velocity magnitude. From the figure it can be clearly observed that at lesser fin diameter the flow is more pronounced, and the velocity magnitude is also higher in comparison with higher fin diameter. With lesser diameter of fin, the flow is observed to exist in between the fins and at the space between fins and shell which resulted in faster propagation of melt front in axial direction. On the other hand, with higher diameter of fins, the flow is mostly confined to the space between fins. Hence, it can be said that increase in diameter dampened the natural convective flow and hence melting rate may get deteriorated which can be examined by analyzing melt fraction evolution and total melting time.

Figure 8.10(a) shows the melt fraction evolution for different fin diameters and for 15 number of fins. With the increase in fin diameter one would expect a reduction in melting time. But, as discussed above because of the restriction of natural convective flow, total melting time is increased with the increase in fin diameter. 13.15% reduction in melting time is noted by reducing the value of "λ" from 0.9 to 0.6. Reduction of "λ" from 0.7 to 0.6 did not result in a considerable reduction in melting time and hence the diameter is not reduced further. From this analysis it can be said that though there is an increase in the heat transfer surface area by increasing fin diameter, melting rate got reduced when 15 number of fins are employed. However, this behavior cannot be same for different number of fins as the space between two fins gets altered which in turn influences natural convection. Figure 8.10(b) shows the total melting time of PCM at different values of "λ" and different fin numbers. It can be observed that the results corresponding to 20 number of fins are also similar to that of 15 number of fins.

However, when 5 number of fins are employed melting time is decreased with the increase in fin diameter. When lesser number of fins are used the space available between two successive fins is more which promoted more circulation in between the fins. Hence, the disadvantage of restricting the flow of PCM towards top of LHSU with higher fin diameter is shadowed by the advantage of increase in heat transfer area. When number of fins is less melting is mostly promoted by the circulation of melted PCM in between the fins whereas, when fin number is more the melting is also aided by the flow of PCM in the space between fin and shell wall. Hence with 5 number of fins, higher fin diameter is suggested and at 15, 20 number of fins lower fin diameter is preferrable. Another interesting result is observed when number of fins is 10. Increasing the ration from 0.6 to 0.7 resulted in lesser melting time. Further increase in the ration led to increase in the melting time. Increasing the ratio up to 0.7 did not result in deterioration of convection currents but increasing the ratio above 0.7, the restriction to convective flow has dominated the benefit of increase in heat transfer area. By comparing the total melting times, it is recommended to use lesser fin diameter and a greater number of fins to obtain higher melting rate.

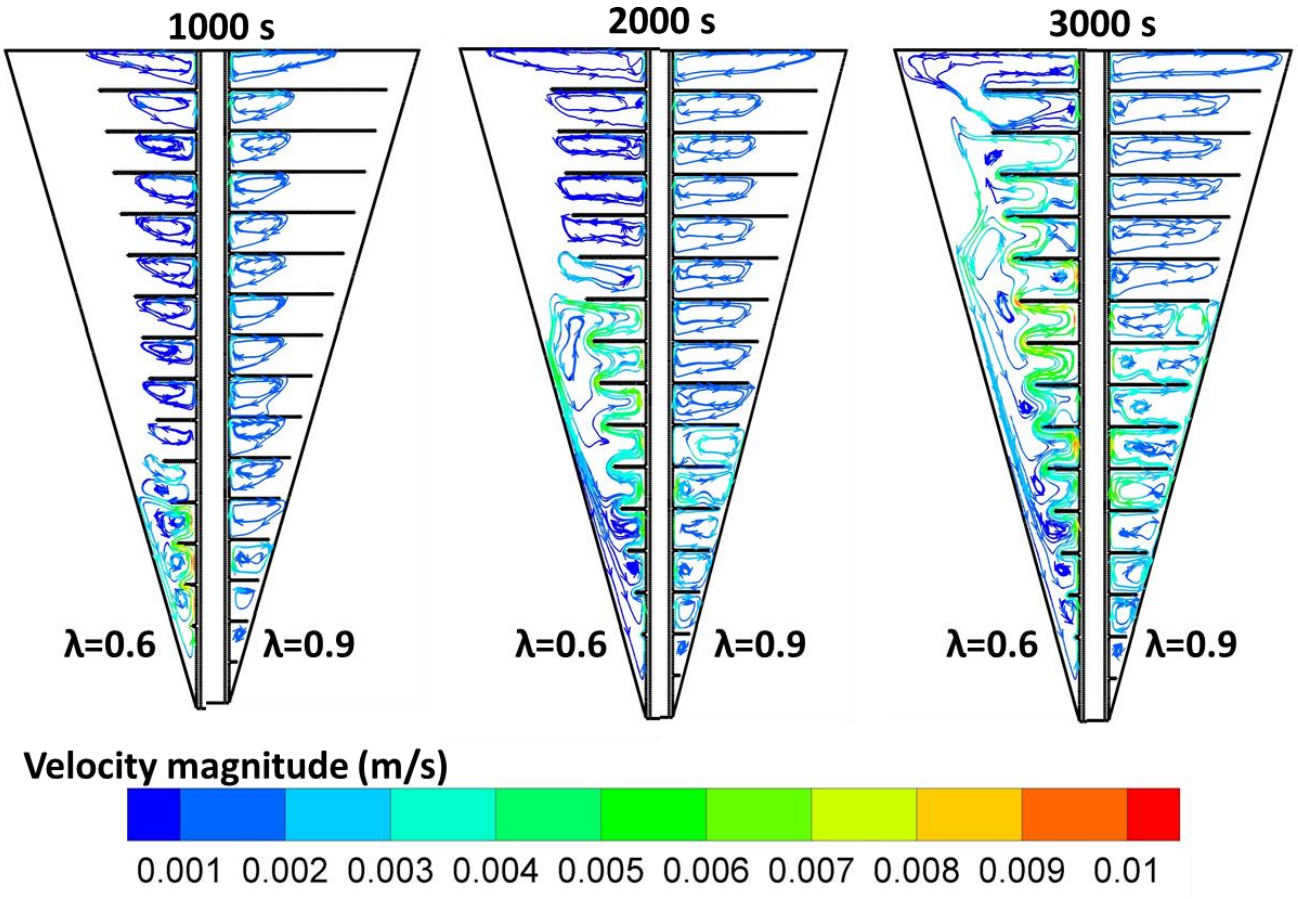

Figure 8.9: Streamlines depicting the flow behavior at λ=0.6(left) and λ=0.9 (right)

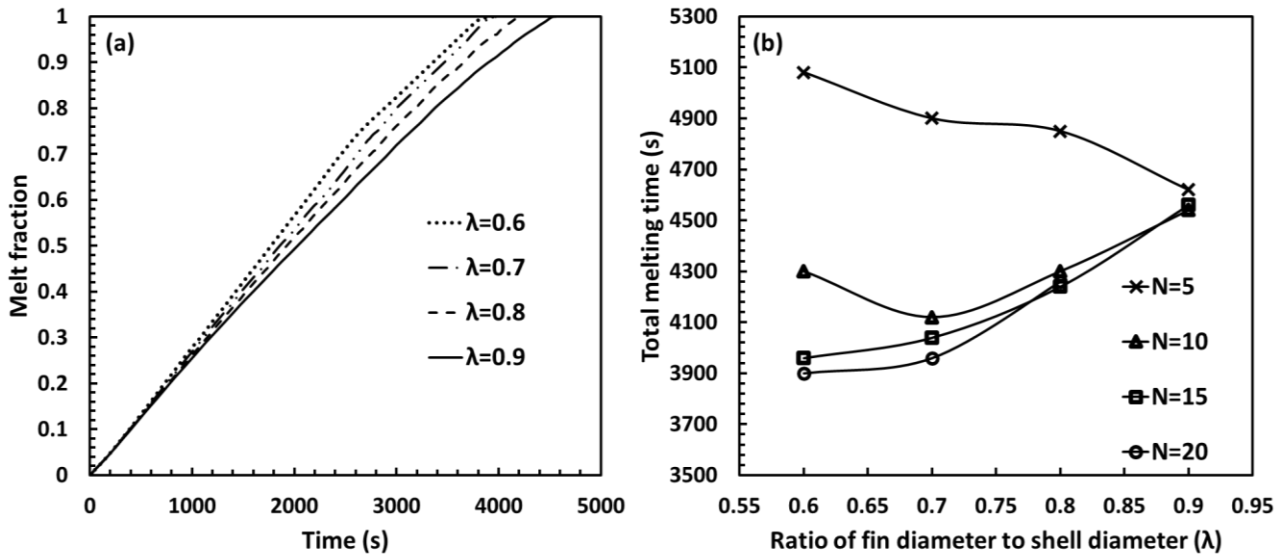

Figure 8.10: (a) Melt fraction evolution at different "λ" values for 15 number of fins (b) Variation in total melting time with λ at different number of fins

Figure 8.11 shows the comparison of energy stored at the end of melting and average rate of energy storage over the period of complete melting for different "λ" values with 15 number of fins. Though a difference in energy stored is noted with varying fin diameter, percentage change in the energy stored is very less. Maximum percentage difference in the energy stored is merely 3.5%. It infers that the effect of fin diameter on energy stored is very less. It is to be noted that the presented values of energy stored are the values at the completion of melting. As there is a difference in total melting time it is appropriate to analyze rate of energy stored. As can be noted from the figure, there is reduction in rate of energy stored with an increase in the value of "λ". 14.45% reduction in energy storage rate is observed by increasing the ratio "λ" from 0.6 from 0.9. As discussed earlier when 15 number of fins are employed, increase in "λ" caused a reduction in natural convection currents which led to higher melting time and thus rate of energy stored got reduced. For other cases also (other fin numbers), energy storage rate is in line to the melting time i.e. lesser melting time led to higher energy storage rate.

Figure 8.12 shows time averaged energy and exergy efficiencies corresponding to 15 number of fins and with different "λ" values. As can be observed from the figure, both energy and exergy efficiencies showed an increasing trend with the increase in ratio. With the increase in ratio, average outlet temperature of HTF is increased which indicates that the energy input is less because of which efficiency is increased. This behavior is observed to be similar irrespective of number of fins.

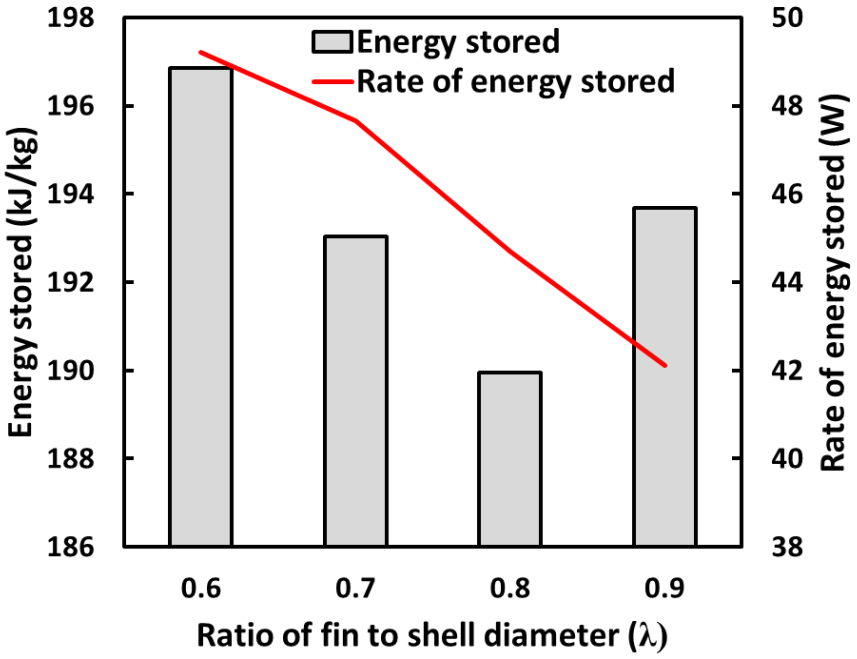

Figure 8.11: Comparison of energy stored, and rate of energy stored at different values of "λ" and for 15 number of fins

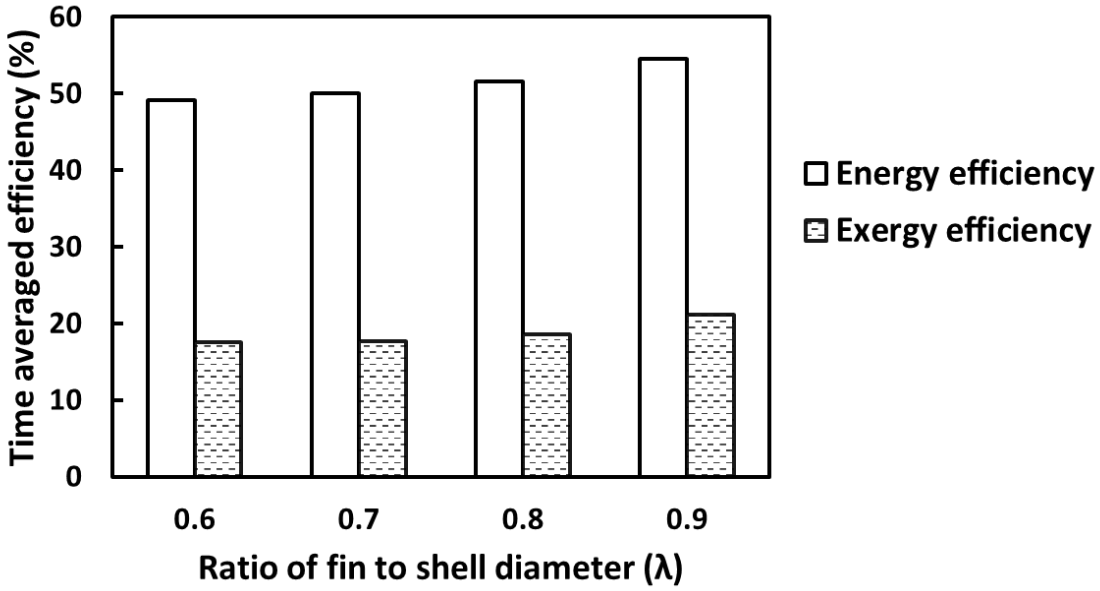

Figure 8.12: Time averaged energy and exergy efficiencies at 15 number of fins and λ=0.6,0.7,0.8 and 0.9

Similar to the fin diameter, number of fins also affects the natural convection as the space between two successive fins get altered by varying fin number. If excessive number of fins is used, there is a possibility of attenuation of natural convection and hence it is necessary to

analyze the effect of number of fins. Figure 8.13 depicts the influence of fin number on total melting time at various values of "λ". Figure 14 also presented the percentage variation in melting times in comparison to 5 number of fins at each fin to shell diameter ratio. It can be noted that at lesser "λ" value, the effect of fin number is more. At λ = 0.6, 21.26% reduction in melting time is noted by increasing the fins from 5 to 15. On the other hand, for λ = 0.9 the reduction in meting time is merely 0.43%. As reported by Kozak et al.[251] annular fins act as non-isothermal surfaces which makes the melting starts from fin surfaces. So, when more number of fins are used the number of surfaces from which melting initiates is more and hence melting time reduces. However, at higher diameter this phenomenon did not favor melting rate much, because the melted PCM is not allowed to move freely which resulted in weaker circulation. In the case of lesser diameter, the commencement of melting from all the fin surfaces aided in enhancing the convection currents which resulted in higher melting rate. Hence, it can be concluded that the effect of fin number is more at lesser diameter of fins. In other words, at higher fin diameter increasing the number of fins is not advantageous.

Rate of energy stored, energy efficiency and exergy efficiency are noted to be increasing with the increase in number of fins irrespective of fin diameter. However, the increase in efficiency from 15 to 20 number of fins is noted to be very less which is shown in Fig. 8.14. Similar trend in results are also obtained for energy storage rate and exergy efficiency also.

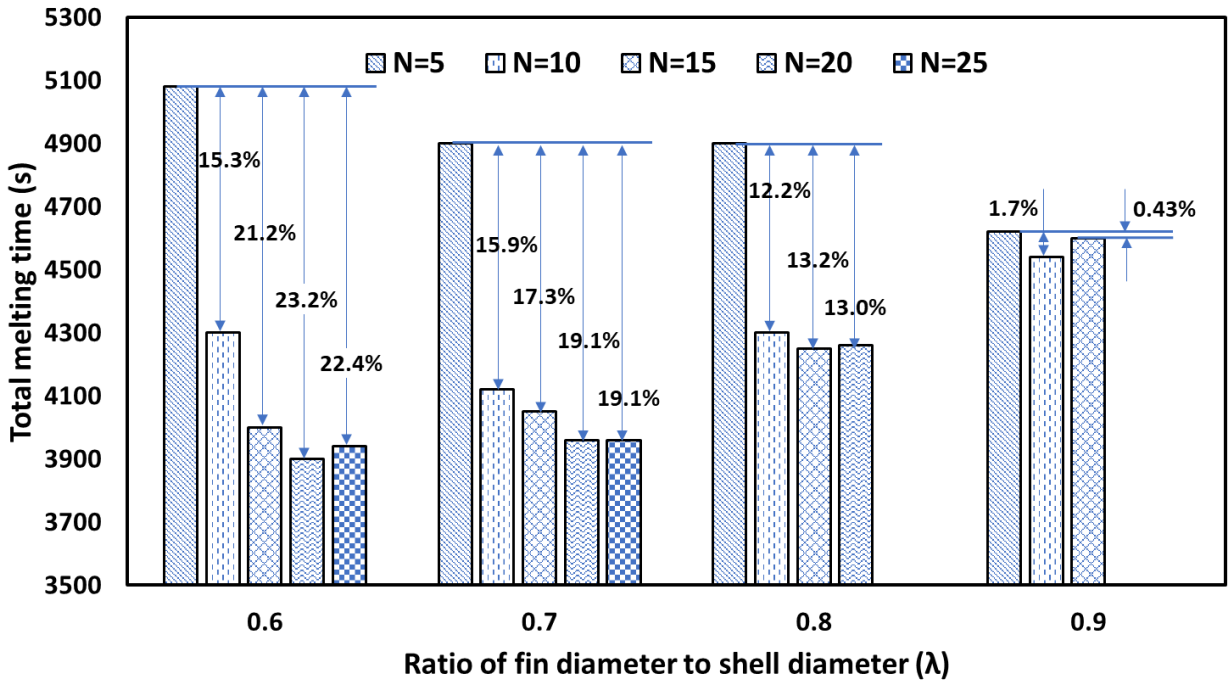

Figure 8.13: Effect of number of fins on total melting time

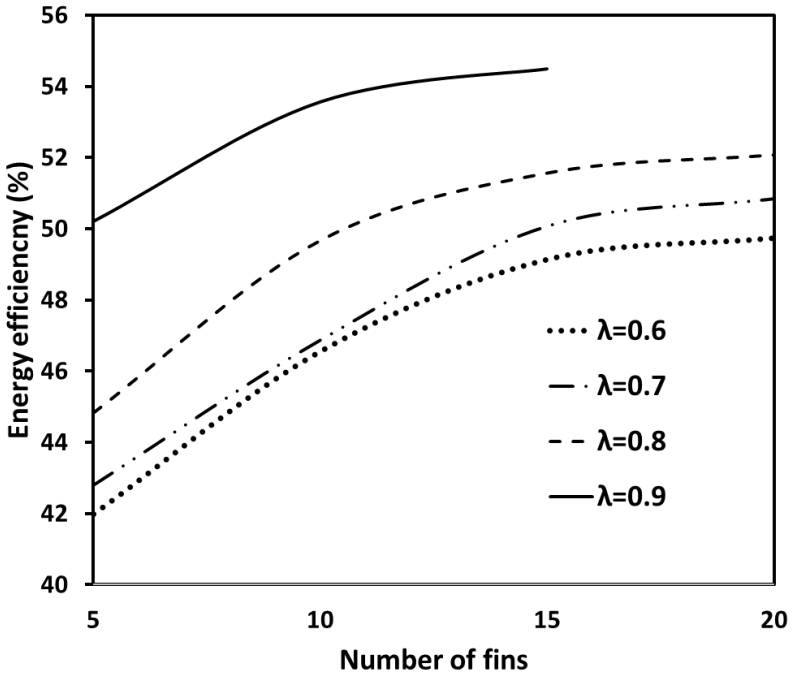

Figure 8.14: Energy efficiency vs number of fins at various fin to shell diameter ratios

8.5.2 Discharging process

The analysis of discharging process is carried out by introducing HTF at a temperature of 15°C and initial temperature of the PCM is kept as 60°C. Similar to the charging process, initially comparison of thermal performance of unfinned cylindrical and conical shell is presented. Later the effect of annular fin parameters is discussed.

8.5.2.1 Comparison of thermal performance of cylindrical and conical shell LHSU without fins during solidification process

Figure 8.15 shows the liquid fraction contours and streamlines at various time levels for both cylindrical and conical shells. It can be observed that the solidification front tends to proceed in inverted conical shape. This is because the solidified PCM moved towards bottom of the LHSU and the liquid PCM remained at top of the LHSU. Hence it can be said that at the top portion of LHSU solidification rate will be very less. As conical shell packs more PCM at the top more amount of melted PCM is observed at the top when compared to cylindrical shell. By observing the streamlines it can be noted that the velocity magnitude is very less for both the shell designs and hence it can be affirmed that there is no major role of convection during solidification process when no fins are employed. Therefore, no advantage can be extracted out of conical shell during solidification process, as the main objective of the conical shell is to

promote natural convection. Quantitative comparison of the liquid fraction is shown in Fig. 8.16 (a) from which it can be observed that the solidification rate is lesser with conical shell. 63.79% increase in total solidification time is noted with conical shell when compared to cylindrical shell. Figure 8.16(b) shows the transient variation in average temperature and energy discharged by the PCM. Up to 20000s time level, the difference in average temperature is very marginal. As the time progressed, more reduction in temperature is noted for cylindrical shell. As the diameter at the top of LHSU is more for conical shell and conduction being the dominant heat transfer mechanism, it took more amount of time for the reduction of temperature. Whereas in cylindrical shell because of same diameter along the length the rate of temperature reduction is more in comparison with conical shell. From the Fig. 8.16(b) it can also be observed that the energy discharge rate is less for conical shell.

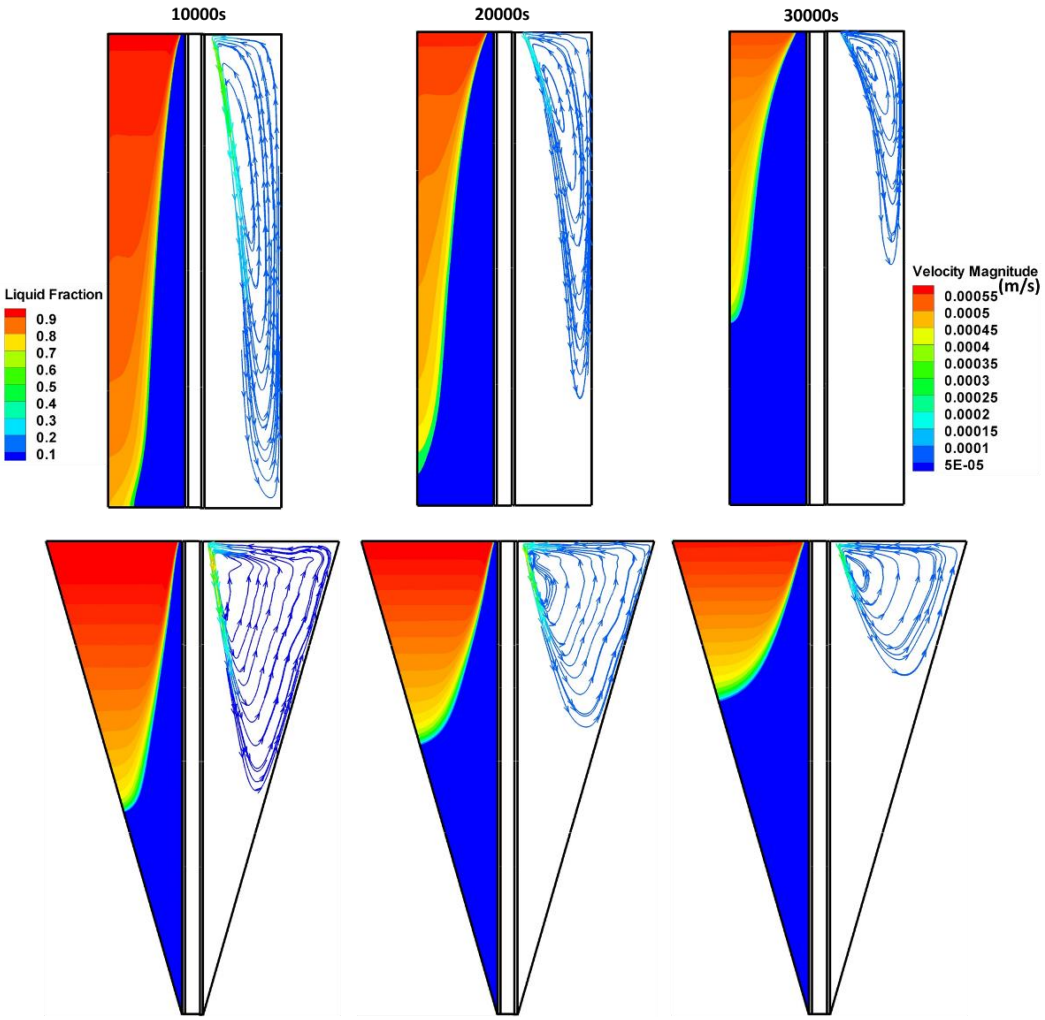

Figure 8.15: Liquid fraction contours and streamlines at various time levels during solidification process

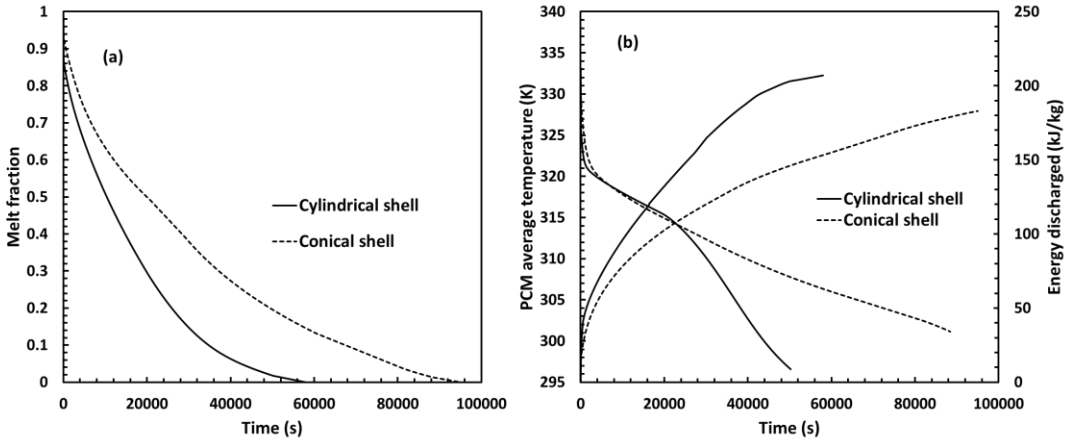

Figure 8.16: Temporal variation in (a) melt fraction (b) PCM average temperature and energy discharged

Figure 8.17 depicts energy and exergy efficiencies' comparison among cylindrical and conical shell. Similar to the melting process, energy efficiency started from a higher value and became constant after some time. This is justified as at the starting of solidification, convection currents are present which are gradually vanished with time. Hence, efficiency is observed to be more at the initial stages. Exergy efficiency is also noted to be following the same trend. With the progression in solidification process, the temperature difference between outlet and inlet of HTF is decreased which infers the reduction in energy retrieval. Hence energy and exergy efficiencies are reduced with time. cylindrical shell is observed to perform better than conical shell in terms of energy and exergy efficiencies. As mentioned earlier, conical shell did not favor solidification as its geometry is exactly opposite to the nature of solidification front propagation. However, this drawback can be resolved by employing fins which is discussed in the next section.

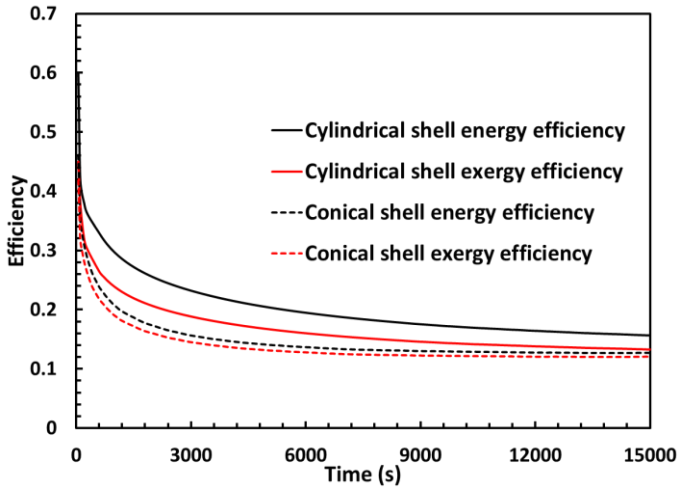

Figure 8.17: Temporal variation in energy and exergy efficiencies

8.5.2.2 Effect of fin parameters on discharging process

Similar to the melting process, the effect of fin parameters on solidification process is also analyzed by varying the fin dimensions as given in Table 8.1. Figure 8.18 shows the melt fraction contours and streamlines at various time levels for $\lambda = 0.6$ and 0.9 (for 15 number of fins). It can be noted that at lesser diameter i.e. for $\lambda = 0.6$, more thermal mixing took place because of the flow between fin and shell walls. From the figure it can be observed that at $\lambda = 0.6$, flow is occurring between fins and shell wall. On the other hand, at $\lambda = 0.9$, flow is confined to occur in between the fins. It can also be observed that the velocity magnitude does not vary much with λ. Increase in fin diameter results in more heat transfer area but lesser diameter resulted in more circulation of fluid. Hence, similar to the melting process solidification process also has both positive and negative influence of fin diameter. Figure 8.19 shows the melt fraction evolution for various λ values and 15 number of fins. With the increase in fin diameter total solidification time is increased which means that the circulation resulted from lesser fin diameter is more beneficial than increase in heat transfer area. 27.1% more time is required for complete solidification with the increase in from 0.6 to 0.9. irrespective of fin number, this behavior is observed to be same, however, for 5 number of fins, the difference in solidification time is very less. Variation in PCM average temperature and energy discharged by the PCM. are also observed to be in line to the melt fraction variation.

Solidification of PCM starts from HTF tube outer wall and over the time solidification also initiated from fin surfaces. Hence with the increase in number of fins, solidification rate is expected to increase. Fig 8.20 shows the streamlines during initial stages of solidification process when 5 and 20 number of fins are employed. When number of fin are less, the velocity magnitude of the unsolidified PCM is observed to be more when compared to higher fin number. Though in both the cases circulation of liquid PCM took place, velocity magnitude is higher when fin number is 5. Hence it can be said that increase in number of fins may dampen the solidification rate also. However, the circulation existed only at the initial stages of solidification and afterwards the solidification becomes conduction dominant because of which increase in number of fins has a positive impact on solidification rate. The same can be realized from Fig 8.20 in which a greater portion of solidified PCM can be noticed (where no streamlines are visible) when the number of fins is more. But the effect of fin number is less when compared to effect of fin diameter. Figure 8.21 shows total solidification times for all the cases considered. From this it can be observed that, at lesser diameter employing more number of fins with lesser diameter is beneficial rather than lesser number of fins with higher diameter.

The influence of fin number on energy discharged, average temperature are also similar to the effect on solidification time. similar to fin diameter, fin number also did not have an ample effect on energy and exergy efficiencies.

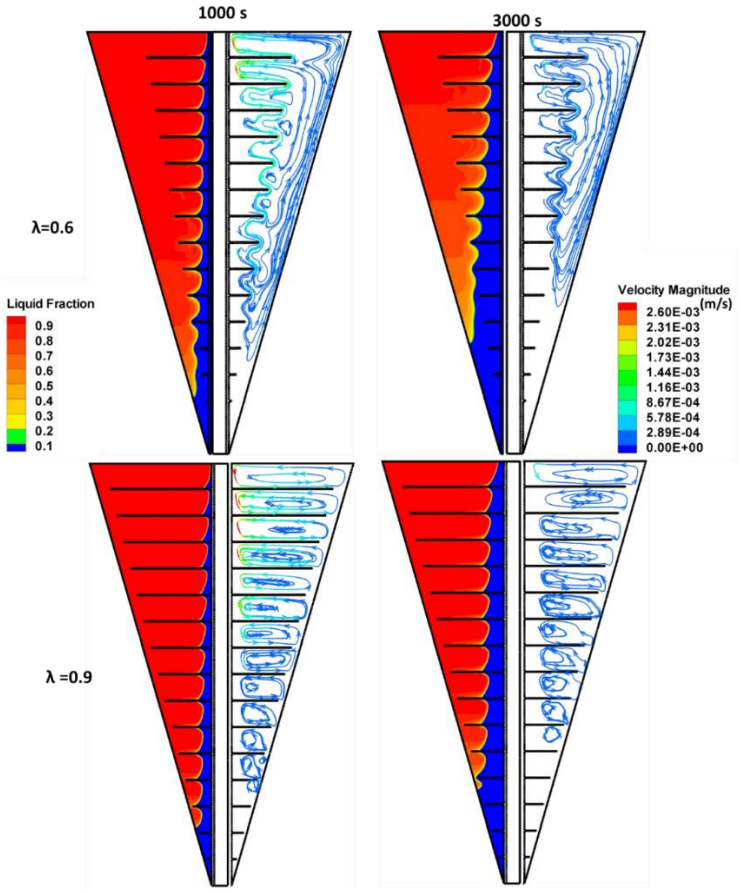

Figure 8.18: Melt fraction contours and streamlines at various time levels during solidification process

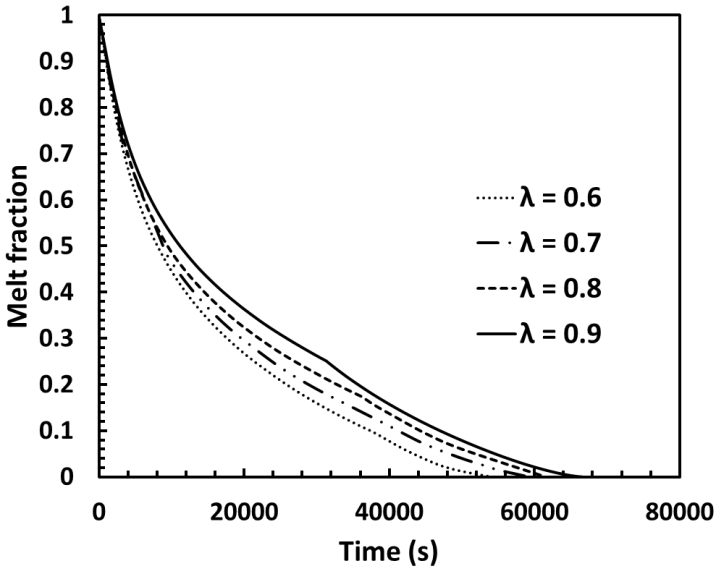

Figure 8.19: Effect of fin diameter on melt fraction variation during discharging process

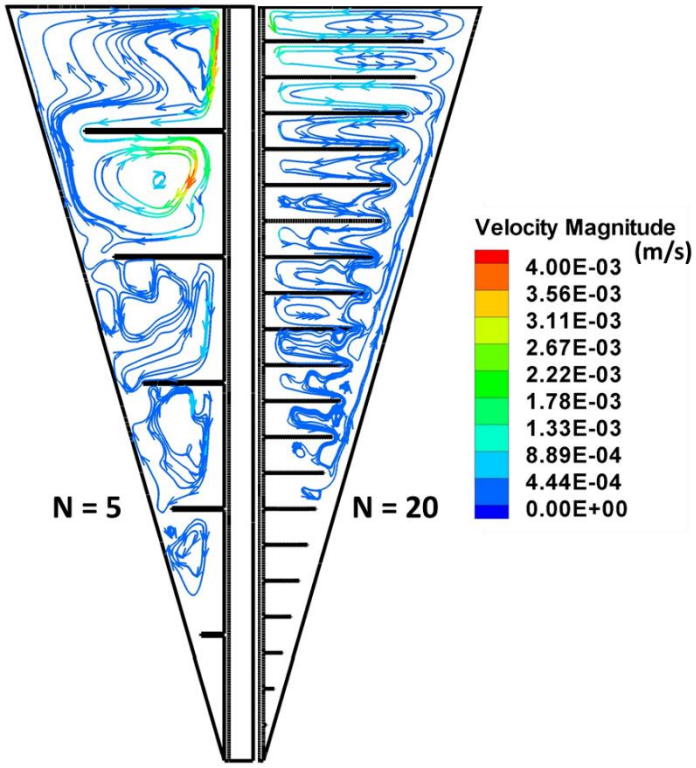

Figure 8.20: Effect of fin number on flow behavior during discharging process

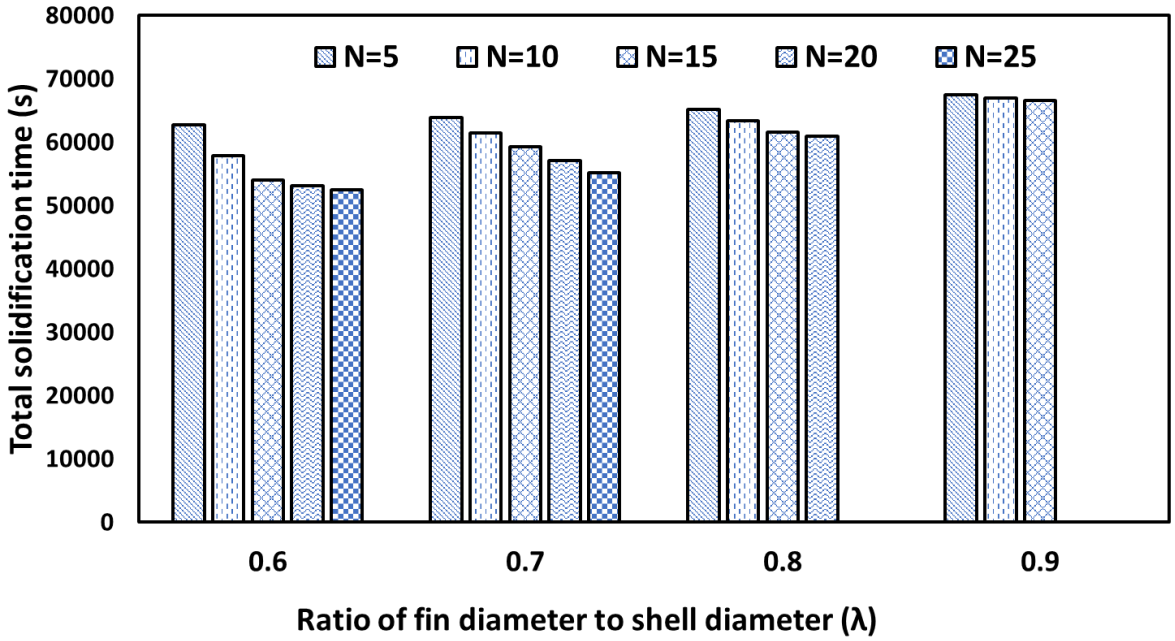

Figure 8.21: Total solidification time for all the considered cases

With the analysis of both charging and discharging processes, it can be concluded that higher number of fins with lesser diameter are beneficial for both charging and discharging processes.

8.6 Closure

Comparison of conical shell LHSU and cylindrical shell LHSU is made without fins for both charging and discharging processes. Annular fins are employed for heat transfer augmentation in conical shell LHSU and the effect of fin parameters is analyzed. The following conclusions are extracted from the current study.

- In the case of unfinned LHSU, conical shell resulted in 34.46% reduction in melting time, but total solidification time is increased by 63.79% when compared with the cylindrical shell.
- For the melting process effect of fin diameter depend on the number of fins. when 5 number of fins are attached increase in fin diameter caused a reduction in melting time but at 20 number of fins increase in fin diameter dampened the melting rate.
- Effect of the number of fins is more at lesser fin diameter during the melting process (for $\lambda = 0.6$, 21.2% reduction in melting time by increasing fin number from 5 to 15 whereas it is mere 0.43% if $\lambda = 0.9$).
- Energy and exergy efficiencies did not depend much on the fin parameters.
- For both melting and solidification process it is recommended to use 20 number of fins with $\lambda = 0.6$

Chapter 9

Conclusions and scope for future work

The present research work is aimed at analyzing the influence of different parameters on the thermal performance of a latent heat storage unit (LHSU). Lauric acid is chosen as the phase change material (PCM) which is filled in the annular space of shell and tube. Two types of annular fins: solid fins and perforated fins are considered for heat transfer augmentation. Experiments were performed to compare the performance of these two kinds of fins and to realize the effect of LHSU orientation on its thermal performance. Numerical simulations based on the enthalpy porosity approach are also carried out for the proper understanding of melting and solidification behavior of PCM and to optimize design parameters of annular fins. Fin parameters: fin diameter and number of fins are optimized by considering the energy and exergetic performance of LHSU. Finally, the geometry of the shell is modified to a conical shape for effective utilization of natural convection and the effect of fin parameters on conical shell LHSU is also analyzed. From the present experimental and numerical investigations, the following conclusions are drawn.

- Melting of PCM proceeded in a conical manner in vertical configuration and melting is assisted by natural convection. But towards the end of the melting process natural convection got diminished, and the mode of heat transfer became conduction dominant.
- Out of various operating and design parameters, Stefan number and Rayleigh number are the most influencing parameters which depend on HTF inlet temperature and shell diameter. 60.78% reduction in melting time is noted by increasing the inlet temperature by 40° C i.e. by increasing Stefan number from 0.2 to 0.6. Similarly, 36.37% reduction in total non-dimensional melting time is observed by increasing the Rayleigh number from 2.04×10^5 to 2.32×10^6.
- The influence of Reynolds number of HTF (mass flow rate) on melting time is very less. Increasing Reynolds from 500 to 2000 caused a reduction of 9.03% in total melting time.
- Tube material and tube thickness have a negligible effect on the total melting time. Hence, the selection of tube material can be made by considering its compatibility with the PCM chosen.

- The developed correlation satisfactorily estimated the total melting time with a maximum error of 5%.
- By analyzing experimental results on the effect of orientation it is observed that the temperature evolution during the melting process followed axisymmetric nature in vertical configuration and asymmetric for other inclinations.
- Horizontal configuration exhibited better melting rate at the initial stages of melting but for complete melting vertical configuration is preferred. To reach 0.5 melt fraction 37.17% lesser time is taken by horizontal configuration whereas total melting time is almost tripled in comparison to vertical orientation.
- Irrespective of orientation, energy efficiency is observed to be increasing up to some time and then energy efficiency started to decrease. Maximum efficiency is observed for vertical configuration which is equal to 43%.
- Exergy efficiency provided more insight on the thermal behavior of the LHSU. The zone of reducing exergy efficiency can be considered as a convection diminishing zone and the LHSU should be designed in such a way that this convection diminishing zone is minimized.
- When solid fins and perforated fins are compared, perforated fins in the vertical orientation of LHSU resulted in faster melting rate at the initial stages but towards the end of the melting process solid fins showed better performance
- Time-averaged energy storage rate is approximately 10% more in the case of solid fins when compared to perforated fins for all inclinations except in horizontal configuration.
- For solid finned LHSU fin effectiveness is observed to be nearly 5% more than the perforated fins at all the inclinations.
- For all the cases: unfinned, solid finned and perforated finned LHSU, orientation did not have any effect on the solidification process.
- Excessive number of fins resulted in attenuation of natural convection effect because of which melting time is increased
- Increase in the number of fins reduced the entropy generation whereas an increase in fin diameter caused an increase in entropy generation. By carrying out multi-objective optimization, the recommended fin parameters for the considered dimensions of LHSU are: Number of fins = 15, Fin diameter = 80 mm.
- Optimized fin parameters in the non-dimensional form are:

Non dimensional fin diameter = 0.8

Non dimensional fin spacing = 0.373

- Conical shell is preferred for the melting process but not for the solidification process (34.46% reduction in melting time, 63.17% increment in solidification time). Packing more amount of PCM at the top favored melting phenomenon but it has an adverse effect on the solidification process.
- At the higher number of fins (15 or more), an increase in fin diameter caused a reduction in melting rate because the higher diameter of fins led to poor thermal mixing.
- Effect of number of fins is more at lesser fin diameter (for $\lambda = 0.6$, 21.2% reduction in melting time by increasing fin number from 5 to 15 whereas it is mere 0.43% if $\lambda = 0.9$)
- Energy and exergy efficiencies did not depend much on fin parameters
- For both melting and solidification process it is recommended to use 20 number of fins with $\lambda = 0.6$

Scope for future work

- Employing perforated fins in the vertical configuration showed improvement in the performance of LHSU. But in the present study, the shape, dimensions and number of perforations are not optimized. Optimization of these parameters could result in better melting and solidification rates.
- Hybrid heat transfer enhancement techniques such as fins + nanoparticles, fins + metal foam can be implemented for further enhancement in heat transfer.
- Optimization of the container geometry can be done to make it efficient for both charging and discharging processes.
- The average temperature difference between inlet and outlet of HTF is nearly 2°C which is very low and hence multi-pass tube will be a good option to explore.
- Simultaneous charging and discharging has more practical relevance and hence it requires an in-depth analysis. Various configurations and enhancement techniques can be compared in this regard.

REFERENCES

[1] Data & Statistics - IEA, (n.d.). https://www.iea.org/data-and-statistics?country=WORLD&fuel=Energy consumption&indicator=Electricity consumption (accessed July 22, 2020).

[2] A. Schneider, S.H., S. Semenov, A. Patwardhan, I. Burton, C.H.D. Magadza, M. Oppenheimer, A.B. Pittock, A. Rahman, J.B. Smith, Suarez and F. Yamin, Assessing key vulnerabilities and the risk from climate change., in: P.J. van der L. and C.E.H. M.L. Parry, O.F. Canziani, J.P. Palutikof (Ed.), Clim. Chang. 2007 Impacts, Adapt. Vulnerability. Contrib. Work. Gr. II to Fourth Assess. Rep. Intergov. Panel Clim. Chang., Cambridge University Press, Cambridge, UK, 2007: pp. 779–810.

[3] SolarPayback, SOLAR HEAT FOR INDUSTRY, 2020. https://www.solar-payback.com/wp-content/uploads/2020/06/SHIP-india-26-06-20.pdf.

[4] C. Lauterbach, B. Schmitt, U. Jordan, K. Vajen, The potential of solar heat for industrial processes in Germany, Renew. Sustain. Energy Rev. 16 (2012) 5121–5130. doi:10.1016/j.rser.2012.04.032.

[5] S. Mekhilef, R. Saidur, A. Safari, A review on solar energy use in industries, Renew. Sustain. Energy Rev. 15 (2011) 1777–1790. doi:10.1016/j.rser.2010.12.018.

[6] H. Schnitzer, C. Brunner, G. Gwehenberger, Minimizing greenhouse gas emissions through the application of solar thermal energy in industrial processes, J. Clean. Prod. 15 (2007) 1271–1286. doi:10.1016/j.jclepro.2006.07.023.

[7] S. Kalogirou, The potential of solar industrial process heat applications, Appl. Energy. 76 (2003) 337–361. doi:10.1016/S0306-2619(02)00176-9.

[8] E. Morofsky, History of Thermal Energy Storage, Therm. Energy Storage Sustain. Energy Consum. (2007) 3–22. doi:10.1007/978-1-4020-5290-3_1.

[9] H.P. Garg, S.C. Mullick, A.K. Bhargava, Solar Thermal Energy Storage, Springer Netherlands, 1985.

https://books.google.co.in/books?id=ut_qCAAAQBAJ&printsec=frontcover&dq=Storage+of+solar+thermal+energy&hl=en&sa=X&ved=0ahUKEwj55v---Z_aAhWKNo8KHbFYCZcQ6AEIKDAA#v=onepage&q=Storage of solar thermal energy&f=false (accessed April 4, 2018).

[10] F. Wang, G. Maidment, J. Missenden, R. Tozer, A review of research concerning the use of PCMS in air conditioning and refrigeration engineering, Adv. Build. Technol. 2 (2002) 1273–1280. doi:10.1016/b978-008044100-9/50158-3.

[11] I. Dincer, M.A. Rosen, Thermal energy storage systems and applications, 2nd editio, Wiley, 2010.

[12] S. Arunachalam, Latent Heat Storage: Container geometry, enhancement techniques, and applications-A review, J. Sol. Energy Eng. Trans. ASME. 141 (2019). doi:10.1115/1.4043126.

[13] S.D. Sharma, K. Sagara, Latent Heat Storage Materials and Systems: A Review, Int. J. Green Energy. 2 (2005) 1–56. doi:10.1081/GE-200051299.

[14] M.M. Farid, A.M. Khudhair, S.A.K. Razack, S. Al-Hallaj, A review on phase change energy storage: Materials and applications, Energy Convers. Manag. 45 (2004) 1597–1615. doi:10.1016/j.enconman.2003.09.015.

[15] D.N. Nkwetta, F. Haghighat, Thermal energy storage with phase change material - A state-of-the art review, Sustain. Cities Soc. 10 (2014) 87–100. doi:10.1016/j.scs.2013.05.007.

[16] H. Akeiber, P. Nejat, M. Zaimi, A. Majid, M.A. Wahid, F. Jomehzadeh, I. Zeynali, J. Kaiser, B. Richard, S. Ahmad, A review on phase change material (PCM) for sustainable passive cooling in building envelopes, Renew. Sustain. Energy Rev. 60 (2016) 1470–1497. doi:10.1016/j.rser.2016.03.036.

[17] A. Kasaeian, F. Pourfayaz, E. Khodabandeh, Experimental studies on the applications of PCMs and nano-PCMs in buildings : A critical review, Energy Build. 154 (2017) 96–112. doi:10.1016/j.enbuild.2017.08.037.

[18] F. Souayfane, F. Fardoun, P. Biwole, Phase change materials (PCM) for cooling applications in buildings : A review, Energy Build. 129 (2016) 396–431. doi:10.1016/j.enbuild.2016.04.006.

[19] T. Silva, R. Vicente, F. Rodrigues, Literature review on the use of phase change materials in glazing and shading solutions, Renew. Sustain. Energy Rev. 53 (2016) 515–535. doi:10.1016/j.rser.2015.07.201.

[20] A. Sharma, V. V. Tyagi, C.R. Chen, D. Buddhi, Review on thermal energy storage with phase change materials and applications, Renew. Sustain. Energy Rev. 13 (2009) 318–345. doi:10.1016/j.rser.2007.10.005.

[21] Z. Wang, F. Qiu, W. Yang, X. Zhao, Applications of solar water heating system with phase change material, Renew. Sustain. Energy Rev. 52 (2015) 645–652. doi:10.1016/j.rser.2015.07.184.

[22] E. Oró, A. De Gracia, A. Castell, M.M. Farid, L.F. Cabeza, Review on phase change materials (PCMs) for cold thermal energy storage applications, Appl. Energy. 99 (2012) 513–533. doi:10.1016/j.apenergy.2012.03.058.

[23] C. Veerakumar, A. Sreekumar, Phase change material based cold thermal energy storage : Materials , techniques and applications – A review, Int. J. Refrig. 67 (2016) 271–289. doi:10.1016/j.ijrefrig.2015.12.005.

[24] L. Nkhonjera, T. Bello-ochende, C.K. King, A review of thermal energy storage designs , heat storage materials and cooking performance of solar cookers with heat storage, Renew. Sustain. Energy Rev. 75 (2017) 157–167. doi:10.1016/j.rser.2016.10.059.

[25] B. Zalba, J.M. Marín, L.F. Cabeza, H. Mehling, Review on thermal energy storage with phase change: Materials, heat transfer analysis and applications, Appl. Therm. Eng. 23 (2003) 251–283. doi:10.1016/S1359-4311(02)00192-8.

[26] Z. Zhang, J. Wang, X. Feng, L. Chang, Y. Chen, X. Wang, The solutions to electric vehicle air conditioning systems : A review, Renew. Sustain. Energy Rev. 91 (2018) 443–463. doi:10.1016/j.rser.2018.04.005.

[27] T. Markandeyulu, J. Krishna Devanuri, K. Kiran Kumar, On the suitability of phase change material (PCM) for thermal management of electronic components, Indian J. Sci. Technol. 9 (2016) 1–4. doi:10.17485/ijst/2016/v9iS1/107939.

[28] S. Kumar, M.K. Das, P. Rath, Application of TCE-PCM based heat sinks for cooling of electronic components : A review, Renew. Sustain. Energy Rev. 59 (2016) 550–582. doi:10.1016/j.rser.2015.12.238.

[29] D.J. Krishna, Operational Time and Melt Fraction Based Optimization of a Phase Change Material Longitudinal Fin Heat Sink, J. Therm. Sci. Eng. Appl. 10 (2018) 1–4. doi:10.1115/1.4040988.

[30] P.B. Salunkhe, D. Jaya Krishna, Investigations on latent heat storage materials for solar water and space heating applications, J. Energy Storage. 12 (2017) 243–260. doi:10.1016/j.est.2017.05.008.

[31] F. Agyenim, N. Hewitt, P. Eames, M. Smyth, A review of materials, heat transfer and phase change problem formulation for latent heat thermal energy storage systems (LHTESS), Renew. Sustain. Energy Rev. 14 (2010) 615–628. doi:10.1016/j.rser.2009.10.015.

[32] Y. Cao, A. Faghri, Performance characteristics of a thermal energy storage module: a transient PCM / forced convection conjugate analysis, Int. J. Heat Mass Transf. 34 (1991) 93–101. doi:https://doi.org/10.1016/0017-9310(91)90177-G.

[33] W.W. Wang, K. Zhang, L.B. Wang, Y.L. He, Numerical study of the heat charging and discharging characteristics of a shell-and-tube phase change heat storage unit, Appl. Therm. Eng. 58 (2013) 542–553. doi:10.1016/j.applthermaleng.2013.04.063.

[34] A. Agarwal, R.M. Sarviya, An experimental investigation of shell and tube latent heat storage for solar dryer using paraffin wax as heat storage material, Eng. Sci. Technol. an Int. J. 19 (2016) 619–631. doi:10.1016/j.jestch.2015.09.014.

[35] S. Seddegh, X. Wang, A.D. Henderson, A comparative study of thermal behaviour of a horizontal and vertical shell-and-tube energy storage using phase change materials, Appl. Therm. Eng. 93 (2016) 348–358. doi:10.1016/j.applthermaleng.2015.09.107.

[36] M.A. Kibria, M.R. Anisur, M.H. Mahfuz, R. Saidur, I.H.S.C. Metselaar, Numerical and experimental investigation of heat transfer in a shell and tube thermal energy storage system, Int. Commun. Heat Mass Transf. 53 (2014) 71–78. doi:10.1016/j.icheatmasstransfer.2014.02.023.

[37] M. Esen, A. Durmuş, A. Durmuş, Geometric design of solar-aided latent heat store depending on various parameters and phase change materials, Sol. Energy. 62 (1998) 19–28. doi:10.1016/S0038-092X(97)00104-7.

[38] M. Akgün, O. Aydin, K. Kaygusuz, Experimental study on melting/solidification characteristics of a paraffin as PCM, Energy Convers. Manag. 48 (2007) 669–678. doi:10.1016/j.enconman.2006.05.014.

[39] M.K. Rathod, J. Banerjee, Experimental investigations on latent heat storage unit using paraffin wax as phase change material, Exp. Heat Transf. 27 (2014) 40–55. doi:10.1080/08916152.2012.719065.

[40] E.S. Fath, Heat Exchanger Performance for Latent Heat Thermal Energy Storage System, Energy Convers. Manag. 31 (1991) 149–155. doi:https://doi.org/10.1016/0196-8904(91)90067-S.

[41] Z. Gong, A. Majumdar, Finite-element analysis of cyclic heat transfer in a shell-and-tube latent heat energy storage exchanger, Appl. Therm. Eng. 17 (1997) 583–591.

doi:10.1016/S1359-4311(96)00054-3.

[42] M. Lacroix, Numerical simulation of a shell-and-tube latent heat thermal energy storage unit, Sol. Energy. 50 (1993) 357–367. doi:10.1016/0038-092X(93)90029-N.

[43] Y. Wang, L. Wang, N. Xie, X. Lin, H. Chen, Experimental study on the melting and solidification behavior of erythritol in a vertical shell-and-tube latent heat thermal storage unit, Int. J. Heat Mass Transf. 99 (2016) 770–781. doi:10.1016/j.ijheatmasstransfer.2016.03.125.

[44] S. Seddegh, X. Wang, M.M. Joybari, F. Haghighat, Investigation of the effect of geometric and operating parameters on thermal behavior of vertical shell-and-tube latent heat energy storage systems, Energy. 137 (2017) 69–82. doi:10.1016/j.energy.2017.07.014.

[45] M. Avci, M.Y. Yazici, Experimental study of thermal energy storage characteristics of a paraffin in a horizontal tube-in-shell storage unit, Energy Convers. Manag. 73 (2013) 271–277. doi:10.1016/j.enconman.2013.04.030.

[46] M.A. Ezan, M. Ozdogan, A. Erek, Experimental study on charging and discharging periods of water in a latent heat storage unit, Int. J. Therm. Sci. 50 (2011) 2205–2219. doi:10.1016/j.ijthermalsci.2011.06.010.

[47] A. Sari, K. Kaygusuz, Thermal performance of a eutectic mixture of lauric and stearic acids as PCM encapsulated in the annulus of two concentric pipes, Sol. Energy. 72 (2002) 493–504. doi:10.1016/S0038-092X(02)00026-9.

[48] A. Trp, K. Lenic, B. Frankovic, Analysis of the influence of operating conditions and geometric parameters on heat transfer in water-paraffin shell-and-tube latent thermal energy storage unit, Appl. Therm. Eng. 26 (2006) 1830–1839. doi:10.1016/j.applthermaleng.2006.02.004.

[49] M.K. Rathod, J. Banerjee, Thermal Performance of a Phase Change Material-Based Latent Heat Thermal Storage Unit, Heat Transf. Res. 43 (2014) 706–719. doi:10.1002/htj.21120.

[50] W. Li, C. Kong, Numerical study on the thermal performance of a shell and tube phase change heat storage unit during melting process, Adv. Mech. Eng. 2014 (2014). doi:10.1155/2014/360283.

[51] C. Bellecci, M. Conti, Phase change thermal storage: transient behaviour analysis of a solar receiver/storage module using the enthalpy method, Int. J. Heat Mass Transf. 36 (1993) 2157–2163. doi:10.1016/S0017-9310(05)80146-2.

[52] K.A.R. Ismail, M.M. Gonçalves, Thermal performance of a pcm storage unit, Energy Convers. Manag. 40 (1999) 115–138. doi:10.1016/S0196-8904(98)00042-9.

[53] R.M. Abdel-Wahed, J.W. Ramsey, E.M. Sparrow, Photographic study of melting about an embedded horizontal heating cylinder, Int. J. Heat Mass Transf. 22 (1979) 171–173. doi:10.1016/0017-9310(79)90110-8.

[54] L.S. Yao, W. Cherney, Transient phase-change around a horizontal cylinder, Int. J. Heat Mass Transf. 24 (1981) 1971–1981. doi:10.1016/0017-9310(81)90119-8.

[55] L. Kalapala, J.K. Devanuri, Parametric investigation to assess the melt fraction and melting time for a latent heat storage material based vertical shell and tube heat

exchanger, Sol. Energy. 193 (2019) 360–371. doi:10.1016/j.solener.2019.09.076.

[56] X.Q. Wang, A.S. Mujumdar, C. Yap, Effect of orientation for phase change material (PCM)-based heat sinks for transient thermal management of electric components, Int. Commun. Heat Mass Transf. 34 (2007) 801–808. doi:10.1016/j.icheatmasstransfer.2007.03.008.

[57] X. Yang, Z. Guo, Y. Liu, L. Jin, Y.L. He, Effect of inclination on the thermal response of composite phase change materials for thermal energy storage, Appl. Energy. 238 (2019) 22–33. doi:10.1016/j.apenergy.2019.01.074.

[58] R. Karami, B. Kamkari, Investigation of the effect of inclination angle on the melting enhancement of phase change material in finned latent heat thermal storage units, Appl. Therm. Eng. 146 (2019) 45–60. doi:10.1016/j.applthermaleng.2018.09.105.

[59] R. Baby, C. Balaji, Experimental investigations on thermal performance enhancement and effect of orientation on porous matrix filled PCM based heat sink, Int. Commun. Heat Mass Transf. 46 (2013) 27–30. doi:10.1016/j.icheatmasstransfer.2013.05.018.

[60] B. Kamkari, H. Shokouhmand, F. Bruno, Experimental investigation of the effect of inclination angle on convection-driven melting of phase change material in a rectangular enclosure, Int. J. Heat Mass Transf. 72 (2014) 186–200. doi:10.1016/j.ijheatmasstransfer.2014.01.014.

[61] M. Avci, M.Y. Yazici, An experimental study on effect of inclination angle on the performance of a PCM-based flat-type heat sink, Appl. Therm. Eng. 131 (2018) 806–814. doi:10.1016/j.applthermaleng.2017.12.069.

[62] M.Y. Yazici, M. Avci, O. Aydin, Combined effects of inclination angle and fin number on thermal performance of a PCM-based heat sink, Appl. Therm. Eng. 159 (2019) 113956. doi:10.1016/j.applthermaleng.2019.113956.

[63] A. Bejan, CONVECTION HEAT TRANSFER, John Wiley & Sons Australia, Limited, 2013.

[64] N. Sharifi, C.W. Robak, T.L. Bergman, A. Faghri, International Journal of Heat and Mass Transfer Three-dimensional PCM melting in a vertical cylindrical enclosure including the effects of tilting, Int. J. Heat Mass Transf. 65 (2013) 798–806. doi:10.1016/j.ijheatmasstransfer.2013.06.070.

[65] N. Kousha, M.J. Hosseini, M.R. Aligoodarz, R. Pakrouh, R. Bahrampoury, Effect of inclination angle on the performance of a shell and tube heat storage unit – An experimental study, Appl. Therm. Eng. 112 (2017) 1497–1509. doi:10.1016/j.applthermaleng.2016.10.203.

[66] Y. Pahamli, M.J. Hosseini, A.A. Ranjbar, R. Bahrampoury, Effect of nanoparticle dispersion and inclination angle on melting of PCM in a shell and tube heat exchanger, J. Taiwan Inst. Chem. Eng. 81 (2017) 316–334. doi:10.1016/j.jtice.2017.09.044.

[67] S. Riahi, W.Y. Saman, F. Bruno, M. Belusko, N.H.S. Tay, Comparative study of melting and solidification processes in different configurations of shell and tube high temperature latent heat storage system, Sol. Energy. 150 (2017) 363–374. doi:10.1016/j.solener.2017.04.061.

[68] I. Al Siyabi, S. Khanna, T. Mallick, S. Sundaram, An experimental and numerical study on the effect of inclination angle of phase change materials thermal energy storage

system, J. Energy Storage. 23 (2019) 57–68. doi:10.1016/j.est.2019.03.010.

[69] D.S. Mehta, K. Solanki, M.K. Rathod, J. Banerjee, Influence of orientation on thermal performance of shell and tube latent heat storage unit, Appl. Therm. Eng. 157 (2019) 113719. doi:10.1016/j.applthermaleng.2019.113719.

[70] D.S. Mehta, K. Solanki, M.K. Rathod, J. Banerjee, Thermal performance of shell and tube latent heat storage unit: Comparative assessment of horizontal and vertical orientation, J. Energy Storage. 23 (2019) 344–362. doi:10.1016/j.est.2019.03.007.

[71] A.D. Solomon, Melt time and heat flux for a simple PCM body, Sol. Energy. 22 (1979) 251–257. doi:10.1016/0038-092X(79)90140-3.

[72] D.S. Riley, F.T. Smith, G. Poots, The inward solidification of spheres and circular cylinders, Int. J. Heat Mass Transf. 17 (1974) 1507–1516. doi:10.1016/0017-9310(74)90061-1.

[73] A. Hasan, Thermal energy storage system with stearic acid as phase change material, Energy Convers. Manag. 35 (1994) 843–856. doi:10.1016/0196-8904(94)90034-5.

[74] A. Hasan, Phase change material energy storage system employing Palmitic acid, Sol. Energy. 52 (1994) 143–154. doi:https://doi.org/10.1016/0038-092X(94)90064-7.

[75] C.-J. Ho, R. Viskanta, Heat Transfer During Melting From an Isothermal Vertical Wall, J. Heat Transfer. 106 (2009) 12. doi:10.1115/1.3246624.

[76] L. Katsman, V. Dubovsky, G. Ziskind, R. Letan, Experimental Investigation of Solid-Liquid Phase Change in Cylindrical Geometry, in: Proc. HT2007, ASME-JSME Therm. Eng. Summer Heat Transf. Conf., ASME, Vancouver, British Columbia, CANADA, 2007: pp. 1–6. doi:10.1115/ht2007-32354.

[77] K.A.R. Ismail, M. das G.E. da Silva, Melting of PCM around a horizontal cylinder with constant surface temperature, Int. J. Therm. Sci. 42 (2003) 1145–1152. doi:10.1016/S1290-0729(03)00093-0.

[78] L.W. Fan, Z.Q. Zhu, Y. Zeng, Q. Lu, Z.T. Yu, Heat transfer during melting of graphene-based composite phase change materials heated from below, Int. J. Heat Mass Transf. 79 (2014) 94–104. doi:10.1016/j.ijheatmasstransfer.2014.08.001.

[79] Y. Xu, M.J. Li, Z.J. Zheng, X.D. Xue, Melting performance enhancement of phase change material by a limited amount of metal foam: Configurational optimization and economic assessment, Appl. Energy. 212 (2018) 868–880. doi:10.1016/j.apenergy.2017.12.082.

[80] Y. Xu, Z.-J. Zheng, M.-J. Li, A half-analytical correlation of total melting time for shell-and-tube latent-heat thermal energy storage unit, Appl. Therm. Eng. 161 (2019) 114176. doi:10.1016/j.applthermaleng.2019.114176.

[81] K. Rathod Manish, B. Jyotirmay, Development of Correlation for Melting Time of Phase Change Material in Latent Heat Storage Unit, Energy Procedia. 75 (2015) 2125–2130. doi:10.1016/j.egypro.2015.07.339.

[82] A.M. Abdulateef, S. Mat, J. Abdulateef, K. Sopian, A.A. Al-Abidi, Geometric and design parameters of fins employed for enhancing thermal energy storage systems: a review, Renew. Sustain. Energy Rev. 82 (2018) 1620–1635. doi:10.1016/j.rser.2017.07.009.

[83] B. Kalhori, S. Ramadhyani, Studies on Heat Transfer From a Vertical Cylinder, With or Without Fins, Embedded in a Solid Phase Change Medium, Trans. ASME. 107 (1985). doi:doi:10.1115/1.3247400.

[84] H. Shokouhmand, B. Kamkari, Numerical Simulation of Phase Change Thermal Storage in Finned Double-Pipe Heat Exchanger, Appl. Mech. Mater. 232 (2012) 742–746. doi:10.4028/www.scientific.net/AMM.232.742.

[85] M.K. Rathod, J. Banerjee, Thermal performance enhancement of shell and tube Latent Heat Storage Unit using longitudinal fins, Appl. Therm. Eng. 75 (2015) 1084–1092. doi:10.1016/j.applthermaleng.2014.10.074.

[86] K.A.R. Ismail, C.L.F. Alves, M.S. Modesto, Numerical and experimental study on the solidification of PCM around a vertical axially finned isothermal cylinder, Appl. Therm. Eng. 21 (2001) 53–77. doi:10.1016/S1359-4311(00)00002-8.

[87] Y.B. Tao, Y.L. He, Effects of natural convection on latent heat storage performance of salt in a horizontal concentric tube, Appl. Energy. 143 (2015) 38–46. doi:10.1016/j.apenergy.2015.01.008.

[88] Y.B. Tao, Y.L. He, Numerical study on performance enhancement of shell-and-tube latent heat storage unit, Int. Commun. Heat Mass Transf. 67 (2015) 147–152. doi:10.1016/j.icheatmasstransfer.2015.07.013.

[89] A. Sciacovelli, F. Gagliardi, V. Verda, Maximization of performance of a PCM latent heat storage system with innovative fins, Appl. Energy. 137 (2015) 707–715. doi:10.1016/j.apenergy.2014.07.015.

[90] H. Walter, A. Beck, M. Hameter, Transient Analysis of an Improved Finned Tube Heat Exchanger for Thermal Energy Storage System, in: ASME 2015 9th Int. Conf. Energy Sustain., San Diego, California, 2015: pp. 1–14. doi:doi:10.1115/ES2015-49144.

[91] A. Pizzolato, A. Sharma, K. Maute, A. Sciacovelli, V. Verda, Design of effective fins for fast PCM melting and solidification in shell-and-tube latent heat thermal energy storage through topology optimization, Appl. Energy. 208 (2017) 210–227. doi:10.1016/j.apenergy.2017.10.050.

[92] J.C. Choi, S.D. Kim, Heat-transfer characteristics of a latent heat storage system using MgCl2· 6H2O, Energy. 17 (1992) 1153–1164. doi:10.1016/0360-5442(92)90004-J.

[93] M. Lacroix, Study of the heat transfer behavior of a latent heat thermal energy storage unit with a finned tube, Int. J. Heat Mass Transf. 36 (1993) 2083–2092. doi:10.1016/S0017-9310(05)80139-5.

[94] W.W. Wang, L.B. Wang, Y.L. He, Parameter effect of a phase change thermal energy storage unit with one shell and one finned tube on its energy efficiency ratio and heat storage rate, Appl. Therm. Eng. 93 (2016) 50–60. doi:10.1016/j.applthermaleng.2015.08.108.

[95] V. Thirunavukkarasu, G. Balaji, M. Sornanathan, Experimental analysis of shell and tube thermal energy storage system with finned tube, J. Chem. Pharm. Sci. 9 (2016) 3138–3141. www.jchps.com.

[96] X. Yang, Z. Lu, Q. Bai, Q. Zhang, L. Jin, J. Yan, Thermal performance of a shell-and-tube latent heat thermal energy storage unit: Role of annular fins, Appl. Energy. 202 (2017) 558–570. doi:10.1016/j.apenergy.2017.05.007.

[97] R. V. Seeniraj, R. Velraj, N.L. Narasimhan, Thermal analysis of a finned-tube LHTS module for a solar dynamic power system, Heat Mass Transf. 38 (2002) 409–417. doi:10.1007/s002310100268.

[98] D. Groulx, W. Ogoh, Solid-liquid phase change simulation applied to a cylindrical latent heat energy storage system, in: Proc. 5th Annu. COMSOL Conf., Boston, 2009: p. 7 p. doi:doi=10.1.1.476.3369.

[99] D. Zhao, G. Tan, Numerical analysis of a shell-and-tube latent heat storage unit with fins for air-conditioning application, Appl. Energy. 138 (2015) 381–392. doi:10.1016/j.apenergy.2014.10.051.

[100] M.J. Hosseini, M. Rahimi, R. Bahrampoury, Thermal analysis of PCM containing heat exchanger enhanced with normal annular fines, Mech. Sci. 6 (2015) 221–234. doi:10.5194/ms-6-221-2015.

[101] K.A.R. Ismail, F.A.M. Lino, Fins and turbulence promoters for heat transfer enhancement in latent heat storage systems, Exp. Therm. Fluid Sci. 35 (2011) 1010–1018. doi:10.1016/j.expthermflusci.2011.02.002.

[102] I. Jmal, M. Baccar, Numerical study of PCM solidification in a finned tube thermal storage including natural convection, Appl. Therm. Eng. 84 (2015) 320–330. doi:10.1016/j.applthermaleng.2015.03.065.

[103] X.Q. Zhai, X.W. Cheng, C. Wang, R.Z. Wang, Experimental investigation and performance analysis of a fin tube phase change cold storage unit for high temperature cooling application, Energy Build. 89 (2015) 9–17. doi:10.1016/j.enbuild.2014.12.021.

[104] F.S. dos Santos, K.A.R. Ismail, F.A.M. Lino, A. Arabkoohsar, T.G.S. Lago, Parametric investigation of the enhancing effects of finned tubes on the solidification of PCM, Int. J. Heat Mass Transf. 152 (2020) 119485. doi:10.1016/j.ijheatmasstransfer.2020.119485.

[105] S. Kuboth, A. König-Haagen, D. Brüggemann, Numerical analysis of shell-and-tube type latent thermal energy storage performance with different arrangements of circular fins, Energies. 10 (2017) 274. doi:10.3390/en10030274.

[106] A. Erek, Z. Ilken, M.A. Acar, Experimental and numerical investigation of thermal energy storage with a finned tube, Int. J. Energy Res. 29 (2005) 283–301. doi:10.1002/er.1057.

[107] S. Paria, S. Baradaran, A. Amiri, A.A.D. Sarhan, S.N. Kazi, Performance evaluation of latent heat energy storage in horizontal shell-and-finned tube for solar application, J. Therm. Anal. Calorim. 123 (2016) 1371–1381. doi:10.1007/s10973-015-5006-1.

[108] R. Karami, B. Kamkari, Experimental investigation of the effect of perforated fins on thermal performance enhancement of vertical shell and tube latent heat energy storage systems, Energy Convers. Manag. 210 (2020) 112679. doi:10.1016/j.enconman.2020.112679.

[109] A. Maji, D. Bhanja, P.K. Patowari, Numerical investigation on heat transfer enhancement of heat sink using perforated pin fins with inline and staggered arrangement, Appl. Therm. Eng. 125 (2017) 596–616. doi:10.1016/j.applthermaleng.2017.07.053.

[110] A. Keyhani Asl, S. Hossainpour, M.M. Rashidi, M.A. Sheremet, Z. Yang, Comprehensive investigation of solid and porous fins influence on natural convection in

an inclined rectangular enclosure, Int. J. Heat Mass Transf. 133 (2019) 729–744. doi:10.1016/j.ijheatmasstransfer.2018.12.156.

[111] F. Agyenim, P. Eames, M. Smyth, A comparison of heat transfer enhancement in a medium temperature thermal energy storage heat exchanger using fins, Sol. Energy. 83 (2009) 1509–1520. doi:10.1016/j.solener.2009.04.007.

[112] F. Agyenim, P. Eames, M. Smyth, A Comparison of Heat Transfer Enhancement in Medium Temperature Thermal Energy Storage Heat Exchanger Using Fins and Multitubes, in: Proc. ISES World Congr. 2007 (Vol. I – Vol. V), Springer Berlin Heidelberg, Berlin, Heidelberg, 2008: pp. 2726–2730. doi:10.1007/978-3-540-75997-3_550.

[113] J. Abdulateef, M.S. Mahdi, A.F. Hasan, Experimental evaluation of thermal performance of two different finned latent heat storage systems, Case Stud. Therm. Eng. (2020) 100675. doi:10.1016/j.csite.2020.100675.

[114] N.H.S. Tay, F. Bruno, M. Belusko, Comparison of pinned and finned tubes in a phase change thermal energy storage system using CFD, Appl. Energy. 104 (2013) 79–86. doi:10.1016/j.apenergy.2012.10.040.

[115] M.M. Farid, A. Kanzawa, Thermal Performance of a Heat Storage Module Using PCM's With Different Melting Temperatures: Mathematical Modeling, J. Sol. Energy Eng. 111 (1989) 152. doi:10.1115/1.3268301.

[116] G. a. Adebiyi, A Second-Law Study on Packed Bed Energy Storage Systems Utilizing Phase-Change Materials, J. Sol. Energy Eng. 113 (1991) 146. doi:10.1115/1.2930486.

[117] J. Lim, A. Bejan, J. Kim, Thermodynamic optimization of phase-change energy-storage using 2 or more materials, J. Energy Resour. Technol. Asme. 114 (1992) 84–90. doi:https://doi.org/10.1115/1.2905925.

[118] T. Watanabe, H. Kikuchi, A. Kanzawa, Enhancement of charging and discharging rates in a latent heat storage system by use of PCM with different melting temperatures, Heat Recover. Syst. CHP. 13 (1993) 57–66. doi:10.1016/0890-4332(93)90025-Q.

[119] R. V. Seeniraj, N. Lakshmi Narasimhan, Performance enhancement of a solar dynamic LHTS module having both fins and multiple PCMs, Sol. Energy. 82 (2008) 535–542. doi:10.1016/j.solener.2007.11.001.

[120] Z.-X. Gong, A.S. Mujumdar, Enhancement of energy charge-discharge rates in composite slabs of different phase change materials, Int. J. Heat Mass Transf. 39 (1996) 725–733. doi:https://doi.org/10.1016/0017-9310(95)00179-4.

[121] Z.. Gong, A.S. Mujumdar, Exergetic Analysis of Energy Storage Using Multiple Phase-Change Materiais, in: Trans. ASME, 1996. doi:doi:10.1115/1.2793869.

[122] Z.-X. Gong, A.S. Mujumdar, Thermodynamic optimization of the thermal process in energy storage using multiple phase change materials, Appl. Therm. Eng. 17 (1997) 1067–1083. doi:10.1016/S1359-4311(97)00012-4.

[123] M. Ezra, Y. Kozak, V. Dubovsky, G. Ziskind, Analysis and optimization of melting temperature span for a multiple-PCM latent heat thermal energy storage unit, Appl. Therm. Eng. 93 (2016) 315–329. doi:10.1016/j.applthermaleng.2015.09.040.

[124] O. Meshally, K. Lafdi, A. Elgafy, K. Bowman, Numerical study for enhancing the

thermal conductivity of phase change material (PCM) storage using high thermal conductivity porous matrix, Energy Convers. Manag. 46 (2005) 847–867. doi:https://doi.org/10.1016/j.enconman.2004.06.010.

[125] A. Atal, Y. Wang, M. Harsha, S. Sengupta, Effect of porosity of conducting matrix on a phas change energy storage device, Int. J. Heat Mass Transf. 93 (2016) 9–16. doi:https://doi.org/10.1016/j.ijheatmasstransfer.2015.09.033.

[126] Z. Li, Z.-G. Wu, Numerical study on the thermal behaviour of phase change materials (PCMs) embedded in porous metal matrix, Sol. Energy. 99 (2014) 172–184. doi:https://doi.org/10.1016/j.solener.2013.11.017.

[127] A. Mills, M. Farid, J.R. Selman, S. Al-Hallaj, Thermal conductivity enhancement of phase change materials using a graphite matrix, Appl. Therm. Eng. 26 (2006) 1652–1661. doi:10.1016/j.applthermaleng.2005.11.022.

[128] Y. Zhong, Q. Guo, S. Li, J. Shi, L. Liu, Heat transfer enhancement of paraffin wax using graphite foam for thermal energy storage, Sol. Energy Mater. Sol. Cells. 94 (2010) 1011–1014. doi:10.1016/j.solmat.2010.02.004.

[129] Y. Zhong, S. Li, X. Wei, Z. Liu, Q. Guo, J. Shi, L. Liu, Heat transfer enhancement of paraffin wax using compressed expanded natural graphite for thermal energy storage, Carbon N. Y. 48 (2010) 300–304. doi:10.1016/j.carbon.2009.09.033.

[130] M. Moeini Sedeh, J.M. Khodadadi, Thermal conductivity improvement of phase change materials/graphite foam composites, Carbon N. Y. 60 (2013) 117–128. doi:10.1016/j.carbon.2013.04.004.

[131] W. Zhao, D.M. France, W. Yu, T. Kim, D. Singh, Phase change material with graphite foam for applications in high-temperature latent heat storage systems of concentrated solar power plants, Renew. Energy. 69 (2014) 134–146. doi:https://doi.org/10.1016/j.renene.2014.03.031.

[132] A. Sari, A. Karaipekli, Thermal conductivity and latent heat thermal energy storage characteristics of paraffin/expanded graphite composite as phase change material, Appl. Therm. Eng. 27 (2007) 1271–1277. doi:10.1016/j.applthermaleng.2006.11.004.

[133] Z. Li, W.G. Sun, G. Wang, Z.G. Wu, Experimental and numerical study on the effective thermal conductivity of paraffin/expanded graphite composite, Sol. Energy Mater. Sol. Cells. 128 (2014) 447–455. doi:10.1016/j.solmat.2014.06.023.

[134] Z.G. Wu, C.Y. Zhao, Experimental investigations of porous materials in high temperature thermal energy storage systems, Sol. Energy. 85 (2011) 1371–1380. doi:10.1016/j.solener.2011.03.021.

[135] C.Y. Zhao, Z.G. Wu, Heat transfer enhancement of high temperature thermal energy storage using metal foams and expanded graphite, Sol. Energy Mater. Sol. Cells. 95 (2011) 636–643. doi:10.1016/j.solmat.2010.09.032.

[136] L. Zhong, X. Zhang, Y. Luan, G. Wang, Y. Feng, D. Feng, Preparation and thermal properties of porous heterogeneous composite phase change materials based on molten salts/expanded graphite, Sol. Energy. 107 (2014) 63–73. doi:10.1016/j.solener.2014.05.019.

[137] X. Xiao, P. Zhang, M. Li, Experimental and numerical study of heat transfer performance of nitrate/expanded graphite composite PCM for solar energy storage,

Energy Convers. Manag. 105 (2015) 272–284. doi:10.1016/j.enconman.2015.07.074.

[138] Z. Duan, H. Zhang, L. Sun, Z. Cao, F. Xu, Y. Zou, H. Chu, S. Qiu, C. Xiang, H. Zhou, CaCl2·6H2O/Expanded graphite composite as form-stable phase change materials for thermal energy storage, J. Therm. Anal. Calorim. 115 (2014) 111–117. doi:10.1007/s10973-013-3311-0.

[139] Y. Tian, C.Y. Zhao, A numerical investigation of heat transfer in phase change materials (PCMs) embedded in porous metals, Energy. 36 (2011) 5539–5546. doi:10.1016/j.energy.2011.07.019.

[140] A. Siahpush, J. O'Brien, J. Crepeau, Phase Change Heat Transfer Enhancement Using Copper Porous Foam, J. Heat Transfer. 130 (2008) 082301. doi:10.1115/1.2928010.

[141] Z. Li, Z.G. Wu, Numerical study on the thermal behavior of phase change materials (PCMs) embedded in porous metal matrix, Sol. Energy. 99 (2014) 172–184. doi:10.1016/j.solener.2013.11.017.

[142] C. Wang, T. Lin, H. Zheng, Heat transfer enhancement of phase change composite material: Copper foam/paraffin, Renew. Energy. 96 (2016) 960–965. doi:https://doi.org/10.1016/j.renene.2016.04.039.

[143] P.Zhang, Z.N. Meng, H. Zhu, Y.L. Wang, S.P. Peng, Melting heat transfer characteristics of a composite phase cahnge material fabricated by paraffin and metal foam, Appl. Energy. 185 (2017) 1971–1983. doi:https://doi.org/10.1016/j.apenergy.2015.10.075.

[144] C.Y.Zhao, W.Lu, Y.Tian, Heat transfer enhancement for thermal energy storage using metal foams embedded within phase cahnge materials (PCMs), Sol. Energy. 84 (2010) 1042–1412. doi:https://doi.org/10.1016/j.solener.2010.04.022.

[145] N. Dukhan, S. Bodke, An improved PCM heat storage technology utilizing metal foam, 12th IEEE Intersoc. Conf. Therm. Thermomechanical Phenom. Electron. Syst. ITherm. (2010). doi:10.1109/ITHERM.2010.5501364.

[146] K. Lafdi, O. Mesalhy, S. Shaikh, Experimental study on the influence of foam porosity and pore size on the melting of phase change materials, J. Appl. Phys. 102 (2007). doi:10.1063/1.2802183.

[147] P.V.S.S. Srivatsa, R. Baby, C. Balaji, Numerical investigation of PCM based heat sinks with embedded metal foam/crossed plate fins, Numer. Heat Transf. Part A Appl. 66 (2014) 1131–1153. doi:10.1080/10407782.2014.894371.

[148] E. Fleming, S. Wen, L. Shi, A.K. Da Silva, Experimental and theoretical analysis of an aluminum foam enhanced phase change thermal storage unit, Int. J. Heat Mass Transf. 82 (2015) 273–281. doi:10.1016/j.ijheatmasstransfer.2014.11.022.

[149] A. Sari, Form-stable paraffin/high density polyethylene composites as solid-liquid phase change material for thermal energy storage: Preparation and thermal properties, Energy Convers. Manag. 45 (2004) 2033–2042. doi:10.1016/j.enconman.2003.10.022.

[150] W. Wang, X. Yang, Y. Fang, J. Ding, J. Yan, Enhanced thermal conductivity and thermal performance of form-stable composite phase change materials by using β-Aluminum nitride, Appl. Energy. 86 (2009) 1196–1200. doi:10.1016/j.apenergy.2008.10.020.

[151] Z. Liu, Y. Yao, H. Wu, Numerical modeling for solid-liquid phase change phenomena in porous media: Shell-and-tube type latent heat thermal energy storage, Appl. Energy. 112 (2013) 1222–1232. doi:https://doi.org/10.1016/j.apenergy.2013.02.022.

[152] J. Yang, Lijun Yang, C. Xu, X. Du, Numerical analysis on thermal behaviour of solid-liquid phase change within copper foam with varying porosity, Int. J. Heat Mass Transf. 84 (2015) 1008–1018. doi:https://doi.org/10.1016/j.ijheatmasstransfer.2015.01.088.

[153] Y. Xu, Q. Ren, Z.J. Zheng, Y.L. He, Evaluation and optimization of melting performance for a latent heat thermal energy storage unit partially filled with porous media, Appl. Energy. 193 (2017) 84–95. doi:10.1016/j.apenergy.2017.02.019.

[154] A.M. DYUGAEV, THERMAL CONDUCTIVITY AND VISCOSITV OF LIQUID 3He, Phys. Lett. 111A (1985) 307–309.

[155] S.U.S. Choi, J.A.. S.. " Eastman, Enhancing thermal conductivity of fluids with nanoparticles., in: Dev. Appl. Non-Newtonian Flows, ASME, 1995: pp. 99–105. doi:doi:. https://www.osti.gov/servlets/purl/196525.

[156] J.M. Khodadadi, S.F. Hosseinizadeh, Nanoparticle-enhanced phase change materials (NEPCM) with great potential for improved thermal energy storage, Int. Commun. Heat Mass Transf. 34 (2007) 534–543. doi:https://doi.org/10.1016/j.icheatmasstransfer.2007.02.005.

[157] S. Shaikh, K. Lafdi, K. Hallinan, Carbon nanoadditives to enhance latent energy storage of phase change materials, J. Appl. Phys. 103 (2008). doi:10.1063/1.2903538.

[158] J. Wang, H. Xie, Z. Xin, Thermal properties of paraffin based composites containing multi-walled carbon nanotubes, Thermochim. Acta. 488 (2009) 39–42. doi:10.1016/j.tca.2009.01.022.

[159] V. Kumaresan, R. Velraj, S.K. Das, The effect of carbon nanotubes in enhancing the thermal transport properties of PCM during solidification, Heat Mass Transf. Und Stoffuebertragung. 48 (2012) 1345–1355. doi:10.1007/s00231-012-0980-3.

[160] T.P. Teng, C.M. Cheng, C.P. Cheng, Performance assessment of heat storage by phase change materials containing MWCNTs and graphite, Appl. Therm. Eng. 50 (2013) 637–644. doi:10.1016/j.applthermaleng.2012.07.002.

[161] Z.T. Yu, X. Fang, L.W. Fan, X. Wang, Y.Q. Xiao, Y. Zeng, X. Xu, Y.C. Hu, K.F. Cen, Increased thermal conductivity of liquid paraffin-based suspensions in the presence of carbon nano-additives of various sizes and shapes, Carbon N. Y. 53 (2013) 277–285. doi:10.1016/j.carbon.2012.10.059.

[162] J. Wang, H. Xie, Z. Xin, Thermal properties of heat storage composites containing multiwalled carbon nanotubes, J. Appl. Phys. 104 (2008). doi:10.1063/1.3041495.

[163] J. Wang, H. Xie, Z. Xin, Y. Li, L. Chen, Enhancing thermal conductivity of palmitic acid based phase change materials with carbon nanotubes as fillers, Sol. Energy. 84 (2010) 339–344. doi:10.1016/j.solener.2009.12.004.

[164] J.L. Zeng, Z. Cao, D.W. Yang, F. Xu, L.X. Sun, X.F. Zhang, L. Zhang, Effects of MWNTs on phase change enthalpy and thermal conductivity of a solid-liquid organic PCM, J. Therm. Anal. Calorim. 95 (2009) 507–512. doi:10.1007/s10973-008-9275-9.

[165] T.X. Li, J.H. Lee, R.Z. Wang, Y.T. Kang, Enhancement of heat transfer for thermal

energy storage application using stearic acid nanocomposite with multi-walled carbon nanotubes, Energy. 55 (2013) 752–761. doi:10.1016/j.energy.2013.04.010.

[166] L.W. Fan, X. Fang, X. Wang, Y. Zeng, Y.Q. Xiao, Z.T. Yu, X. Xu, Y.C. Hu, K.F. Cen, Effects of various carbon nanofillers on the thermal conductivity and energy storage properties of paraffin-based nanocomposite phase change materials, Appl. Energy. 110 (2013) 163–172. doi:10.1016/j.apenergy.2013.04.043.

[167] Y. Cui, C. Liu, S. Hu, X. Yu, The experimental exploration of carbon nanofiber and carbon nanotube additives on thermal behavior of phase change materials, Sol. Energy Mater. Sol. Cells. 95 (2011) 1208–1212. doi:10.1016/j.solmat.2011.01.021.

[168] D.H. Choi, J. Lee, H. Hong, Y.T. Kang, Thermal conductivity and heat transfer performance enhancement of phase change materials (PCM) containing carbon additives for heat storage application, Int. J. Refrig. 42 (2014) 112–120. doi:10.1016/j.ijrefrig.2014.02.004.

[169] S. Harish, D. Orejon, Y. Takata, M. Kohno, Thermal conductivity enhancement of lauric acid phase change nanocomposite with graphene nanoplatelets, Appl. Therm. Eng. 80 (2015) 205–211. doi:10.1016/j.applthermaleng.2015.01.056.

[170] X. Fang, L.-W. Fan, Q. Ding, X. Wang, X.-L. Yao, J.-F. Hou, Z.-T. Yu, G.-H. Chen, Y.-C. Hu, K.-F. Cen, Increased Thermal Conductivity of Eicosane-Based Composite Phase Change Materials in the Presence of Graphene Nanoplatelets BT - Energy & Fuels, Energy and Fuels. 27 (2013) 4041–4047. doi:10.1021/ef400702a.

[171] L.W. Fan, Z.Q. Zhu, Y. Zeng, Y.Q. Xiao, X.L. Liu, Y.Y. Wu, Q. Ding, Z.T. Yu, K.F. Cen, Transient performance of a PCM-based heat sink with high aspect-ratio carbon nanofillers, Appl. Therm. Eng. 75 (2015) 532–540. doi:10.1016/j.applthermaleng.2014.10.050.

[172] E.B.S. Mettawee, G.M.R. Assassa, Thermal conductivity enhancement in a latent heat storage system, Sol. Energy. 81 (2007) 839–845. doi:10.1016/j.solener.2006.11.009.

[173] C.J. Ho, J.Y. Gao, An experimental study on melting heat transfer of paraffin dispersed with Al2O3 nanoparticles in a vertical enclosure, Int. J. Heat Mass Transf. 62 (2013) 2–8. doi:10.1016/j.ijheatmasstransfer.2013.02.065.

[174] S. Motahar, N. Nikkam, A.A. Alemrajabi, R. Khodabandeh, M.S. Toprak, M. Muhammed, Experimental investigation on thermal and rheological properties of n-octadecane with dispersed TiO2nanoparticles, Int. Commun. Heat Mass Transf. 59 (2014) 68–74. doi:10.1016/j.icheatmasstransfer.2014.10.016.

[175] J. Zeng, F. Zhu, S. Yu, L. Zhu, Z. Cao, L. Sun, G. Deng, Solar Energy Materials & Solar Cells Effects of copper nanowires on the properties of an organic phase change material, Sol. Energy Mater. Sol. Cells. 105 (2012) 174–178. doi:10.1016/j.solmat.2012.06.013.

[176] L. Zhang, Thermal conductivity enhancement of Ag nanowires on an organic phase change material, J. Therm. Anal. Calorim. 101 (2010) 385–389. doi:10.1007/s10973-009-0472-y.

[177] X. Xiao, P. Zhang, Numerical and experimental study of heat transfer characteristics of a shell-tube latent heat storage system: Part I-Charging process, Energy. 79 (2015) 337–350. doi:https://doi.org/10.1016/j.energy.2014.11.020.

[178] N. Das, Y. Takata, M. Kohno, S. Harish, Melting of graphene based phase change

nanocomposites in vertical latent heat thermal energy storage unit, Appl. Therm. Eng. 107 (2016) 101–113. doi:https://doi.org/10.1016/j.applthermaleng.2016.06.166.

[179] M. Parsazadeh, X. Duan, Numerical and statistical study on melting of nanoparticle enhanced phase change material in a shell-and-tube thermal energy storage system, Appl. Therm. Eng. 111 (2017) 950–960. doi:10.1016/j.applthermaleng.2016.09.133.

[180] S. Fomin, A. Wilchinsky, T. Saitoh, Close-contact melting inside an elliptic cylinder, Sol. Energy Eng. Trans. ASME. 122 (2000) 192–195. doi:10.1115/1.1330724.

[181] E.M. Alawadhi, A solidification process with free convection of water in an elliptical enclosure, Energy Convers. Manag. 50 (2009) 360–364. doi:10.1016/j.enconman.2008.09.015.

[182] M. Akgün, O. Aydin, K. Kaygusuz, Thermal energy storage performance of paraffin in a novel tube-in-shell system, Appl. Therm. Eng. 28 (2008) 405–413. doi:10.1016/j.applthermaleng.2007.05.013.

[183] Z. Hu, A. Li, R. Gao, H. Yin, Enhanced heat transfer for PCM melting in the frustum-shaped unit with multiple PCMs, J. Therm. Anal. Calorim. 120 (2015) 1407–1416. doi:10.1007/s10973-014-4370-6.

[184] A.D. Korawan, S. Soeparman, W. Wijayanti, D. Widhiyanuriyawan, 3D numerical and experimental study on paraffin wax melting in thermal storage for the nozzle-and-shell, tube-and-shell, and reducer-and-shell models, Model. Simul. Eng. 2017 (2017). doi:10.1155/2017/9590214.

[185] A.D. Korawan, S. Soeparman, W. Wijayanti, D. Widhiyanuriyawan, Increased Melting Heat Transfer in the Latent Heat Energy Storage from the Tube-and-Shell Model to the Combine-and-Shell Model, Model. Simul. Eng. 2017 (2017). doi:10.1155/2017/8574184.

[186] A.A. Rabienataj Darzi, M. Jourabian, M. Farhadi, Melting and solidification of PCM enhanced by radial conductive fins and nanoparticles in cylindrical annulus, Energy Convers. Manag. 118 (2016) 253–263. doi:10.1016/j.enconman.2016.04.016.

[187] M. Faghani, M.J. Hosseini, R. Bahrampoury, Numerical simulation of melting between two elliptical cylinders, Alexandria Eng. J. (2016) 1–10. doi:10.1016/j.aej.2017.02.003.

[188] K. Muralidhar, J. Banerjee, Conduction and Radiation, Alpha Science International, 2010. https://books.google.co.in/books?id=FnqQSQAACAAJ.

[189] M.N. Özışık, Heat conduction, John Wiley & Sons Australia, Limited, 1980. https://books.google.co.in/books?id=8H4pAQAAMAAJ.

[190] T. Cheng, Numerical analysis of nonlinear multiphase Stefan problems, Comput. Struct. 75 (2000) 225–233.

[191] K.B. Radhakrishnan, A.R. Balakrishnan, Storage using phase change, Heat Recover. Syst. CHP. 12 (1992) 427–435.

[192] H. Hu, S.A. Argyropoulos, Mathematical modelling of solidification and melting : a review, Model. Simul. Mater. Sci. Eng. 4 (1996) 371–396. doi:https://doi.org/10.1088/0965-0393/4/4/004.

[193] D. Poirier, M. Salcudean, On Numerical Methods Used in Mathematical Modeling of

Phase Change in Liquid Metals, Trans. ASME. 110 (1988). doi:doi:10.1115/1.3250529.

[194] E.M. Sparrow, S. V. Patankar, S. Ramadhyani, Analysis of Melting in the Presence of Natural Confection in the Melt Region, Trans. ASME. 99 (1977). doi:doi:10.1115/1.3450736.

[195] L.S. Yao, F.F. Chen, Effects of Natural Convection in the Melted Region Around a Heated Horizontal Cylinder, J. Heat Transfer. 102 (1980) 667. doi:10.1115/1.3244369.

[196] D. Buddhi, N.. Bansal, R.. Sawhney, M.. Sodha, Solar thermal storage systems using phase change materials, Int. J. Energy Res. 12 (1988) 547–555. doi:10.1002/er.4440120318.

[197] M. Lacroix, T. Duong, Experimental IMPROVEMENTS OF HEAT TRANSFER IN A LATENT HEAT THERMAL ENERGY STORAGE UNIT WITH EMBEDDED HEAT SOURCES, Energy Convers. Manag. 39 (1998) 703–716. doi:10.1016/S0196-8904(97)10011-5.

[198] A.D. Brent, V.R. Voller, K.T.J. Reid, Enthalpy-porosity technique for modeling convection-diffusion phase change: application to the melting of a pure metal, Numer. Heat Transf. Part A Appl. 13 (1988) 297–318. doi:10.1080/10407788808913615.

[199] D.K. Gartling, Finite element analysis of convective heat transfer problems with change of phase, Sandia Labs., 1978.

[200] O.J. Ilegbusi, M.D. Mat, A hybrid model of the mushy region in phase-change problems, J. Mater. Process. Manuf. Sci. 5 (1997) 209–223.

[201] M. Kumar, D.J. Krishna, Influence of mushy zone constant on thermohydraulics of a PCM, Energy Procedia. 109 (2017) 314–321. doi:10.1016/j.egypro.2017.03.074.

[202] R. Kandasamy, X. Wang, A.S. Mujumdar, Transient cooling of electronics using phase change material (PCM) -based heat sinks, Appl. Mech. Mater. 28 (2008) 1047–1057. doi:10.1016/j.applthermaleng.2007.06.010.

[203] M.M. Farid, A.K. Mohamed, Effect of Natural Convection on the Process of Melting and Solidification of Paraffin Wax, Chem. Eng. Commun. 57 (1987) 297–316. doi:10.1080/00986448708960492.

[204] M. Farid, Y. Kim, T. Honda, A. Kanzawa, the Role of Natural Convection During Melting and Solidification of Pcm in a Vertical Cylinder, Chem. Eng. Commun. 84 (1989) 43–60. doi:10.1080/00986448908940334.

[205] M. Belusko, F. Bruno, Design methodology of PCM thermal storage systems with parallel plates, in: 1st Int. Congr. Heating, Cool. Build., EUROSUN, 2008: pp. 1–8. doi:oai:urm_publish:53119925780001831.

[206] N.H.S. Tay, M. Belusko, F. Bruno, An effectiveness-NTU technique for characterising tube-in-tank phase change thermal energy storage systems, Appl. Energy. 91 (2012) 309–319. doi:10.1016/j.apenergy.2011.09.039.

[207] D. Jaya Krishna, S. Kochar, The metallographic study of corrosion of metals with latent heat storage materials suitable for solar hot water system, Trans. Indian Ceram. Soc. 76 (2017) 133–141. doi:10.1080/0371750X.2016.1268072.

[208] U.M. Gaddala, J.K. Devanuri, A Hybrid Decision-Making Method for the Selection of

a PCM for Thermal Energy Storage, J. Therm. Sci. Eng. Appl. 12 (2020) 1–11. doi:10.1115/1.4046056.

[209] A.M. Abdulateef, S. Mat, K. Sopian, J. Abdulateef, A.A. Gitan, Experimental and computational study of melting phase-change material in a triplex tube heat exchanger with longitudinal/triangular fins, Sol. Energy. 155 (2017) 142–153. doi:10.1016/j.solener.2017.06.024.

[210] S. Mat, A.A. Al-Abidi, K. Sopian, M.Y. Sulaiman, A.T. Mohammad, Enhance heat transfer for PCM melting in triplex tube with internal-external fins, Energy Convers. Manag. 74 (2013) 223–236. doi:10.1016/j.enconman.2013.05.003.

[211] P. Wang, H. Yao, Z. Lan, Z. Peng, Y. Huang, Y. Ding, Numerical investigation of PCM melting process in sleeve tube with internal fins, Energy Convers. Manag. 110 (2016) 428–435. doi:10.1016/j.enconman.2015.12.042.

[212] J.M. Mahdi, S. Lohrasbi, D.D. Ganji, E.C. Nsofor, Simultaneous energy storage and recovery in the triplex-tube heat exchanger with PCM, copper fins and Al2O3 nanoparticles, Energy Convers. Manag. 180 (2019) 949–961. doi:10.1016/j.enconman.2018.11.038.

[213] W.B. Ye, D.S. Zhu, N. Wang, Numerical simulation on phase-change thermal storage/release in a plate-fin unit, Appl. Therm. Eng. 31 (2011) 3871–3884. doi:10.1016/j.applthermaleng.2011.07.035.

[214] S. Seddegh, X. Wang, A.D. Henderson, A comparative study of thermal behaviour of a horizontal and vertical shell-and-tube energy storage using phase change materials, Appl. Therm. Eng. 93 (2016) 348–358. doi:10.1016/j.applthermaleng.2015.09.107.

[215] B. Buonomo, H. Celik, D. Ercole, O. Manca, M. Mobedi, Numerical study on latent thermal energy storage systems with aluminum foam in local thermal equilibrium, Appl. Therm. Eng. 159 (2019) 113980. doi:10.1016/j.applthermaleng.2019.113980.

[216] A. Shahsavar, H.M. Ali, R.B. Mahani, P. Talebizadehsardari, Numerical study of melting and solidification in a wavy double-pipe latent heat thermal energy storage system, J. Therm. Anal. Calorim. (2020). doi:10.1007/s10973-020-09864-9.

[217] B. Buonomo, D. Ercole, O. Manca, S. Nardini, Numerical Analysis on a Latent Thermal Energy Storage System with Phase Change Materials and Aluminum Foam, Heat Transf. Eng. 41 (2020) 1075–1084. doi:10.1080/01457632.2019.1600875.

[218] B. Buonomo, H. Celik, D. Ercole, O. Manca, M. Mobedi, Numerical study on latent thermal energy storage systems with aluminum foam in local thermal equilibrium, Appl. Therm. Eng. 159 (2019) 113980. doi:https://doi.org/10.1016/j.applthermaleng.113980.

[219] M. Longeon, A. Soupart, J.F. Fourmigué, A. Bruch, P. Marty, Experimental and numerical study of annular PCM storage in the presence of natural convection, Appl. Energy. 112 (2013) 175–184. doi:10.1016/j.apenergy.2013.06.007.

[220] Y. Yuan, X. Cao, B. Xiang, Y. Du, Effect of installation angle of fins on melting characteristics of annular unit for latent heat thermal energy storage, Sol. Energy. 136 (2016) 365–378. doi:10.1016/j.solener.2016.07.014.

[221] M. Bechiri, K. Mansouri, Study of heat and fluid flow during melting of PCM inside vertical cylindrical tube, Int. J. Therm. Sci. 135 (2019) 235–246. doi:10.1016/j.ijthermalsci.2018.09.017.

[222] F.L. Tan, S.C. Fok, Numerical investigation of phase change material-based heat storage unit on cooling of mobile phone, Heat Transf. Eng. 33 (2012) 494–504. doi:10.1080/01457632.2012.624852.

[223] G. Li, Energy and exergy performance assessments for latent heat thermal energy storage systems, Renew. Sustain. Energy Rev. 51 (2015) 926–954. doi:10.1016/j.rser.2015.06.052.

[224] K. Kaygusuz, Ahmet Sari, Energy and exergy calculations of latent heat energy storage systems, Energy Sources. 22 (2002) 117–126. doi:10.1080/00908310050014090.

[225] H.H. Öztürk, Experimental evaluation of energy and exergy efficiency of a seasonal latent heat storage system for greenhouse heating, Energy Convers. Manag. 46 (2005) 1523–1542. doi:10.1016/j.enconman.2004.07.001.

[226] A. Erek, I. Dincer, A new approach to energy and exergy analyses of latent heat storage unit, Heat Transf. Eng. 30 (2009) 506–515. doi:10.1080/01457630802529271.

[227] E. Guelpa, A. Sciacovelli, V. Verda, Entropy generation analysis for the design improvement of a latent heat storage system, Energy. 53 (2013) 128–138. doi:10.1016/j.energy.2013.02.017.

[228] M.H. Mahfuz, M.R. Anisur, M.A. Kibria, R. Saidur, I.H.S.C. Metselaar, Performance investigation of thermal energy storage system with Phase Change Material (PCM) for solar water heating application, Int. Commun. Heat Mass Transf. 57 (2014) 132–139. doi:10.1016/j.icheatmasstransfer.2014.07.022.

[229] M. Rezaei, M.R. Anisur, M.H. Mahfuz, M.A. Kibria, R. Saidur, I.H.S.C. Metselaar, Performance and cost analysis of phase change materials with different melting temperatures in heating systems, Energy. 53 (2013) 173–178. doi:10.1016/j.energy.2013.02.031.

[230] R.J. Moffat, Describing the uncertainties in experimental results, Exp. Therm. Fluid Sci. 1 (1988) 3–17. doi:10.1016/0894-1777(88)90043-X.

[231] U.M. G., A. Majumadar, T. Niphadkar, J.K. D., An image processing algorithm to estimate the melt fraction and energy storage of a PCM enclosed in a spherical capsule, Int. J. Energy Res. 43 (2019) 5535–5547. doi:10.1002/er.4668.

[232] A. Bejan, Two Thermodynamic Optima in the Design of Sensible Heat Units for Energy Storage, J. Heat Transfer. 100 (1978) 708–712. doi:10.1115/1.3450882.

[233] S. Jegadheeswaran, S.D. Pohekar, T. Kousksou, Exergy based performance evaluation of latent heat thermal storage system: A review, Renew. Sustain. Energy Rev. 14 (2010) 2580–2595. doi:10.1016/j.rser.2010.07.051.

[234] K.Y. Leong, M.R. Abdul Rahman, B.A. Gurunathan, Nano-enhanced phase change materials: A review of thermo-physical properties, applications and challenges, J. Energy Storage. 21 (2019) 18–31. doi:10.1016/j.est.2018.11.008.

[235] M.S. Mahdi, A.F. Hasan, H.B. Mahood, A.N. Campbell, A.A. Khadom, A.M. em A. Karim, A.O. Sharif, Numerical study and experimental validation of the effects of orientation and configuration on melting in a latent heat thermal storage unit, J. Energy Storage. 23 (2019) 456–468. doi:10.1016/j.est.2019.04.013.

[236] S.M. Borhani, M.J. Hosseini, A.A. Ranjbar, R. Bahrampoury, Investigation of phase

change in a spiral-fin heat exchanger, Appl. Math. Model. 67 (2019) 297–314. doi:10.1016/j.apm.2018.10.029.

[237] S. Zhang, L. Pu, L. Xu, R. Liu, Y. Li, Melting performance analysis of phase change materials in different finned thermal energy storage, Appl. Therm. Eng. 176 (2020) 115425. doi:10.1016/j.applthermaleng.2020.115425.

[238] L. Kalapala, J.K. Devanuri, Energy and exergy analyses of latent heat storage unit positioned at different orientations – An experimental study, Energy. 194 (2020) 116924. doi:10.1016/j.energy.2020.116924.

[239] A. Bejan, Entropy generation minimization, CRC Press, London (England), 1996.

[240] M.K. Rathod, J. Banerjee, Entropy generation assessment of shell and tube latent heat storage unit, Int. J. Exergy. 16 (2015) 97–108. doi:10.1504/IJEX.2015.067301.

[241] G. Li, Energy and exergy performance assessments for latent heat thermal energy storage systems, Renew. Sustain. Energy Rev. 51 (2015) 926–954. doi:10.1016/j.rser.2015.06.052.

[242] M.M.A. Khan, N.I. Ibrahim, R. Saidur, I.M. Mahbubul, F.A. Al-Sulaiman, Performance assessment of a solar powered ammonia–water absorption refrigeration system with storage units, Energy Convers. Manag. 126 (2016) 316–328. doi:10.1016/j.enconman.2016.08.004.

[243] X.H. Yang, S.C. Tan, J. Liu, Numerical investigation of the phase change process of low melting point metal, Int. J. Heat Mass Transf. 100 (2016) 899–907. doi:10.1016/j.ijheatmasstransfer.2016.04.109.

[244] S. Chakraborty, Applications of the MOORA method for decision making in manufacturing environment, Int. J. Adv. Manuf. Technol. 54 (2011) 1155–1166. doi:10.1007/s00170-010-2972-0.

[245] W.K. Brauers, Optimization methods for a stakeholder society : a revolution in economic thinking by multi-objective optimization, Kluwer Academic Publishers, 2004.

[246] W.K.M. Brauers, E.K. Zavadskas, F. Peldschus, Z. Turskis, Multi-objective decision-making for road design, Transport. 23 (2008) 183–193. doi:10.3846/1648-4142.2008.23.183-193.

[247] S. Seddegh, S.S.M. Tehrani, X. Wang, F. Cao, R.A. Taylor, Comparison of heat transfer between cylindrical and conical vertical shell-and-tube latent heat thermal energy storage systems, Appl. Therm. Eng. 130 (2018) 1349–1362. doi:10.1016/j.applthermaleng.2017.11.130.

[248] G. Shen, X. Wang, A. Chan, F. Cao, X. Yin, Study of the effect of tilting lateral surface angle and operating parameters on the performance of a vertical shell-and-tube latent heat energy storage system, Sol. Energy. 194 (2019) 103–113. doi:10.1016/j.solener.2019.10.077.

[249] G.S. Sodhi, A.K. Jaiswal, K. Vigneshwaran, P. Muthukumar, Investigation of charging and discharging characteristics of a horizontal conical shell and tube latent thermal energy storage device, Energy Convers. Manag. 188 (2019) 381–397. doi:10.1016/j.enconman.2019.03.022.

[250] R.P. Singh, H. Xu, S.C. Kaushik, D. Rakshit, A. Romagnoli, Charging performance

evaluation of finned conical thermal storage system encapsulated with nano-enhanced phase change material, Appl. Therm. Eng. 151 (2019) 176–190. doi:10.1016/j.applthermaleng.2019.01.072.

[251] Y. Kozak, T. Rozenfeld, G. Ziskind, Close-contact melting in vertical annular enclosures with a non-isothermal base: Theoretical modeling and application to thermal storage, Int. J. Heat Mass Transf. 72 (2014) 114–127. doi:10.1016/j.ijheatmasstransfer.2013.12.058.

ARTICLES PUBLISHED BASED ON THE PRESENT WORK

1. L. Kalapala, J.K. Devanuri, Influence of operational and design parameters on the performance of a PCM based heat exchanger for thermal energy storage – A review, **J. Energy Storage**. 20 (2018) 497–519. doi:10.1016/j.est.2018.10.024. **(I.F – 3.762)**

2. L. Kalapala, J.K. Devanuri, Parametric investigation to assess the melt fraction and melting time for a latent heat storage material based vertical shell and tube heat exchanger, **Sol. Energy**. 193 (2019) 360–371. doi:10.1016/j.solener.2019.09.076. **(I.F – 4.608)**

3. L. Kalapala, J.K. Devanuri, Energy and exergy analyses of latent heat storage unit positioned at different orientations – An experimental study, **Energy**. 194 (2020) 116924. doi:10.1016/j.energy.2020.116924. **(I.F – 6.082)**

4. L. Kalapala, J.K. Devanuri, Optimization of Fin Parameters to Reduce Entropy Generation and Melting Time of a Latent Heat Storage Unit, **ASME J. Sol. Energy Eng.** 142 (2020) 1–12. doi:10.1115/1.4046878. **(I.F – 1.641)**

5. L. Kalapala, J.K. Devanuri, Effect of orientation on thermal performance of a latent heat storage system equipped with annular fins – An experimental and numerical investigation, **Appl. Therm. Eng**. 183 (2021) doi: 10.1016/ j. applthermaleng .2020. 116244. **(I.F – 4.725)**

6. L. Kalapala, J.K. Devanuri, Comparative analysis of solid and perforated fins for thermal enhancement of a latent heat storage unit positioned at various inclinations, **Energy Sources, Part A Recover. Util. Environ. Eff**. (2021) 1–20. doi:10.1080/15567036.2021.1886202. **(I.F – 1.184)**

7. Effect of fin parameters on thermal performance of conical shell and tube latent heat storage unit (Under review - Submitted to ASME Journal of Energy Resource Technology)